The Microlaser: Study of Laser Oscillation with One Atom in an Optical Resonator

by

Kyungwon An

B.S., Seoul National University (1983)
M.S., Seoul National University (1985)

Submitted to the Department of Physics
in partial fulfillment of the requirements for the degree of

Doctor of Philosophy

at the

MASSACHUSETTS INSTITUTE OF TECHNOLOGY

February 1995

Author ....
Department of Physics
November 28, 1994

Certified by ....
Michael S. Feld
Professor
Thesis Supervisor

Accepted by ....
George F. Koster
Chairman, Departmental Committee on Graduate Students

The Microlaser: Study of Laser Oscillation with One Atom in an Optical Resonator

by

Kyungwon An

Submitted to the Department of Physics
on November 28, 1994, in partial fulfillment of the
requirements for the degree of
Doctor of Philosophy

Abstract

This thesis describes the first realization of one-atom laser, a laser oscillator with only one atom in an optical resonator. In our experiment a beam of ^{138}Ba atoms traverses a high-Q optical cavity with a finesse of 8×10^5. The atoms are excited from the $^1S_0$ ground state to the $^3P_1$ (m=0) excited state by a π-pulse before they enter the cavity. Laser oscillation at 791 nm ($^3P_1 \rightarrow {}^1S_0$) has been observed with the mean number of atoms inside the cavity mode varied between 0.1 and 1.0, resulting in the mean number of photons inside the cavity changing from 0.14 to 11. To understand the data quantitatively, two different theoretical approaches were taken. First a pendulum equation based on the Maxwell-Schrodinger equation provides physical insights on the evolution of the one-atom laser with limited success in predicting correct signal size. Second approach is based on a fully-quantized one-atom theory. In this approach, a new photon recursion relation for the field density matrix was derived. Combined with a simple modification needed for the standing wave nature of the cavity mode, the quantum theory is in good agreement with the experiment.

Thesis Supervisor: Michael S. Feld
Title: Professor

Acknowledgments

This work would not have been possible without boundless support from my wife Youngkyu. She has been alway there whenever I needed her, encouraging me to overcome so many difficult times. The success of this work coincided with the birth of my son Ulzee. He brought us a joy and changed the meaning of life forever. My parents in Korea have also gone through many difficult moments with us. They have been worried about their son in a strange land (to them) and alway prayed for me. I am indebted to them for endless care for those long years at MIT.

I cannot deny even for a second the intellectual influence that Prof. Michael Feld has shed on me. His deep intuition in physics has always amazed me. His optimism, his belief in me and encouragement have been unquestionable driving force to the success of this work. I also owe thousand thanks to Dr. Ramachandra Dasari for supporting me intellectually and financially. I thank him for inviting me to many wonderful Indian diners (breakfast too) and countless enjoyable discussions that we shared beyond physics. Jim Childs has been a good companion in the Spectroscopy Laboratory, where we had been only two physics students for some time, working together day and night. I learned many useful experimental techniques from him, particularly on ion lasers and ring dye lasers.

I deeply appreciate Mrs. Fari Partovi's warm smile and help in many occasions. Her help even encompasses helping me to arrange catering service for my mother-in-law's exhibition in Newbury St.. I also would like to express thanks to all fellow students in the Spectroscopy Laboratory, naming a few, Changhuei Yang for helping me to improve the microlaser setup, George Zonios for lending me a computer account for the calculations for the microlaser, and Dr. Joe Baraga (PhD and MD) for his witts, optimism and attention to a fellow student.

I would like to thank Prof. John Thomas at Duke Univ., and Dr. Michael Otteson for helping me to initiate experiments in the picosecond laboratory in my early years at MIT. In those days Dr. C. Kitttrell also helped me to setup the time-resolved photon counting system there. Dr. Young-Dong Park, now in Inha Univ. in Korea, was a wonderful mentor and friend in those early years. We both worked in the picosecond laboratory, doing some time-decay fluorescence measurement on biomedical samples. I also wish to thank Prof. Dan Heinzen at Univ. at Texas Austin, who initiated early cavity QED experiments in the Spectroscopy Laboratory. Whenever he visited MIT, we had many good discussions, often resulting in significant improvements in the project. Finally, my sincere thanks go to Prof. Dan Kleppner, Prof. Roy Glauber and Prof. Ray Weiss for participating in my thesis committe and for giving me invaluable suggestions and comments on this work.

This entire document was typeset with OzTEX, which is a wonderful public-domain implementation of LaTeX on Macintosh computer.

Contents

List of Figures

List of Tables

Chapter 1

Introduction

One of the simplest but most interesting problems in quantum optics is the interaction of a single atom with a single quantized mode of the electromagnetic field. This problem, treated by Jaynes and Cummings many years ago [2], has an exact solution if irreversible processes which give rise to damping, such as atomic spontaneous emission and decay of the field mode, are negligible. The atom and the field then exchange an energy quantum in a manner characteristic of coupled oscillators. The rate of energy exchange, determined by the atom-field coupling strength, can be appreciable even for a vacuum field. This coupling has been observed in the lineshape splitting for a weakly excited absorbing atom [3].

The atom-cavity interaction process, often referred to as cavity quantum electrodynamics, has been studied extensively in both theory and experiment. One of the best systems to study cavity QED has been the micromaser, one-atom maser [4]. Naturally, there has been great anticipation to realize a microlaser, one-atom laser. This new experimental tool would greatly broaden the scope of the study of cavity QED. One-atom laser would allow detection of photons, as well as atoms, whereas only atoms can be probed in the microwave regime. Photon counting detectors with efficiencies of up to 80 % [5] are now available, making study of the photon statistics in the one-atom laser quite promising. Furthermore, a linewidth measurement would be straightforward, while it is yet to be done in the one-atom maser, where a complicated Ramsy-fringe type configuration is required[6].

One major obstacle in the development of an one-atom laser has been the technical difficulty in fabricating a very high-Q cavity in the optical regime. Recently, supercavity technology has reached the point where a cavity with finesse of 10^6 or even higher [7] can be assembled. The present work builds upon this recent breakthrough.

This thesis describes the first realization of a working one-atom laser. This system undergoes laser oscillation with an average of less than one atom, yielding an average photon number in the cavity much greater than unity.

1.1 Background

Lasers work on the principle of spontaneous as well as stimulated emission. A laser in its simplest form is composed of a resonator and a gain medium. Excited atoms or molecules constituting the gain medium tend to emit photons in the same mode as the photons already in the resonator. This process is called stimulated emission. The rate of the stimulated emission process is roughly proportional to the number of photons already existing in the cavity so that under certain condition, often referred to above-threshold condition, successive photon emission processes are accelerated as the number of photons in the mode increases. Due to the stimulated emission process, the output of a laser is monochromatic and coherent. However such stimulated emission process will not be initiated without spontaneous emission. It is the spontaneous emission process that creates a small number of intracavity photons, which in turn trigger the stimulated emission. The spontaneous emission process also determines an ultimate or intrinsic emission linewidth of a laser [8, 9, 10].

This conventional notion is about to change. Though too simplified, there are basically two kinds of lasers: conventional lasers and the one-atom laser. All conventional lasers work on the principle of the spontaneous and stimulated emission as explained before whereas the one-atom laser, which is the subject of this thesis, works on a quite different principle, so called Rabi oscillation in cavity quantum electrodynamics (QED) [11].

What is the cavity QED? The cavity QED can be defined as the study of an atom or atoms in a vacuum modified by the presence of a cavity. When an excited atom is in free space, the vacuum fluctuations induces the atom to couple to the continuum of free space modes. As a result, the atom undergoes spontaneous emission. The coupling constant between the atom and one of the free-space modes is given by the following formula [25].

$$g = \frac{\mu E_{vac}}{\hbar} . \tag{1.1}$$

where E_{vac} is the rms size of an electric field associated with the vacuum fluctuations, and it is given by

$$E_{vac} = \sqrt{\frac{2\pi\hbar\omega}{V_m}} . \tag{1.2}$$

Since E_{vac} is inversely proportional to the square root of the mode volume V_m, which is infinite for free space, the coupling constant to one of the free space mode is practically zero.

Now suppose we place the atom in a cavity. Then the vacuum fluctuations associated with the cavity mode is greatly enhanced because the volume determining the size of E_{vac} is nothing but the cavity mode volume, which can be made very small. Since the emission rate into the cavity mode is proportional to the square of the coupling constant, we can make the emission rate even much larger than the unmodified free-space spontaneous decay rate. This has been the basic idea behind many cavity QED experiments, including the suppression/enhancement of spontaneous emission [12, 13, 14, 15, 16, 17], radiative level shift [18, 19, 20], and some experiments directly related to the coupling constant g such as collective atom-cavity oscillation [21], normal mode splitting in the transmission/absorption spectra of atom-cavity combined systems [22, 23, 24]. For a complete list of cavity-QED experiments, readers are referred to the excellent articles in Refs. [25, 26] and references therein.

So far the study of the cavity QED has been mostly devoted to the spontaneous emission process. Now it seems quite logical to ask about stimulated emission in the cavity QED. An obvious choice for the study of stimulated emission is a laser in the cavity QED setting, one-atom laser.

The ideas of one-atom lasers, have been discussed in the literature for some time

[27, 28, 29, 30, 31, 32]. At the same time, many experimental schemes of one-atom lasers have been proposed including a single atom trapped in a cavity [27, 32], single-atom dressed-state gain [33], a new breed of cavity utilizing whispering gallery modes of a sphere [32], and a microlaser, an optical analogy of the micromaser [4]. The present work is based on the microlaser idea.

So why do we bother to construct a laser with only one atom? There are many reasons but the most important one is that a single atom laser is a fundamental quantum oscillator, consisting of a single atom and a single radiation mode. Because of the quantum mechanical nature of the coherent interaction between a single atom and a single radiation mode, it can in principle generate nonclassical radiation at visible wavelengths. Because it is still a laser, such radiation can be quite intense. For example, the one-atom laser of the present work, can generate up to 10^7 photons per second. Another reason is that a single atom laser can also serve as a testing ground of various quantum mechanical theories. For example, we can test many quantum mechanical theories predicting the linewidth of the micromaser [34, 35, 36, 37, 38] by actually measuring the linewidth of the one-atom laser.

1.2 Basic concept

Let's examine the basic concept of the one-atom laser. The components of our experiment are two-level atoms, a high-Q single-mode cavity resonant with the atom, a light source to excite the atom into the upper energy level, and photon-counting detectors (Figure 1-1). The two-level atoms from an atomic beam are excited to the upper energy level by a pump laser just before they enter the cavity. The intensity and waist of the pump laser are adjusted in such a way that the atoms are completely excited to the excited state when they leave the pump region. In a pendulum analogy, the atoms are said to be inverted by the pump. The spontaneous emission has to be very small so that it can be neglected while the atoms are traveling from the pump region to the cavity as well as they are in the cavity. Since both the atomic damping and cavity damping are very small, laser dynamics is determined solely by

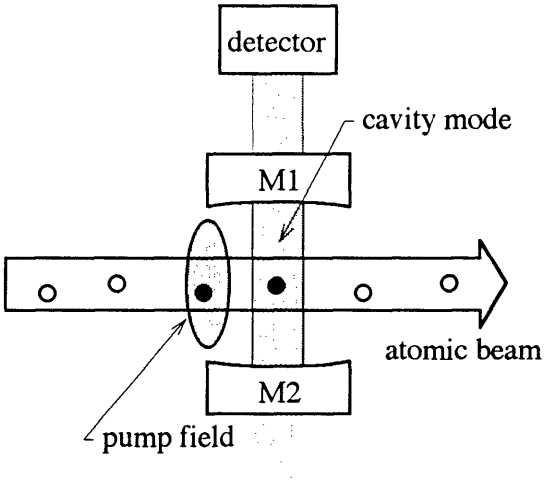

Figure 1-1: Schematic of the one-atom laser experiment.

the Rabi oscillation between the atom and the cavity field. This Rabi oscillation is fully characterized by the atom-cavity coupling constant g and the transit time or interaction time T_{transit}.

In Figure 1-2, the excited-state probability of the atom, which is just the absolute square of the excited state wave function, is plotted as a function of time. As we will see later, the one-atom laser behaves like a pendulum. Initially the pendulum is inverted and it rotates as the system evolves. Suppose an excited atom is injected with no photon in the cavity. The atom enters the cavity at $t = 0$ and exits at $t = T_{\text{transit}}$. Once inside the cavity, the atom has a probability of undergoing a downward transition due to vacuum Rabi oscillation at frequency g_o, emitting a photon into the cavity mode. For the value of $2gT_{\text{transit}}$ of unity, which is roughly the value in our one-atom laser, the first atom has about 30 % chance of emitting a photon. In other words, after three atoms, one photon will be emitted.

Once a photon is emitted, it will stay in the cavity for a long time, so the next atom will see a photon already in the cavity, and therefore the Rabi frequency for the atom is enhanced by $\sqrt{n+1}$ with n the number of photons already in the cavity. So the atom has more chance of emitting a photon. Therefore, after many passages, a situation can occur in which the atom leaves the cavity completely in the ground

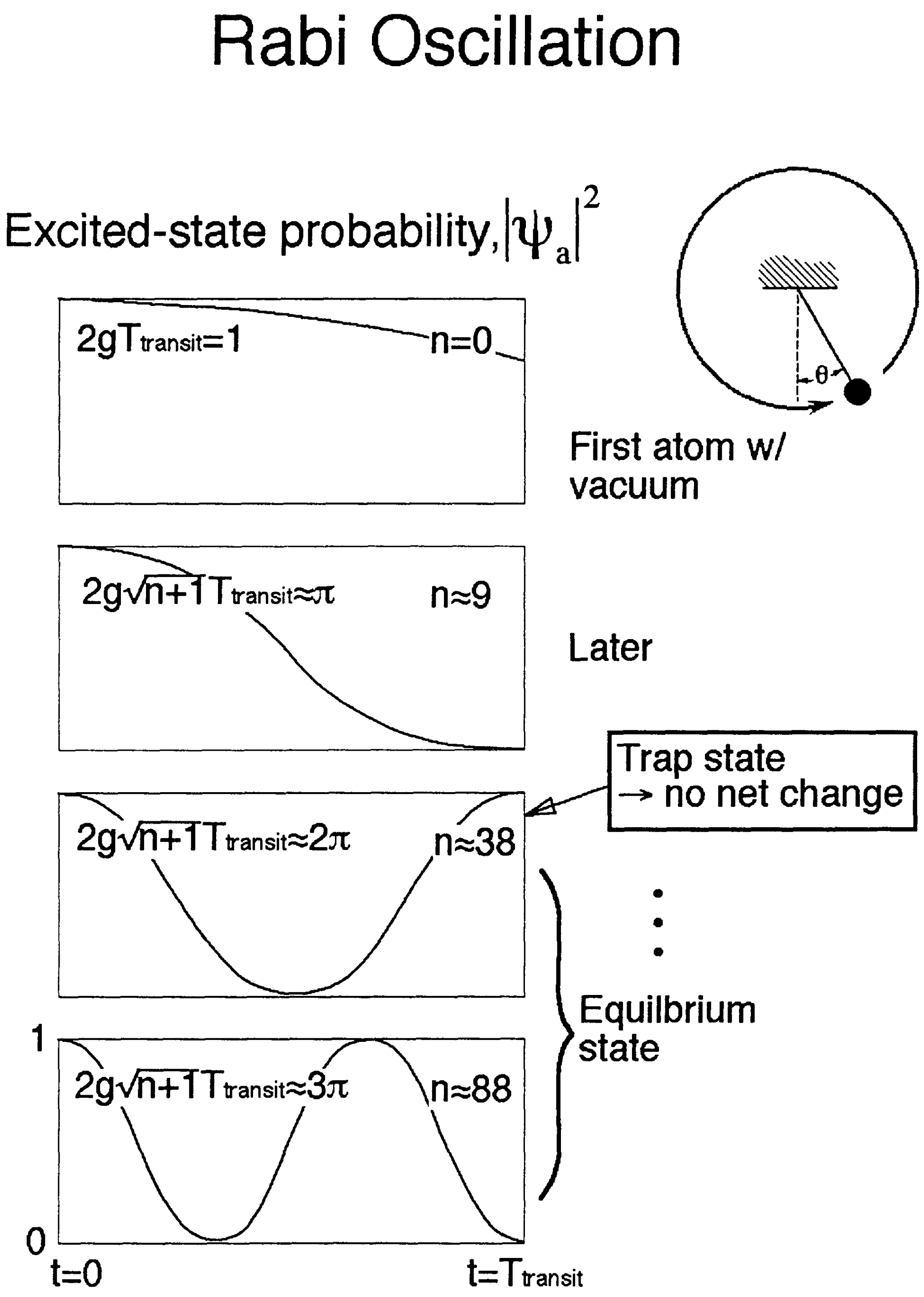

Figure 1-2: Rabi oscillation as an analogy to a rotating pendulum.

state, thereby having 100 % probability of emitting a photon. In pendulum analogy, it corresponds to a half rotation of the pendulum from top to bottom position.

Photon buildup does not stop there, so after a while the atom can undergo a complete rotation, leaving the cavity in the same state as its initial state, which is often called a trap state [39, 40], or it may undergo a half more turn, leaving the cavity again in the ground state. This process continues until an equilibrium situation is reached. In the equilibrium, the small energy loss due to cavity decay and atomic spontaneous decay is exactly balanced by the mean energy transfer from the excited atom to the field mode. This is the basic idea how the one-atom laser works.

A similar idea was introduced in the micromaser 9 years ago [4]. The micromaser itself has been a very interesting microwave device. This system has made possible the study of quantum collapse and revival [41] and non-classical atom statistics [42]. It has also invoked many theoretical studies on linewidth [34], number state generation [43], quantum non-demolition measurements [19, 20], squeezing [44], and trap states [39], but most of these have yet to be realized experimentally.

1.3 Effects of strong coupling on the one-atom laser

In the cavity QED, there exists an interesting regime in which g is made much larger than the free-space total spontaneous decay rate, Γ_a. For the one-atom laser, for example, the spontaneous emission process during the interaction time is negligibly small whereas the coupling constant g is appreciably large. Interestingly, both g and Γ_a are proportional to the dipole moment, either linearly(g) or quadratically(Γ_a).

In laser physics, β parameter is often used to characterize the efficiency of the emission process into a laser cavity mode. The parameter is defined as the ratio of the emission rate into the cavity mode, defined as A_{enh} below, to the total emission rate including the free-space spontaneous emission rate. In a steady state, the emission rate into the cavity mode A_{enh} is given by [24],

$$A_{\text{enh}} = 4g^2/\Gamma_c \ , \tag{1.3}$$

where Γ_c is the cavity decay rate. In our case $A_{\text{enh}}/\Gamma_a \approx 52$ so that

$$\beta = \frac{A_{\text{enh}}}{A_{\text{enh}} + \Gamma_a} = \frac{52}{52+1} = 0.98 \ . \tag{1.4}$$

This β or A_{enh}/Γ_a is, in fact, a physically meaningful parameter only for continuous wave (CW) lasers. In our case, where atoms are inverted temporarily, rather g and T_{transit} are truly meaningful parameters. However under certain conditions, e.g., many atom operation and rate equation regime as discussed in Chap.2, the microlaser can well be characterized by A_{enh}/Γ_a factor. Under such conditions, the factor is nothing but an unsaturated multi-pass gain, the ratio of an unsaturated single-pass gain to a single-pass loss.

It is interesting to note that the resonator used in the one-atom laser is just like an ordinary laser cavity in characteristics, except that the length of the cavity is relatively small ($\sim 1mm$) and the finesse is very high. However, the volume of the TEM_{00} mode of the cavity is small enough that the coupling constant between the atom and the cavity field is much larger than irreversible damping rates, Γ_a and Γ_c. Note that the absolute magnitude of g is not so large. In fact, in many recent cavity-QED experiments g has been often a few MHz [22, 3] whereas our g is only 0.4 MHz. But its relative size compared to Γ_a and Γ_c, or equivalently β parameter, is unprecedented in recent cavity-QED experiments in the visible wavelength region. The enhancement factor A_{enh}/Γ_a in Ref. [3] was only $(6.4)^2/(5.0 \times 1.9) = 4.3$, compared to our value of whopping 52 !

In order to get some idea how make the ratio $2g/\Gamma_a$ much larger than unity, lets consider an atom in a small cube with no cavity damping. The the square of the ratio can be rewritten as

$$\begin{aligned}\left(\frac{2g}{\Gamma_a}\right)^2 &= \frac{4\frac{\mu^2}{\hbar^2}\left(\frac{2\pi\hbar\omega}{V_m}\right)}{\Gamma_a\frac{4\mu^2(\omega/c)^3}{3\hbar}} \\ &= \frac{1}{(2\pi)^2}\left(\frac{\omega}{\Gamma_a}\right)\left(\frac{\lambda^3}{V_m}\right) \,. \qquad (1.5)\end{aligned}$$

Therefore, there are practically two parameters that can be controlled: the mode volume and the free-space spontaneous decay rate. In order to make the ratio as large as possible, we need to make both parameters as small as possible. It is rather ironical that the smaller spontaneous decay rate is the better, considering that the larger the coupling constant is, the larger the spontaneous decay rate must be.

Appreciating this idea, we can realize that there is no limit to which the coupling constant can be enhanced. We can imagine an atom placed in a cube with its dimension comparable to the wavelength. If the dimension of the cube is smaller than the wavelength, obviously the atom can never decay because the mode frequencies supported by the cube is higher than the transition frequency so that the coupling constant for the transition frequency is zero. The smallest volume leading to largest coupling constant is, therefore, $(\lambda/2)^3$. Then the largest $2g/\Gamma_a$ is

$$\left(\frac{2g}{\Gamma_a}\right)_{\max} = \frac{2}{\pi^2}\left(\frac{\omega}{\Gamma_a}\right) \,. \qquad (1.6)$$

However, once the ratio is much larger than unity, nothing is gained by by enhancing the ratio further. In our one-atom laser, $2g$ is about 700 kHz compared to Γ_a about 50 kHz, yielding the ratio, $14 \gg 1$.

1.4 Feasibility

Before we start to construct one-atom laser, obviously we want to make sure that such a laser is feasible. As mentioned before briefly, in an equilibrium state, the energy input rate is exactly matched by the energy loss rate. So we can write down a rate equation for the mean number of photons in the cavity,

$$\frac{d\langle n\rangle}{dt} = \frac{N}{T_{\text{transit}}} - \Gamma_c\langle n\rangle \ = 0 \ , \tag{1.7}$$

where we assume that N excited atoms are injected during T_{transit}, and the photons are lost by the cavity decay Γ_c. Then in an equilibrium state, the mean photon number is given by

$$\langle n\rangle \ = \frac{N}{\Gamma_c T_{\text{transit}}} \tag{1.8}$$

The feasibility of the one-atom laser critically hinges on efficient photon storage as well as a strong atom-cavity coupling. In the experiment, a supercavity optical resonator with optical Q of 2×10^9 was used to realize very long cavity decay time. An inequality to be satisfied is

$$\Gamma_c \ , \ \Gamma_a \ \ll 2g \ , T_{\text{transit}}^{-1} \ , \tag{1.9}$$

so that the strong coupling condition in the cavity QED has to be satisfied.

Now let's check the feasibility with some numbers. In our experiment, we used ^{138}Ba atom as a two-level system. The atoms are inverted from the ^{1}S$_0$ ground state to ^{3}P$_1$ excited state by a pump laser. The wavelength is 791 nm and the spontaneous decay time is about 3 μsec. We also used a supercavity resonator, the finesse of which was 8×10^5, length of 1 mm, radius curvature of the mirrors were 10 cm, so that the cavity mode waist was 45 μm. Using these figures, we obtain the cavity decay time about 1 μsec, and the inverse of the coupling constant 0.4 μsec. If we assume a velocity of 300 m/s, the transit time is $\frac{2\times45\mu m}{300m/s} = 0.3$ μsec. Using these numbers, the mean photon number for one-atom case is expected to be about 3 photons, much greater than unity. So it should be possible to build an one-atom laser.

1.5 Contribution of present work

In the present work we have realized one-atom laser. The laser oscillation was obtained with the mean number of atoms in the cavity mode varied between 0.1 and 1.0, resulting in the mean photon number in the cavity changing from 0.14 to 11.

The largest mean photon number corresponds to 10^7 photons emitted per second. In addition, we obtained the following results.

a. No distinct threshold behavior was observed.

b. The measured mean photon number agrees with a fully quantized one-atom theory (to be described in Chap.2) as long as the mean number of atoms is much less than unity.

c. When the mean number of atoms is comparable to unity, the measured mean photon number is much larger than the prediction of the one-atom theory. This discrepancy can be explained by incorporating the standing-wave nature of the cavity mode into the theory.

1.6 Organization of thesis

In Chapter 2, a semiclassical theory of the one-atom laser is first described, followed by a fully-quantized theory. It will be shown that the semiclassical theory leads to a pendulum equation, which provides intuitive description of the evolution of the one-atom laser. The quantum theory, based on the theory of the one-atom maser, provides a new photon recursion relation for the field density matrix for correct description of the one-atom laser. A heuristic argument is given for accounting the standing wave nature of the cavity mode. At the end of the chapter, a semiclassical theory of the many-atom laser is presented for comparison purpose. It is shown that this theory can generate simple laser rate equations under certain conditions.

In Chapter 3, the experimental study of the one-atom laser is presented. First the core components of the experiment are closely examined and necessary requirements on each component are discussed. Then the experimental procedures in taking various data are described and the data are analyzed using the quantum theory as well as the semiclassical theory.

In Chapter 4, possible future experiments are proposed and briefly explained.

Chapter 2

Theory of the One-Atom Laser

The micromaser, i.e., the one-atom maser[4] has been the subject of numerous theoretical studies because the system itself is simple enough to permit rigorous theoretical considerations. There exist full-quantized theories, addressing various aspects of the micromaser [45, 44, 46, 47, 39, 48, 49, 34, 35], when the mean number of atoms involved is far less than one so that at most only one atom interacts with the cavity field. As seen below, this theory can be readily applicable to the one-atom laser with appropriate modifications.

When the mean number of the atoms becomes comparable to or larger than one, any quantum theory should account for the cases where more than one atom can simultaneously interact with a common cavity field. As one can easily imagine, a quantum modeling would become prohibitively complicated due to the large number of degrees of freedom in the problem. As shown in the next chapter, the mean number of photons grows quickly as the mean number of atoms increases. Hence the field Fock states to be considered can be a few hundreds even for a few atoms, resulting in 10^4 - 10^5 field density matrix elements to be evaluated. At best we can only rely on a numerical simulation on computers. However if the number of the involved atoms is macroscopically large, a semiclassical approach employing the coupled Maxwell-Schrödinger equations should correctly describe the system. Therefore, it will be interesting to see how the characteristics of the one-atom maser/laser change as the number of atoms is varied from far below one to many.

In this chapter, a review of a fully quantized one-atom maser theory is presented first (Sec.2.1.1). We then examine necessary modifications in the model to correctly describe the one-atom laser. It will be shown in Chapter 3 that the micromaser theory, with the photon recursion relation as it is, simply cannot fit our experimental data (see Fig. 3-42). Therefore, we need to derive a new recursion relation for the field density matrix (Sec.2.1.3). Then the standing wave nature of the cavity mode is examined and properly incorporated into the quantum theory (Sec.2.1.4). Following this, a semiclassical theory of the one-atom laser is formulated (Sec.2.2). The purpose of the semiclassical theory is to elucidate an analogy between the one-atom laser and a rotating pendulum, and to clarify the role of a pump laser field, particularly when it is placed *inside* the cavity. Our quantum theory at present status simply cannot address a situation in which the pump field overlaps with the cavity field. Finally a semiclassical theory for a many-atom laser is presented (Sec.2.3). Under the assumption that atomic dipoles are rapidly dephasing, this theory reduces to a pair of rate equations resembling those of conventional lasers (Sec.2.3.3). These equations should describe the system when the number of atoms in the cavity is macroscopically large. The theories developed in this chapter will be used to analyze the experimental data presented in the next chapter.

2.1 Quantum Mechanical Theory of the One-Atom Laser

2.1.1 Review of Micromaser Theory

The theory presented here is a recapitulation of the quantum theory of the microlaser developed by Filipowicz et al.[47]. In Sec. 2.1.3 we extend this theory to describe our one-atom laser. In this theory, a series of *excited* two-level atoms at velocity v are injected into a low-order single-mode microwave cavity, which is tuned to the atomic transition. The way the atoms are excited is not important but the pumping process used to excited the atoms should not interfere with the atom-cavity interaction. The

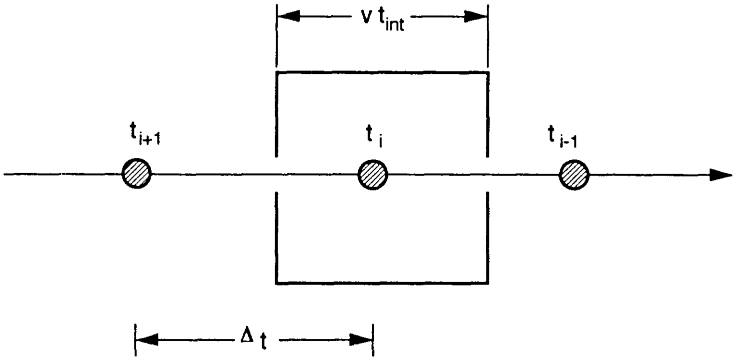

Figure 2-1: Schematic of the one-atom maser. Two-level atoms are injected into a microwave cavity at a mean time interval of Δt. The transit time t_{int} is assumed to be much shorter than Δt so that at most one atom is present inside the cavity at any instance.

atoms should be also completely excited to the excited state so that only an incoherent population gain is present. We assume the atoms are apart in time by Δt and the traverse time through the cavity is t_{int} (following original notation in Ref.[47]), which is identical to T_{transit} introduced in Chapter 1. We also assume that $t_{int} << \Delta t$ so that at most only one atom is present in the cavity (Figure 2-1).

When an atom is present in the cavity, the system can be described by the Jaynes-Cummings hamiltonian [2] given by

$$H = \frac{1}{2}\hbar\omega_a S_z + \hbar\omega a^\dagger a + \hbar g \left(S_+ a + S_- a^\dagger\right) \tag{2.1}$$

where g is the atom-field coupling constant defined in Eqs. 1.1 and 1.2, ω_a is the atomic transition frequency, $a^\dagger$ and a are the creation and the annihilation operator for the photons in the field mode, respectively, and S_+, S_- and S_z are the Pauli matrices. When no atom is present in the cavity, the last term, accounting for the coupling between the atom and the cavity field, vanishes.

We assume the i-th atom in the sequence enters the cavity at $t = t_i$ and the next atom at $t = t_{i+1}$, and so on. The system is described by a density operator ρ, with ρ_f and ρ_a being the projection of the ρ into the field space and the atom space, respectively.

For $t_i < t < t_{i+1}$, i.e., when an atom is inside the cavity, the evolution of the system is described by an unitary operator

$$U(t) = \exp\left(-iHt/\hbar\right) \tag{2.2}$$

so that

$$\begin{aligned} \rho_f(t_i + t_{int}) &= \mathrm{Tr}_{atom}\left[U(t_{int})\rho(t_i)U^\dagger(t_{int})\right] \\ &\equiv F(t_{int})\rho_f(t_i) \end{aligned} \tag{2.3}$$

where Tr_{atom} is a projected trace operator into the atom space. Eq. 2.3 also defines $F(t_{int})$. On the other hand, for $t_i + t_{int} < t < t_{i+1}$, i.e., when no atom is present in the cavity, the field component of the density operator undergoes decay due to the cavity damping process.

$$\begin{aligned} \dot{\rho_f} &= \frac{\Gamma_c}{2}(n_b+1)\left(2a\rho_f a^\dagger - a^\dagger a\rho_f - \rho_f a^\dagger a\right) + \frac{\Gamma_c}{2}n_b\left(2a^\dagger\rho_f a - aa^\dagger\rho_f - \rho_f aa^\dagger\right) \\ &\equiv \mathrm{L}\rho_f \end{aligned} \tag{2.4}$$

where n_b is the number of photons due to black-body radiation in the cavity. Then from Eqs.2.3 and 2.4,

$$\begin{aligned} \rho_f(t_{i+1}) &= \exp(\mathrm{L}t_p)\rho_f(t_i + t_{int}) \\ &= \exp(\mathrm{L}t_p)F(t_{int})\rho_f(t_i) \end{aligned} \tag{2.5}$$

where $t_p \equiv t_{i+1} - (t_i + t_{int})$.

The probability of having n photons in the cavity mode is given by

$$P_n = \langle n \,|\rho_f|\, n\rangle \tag{2.6}$$

From Eq.2.3, a recursion relationship for P_n can be obtained.

$$P_n(t_i + t_{int}) = P_n(t_i) + \underbrace{\beta_{n-1}P_{n-1}(t_i)}_{\text{emission: } n-1\to n} - \underbrace{\beta_n P_n(t_i)}_{\text{emission: } n\to n+1} \quad , \tag{2.7}$$

where

$$\beta_n = \frac{(n+1)g^2}{(n+1)g^2 + (\Delta/2)^2} \sin^2\left(\sqrt{(n+1)g^2 + (\Delta/2)^2}\, t_{int}\right) \tag{2.8}$$

where $2\sqrt{n+1}g$ is the Rabi frequency associated with n photons and $\Delta = \omega - \omega_a$, a cavity-atom frequency detuning. This recursion relation reflects the coherent interaction between the atom and the cavity field while the atom traverses the cavity. When no atom in the cavity, the evolution of P_n is determined by

$$\dot{P}_n = \Gamma_c(n_b+1)\left[(n+1)P_{n+1} - nP_n\right] + \Gamma_c n_b \left[nP_{n-1} - (n+1)P_n\right] \tag{2.9}$$

which is derived from Eq.2.4.

In reality, the arrival times of the atoms at the cavity are not regularly spaced. Rather the time interval between two successive atoms follows Poissonian distribution.

$$f(t_p) = \frac{1}{\Delta t}\exp\left[-\frac{t_p + t_{int}}{\Delta t}\right] \tag{2.10}$$

Averaging Eq.2.5 over the distribution,

$$\begin{aligned} \bar{\rho}_f(t_{i+1}) &\equiv \langle \rho_f(t_{i+1})\rangle_{t_p} \\ &= \langle \exp(\mathrm{L}t_p)\rangle_{t_p} \langle F(t_{int})\rho_f(t_i)\rangle_{t_p} \\ &= \langle \exp(\mathrm{L}t_p)\rangle_{t_p} \langle \rho_f(t_i + t_{int})\rangle_{t_p} \end{aligned} \tag{2.11}$$

where we assume that the arrival time of the (i+1)-th atom is statistically independent from that of the i-th atom. Note that

$$\begin{aligned}\langle \exp(\mathrm{L}t_p)\rangle_{t_p} &= \frac{1}{\Delta t}\int_0^\infty dt_p \, \mathrm{e}^{-\frac{t_p+t_{int}}{\Delta t}} \, \mathrm{e}^{\mathrm{L}t_p} \\ &= \frac{\mathrm{e}^{-\frac{t_{int}}{\Delta t}}}{1-\mathrm{L}\Delta t} \\ &\approx \frac{1}{1-\mathrm{L}\Delta t} \end{aligned} \tag{2.12}$$

because $t_{int} \ll \Delta t$ for true one-atom operation. So

$$(1-\mathrm{L}\Delta t)\,\bar{\rho}_f(t_{i+1}) = \langle \rho_f(t_i+t_{int})\rangle_{t_p} \ . \tag{2.13}$$

In an equilibrium state, the averaged field component of the density matrix, $\bar{\rho}_f(t)$, at the end of the every atom transit, should remain constant.

$$\bar{\rho}_f(t_{i+1})\,|_{SS} = \bar{\rho}_f(t_i)|_{SS} \equiv \bar{\rho}_{f,SS} \ , \tag{2.14}$$

which is called "a steady state of a return map" in Ref.[47]. Therefore

$$(1-\mathrm{L}\Delta t)\,\bar{\rho}_f(t_i)\,|_{SS} = \bar{\rho}_f(t_i+t_{int})|_{SS} \ ,$$

which is rewritten as

$$\bar{\rho}_f(t_i)\,\Big|_{SS} - \Delta t\dot{\bar{\rho}}_f(t_i)\Big|_{SS} = \bar{\rho}_f(t_i+t_{int})\,|_{SS} \ \ , \tag{2.15}$$

using Eq.2.4.

With the define of an averaged photon distribution function

$$\bar{P}_n \equiv \langle n\,|\bar{\rho}_{f,SS}|\,n\rangle \ \ , \tag{2.16}$$

Eq.2.15 reduces to

$$\bar{P}_n - \Delta t\dot{\bar{P}}_n = (1-\beta_n)\bar{P}_n + \beta_{n-1}\bar{P}_{n-1} \ , \tag{2.17}$$

which simplifies to

$$\begin{aligned}
S_n &\equiv \Gamma_c \Delta t \left[(n_b + 1) n \bar{P}_n - n_b n \bar{P}_{n-1} \right] - \beta_{n-1} \bar{P}_{n-1} \\
&= \Gamma_c \Delta t \left[(n_b + 1)(n+1) \bar{P}_{n+1} - n_b (n+1) \bar{P}_n \right] - \beta_n \bar{P}_n \\
&\equiv S_{n+1}, \qquad\qquad n \geq 1 \,. \qquad (2.18)
\end{aligned}$$

For a physical photon distribution, $n\bar{P}_n \rightarrow 0$ for $n \rightarrow \infty$, resulting in $S_n \rightarrow 0$. Since $S_{n+1} = S_n$ for all $n(\geq 1)$, $S_n = 0$ for all $n(\geq 1)$. Hence

$$\bar{P}_n = \left[\frac{\Gamma_c \Delta t n_b n + \beta_{n-1}}{\Gamma_c \Delta t (n_b + 1) n} \right] \bar{P}_{n-1}, \; n \geq 1 \qquad (2.19)$$

This recursion relation reduces to

$$\bar{P}_n = \bar{P}_0 \prod_{k=1}^{n} \left[\frac{\Gamma_c \Delta t n_b k + \beta_{k-1}}{\Gamma_c \Delta t (n_b + 1) k} \right] \qquad (2.20)$$

In optical regime, n_b is practically zero, so

$$\bar{P}_n = \frac{\bar{P}_0}{(\Gamma_c \Delta t)^n} \prod_{k=1}^{n} \left(\frac{\beta_{k-1}}{k} \right) \qquad (2.21)$$

The series is well convergent. By normalizing the series we can find $\bar{P}_0$ and then all the $\bar{P}_n$'s. Once all $\bar{P}_n$'s are known, the averaged photon number can be calculated using

$$\langle n \rangle = \sum_{k=1}^{\infty} k \bar{P}_k \qquad (2.22)$$

The averaged number of atoms in the cavity mode is simply

$$\langle N_{atom} \rangle = t_{int} \Delta t \qquad (2.23)$$

Interpretation of the Result

Let's consider a special case in which $\bar{P}_k$ distribution is peaked at $k = m$. We assume that m is much larger than one so that the fractional change of the distribution when

k changes by unity near m is quite small,

$$\left|\bar{P}_m - \bar{P}_{m-1}\right| \ll \bar{P}_m \tag{2.24}$$

or

$$\begin{aligned} 1 &\approx \frac{\bar{P}_m}{\bar{P}_{m-1}} \\ &= \frac{\Gamma_c \Delta t n_b m + \beta_{m-1}}{\Gamma_c \Delta t (n_b + 1) m} \end{aligned}$$

so that

$$\langle n \rangle \approx m \approx \frac{1}{\Gamma_c \Delta t} \beta_{m-1} \tag{2.25}$$

We can cast this equation in the form of a rate equation

$$\frac{1}{\Delta t} \beta_{\langle n \rangle - 1} - \Gamma_c \langle n \rangle \approx 0 = \frac{d \langle n \rangle}{dt} \tag{2.26}$$

Note that $\frac{1}{\Delta t}$ is the injection rate of the excited atoms. The $\beta_{\langle n \rangle - 1}$ can be thought as the probability of having the atom have undergone the transition from the excited state to the ground state at the end of the passage in the presence of $(\langle n \rangle - 1)$ photons already in the cavity. Such transition will increase the photon number from $(\langle n \rangle - 1)$ to $\langle n \rangle$. Hence the the first term in Eq.2.26 can be thought as the number of energy quanta transferred to the field mode per unit time, and the second term as the number of energy quanta lost by the cavity leakage per unit time.

Note that Eq.2.26 resembles the heuristic rate equation derived in Sec.1.4, Eq.1.7. In deriving Eq.1.7, in fact, we assume that any injected excited atom dumps a photon to the cavity with 100 % probability. The quantum theory tells that this is not the case: the atom have certain probability of emitting a photon and the probability has to be determined by the Rabi dynamics between the atom and the field. The rate equation interpretations, however, are valid only when $\langle n \rangle$ is much larger than unity (i.e., classical limit).

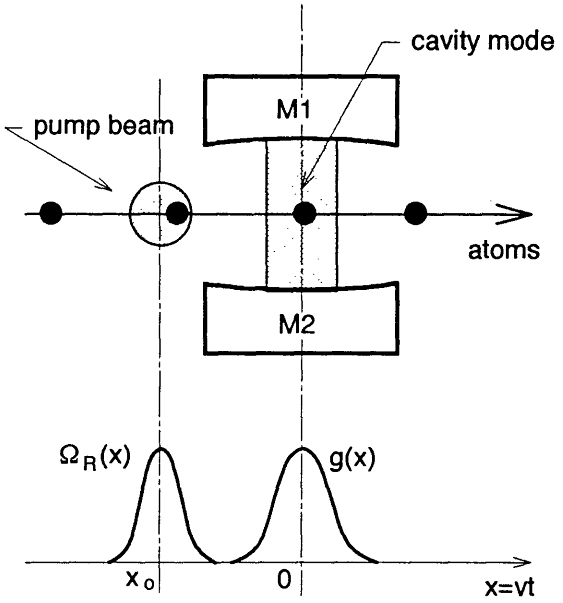

Figure 2-2: The pump beam located at $x = x_o$ is a gaussian beam with a waist of w_p. The center of the cavity is located at $x = 0$.

2.1.2 π-pulse pumping

In the microlaser, i.e., the one-atom laser, two-level atoms are inverted by a pump laser before they enter the cavity. This pump laser is a CW laser with a certain waist, intersecting the atomic beam perpendicularly.

The frequency of the pump laser is tuned to the atomic transition. If the atoms have the same velocity v, by adjusting the intensity and the beam waist of the pump, the atoms can be excited to the excited state completely (i.e., inverted) when they exit the pump beam. To see how this pumping process works, assume that a gaussian laser beam is located at $x = x_p (< 0)$ and the center of the cavity is located at $x = 0$ as shown in Figure 2-2. We also assume that the two-level atoms are traveling from $x = -\infty$ to $+\infty$. We also assume that the waist of the pump beam is so small that both the spontaneous emission and the cavity damping are neglected while an atom is traversing the pump beam.

$$\Gamma_a, \Gamma_c \ll \frac{v}{2w_p} \tag{2.27}$$

The Schrödinger equations for the probability amplitudes in the slowly varying envelope approximation are

$$\dot{C}_b = \frac{i}{2}\Omega_R(t)C_a \tag{2.28}$$

$$\dot{C}_a = -\frac{i}{2}\Omega_R(t)C_b \tag{2.29}$$

where C_a and C_b are the probability amplitudes of level a (excited state) and level b (ground state), respectively, and $\Omega_R(t)$ is the Rabi frequency associated with the pump laser given by

$$\Omega_R(t) = \Omega_R^o \exp - \left(\frac{x - x_p}{w_p}\right)^2 \Bigg|_{x=vt} \tag{2.30}$$

In writing the equations we neglected the atomic and the cavity damping. The solution of the coupled equations is

$$C_a(t) = i \sin\left(\frac{1}{2}\int_{-\infty}^{t} \Omega_R(t')dt'\right) \tag{2.31}$$

$$C_b(t) = \cos\left(\frac{1}{2}\int_{-\infty}^{t} \Omega_R(t')dt'\right) \tag{2.32}$$

assuming the atom of interest is in the ground state (level a) at $x = -\infty$ (or $t = -\infty$). Then the probability of finding the atom in the excited state is

$$\begin{aligned}
|C_a(t)|^2 &= \sin^2\left(\frac{1}{2}\int_{-\infty}^{t} \Omega_R(t')dt'\right) \\
&= \sin^2\left(\frac{\Omega_R^o}{2}\int_{-\infty}^{t} \exp - \left(\frac{vt' - x_p}{w_p}\right)^2 dt'\right) \\
&= \sin^2\left(\frac{\Omega_R^o w_p}{2v}\int_{-\infty}^{\frac{vt}{w_p}} \exp - \left(q - \frac{x_p}{w_p}\right)^2 dq\right) \qquad (2.33)
\end{aligned}$$

For $t >> \frac{w_p}{v}$, i.e., far from the pump region, the probability is simplified to

$$\begin{aligned}
|C_a(t)|^2 &\simeq \sin^2\left(\frac{\Omega_R^o w_p}{2v}\int_{-\infty}^{\infty} \exp - \left(q - \frac{x_p}{w_p}\right)^2 dq\right) \\
&= \sin^2\left(\frac{\Omega_R^o w_p}{2v}\sqrt{\pi}\right) \qquad (2.34)
\end{aligned}$$

Then a complete excitation occurs if

$$\frac{\sqrt{\pi}\Omega_R^o w_p}{v} = \pi \tag{2.35}$$

or

$$\Omega_R^o = \Omega_R^\pi \equiv \frac{\sqrt{\pi} v}{w_p} \tag{2.36}$$

In the one-atom laser experiments, an effusive atomic beam is used. Then we have to perform an averaging over the velocity distribution of the atomic beam.

$$\begin{aligned} |C_a(t)|^2 &\Rightarrow dv f_B(v) \sin^2\left(\frac{\sqrt{\pi}\Omega_R^o w_p}{2v}\right) \\ &= dv f_B(v) \sin^2\left[\frac{\pi}{2}\left(\frac{u}{v}\right)\left(\frac{\Omega_R^o}{\Omega_{R,th}^\pi}\right)\right] \end{aligned} \tag{2.37}$$

where $f_B(v)$ is the Maxwell-Boltzmann velocity distribution for the atomic beam, given by

$$f_B(v)dv = \frac{4}{\sqrt{\pi}}\left(\frac{v}{u}\right)^2 e^{-\left(\frac{v}{u}\right)^2} d\left(\frac{v}{u}\right) \tag{2.38}$$

and $\Omega_{R,th}^\pi$ is defined for u, a mean thermal velocity,

$$\Omega_{R,th}^\pi \equiv \frac{\sqrt{\pi} u}{w_p} \tag{2.39}$$

$$u \equiv \sqrt{\frac{2k_B T}{M}} \tag{2.40}$$

where k_B is the Boltzmann constant, T is the absolute temperature of the atomic beam source and M is the mass of the atom.

2.1.3 New Photon Recursion Relation

An atom can be perfectly excited to the excited state, and consequently the induced dipole moment vanishes only when the condition for the π-pulse excitation is satisfied. The condition, however, cannot be satisfied for all the atoms in the effusive beam because the velocities of the atoms are not the same.

Since the atoms are not completely excited, unexcited atoms will absorb the photons from the cavity field, and, therefore, the photon distribution is influenced. There are also effects due to the coherence in the atomic state [48] if the atoms are not completely inverted. In fact, the micromaser theory, which considers only the diagonal elements of the field density operator, simply cannot fit our experimental data in Chapter 3. Therefore, a new photon recursion relation including the off-diagonal elements of the density operator for the cavity field needs to be derived. Only when the atoms are prepared in a pure population state, this relation reduces to Eq.2.7. When the atoms are prepared in a superposition state, the off-diagonal elements are as important as the diagonal elements. This is illustrated in Figure 2-3. In Chapter 3, it will be shown that the prediction based on Eq.2.21 cannot fit our data whereas the new recursion relation successfully fits the data (Fig. 3-42).

derivation of the recursion relation

Let's consider a system of a two-level atom and a single field mode with a total of $(n+1)$ energy quanta in the system. The wavefunction is a superposition of two possible amplitudes,

$$|\Psi(t)\rangle = \{c_{a,n}(t)|a,n\rangle + c_{b,n+1}(t)|b,n+1\rangle\} \; e^{-i\omega(n+1/2)t} \tag{2.41}$$

where $|a,n\rangle$ represents a state in which the atom is in the excited state (state a) and the field is in n-photon state, and $|b,n+1\rangle$ represents a state in which the atom is in the ground state (state b) and the field is in $(n+1)$-photon state. The Schrödinger equation is

$$i\hbar|\dot{\Psi}\rangle = H|\Psi\rangle = \hbar\left[\tfrac{1}{2}\omega_a S_z + \omega a^\dagger a + g\left(aS_+ + a^\dagger S_-\right)\right]|\Psi\rangle \tag{2.42}$$

Substituting Eq.2.41 into Eq.2.42,

$$i\hbar\left\{\left[\dot{c_{a,n}} - i\omega\left(n+\tfrac{1}{2}\right)c_{a,n}\right]|a,n\rangle + \left[\dot{c_{b,n+1}} - i\omega\left(n+\tfrac{1}{2}\right)c_{b,n+1}\right]|b,n+1\rangle\right\}$$

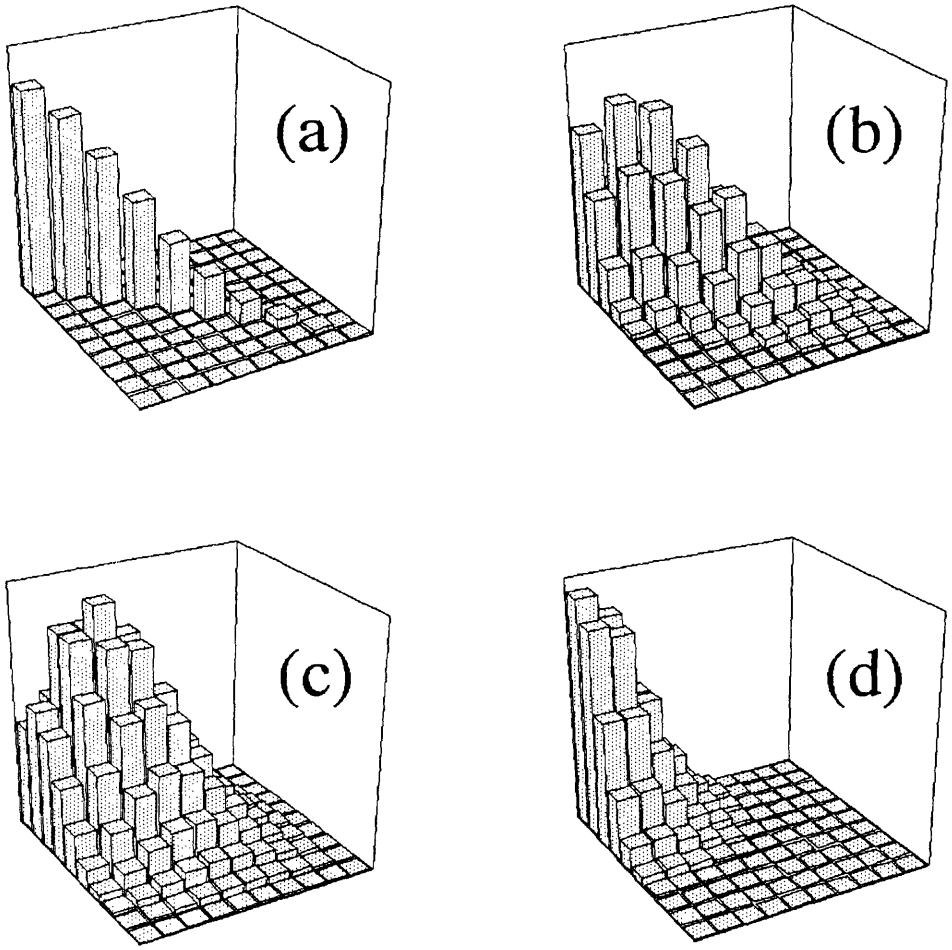

Figure 2-3: Magnitudes of the field density matrix elements, $Q_{n,m}$, which is defined in Eq. 2.75 for various initial atom states prepared by a pump beam with pulse area of (a)π, (b)$\frac{7}{8}\pi$, (c)$\frac{2}{3}\pi$, and (d)$\frac{1}{3}\pi$. The pump pulse area is the argument of the sine function in Eq.2.34. The left upper corner corresponds to $Q_{0,0}$ and the right lower corner $Q_{9,9}$. Only (a) corresponds to a pure population state. The others correspond to coherent superposition states. Parameter values used in these plots are listed in page 56.

$$
\begin{aligned}
= \;& \hbar\left[\tfrac{1}{2}\omega_a + \omega n\right] c_{a,n}|a,n\,\rangle \;+ \hbar\left[-\tfrac{1}{2}\omega_a + \omega(n+1)\right] c_{b,n+1}|b,n+1\,\rangle \\
& +\hbar g\left[\sqrt{n+1}\,c_{a,n}|b,n+1\,\rangle \;+ \sqrt{n+1}\,c_{b,n+1}|a,n\,\rangle\,\right]
\end{aligned}
\tag{2.43}
$$

Applying $\langle a,n\,|$ or $\langle b,n+1\,|$ to both side, we obtain

$$\dot{c}_{a,n} - \frac{i}{2}\Delta c_{a,n} = -ig\sqrt{n+1}\,c_{b,n+1} \tag{2.44}$$

$$\dot{c}_{b,n+1} + \frac{i}{2}\Delta c_{b,n+1} = -ig\sqrt{n+1}\,c_{a,n} \tag{2.45}$$

These coupled equations have an exact solution.

$$c_{a,n}(t) = c^o_{a,n}C_n(t) - i\left(\kappa_n c^o_{b,n+1} - \delta_n c^o_{a,n}\right)S_n(t) \tag{2.46}$$

$$c_{b,n+1}(t) = c^o_{b,n+1}C_n(t) - i\left(\kappa_n c^o_{a,n} + \delta_n c^o_{b,n+1}\right)S_n(t) \tag{2.47}$$

where

$$c^o_{a,n} \equiv c_{a,n}(0) \equiv c_a\gamma_n \tag{2.48}$$

$$c^o_{b,n+1} \equiv c_{b,n+1}(0) \equiv c_b\gamma_{n+1} \tag{2.49}$$

$$\kappa_n \equiv \frac{g\sqrt{n+1}}{\sqrt{g^2(n+1)+(\Delta/2)^2}} \tag{2.50}$$

$$\delta_n \equiv \frac{\Delta/2}{\sqrt{g^2(n+1)+(\Delta/2)^2}} \tag{2.51}$$

$$C_n(t) \equiv \cos\left[\sqrt{g^2(n+1)+(\Delta/2)^2}\,t\right] \tag{2.52}$$

$$S_n(t) \equiv \sin\left[\sqrt{g^2(n+1)+(\Delta/2)^2}\,t\right] \tag{2.53}$$

In general, $|\Psi\,\rangle$ is a linear combination all possible such states,

$$|\Psi\,\rangle = \sum_{n=0}^{\infty}\left[c_{a,n}|a,n\,\rangle + c_{b,n+1}|b,n+1\,\rangle\,\right]\,e^{-i\omega(n+1/2)t} + c_{b,0}|b,0\,\rangle\; e^{i\omega t/2} \tag{2.54}$$

which reduces to coupled equations same as Eqs.2.44 and 2.45 for $n = 0, 1, 2\ldots$, and

$$\dot{c_{b,0}} = 0 \quad \text{or} \quad c_{b,0} = \text{const} \tag{2.55}$$

Hence the solution is the same as Eqs.2.46 and 2.47 for every $n \geq 0$.

The density operator for the field, ρ_f, which is the projection of the density operator ρ into the field space, is

$$\rho_f = \mathrm{Tr}_{\mathbf{atom}}\left[\rho\right] = \langle a\,|\Psi\rangle\,\langle\Psi\,|a\rangle + \langle b\,|\Psi\rangle\,\langle\Psi\,|b\rangle \tag{2.56}$$

The slow-varying envelopes of the matrix elements of ρ_f are

$$\begin{aligned} \rho^F_{n,m}(t) &\equiv \langle n\,|\rho_f(t)|\,m\rangle\ \mathrm{e}^{i\omega(n-m)t} \\ &= \left[\langle a,n\,|\Psi(t)\rangle\,\langle\Psi(t)\,|a,m\rangle + \langle b,n\,|\Psi(t)\rangle\,\langle\Psi(t)\,|b,m\rangle\right]\ \mathrm{e}^{i\omega(n-m)t} \\ &= c_{a,n}(t)c^*_{a,m}(t) + c_{b,n}(t)c^*_{b,m}(t) \end{aligned} \tag{2.57}$$

Using Eqs.2.46 and 2.47,

$$\begin{aligned} &\rho^F_{n,m}(t) \\ &\quad = \left[c_a\gamma_n C_n(t) - i(\kappa_n c_b\gamma_{n+1} - \delta_n c_a\gamma_n)S_n(t)\right]\left[c^*_a\gamma^*_m C_m(t) + i(\kappa_m c^*_b\gamma^*_{m+1} - \delta_m c^*_a\gamma^*_m)S_m(t)\right] \\ &\qquad + \left[c_b\gamma_n C_{n-1}(t) - i(\kappa_{n-1}c_a\gamma_{n-1} + \delta_{n-1}c_b\gamma_n)S_{n-1}(t)\right] \\ &\qquad\qquad \times\left[c^*_b\gamma^*_m C_{m-1}(t) + i(\kappa_{m-1}c^*_a\gamma^*_{m-1} + \delta_{m-1}c^*_b\gamma^*_m)S_{m-1}(t)\right] \end{aligned} \tag{2.58}$$

Noting that

$$\begin{aligned} \rho^F_{n,m}(0) &= c_{a,n}(0)c^*_{a,m} + c_{b,n}(0)c^*_{b,m}(0) \\ &= |c_a|^2\gamma_n\gamma^*_m + |c_b|^2\gamma_n\gamma^*_m = \gamma_n\gamma^*_m \end{aligned} \tag{2.59}$$

and defining

$$\begin{aligned}
\rho^A_{xy} &\equiv c_x c^*_y, \quad x, y = a, b && (2.60)\\
S^\delta{}_k(t) &\equiv \delta_k S_k(t) = \frac{\Delta/2}{\sqrt{g^2(k+1)+(\Delta/2)^2}} \sin\left[\sqrt{g^2(k+1)+(\Delta/2)^2}\, t\right] && (2.61)\\
S^\kappa{}_k(t) &\equiv \kappa_k S_k(t) = \frac{g\sqrt{k+1}}{\sqrt{g^2(k+1)+(\Delta/2)^2}} \sin\left[\sqrt{g^2(k+1)+(\Delta/2)^2}\, t\right] && (2.62)
\end{aligned}$$

we obtain

$$\begin{aligned}
&\rho^F_{n,m}(t)\\
&= \rho^F_{n,m}(0)\Big\{\rho^A_{aa}\left[C_n(t)C_m(t) + S^\delta{}_n(t)S^\delta{}_m(t) - i\left(C_n(t)S^\delta{}_m(t) - C_m(t)S^\delta{}_n(t)\right)\right]\\
&\quad + \rho^A_{bb}\left[C_{n-1}(t)C_{m-1}(t) + S^\delta{}_{n-1}(t)S^\delta{}_{m-1}(t) + i\left(C_{n-1}(t)S^\delta{}_{m-1}(t) - C_{m-1}(t)S^\delta{}_{n-1}(t)\right)\right]\Big\}\\
&\quad + \rho^F_{n+1,m+1}(0)\rho^A_{bb}S^\kappa{}_n(t)S^\kappa{}_m(t) + \rho^F_{n-1,m-1}(0)\rho^A_{aa}S^\kappa{}_{n-1}(t)S^\kappa{}_{m-1}(t)\\
&\quad + i\rho^F_{n,m+1}(0)\rho^A_{ab}\left(C_n(t) + iS^\delta{}_n(t)\right)S^\kappa{}_m(t) - i\rho^F_{n+1,m}(0)\rho^A_{ba}S^\kappa{}_n(t)\left(C_m(t) - iS^\delta{}_m(t)\right)\\
&\quad + i\rho^F_{n,m-1}(0)\rho^A_{ba}\left(C_{n-1}(t) - iS^\delta{}_{n-1}(t)\right)S^\kappa{}_{m-1}(t)\\
&\quad - i\rho^F_{n-1,m}(0)\rho^A_{ab}S^\kappa{}_{n-1}(t)\left(C_{m-1}(t) + iS^\delta{}_{m-1}(t)\right) \qquad (2.63)
\end{aligned}$$

The above solution can be applied to our one-atom laser. When the atom is traversing the cavity mode, we can neglect the atomic and the cavity damping since we assume

$$\Gamma_a, \Gamma_c \ll \frac{1}{\Delta t} \qquad (2.64)$$

Hence Eq.2.63 describe the evolution of the system for $0 < t < t_{int}$. When no atom is present in the mode, on the other hand, the field simply decays according to Eq.2.65. In terms of the matrix elements, this equation is

$$\dot{\rho^F_{n,m}} = \Gamma_c\left[\sqrt{(n+1)(m+1)}\rho^F_{n+1,m+1} - \tfrac{1}{2}(n+m)\rho^F_{n,m}\right] \qquad (2.65)$$

In writing this, we set $n_b = 0$.

Eqs.2.63 and 2.65 describe the one-atom laser for all cases. We can derive the results for the micromaser in Sec. 2.1.1 as a special case. Suppose we turn on the

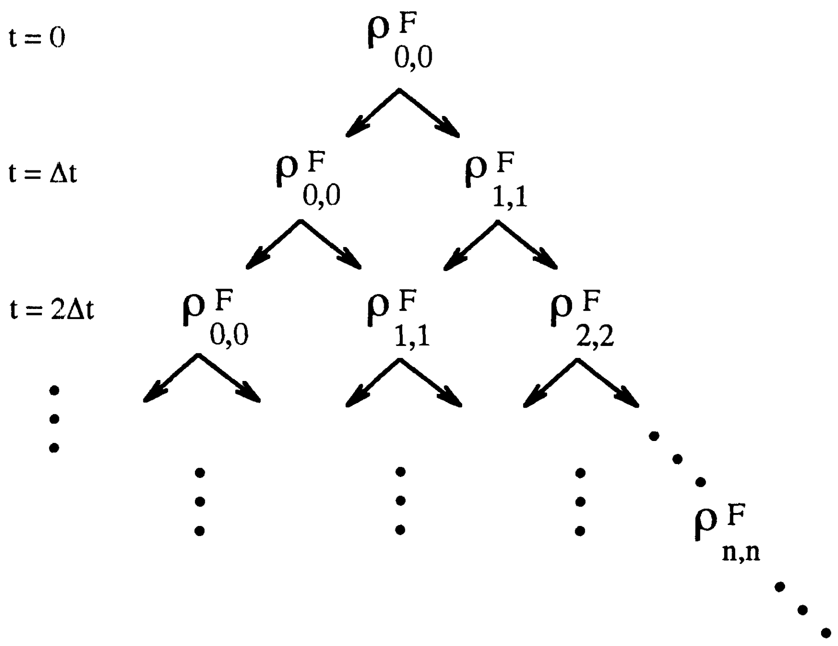

Figure 2-4: Evolution of nonzero components of $\rho^F_{n,m}$ when the atoms are prepared in the excited state perfectly. Only the diagonal matrix elements are excited.

system at $t = 0$, and the incoming atoms are perfectly excited.

$$\begin{aligned}\rho^F_{0,0}(0) &= 1\ (\text{vacuum}),\ \ \rho^F_{n,m}(0) = 0\ \ \text{otherwise} && (2.66)\\ \rho^A_{aa} &= 1,\ \ \rho^A_{bb} = \rho^A_{ab} = 0\ \ \text{at}\ t = 0 && (2.67)\end{aligned}$$

Then Eq.2.63 reduces to

$$\begin{aligned}\rho^F_{n,m}(t_{int}) &= \rho^F_{n,m}(0)\left[C_n(t)C_m(t) + S^{\delta}{}_n(t)S^{\delta}{}_m(t) - i\left(C_n(t)S^{\delta}{}_m(t) - C_m(t)S^{\delta}{}_n(t)\right)\right]\\ &\quad + \rho^F_{n-1,m-1}(0)S^{\kappa}{}_{n-1}(t)S^{\kappa}{}_{m-1}(t) && (2.68)\end{aligned}$$

Note that the (n,m)-th element is only connected to the (n-1,m-1)-th element and itself. Hence, when the first atom is exiting the cavity mode ($t = \Delta t$), $\rho^F_{1,1}$ and $\rho^F_{0,0}$ are the only nonzero elements. Before the next atom comes in, these matrix elements decay according to Eq.2.65. The interaction with the following atoms will generate more nonzero matrix elements, but however they are all diagonal elements as depicted in Figure 2-4. The growth of the number of nonzero diagonal elements will eventually taper off due the field decay, resulting in a steady state solution.

Eqs.2.68 and 2.65 together reduce to the recursion relation of the photon distribution function in Sec.2.1.1. For diagonal elements,

$$\rho^F_{n,n}(t_{int}) = \rho^F_{n,n}(0)\left[(C_n(t))^2 + \left({S^\delta}_n(t)\right)^2\right] + \rho^F_{n-1,n-1}(0)\left({S^\kappa}_{n-1}(t)\right)^2 \tag{2.69}$$

Noting that

$$\begin{align}
\rho^F_{n,n} &= \langle n\,|\rho_f|\,n\rangle \equiv P_n \tag{2.70}\\
{S^\kappa}^2_n(t_{int}) &= \frac{(n+1)g^2}{(n+1)g^2 + (\Delta/2)^2}\sin^2\left[\sqrt{(\Delta/2)^2 + (n+1)g^2}\;t_{int}\right] \notag\\
&\equiv \beta_n \tag{2.71}\\
\left({S^\delta}_n\right)^2 + \left({S^\kappa}_n\right)^2 &= S^2_n\,, \tag{2.72}
\end{align}$$

we find

$$\begin{align}
P_n(t_{int}) &= P_n(0)\left[C^2_n + \left({S^\delta}_n\right)^2\right] + P_{n-1}(0)\left({S^\kappa}_{n-1}\right)^2 \notag\\
&= P_n(0)\left[1 - \left({S^\kappa}_n\right)^2\right] + P_{n-1}(0)\left({S^\kappa}_{n-1}\right)^2 \notag\\
&= P_n(0)\left[1 - \beta_n(t_{int})\right] + P_{n-1}(0)\beta_{n-1}(t_{int}) \tag{2.73}
\end{align}$$

which is exactly Eq.2.7.

Now we derive a recursion relation in general case. From Eqs.2.15,

$$\overline{\rho_f(t_i)}\,|_{SS} - \Delta t\,\overline{\dot{\rho}_f(t_i)}\,|_{SS} = \overline{\rho_f(t_i + t_{int})}\,|_{SS} \tag{2.74}$$

Define

$$Q_{n,m} \equiv \langle n\,|\rho_{f,SS}|\,m\rangle = \overline{\rho^F_{n,m}}\,|_{SS} \tag{2.75}$$

Then using Eq.2.65, Eq.2.74 can be rewritten as

$$Q_{n,m}(0) - \Gamma_c\Delta t\left[\sqrt{(n+1)(m+1)}\,Q_{n+1,m+1}(0) - \tfrac{1}{2}(n+m)Q_{n,m}(0)\right] = Q_{n,m}(t_{int}) \tag{2.76}$$

which reduces to a recursion relation

$$\begin{aligned}
&Q_{n,m} - \Gamma_c \Delta t \left[\sqrt{(n+1)(m+1)}\, Q_{n+1,m+1} - \tfrac{1}{2}(n+m) Q_{n,m}\right] \\
&= \; Q_{n,m} \left\{ \rho^A_{aa} \left[C_n C_m + {S^{\delta}}_n {S^{\delta}}_m - i \left(C_n {S^{\delta}}_m - C_m {S^{\delta}}_n \right) \right] \right. \\
&\qquad \left. + \; \rho^A_{bb} \left[C_{n-1} C_{m-1} + {S^{\delta}}_{n-1} {S^{\delta}}_{m-1} + i \left(C_{n-1} {S^{\delta}}_{m-1} - C_{m-1} {S^{\delta}}_{n-1} \right) \right] \right\} \\
&\qquad + Q_{n+1,m+1} \rho^A_{bb} {S^{\kappa}}_n {S^{\kappa}}_m + Q_{n-1,m-1} \rho^A_{aa} {S^{\kappa}}_{n-1} {S^{\kappa}}_{m-1} \\
&\qquad + i Q_{n,m+1} \rho^A_{ab} \left(C_n + i {S^{\delta}}_n \right) {S^{\kappa}}_m - i Q_{n+1,m} \rho^A_{ba} {S^{\kappa}}_n \left(C_m - i {S^{\delta}}_m \right) \\
&\qquad + i Q_{n,m-1} \rho^A_{ba} \left(C_{n-1} - i {S^{\delta}}_{n-1} \right) {S^{\kappa}}_{m-1} - i Q_{n-1,m} \rho^A_{ab} {S^{\kappa}}_{n-1} \left(C_{m-1} + i {S^{\delta}}_{m-1} \right)
\end{aligned} \tag{2.77}$$

where $C_n, {S^{\kappa}}_n$ and ${S^{\delta}}_n$ are evaluated at $t = t_{int}$,

$$C_n \equiv C_n(t_{int}), \text{etc} \tag{2.78}$$

Noting that

$$c_a \; = \; i \sin\left(\frac{\sqrt{\pi}\,\Omega^o_R w_p}{2v} \right) = i\sqrt{\rho^A_{aa}} \tag{2.79}$$

$$c_b \; = \; \cos\left(\frac{\sqrt{\pi}\,\Omega^o_R w_p}{2v} \right) = \sqrt{\rho^A_{bb}} \tag{2.80}$$

$$\rho^A_{ba} \; = \; c_b c_a^* = -i\sqrt{\rho^A_{aa}\rho^A_{bb}} = \left(\rho^A_{ab}\right)^* \tag{2.81}$$

we can rewrite the recursion relation as

$$\begin{aligned}
&\left[1 + \tfrac{1}{2}\Gamma_c \Delta t (n+m)\right] Q_{n,m} \\
&= \; Q_{n,m} \left\{ \rho^A_{aa} \left[C_n C_m + {S^{\delta}}_n {S^{\delta}}_m - i \left(C_n {S^{\delta}}_m - C_m {S^{\delta}}_n \right) \right] \right. \\
&\qquad\qquad \left. (1 - \rho^A_{aa}) \left[C_{n-1} C_{m-1} + {S^{\delta}}_{n-1} {S^{\delta}}_{m-1} + i \left(C_{n-1} {S^{\delta}}_{m-1} - C_{m-1} {S^{\delta}}_{n-1} \right) \right] \right\} \\
&\quad + Q_{n+1,m+1} \left[(1 - \rho^A_{aa}) {S^{\kappa}}_n {S^{\kappa}}_m + \Gamma_c \Delta t \sqrt{(n+1)(m+1)} \right] \\
&\quad + Q_{n-1,m-1} \rho^A_{aa} {S^{\kappa}}_{n-1} {S^{\kappa}}_{m-1} \\
&\quad + \sqrt{\rho^A_{aa}(1 - \rho^A_{aa})} \left[Q_{n,m-1} \left(C_{n-1} - i {S^{\delta}}_{n-1} \right) {S^{\kappa}}_{m-1} + Q_{n-1,m} {S^{\kappa}}_{n-1} \left(C_{m-1} + i {S^{\delta}}_{m-1} \right) \right.
\end{aligned}$$

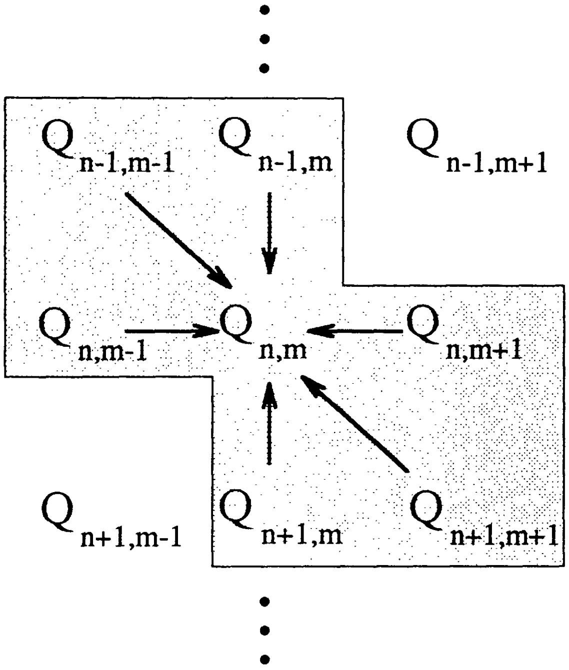

Figure 2-5: Connection between $Q_{n,m}$ and its neighbors.

$$- Q_{n,m+1}\left(C_n + iS^{\delta}{}_n\right) S^{\kappa}{}_m - Q_{n+1,m} S^{\kappa}{}_n \left(C_m - iS^{\delta}{}_m\right)\Big] \tag{2.82}$$

Note that $Q_{n,m}$ is related with its nearest neighbors except $Q_{n-1,m+1}$ and $Q_{n+1,m-1}$, as shown in Figure 2-5. When the atoms are prepared in a superposition state, even if we start from a vacuum state($Q_{0,0} = 1$), eventually all the matrix elements are excited. Suppose we turn on the system at $t = 0$. Just after the first atom-field iteration, not only $Q_{1,1}$ and $Q_{0,0}$, but also $Q_{1,0}$ and $Q_{0,1}$ components become nonzero according to Eq.2.82. The interaction with the second atom will excite any $Q_{n,m}$ with $n, m = 0, 1, 2$. In general all the $Q_{n,m}$ components with $n, m = 0, 1, \ldots, k$ will be excited after the interaction with the k-th atom, as shown in Figure 2-6. This growth eventually taper off due to the cavity decay.

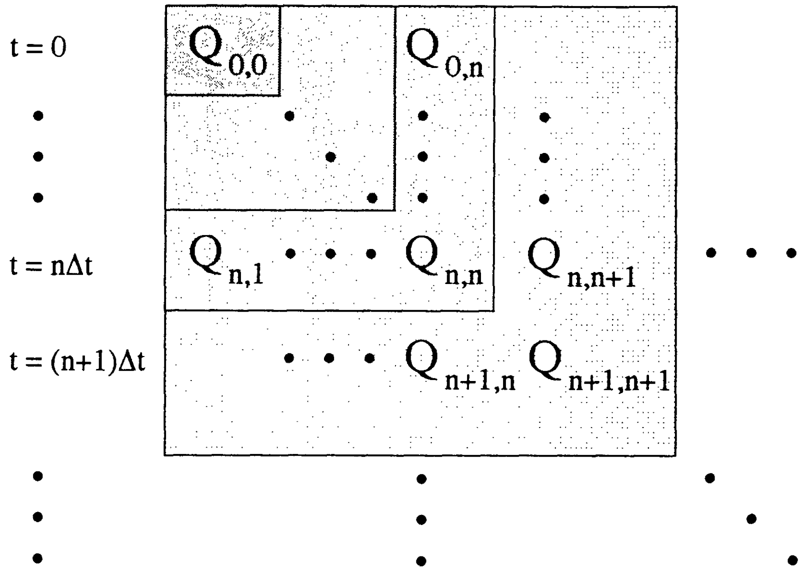

Figure 2-6: Time evolution of $Q_{n,m}$. After the interaction with the k-th atom, any $Q_{n,m}$ elements with $(n, m = 0, 1, \ldots, k)$ are excited.

2.1.4 Standing-Wave Cavity Mode

So far we assume that the coupling constant is uniform inside the cavity. This is a reasonable assumption for the micromaser, where a low-order standing-wave mode of the cavity is excited. A low order means that a few integer multiples of a half wavelength (of a few cm) of the field fits in the cavity. Hence it is relatively easy to align the atomic beam along the antinode of the cavity mode, ensuring that all the atoms have the same coupling constant.

In the one-atom laser, on the other hand, a cavity with high-order standing-wave modes is used. Typically 10^3–10^4 wavelengths fit in the cavity. Since the diameter of the atomic beam is typically much larger than the wavelength, the atom-field coupling constant varies sinusoidally over the beam dimension. In addition, since the cavity mode has a gaussian field distribution in the transverse directions, the coupling constant also varies accordingly. Therefore, the coupling constant g appearing in Eq.2.63 via the definitions of C_n, $S^{\kappa}{}_n$ and $S^{\delta}{}_n$ has to be replaced with a coupling constant $g(\vec{r})$ as a function of the position of an atom of interest.

$$g(\vec{r}) = g_o \exp\left[-\frac{x^2+y^2}{w_m^2}\right] \cos kz \ , \tag{2.83}$$

where g_o is given by

$$g_o = \frac{\mu}{\hbar}\sqrt{\frac{2\pi\hbar\omega}{V_m}} \ , \tag{2.84}$$

w_m is the waist of the cavity mode, and *coskz* accounts for the standing-wave nature of the cavity mode. One thing that should be noted here is that although the coupling constant as defined above can be negative, the sinusoidal functions in the definitions of C_n, $S^{\kappa}{}_n$ and $S^{\delta}{}_n$ have $g^2(\vec{r})$ in their arguments so that the negativeness of the coupling constant makes no difference as far as the Rabi oscillation is concerned.

One may think the position dependence of the coupling constant can be taken into account by simply averaging the final results, the recursion relation, over the distributions of y and z. This averaging scheme would be correct only if the interaction between an atom and the field is completely independent from the interactions between the preceding atoms and the field. However, one event of the atom-field interaction is not independent from the preceding events. The cavity field, which is the result of all the preceding events, does not decay appreciably when the next atom comes in so that the new atom-field interaction is influenced.

In order to show that the post-averaging scheme is wrong, let's consider two infinitely narrow atomic beams going through the field mode at $y = 0$ for both. One beam is going through the field mode at a node ($\cos^2 kz = 0$) and the other is at an anti-node ($\cos^2 kz = 1$) of the mode. The atoms at the node have zero coupling to the cavity field. Therefore, they traverse the cavity as if there were no cavity at all. Contrarily, the atoms at the anti-node interact with the field with a full magnitude of the coupling constant, g_o.

Now recall that the mean time interval between two atoms is defined for the entire atomic beam, i.e., the two atomic beams as a whole. Therefore, the mean time interval only for the atomic beam along the anti-node should be exactly twice of the mean time interval for the whole set of beams. These two beam configuration, therefore, should give rise to the same result as the single atomic beam traversing the cavity along an anti-node with a mean time interval twice as large as the original interval.

The averaging scheme, however, gives a quite different result, which is just an average of two possible configurations: all the atoms traveling either along the anti-node or the node, with the original mean time interval. Since the atomic beam traveling along the node gives nothing, the solution by the averaging scheme is the half of the result that would be obtained with one atomic beam with the original time interval. Because the performance of the one-atom laser does not linearly depend on the time interval, the result by the averaging scheme is incorrect.

The lowest order correction needed in the theory in order to account for the standing-wave mode is to assume that the half of the atoms are located along the nodes of the cavity and the remaining half of them are located along the anti-nodes. Then only the atoms located along the anti-node will interact with the cavity field while the others are just passing by. This assumption is equivalent to count only the half of the atoms in the cavity. In fact, there is another factor of two reduction in the number of atoms due to the gaussian transverse profile of the cavity mode (see next two pages.). Therefore, only a fourth of the number of atoms in the apparent volume of the cavity are counted.

While the number of atoms in the cavity mode is something that can be measured in the experiment, the parameter used in the theory is not the number of atoms but the time interval Δt, which is proportional to the number of atoms. For the micromaser (with a low-order cavity), Eq.2.23 gives Δt in terms of the averaged number of atoms, N_{atom}. However this equation is not correct for the one-atom laser. Because of the gaussian mode profile, rather the equation should be corrected as

$$\langle N_{atom} \rangle = \left(\frac{t_{int}}{\sqrt{2}\Delta t} \right) , \qquad (2.85)$$

where $\langle N_{atom} \rangle$ is an effective mean number of atoms in the cavity, accounting for the standing wave nature and the gaussian profile of the cavity mode.

In order to show how the factor of a fourth comes out, let's consider an atomic

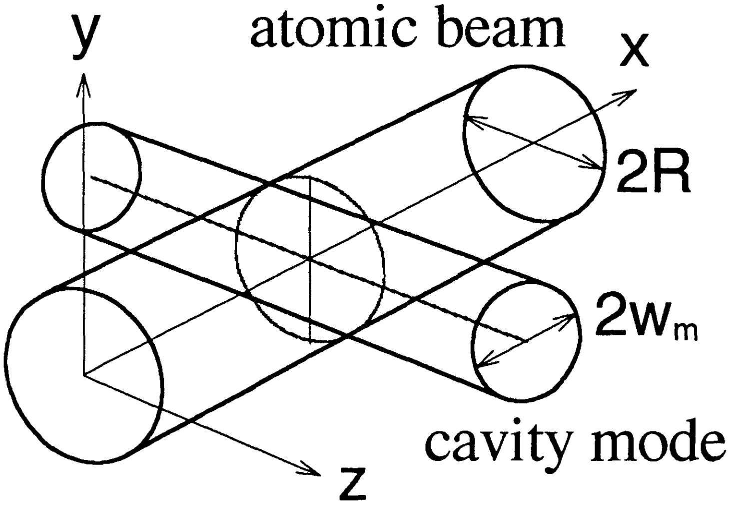

Figure 2-7: An atomic beam crossing the field mode of a high-order single-mode cavity

beam with a diameter $2R$ intersecting the cavity mode as illustrated in Fig.2-7. If $2R$ is smaller than the cavity length, then $\langle N_{atom} \rangle$ is calculated from the following integral.

$$\begin{aligned}
\langle N_{atom} \rangle &= n_o \int_{-\infty}^{+\infty} dx \int_{-R}^{R} dy \; \mathrm{e}^{-2\left(\frac{x^2+y^2}{w_m^2}\right)} \int_{-\sqrt{R^2-y^2}}^{\sqrt{R^2-y^2}} dz \cos^2 kz \\
&\cong n_o w_m \sqrt{\frac{\pi}{2}} \int_{-R}^{R} dy \; \mathrm{e}^{-\frac{2y^2}{w_m^2}} \int_{-\sqrt{R^2-y^2}}^{\sqrt{R^2-y^2}} dz \frac{1}{2} \\
&= n_o R^2 w_m \sqrt{\frac{\pi}{2}} \, R^2 \int_{-1}^{1} dq \sqrt{1-q^2} \; \mathrm{e}^{-2q^2\left(\frac{R}{w_m}\right)^2} \\
&\equiv n_o R^2 w_m \left(\frac{\pi}{2}\right)^{\frac{3}{2}} \eta\left(R/w_m\right) \; , \qquad (2.86)
\end{aligned}$$

where n_o is the density of the atomic beam, which can be measured independently in the experiment, and $\eta(x)$ is defined as

$$\eta(x) \equiv \frac{2}{\pi} \int_{-1}^{1} dq \sqrt{1-q^2} \; \mathrm{e}^{-2q^2x^2} \; . \qquad (2.87)$$

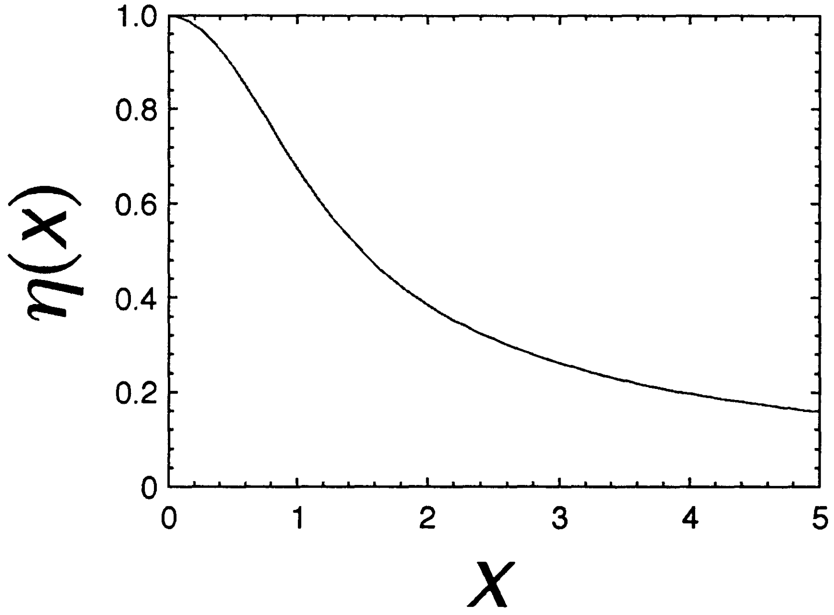

Figure 2-8: Plot of $\eta(x)$

In Figure 2-8, the function $\eta(x)$ is plotted.

The function $\eta(x)$ can be expressed in simple forms in two limiting cases. When $R \ll w_m$,

$$\eta\left(R/w_m\right) \approx \frac{2}{\pi}\int_{-1}^{1} dq\sqrt{1-q^2} = 1 \tag{2.88}$$

and when $R \gg w_m$,

$$\begin{aligned}\eta\left(R/w_m\right) &\approx \frac{2}{\pi}\int_{-1}^{1} dq\ \mathrm{e}^{-2(R/w_m)^2q^2} \\ &\approx \frac{2}{\pi}\int_{-\infty}^{\infty} dq\ \mathrm{e}^{-2(R/w_m)^2q^2} \\ &= \sqrt{\frac{2}{\pi}\frac{w_m}{R}}\ .\end{aligned} \tag{2.89}$$

Therefore,

$$\langle N_{atom}\rangle = \begin{cases} n_o\frac{1}{4}\pi R^2(2w_m)\sqrt{\frac{\pi}{2}} & \text{if } R \ll w_m \\ n_o\frac{1}{4}\pi w_m^2(2R) & \text{if } R \gg w_m\ , \end{cases} \tag{2.90}$$

We can appreciate the physical meaning of this result in the following way. When

$R \gg w_m$, we have the averaging over $cos^2 kz$ dependence as well as the averaging over the gaussian mode profile along both x and y directions. Therefore, in order to get $\langle N_{atom} \rangle$, an overall reduction factor

$$\frac{1}{2} \times \frac{1}{\sqrt{2}} \times \frac{1}{\sqrt{2}} = \frac{1}{4}.$$

has to be multiplied to the mean number of atoms in the apparent volume, which is simply $\pi w_m^2 2R$. On the other hand, if $R \ll w_m$, we do not need the averaging over y dimension so that the reduction factor is

$$\frac{1}{2} \times \frac{1}{\sqrt{2}} = \frac{1}{2\sqrt{2}} ,$$

which is multiplied to an apparent volume of $\pi R^2 \sqrt{\pi} w_m$. Note that we have $\sqrt{\pi} w_m$ instead of $2w_m$ because of the absence of the averaging over y dimension.

In a similar way, we can derive the relation between $\langle N_{atom} \rangle$ and Δt. For this let's consider an infinitely narrow atomic beam ($R \ll w_m, \lambda$) traveling along one of the anti-nodes of the cavity. We assume that the mean time interval between atoms is Δt. The density is then simply

$$n_o = \frac{1}{\pi R^2 v \Delta t} .$$

Since all the atoms are moving along the anti-node, the effective mean number of atoms in the cavity, $\langle N_{atom} \rangle$, is

$$\langle N_{atom} \rangle = n_o \frac{1}{\sqrt{2}} \pi R^2 \sqrt{\pi} w_m ,$$

without the factor of $\frac{1}{2}$. Using the expression for the density, we obtain

$$\begin{aligned} \langle N_{atom} \rangle &= \frac{1}{v \Delta t} \frac{1}{\sqrt{2}} \sqrt{\pi} w_m \\ &= \frac{\pi w_m / v}{\sqrt{2} \Delta t} . \qquad (2.91) \end{aligned}$$

With a known value of $\langle N_{atom} \rangle$, the mean time interval given by this equation is used in the recursion relation, Eq.2.82. With this simple substitution, the y and z spatial dependencies of the coupling constant is taken into account as the lowest-order approximation.

Both $g(\vec{r})$ above and $\Omega_R(t)$ in the π-pulse excitation considered in the preceding section are given by gaussian mode functions. In the π-pulse excitation, the arguments of the sine and the cosine functions was

$$\frac{\Omega_R^o}{2} \frac{\sqrt{\pi} w_m}{v} = \text{Rabi frequency} \times \text{interaction time}$$

Since both $2g_o$ and Ω_R^o are Rabi frequencies, the atom-field interaction time that we should use is

$$t_{int} \equiv \frac{\sqrt{\pi} w_m}{v} \tag{2.92}$$

By this definition, the x dependence of the coupling constant is also incorporated into the theory. Using t_{int}, we can rewrite Eq.2.91 in a simple form,

$$\Delta t = \frac{t_{int}}{\sqrt{2} \langle N_{atom} \rangle} . \tag{2.93}$$

With all these modifications described so far installed into the theory, the mean photon number $\langle n \rangle$ is calculated from

$$\langle n \rangle = \int_0^\infty dv f_B(v) \sum_{k=1}^{\infty} k Q_{k,k}(v) \tag{2.94}$$

where $Q_{k,k}(v)$ is evaluated using the algorithm described before. Note that the dependence on velocity is embedded in ρ_{aa}^A and ρ_{bb}^A as well as $S^\kappa{}_n$, $S^\delta{}_n$ and C_n.

$$\rho_{aa}^A(v) = \sin^2 \left[\frac{\pi}{2} \left(\frac{u}{v} \right) \left(\frac{\Omega_R^o}{\Omega_R^\pi} \right) \right] \quad \rho_{bb}^A(v) = 1 - \rho_{aa}^A(v) \tag{2.95}$$

2.1.5 Numerical Simulation

algorithm for solving recursion relation

In general, $Q_{n,m}$'s are complex quantities. Defining

$$Q_{n,m} \equiv p_{n,m} + iq_{n,m}, \quad p_{n,m}, q_{n,m} \text{ are real} \tag{2.96}$$

the Eq.2.82 reduces to

$$\begin{aligned}
&\left[1+\tfrac{1}{2}\Gamma_c\Delta t(n+m)\right] p_{n,m} \\
&\quad = p_{n,m}\left[\rho^A_{aa}\left(C_nC_m + S^\delta{}_n S^\delta{}_m\right) + (1-\rho^A_{aa})\left(C_{n-1}C_{m-1} + S^\delta{}_{n-1}S^\delta{}_{m-1}\right)\right] \\
&\qquad + q_{n,m}\left[\rho^A_{aa}\left(C_nS^\delta{}_m - C_mS^\delta{}_n\right) + (1-\rho^A_{aa})\left(C_{n-1}S^\delta{}_{m-1} - C_{m-1}S^\delta{}_{n-1}\right)\right] \\
&\qquad + p_{n+1,m+1}\left[(1-\rho^A_{aa})S^\kappa{}_n S^\kappa{}_m + \Gamma_c\Delta t\sqrt{(n+1)(m+1)}\right] + p_{n-1,m-1}\rho^A_{aa}S^\kappa{}_{n-1}S^\kappa{}_{m-1} \\
&\qquad + \sqrt{\rho^A_{aa}(1-\rho^A_{aa})} \\
&\qquad \left\{\left[p_{n,m-1}C_{n-1}S^\kappa{}_{m-1} + p_{n-1,m}S^\kappa{}_{n-1}C_{m-1} - p_{n,m+1}C_nS^\kappa{}_m - p_{n+1,m}S^\kappa{}_nC_m\right]\right. \\
&\qquad \left. + \left[q_{n,m-1}S^\delta{}_{n-1}S^\kappa{}_{m-1} - q_{n-1,m}S^\kappa{}_{n-1}S^\delta{}_{m-1} + q_{n,m+1}S^\delta{}_nS^\kappa{}_m - q_{n+1,m}S^\kappa{}_nS^\delta{}_m\right]\right\}
\end{aligned} \tag{2.97}$$

for real parts, and

$$\begin{aligned}
&\left[1+\tfrac{1}{2}\Gamma_c\Delta t(n+m)\right] q_{n,m} \\
&\quad = q_{n,m}\left[\rho^A_{aa}\left(C_nC_m + S^\delta{}_n S^\delta{}_m\right) + (1-\rho^A_{aa})\left(C_{n-1}C_{m-1} + S^\delta{}_{n-1}S^\delta{}_{m-1}\right)\right] \\
&\qquad + q_{n,m}\left[\rho^A_{aa}\left(C_nS^\delta{}_m - C_mS^\delta{}_n\right) + (1-\rho^A_{aa})\left(C_{n-1}S^\delta{}_{m-1} - C_{m-1}S^\delta{}_{n-1}\right)\right] \\
&\qquad + q_{n+1,m+1}\left[(1-\rho^A_{aa})S^\kappa{}_n S^\kappa{}_m + \Gamma_c\Delta t\sqrt{(n+1)(m+1)}\right] + q_{n-1,m-1}\rho^A_{aa}S^\kappa{}_{n-1}S^\kappa{}_{m-1} \\
&\qquad + \sqrt{\rho^A_{aa}(1-\rho^A_{aa})} \\
&\qquad \left\{\left[q_{n,m-1}C_{n-1}S^\kappa{}_{m-1} + q_{n-1,m}S^\kappa{}_{n-1}C_{m-1} - q_{n,m+1}C_nS^\kappa{}_m - q_{n+1,m}S^\kappa{}_nC_m\right]\right. \\
&\qquad \left. - \left[p_{n,m-1}S^\delta{}_{n-1}S^\kappa{}_{m-1} - p_{n-1,m}S^\kappa{}_{n-1}S^\delta{}_{m-1} + p_{n,m+1}S^\delta{}_nS^\kappa{}_m - p_{n+1,m}S^\kappa{}_nS^\delta{}_m\right]\right\}
\end{aligned} \tag{2.98}$$

for imaginary parts. Unfortunately, these recursion relations do not permit further simplification; no simple closed form is known. We have to rely on numerical evaluation, the algorithm of which is described here. First we start with th 0-th order approximation, corresponding to a vacuum.

$$Q^{(0)}_{n,m} = \begin{cases} 1 & \text{if } n = m = 0 \\ 0 & \text{otherwise} \end{cases} \tag{2.99}$$

Then the first order approximation is obtained using Eq.2.82, i.e., $Q^{(1)}_{n,m}$ is evaluated from $Q^{(0)}_{n\pm 1,m\pm 1}$. Then the result is renormalized.

$$Q^{(1)}_{n,m} \rightarrow \frac{Q^{(1)}_{n,m}}{\sum_{n=0}^{\infty} Q^{(1)}_{n,n}} \tag{2.100}$$

Repeat this procedure recursively until desired convergence is achieved. Practically, we set an upperbound for n and m not only because computational difficulty escalates with a larger number of matrix elements considered, but also because the mean photon number for the one-atom laser is a small number, typically of the order of one. When the upperbound is $(N-1)$, there are N^2 matrix elements to calculate. Since the diagonal elements satisfy a normalization condition

$$\sum_{n=0}^{N} Q_{n,n} = 1 \tag{2.101}$$

and since the matrix is a hermitian,

$$Q_{n,m} = Q^{*}_{m,n} \tag{2.102}$$

the number of independent matrix elements is

$$(N^2 - N)/2 + (N-1) = (N+2)(N-1)/2 \tag{2.103}$$

In our analysis of the experimental data, the upperbound was varied between 20 and 40.

computer program

The algorithm has been coded into a computer program. The program is written in C language and is listed in Appendix B. The main body of the program is `ml3_5.c`. The routines calculating $Q_{n,m}$'s are contained in `micro_Q_core5.c`. For numerical integration the program borrows routines from the library of Numerical Recipes in C [50]. The program can be compiled on many Unix operating systems such as Sun OS 4.1, A/UX 3.1 and DEC OSF 1.3.

When running the program, users can specify experimental parameters such as a finesse of $\mathcal{F}$, a radius of curvature of r_o, a cavity length of L, the atomic natural linewidth of Γ_a, the wavelength of the atomic transition of λ, the thermal velocity of u and the mean number of atoms in the cavity of $\langle N_{atom} \rangle$ through the standard input, `stdin`. From these parameters the following parameters are derived in the program.

`z0` =	$z_o = \sqrt{\frac{r_o L}{2}}$,	confocal parameter
`w0` =	$w_m = \sqrt{\frac{\lambda z_o}{\pi}}$,	cavity field mode waist
`fsr` =	$\Delta\nu_f = \frac{c}{2L}$,	free spectral range
`Gc_over_2pi` =	$\Gamma_c/2\pi = \frac{\Delta\nu_f}{\mathcal{F}}$,	cavity decay rate
`f` =	$f = \frac{3}{4}\left(\frac{\lambda}{\pi w_m}\right)^2$,	solid angle factor
`g_over_2pi` =	$g_o/2\pi = \sqrt{\frac{2}{\pi}\Delta\nu_f f \frac{\Gamma_c}{2\pi}}$,	coupling constant
`t_int` =	$t_{int} = \frac{\sqrt{\pi} w_m}{v}$,	interaction time
`R` =	$\frac{1}{\Delta t} = \sqrt{2}\frac{\langle N_{atom} \rangle_{ens}}{t_{int}}$,	atom flow rate
`Nex` =	$N_{ex} = \frac{1}{\Gamma_c \Delta t}$,	number of atoms injected per cavity decay time
`theta` =	$\theta = \sqrt{N_{ex}}\, g_o\, t_{int}$,	pulse area

The program then calculates $Q_{n,m}$'s and an average number of photons in the cavity for various velocity groups, and then it performs an averaging over all the velocities according to the Maxwell-Boltzmann velocity distribution and the result is written to the standard output, `stdout`.

Users can specify program control parameters such as the upperbound in the indices of $Q_{n,m}$ (`N_CUTOFF`), an error tolerance (`TOLERANCE`) and a maximum number of iteration (`MAX_ITERATION`) in calculating $Q_{n,m}$'s, an error tolerance in the numerical integration for the velocity averaging (`EPS`). These parameters should be contained in a parameter file (`ml3.PARA`), which is read by the program upon execution. Typical parameter values were 30 for `N_CUTOFF`, 1.0×10^{-4} for `TOLERANCE` and 1.0×10^{-3} for `EPS`. With this setting, the calculation of a single data point takes about 20 seconds on a workstation rated at 150 SPECfp92 (alpha processor running at 200 MHz, DEC 3000-500).

Results

As briefly mentioned earlier in this section, when the atoms are prepared in a superposition state of the two energy levels, the off-diagonal elements of the field density matrix are as important as the diagonal ones. Fig.2-3, illustrating this, was calculated by the computer program. The parameters used in the calculations are given below:

$$\begin{aligned} \Theta_m \equiv 2g_o t_{int} &= 1.18 \\ \Theta_p \equiv \frac{\sqrt{\pi}\Omega_R^o w_p}{v} &= \pi, \frac{7}{8}\pi, \frac{2}{3}\pi, \frac{1}{3}\pi \\ \Gamma_c \Delta t &= \frac{0.0987}{\langle N_{atom}\rangle} = \frac{0.0987}{1.0} \\ \Delta &= 0 \end{aligned} \tag{2.104}$$

The significance of the off-diagonal elements can also be seen in Figure 2-9, where $\langle n\rangle$ is plotted as a function of a pump power pulse area, Θ_p. Interestingly a maximum $\langle n\rangle$ is achieved not when the atoms are fully inverted but when they are in a superposition state. This is understandable because not only an inverted atom but also a polarized atom as a dipole can radiate coherently into a resonant field mode. When an atom is slightly under-pumped or over-pumped, ρ_{aa}^A is reduced slightly from unity while $|\rho_{ab}|$ increases significantly. Therefore overall capability of emitting a photon into the field mode can be maximized.

Extensive simulations with the modified quantum mechanical model should be performed to obtain a complete understanding of the one-atom laser. For example,

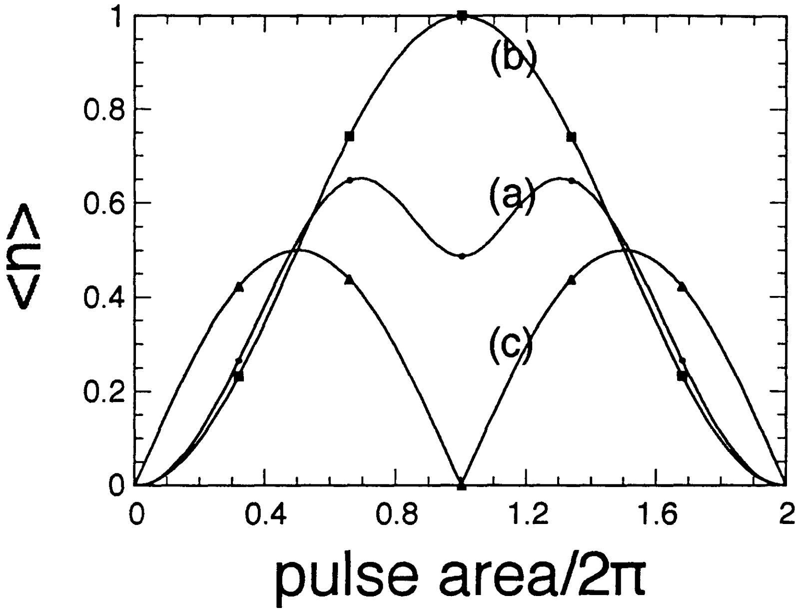

Figure 2-9: Effect of superposition state. (a)$\langle n\rangle$, (b)ρ^A_{aa}, and (c)$\left|\rho^A_{ab}\right|$.

once the field density matrix is found, the photon statistics is easily calculated. However, such extensive study is not covered in this thesis. Only a small region in the parameter space, which corresponds to our experimental conditions, has been studied. The results will be presented in Chap.3 in comparison with experimental data. More extensive studies will be covered in future publications.

2.2 Semiclassical Theory of the One-Atom Laser

2.2.1 Model

In this section, we formulate the one-atom laser based on a semiclassical formalism, in which the atom is treated quantum mechanically by the Schrödinger equation while the field is treated classically, described by the Maxwell equation. We cast the equations in terms of three variables: an induced atomic dipole moment, a population inversion and a cavity field amplitude. These physical observables are represented by properly normalized slow-varying-envelope variables. They are a for the cavity field, σ for the atomic dipole moment, and N for the population inversion. Note that we treat the atom as a two-level system. Then the Maxwell-Schrödinger equations are

$$\begin{aligned} \dot{a} + \frac{\Gamma_c}{2} a &= -g\sigma && (2.105) \\ \dot{\sigma} + \frac{\Gamma_a}{2} \sigma &= -gNa && (2.106) \\ \dot{N} + \Gamma_a(N+1) &= 4g\sigma a \ , && (2.107) \end{aligned}$$

where

$$\begin{aligned} a &\equiv \mathcal{E} \Big/ \sqrt{\frac{8\pi\hbar\omega}{V}} = \frac{\mathcal{E}}{2E_{vac}} && (2.108) \\ \sigma &\equiv \frac{\mathcal{P}}{2i\mu} \ , && (2.109) \end{aligned}$$

where $\mathcal{E}$ and $\mathcal{P}$ are the slowly varying envelopes corresponding to the cavity field $E(t)$ and the dipole moment $P(t)$, respectively.

$$\begin{aligned} E(t) &= \mathrm{Re}\,[\mathcal{E}(t)\,\mathrm{e}^{-}i\omega t] \\ P(t) &= \mathrm{Re}\,[\mathcal{P}(t)\,\mathrm{e}^{-}i\omega t] \ . \end{aligned}$$

Note that $|a|^2$ is nothing but the number of photons in the field.

$$|a|^2 = \frac{|\mathcal{E}|^2 V}{8\pi\hbar\omega} \longrightarrow \langle n \rangle \ . \qquad (2.110)$$

The expression for the π-pulse pump beam is, as defined in Eq.2.30,

$$\Omega_R(x) = \Omega_R^o \, \mathrm{e}^{-\left(\frac{x-x_P}{w_P}\right)^2} \ ,$$

where Ω_R^o is the Rabi frequency corresponding to the pump field, w_P and x_p are the waist and the center position of the pump field, respectively.

The coupling constant g depends on the position of the atom as in Eq.2.83. As discussed before, y and z dependencies can be taken into account by an effective mean number of atoms in the mode. So for simplicity of calculation, we assume that all the atoms are located at the anti-nodes of the cavity field mode with $y = 0$.

$$g(x) = g_o \, \mathrm{e}^{-\left(\frac{x}{w_m}\right)^2},$$

assuming that the cavity center is positioned at $x = 0$. Figure 2-2 illustrates the spatial distribution of the pump beam and the cavity mode.

Now suppose atoms are traveling from $x = -\infty$ to $x = +\infty$ at a velocity of v. The mean time interval between successive atoms is Δt as introduced in Sec.2.1.1, satisfying

$$\Delta t >> \frac{w_p}{v}, \frac{w_m}{v} \, . \tag{2.111}$$

Incorporating the pump beam and the cavity mode distribution and neglecting atomic damping ($\Gamma_a \to 0$), we can rewrite the coupled equations as

$$\begin{aligned} \frac{da(t)}{dt} &= -g(t)\sigma(t) - \frac{\Gamma_c}{2} a(t) & (2.112) \\ \frac{d\sigma(t)}{dt} &= -\left(g(t)a(t) + \Omega_R(t)/2\right) N(t) & (2.113) \\ \frac{dN(t)}{dt} &= 4\left(g(t)a(t) + \Omega_R(t)/2\right) \sigma(t) \, , & (2.114) \end{aligned}$$

where

$$\begin{aligned} g(t) &= g(x)\,|_{x \to vt} = g_o \, \mathrm{e}^{-\left(\frac{vt}{w_m}\right)^2} & (2.115) \\ \Omega_R(t) &= \Omega_R(x)\Big|_{x \to vt,\, x_p \to vt_o} = \Omega_R^o \, \mathrm{e}^{-\left(\frac{v(t-t_o)}{w_P}\right)^2} \, . & (2.116) \end{aligned}$$

with $t_o < 0$.

For well separated one-atom events, we can impose boundary conditions on N, σ, and a. Since the value of $a(t)$ at the end of one-atom event is exactly the initial value of $a(t)$ for the next one-atom event, and since all one-atom events are equivalent, we again obtain a condition of "steady state of return map" (compared to Eq.2.14 in Sec.2.1.1).

$$a(-\Delta t/2) = a(+\Delta t/2) \, , \tag{2.117}$$

For every atom, the initial dipole moment and inversion should be those of an unexcited atom.

$$\begin{aligned} N(-\infty) &= -1 && (2.118) \\ \sigma(-\infty) &= 0\,. && (2.119) \end{aligned}$$

There is a constant of motion obtainable from Eq.2.113 and Eq.2.114. Multiplying N to Eq.2.114 and σ to Eq.2.113 and adding the results together, we find

$$N\dot{N} + 4\sigma\dot{\sigma} = 0 \tag{2.120}$$

or

$$N^2 + 4\sigma^2 = \text{constant} = 1\ , \tag{2.121}$$

where the constant is determined from the boundary condition, Eqs.2.118 and 2.119. Note if $|N| < 1$, which is the case when atom is in the superposition state of the ground state and the excited state, $|\sigma|$ must be nonzero. A different way of stating it is that the dipole moment of the atom is identically zero only when the atom is either in the ground state or in the excited state.

The form of Eq.2.121 suggests that we can express $N(t)$ and $\sigma(t)$ in terms of sine and cosine function

$$\begin{aligned} N(t) &= -\cos\theta(t) && (2.122) \\ \sigma(t) &= \frac{1}{2}\sin\theta(t)\,. && (2.123) \end{aligned}$$

With this substitution,

$$\begin{aligned} \dot{N} &= \sin(\theta)\,\dot{\theta} = 2\sigma\dot{\theta} \\ &= 2\,(2ga + \Omega_R)\,\sigma\ , \end{aligned}$$

so that for $-\frac{\Delta t}{2} < t < \frac{\Delta t}{2}$,

$$\begin{aligned}\dot{\theta} &= [2g(t)a(t) + \Omega_R(t)] \qquad (2.124)\\ \dot{a} &= -\frac{\Gamma_c}{2}a - \frac{g(t)}{2}\sin\theta(t)\ . \qquad (2.125)\end{aligned}$$

These two coupled differential equations should describe the system completely with appropriate boundary conditions, which are

$$\begin{aligned}a(-\Delta t/2) &= a(+\Delta t/2) \qquad (2.126)\\ \theta(-\infty) &= 0 \qquad (2.127)\end{aligned}$$

In general, Eqs.2.124 and 2.125 can be solved only numerically. We first pick up a value for a_o, the initial value of $a(t)$, and then solve the equations to find $a(\frac{\Delta t}{2})$. If this value is not equal to a_o, we change the guess and repeat the calculation until $a(\frac{\Delta t}{2})$ becomes very close to a_o within a desired accuracy. This procedure is equivalent to find the roots to the following equation.

$$a_o = a(\Delta t/2; a_o)\ , \qquad (2.128)$$

where the right hand side is the solution of the differential equations evaluated at $t = \Delta t/2$, with the initial condition, $a(-\frac{\Delta t}{2}) = a_o$. A steady-state mean number of photons is then obtained by taking a time average of a^2 over the interaction time, Δt.

$$\langle n\rangle = \frac{1}{\Delta t}\int_{-\Delta t/2}^{\Delta t/2} a^2(t)dt\ . \qquad (2.129)$$

2.2.2 Stepwise Coupling: Pendulum Equation

The coupled equations, Eqs.2.124 and 2.125 can be reduced to a differential equation describing a rotating pendulum. In order to show this, let's suppose that the cavity mode is sharply edged and the coupling constant is a constant g_o if $|x| < w_m$ and zero otherwise. Let's also assume that the pump laser is placed far away from the cavity

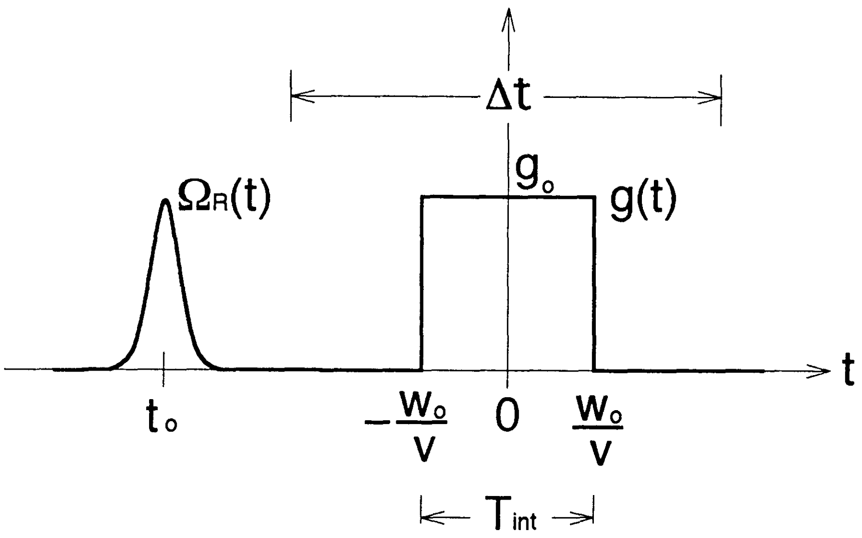

Figure 2-10: A stepwise $g(t)$ centered at $t = 0$ and $\Omega_R(t)$ at $t = t_o$.

as shown in Figure 2-10.

$$-x_o \ll -\frac{v\Delta t}{2} \ll -w_m < 0 \, .$$

Then for $|x| < \frac{T_{int}}{2}$ with $T_{int} \equiv \frac{2w_m}{v}$,

$$\begin{aligned} \dot{\theta} &= 2g_o a(t) && (2.130) \\ \dot{a} &= -\frac{\Gamma_c}{2}a - \frac{g_o}{2}\sin\theta(t) \, , && (2.131) \end{aligned}$$

and for $\frac{T_{int}}{2} < |x| < \frac{\Delta t}{2}$,

$$\begin{aligned} \dot{\theta} &= 0 && (2.132) \\ \dot{a} &= -\frac{\Gamma_c}{2}a \, . && (2.133) \end{aligned}$$

By substituting the expression for a from Eq.2.130 into Eq.2.131, we obtain a pendulum equation for $|x| < \frac{T_{int}}{2}$.

$$\ddot{\theta} + \frac{\Gamma_c}{2}\dot{\theta} + g_o^2 \sin\theta = 0 \, , \qquad (2.134)$$

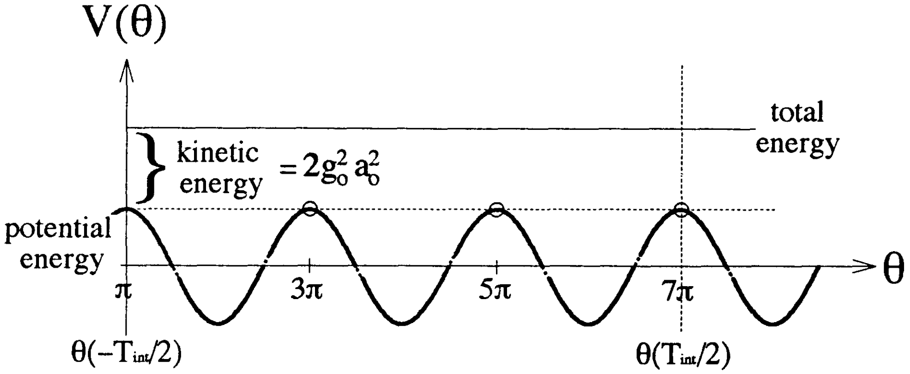

Figure 2-11: The one-atom laser as a pendulum. The atom-field interaction is analogous to a mechanical pendulum in a periodic potential as shown in this figure. By a π-pulse, the pendulum is inverted before it is placed in the potential. At $t = -\frac{T_{int}}{2}$ the pendulum starts to swing with an initial angular velocity $2a_o g_o$. The boundary condition, $\dot{\theta}(T_{int}/2) = \dot{\theta}(T_{int}/2)$, requires that $\theta(T_{int}/2)$ must be $(2k+1)\pi$ with $k = 1, 2, \ldots$. In this plot a case of $k = 3$ is shown.

which is nothing but a differential equation for a mechanical pendulum with damping. For the pendulum, g_o is a normal mode frequency given by

$$g_o \rightarrow \sqrt{\frac{g}{l}}$$

with g being the gravitational acceleration and l being the length of the pendulum.

A. No Cavity Damping

For a perfect cavity with no damping, the solution of the pendulum equation is readily obtained. There exists a constant of motion,

$$\frac{1}{2}\dot{\theta}^2 - g_o^2 \cos\theta = \text{constant} \; , \tag{2.135}$$

which is nothing but a total energy of a classical pendulum except a constant factor, with the first term a kinetic energy and the second term a potential energy. The atom-field interaction is hence analogous to a mechanical pendulum in a periodic potential as shown in Figure 2-11. The boundary conditions, Eqs.2.126 and 2.127, reduce to

$$\begin{aligned} \theta(-T_{int}/2) &= \pi \text{ (initially inverted)} && (2.136) \\ \dot{\theta}(-T_{int}/2) &= 2g_o a_o = \dot{\theta}(T_{int}/2)\ . && (2.137) \end{aligned}$$

The total energy E is simply

$$E = 2g_o^2 a_o^2 + g_o^2 = \frac{1}{2}\dot{\theta}^2 - g_o^2 \cos\theta\ . \qquad (2.138)$$

By a π-pulse, the pendulum is inverted before it is placed in the potential. At $t = -\frac{T_{int}}{2}$ the pendulum starts to swing with an initial angular velocity $2a_o g_o$. It is then obvious that, if $a_o > 0$, in order to satisfy $\dot{\theta}(-T_{int}/2) = \dot{\theta}(T_{int}/2)$,

$$\theta(T_{int}/2) = \theta(\Delta t/2) = 3\pi, 5\pi, \ldots \qquad (2.139)$$

Large Photon Number Limit

In the limit of a large photon number, $a(t)$ during the atom-cavity interaction can be thought as constant a_o since an one-atom event can only change a^2 by only one at most. Then Eq.2.139 simply means,

$$\begin{aligned} \theta\left(T_{int}/2\right) = 2g_o a_o T_{int} + \pi &= 3\pi, 5\pi, \ldots \quad \text{if } a_o > 0 \\ &= -\pi, -3\pi, \ldots \text{ if } a_o < 0\ , && (2.140) \end{aligned}$$

or

$$2g_o a_o T_{int} = \pm 2\pi, \pm 4\pi, \pm 6\pi \ldots\ . \qquad (2.141)$$

In this limit, once an equilibrium is reached, the atoms undergo complete multiple Rabi revolutions, exiting the cavity unchanged, that is, in the excited state. The states of the system satisfying Eq.2.141 are called trap states [39]. The mean photon number is then

$$\langle n \rangle = a_o^2 = \left(\frac{k\pi}{g_o T_{int}}\right)^2 \quad , \quad k = 1, 2, \ldots\ . \qquad (2.142)$$

Interestingly a infinite number of k's give rise to the solutions for $\langle n \rangle$. Note that the semiclassical theory does not tell us which are physically observable solutions. In fact, as shown below, all the trap state solutions are unstable for any small perturbations/fluctuations.

Evolution of Field

Some part of the material discussed in this section can also be found in Ref. [39]. The boundary condition of steady state of return map requires that the field amplitude at the end of n-th one-atom event is exactly the same as the initial field amplitude for the next one-atom event. If we denote the field amplitude of the n-th event by $a_n(t)$, the boundary condition reads

$$a_n(\Delta t/2) = a_{n+1}(-\Delta t/2) \equiv \alpha_n \ , \quad n = 1, 2, \dots \ . \tag{2.143}$$

Eq.2.138 can be rewritten then as

$$\begin{aligned} E &= 2g_o^2 a_{n+1}^2(-\Delta t/2) + g_o^2 \\ &= 2g_o^2 a_{n+1}^2(\Delta t/2) - g_o^2 \cos\theta(\Delta t/2) \ , \end{aligned}$$

or

$$\begin{aligned} E &= 2g_o^2 \alpha_n^2 + g_o^2 \\ &= 2g_o^2 \alpha_{n+1}^2 - g_o^2 \cos\theta(\Delta t/2) \ , \end{aligned}$$

which, in the large photon number limit, simplifies to

$$\begin{aligned} \alpha_{n+1}^2 &= \alpha_n^2 + \frac{1 + \cos\left(\pi + 2g_o \int_{-\Delta t/2}^{\Delta t/2} a_n(t')dt'\right)}{2} \\ &\approx \alpha_n^2 + \frac{1 + \cos\left(\pi + 2g_o \alpha_n T_{int}\right)}{2} \\ &= \alpha_n^2 + \frac{1 - \cos\left(2g_o \alpha_n T_{int}\right)}{2} \\ &= \alpha_n^2 + \sin^2\left(g_o \alpha_n T_{int}\right) \equiv f(\alpha_n^2) \ . \end{aligned} \tag{2.144}$$

This is the recursion relation for the field amplitude. For an arbitrary initial amplitude, α_o, a steady-state field amplitude is obtained by evaluating α_n for $n = 1, 2, \ldots$ until a convergence is achieved. Since $\alpha_n = \alpha_{n+1}$ as $n \to \infty$, a steady-state solution, α_∞, satisfies

$$\sin^2(g_o \alpha_\infty T_{int}) = 0 \ ,$$

or

$$\alpha_\infty = \pm \frac{k\pi}{g_o T_{int}} \equiv \pm \beta^{(k)} \quad , k = 1, 2, \ldots \ , \tag{2.145}$$

which is exactly Eq.2.141. However we are not interested in the solution itself here. Rather note that the recursion relation simulates the evolution of the field as a function of the number of atoms traversing the cavity. Let's assume that the field amplitude is initially α_o before a first atom traverses the cavity. After the first atom, the field is given by α_1, which is the initial field amplitude for the next atom. Using this α_1 and the recursion relation, we then get α_2, and so on, as illustrated in Figure 2-12. We can readily show that the field converges to one of the $\beta^{(k)}$'s given by Eq.2.145, depending on the initial value, α_o. In fact, if α_o is restricted between $\beta^{(m-1)}$ and $\beta^{(m)}$, α_∞ is always equal to or larger than $\beta^{(m)}$. In other words, the mean number of photons in an equilibrium state is always greater than an initial number of photons. This is of course due to the initial population inversions in the atoms. If the atoms are initially in the ground state instead, we will get an opposite result.

Let's consider the initial field being a vacuum. Classically the field never grows since a vanishing α_o gives $\alpha_1 = 0$, $\alpha_2 = 0$, and so forth. However a vacuum is not stable and it fluctuates in quantum mechanics. Therefore, we should introduce random fluctuations of α_o around zero (actually above zero since we assumed $\alpha_n > 0$.). Then the field amplitude converges to one of the $\beta^{(k)}$'s depending on the fluctuations.

Even when the field has converged to $\beta^{(m)}$ with $m > 0$, the resulting field is also subject to the fluctuations. The sources of the fluctuations are the vacuum fluctuation as well as the spontaneous emission process of the atom. The change of the field by the spontaneous emission itself is negligibly small since the solid angle extended by the cavity mode is much smaller than 4π, into which the spontaneous emission occurs.

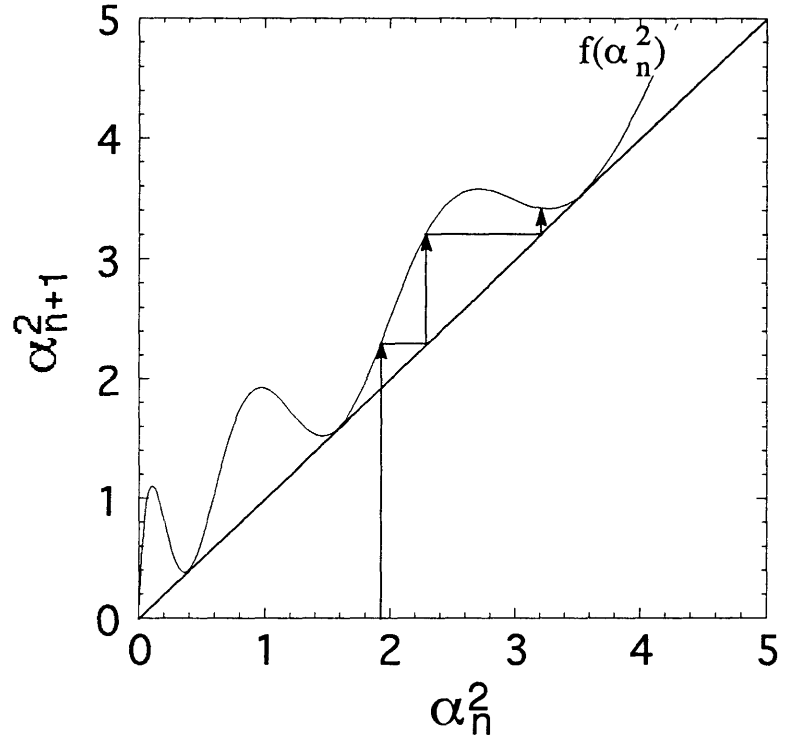

Figure 2-12: Evolution of $a(t)$. Depending on an initial value, $a(t)$ converges to one of the $\beta^{(k)}$'s given by Eq.2.145.

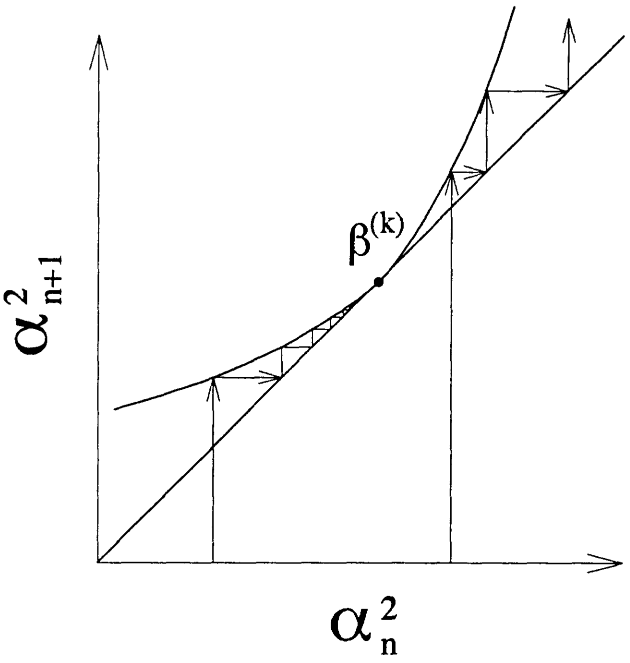

Figure 2-13: $\beta^{(k)}$ solutions are stable when approached from lower amplitude side whereas it is unstable when approached from the other side. Therefore fluctuations eventually push the field amplitude to a higher trap state.

However, the atomic wave function changes abruptly once the spontaneous emission occurs.

Once the field amplitude becomes slightly larger than $\beta^{(m)}$ due to the fluctuations, the amplitude quickly departs from $\beta^{(m)}$ and converges to one of $\beta^{(n)}$ with n larger than m. If the amplitude is slightly less than $\beta^{(m)}$, on the other hand, it can converge back to $\beta^{(m)}$ as illustrated in Figure 2-13

Since this consideration can also be applied to the new $\beta^{(n)}$ evolved from $\beta^{(m)}$, it is not difficult to imagine that the field will eventually evolve to higher and higher n states without any upper limit. In other words, in the absence of the cavity damping, the field will grow indefinitely, and hence there exists *no* steady state. In the presence of the cavity damping, the growth of the field is limited, resulting in a real steady-state solution, as will be shown later.

Arbitrary Number of Photons

The convergent solution, α_∞, for an arbitrary magnitude of the mean photon number can be obtained by integrating Eq.2.138.

$$
\begin{aligned}
\frac{\dot{\theta}^2}{2} - g_o^2(1+\cos\theta) &= 2g_o^2\alpha_\infty^2 \\
\frac{d\theta}{dt} &= \pm 2\alpha_\infty g_o \sqrt{1+\left(\frac{1}{\alpha_\infty}\right)^2 \cos^2\frac{\theta}{2}} \\
\frac{d\theta}{\sqrt{1+\left(\frac{1}{\alpha_\infty}\right)^2\cos^2\frac{\theta}{2}}} &= \pm 2\alpha_\infty g_o dt \\
\int_\pi^{(2k+1)\pi} \frac{d\theta}{\sqrt{1+\left(\frac{1}{\alpha_\infty}\right)^2\cos^2\frac{\theta}{2}}} &= \pm 2\alpha_\infty g_o T_{int}\ .
\end{aligned}
$$

Using the periodicity of the cosine function,

$$
\begin{aligned}
\pm 2\alpha_\infty g_o T_{int} &= 2\int_{\pi/2}^{(2k+1)\pi/2} \frac{d\Phi}{\sqrt{1+\left(\frac{1}{\alpha_\infty}\right)^2\cos^2\Phi}} \\
&= 4k\int_0^{\pi/2} \frac{d\Phi}{\sqrt{1+\left(\frac{1}{\alpha_\infty}\right)^2\cos^2\Phi}} \\
&= 4k\int_0^{\pi/2} \frac{d\Phi}{\sqrt{1+\left(\frac{1}{\alpha_\infty}\right)^2\left(1-\sin^2\Phi\right)}} \\
&= \frac{4k}{\sqrt{1+\alpha_\infty^{-2}}} K\left(\frac{1}{\sqrt{1+\alpha_\infty^2}}\right)\ , \qquad (2.146)
\end{aligned}
$$

where $K(x)$ is the complete elliptic integral defined as

$$
K(x) = \int_0^{\pi/2} \frac{d\Phi}{\sqrt{1-x^2\sin^2\Phi}}\ , \quad x^2 < 1 \qquad (2.147)
$$

and its values are tabulated in many mathematical handbooks [51] and its functional form is shown in Figure 2-14. If $\alpha_\infty^2 \gg 1$, Eq.2.146 is simplified to

$$
\pm\, 2\alpha_\infty g_o T_{int} \approx 4kK(0) = 2k\pi \qquad (2.148)
$$

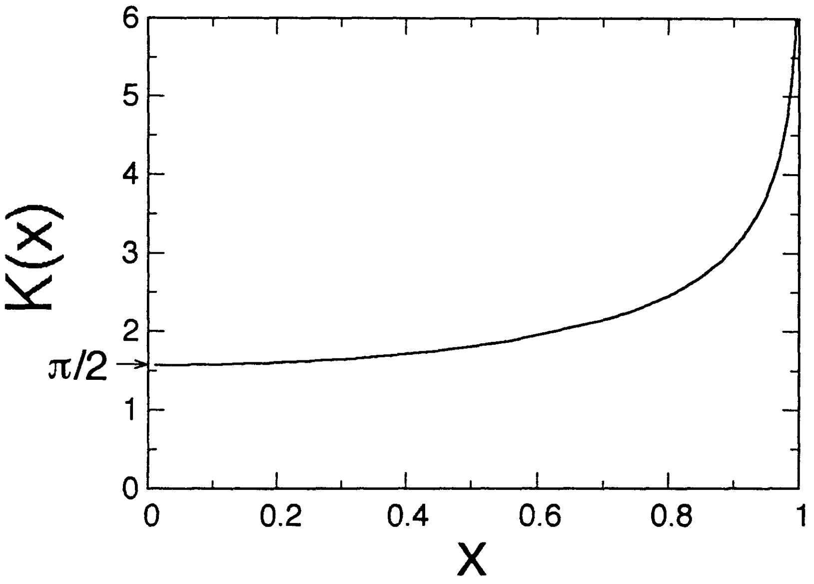

Figure 2-14: Plot of $K(x)$, complete elliptic integral.

which is identical to Eqs.2.141 and 2.145. The general solutions of Eq.2.146 can be found by plotting the right-hand side except the factor of $4k$ and the left-hand side divided by $4k$ as a function of α_∞ and finding all the intersecting points as shown in Figure 2-15. These solutions in fact do not differ much from the trap state solutions even when α_∞ is as small as 0.5 as can be seen in Figure 2-16. Of course if α_∞ gets too small, the discrepancy will be more pronounced.

B. Non-negligible Cavity Damping

If the cavity damping is included, the total energy of the pendulum is not a constant of motion; it decays in time. In this case, how frequently the excited atoms are injected into the cavity is critical. If the injection rate is too slow (i.e., very large Δt), the field would not build up much in an equilibrium state, and hence only a small number of θ values satisfy the boundary condition, $a(-\Delta t/2) = a(\Delta t/2)$, in contrast with the no-damping case, where infinite number of θ solutions exist ($k = 1, 2, \ldots$). In the presence of the damping, the kinetic energy of the pendulum can be equal to its initial value not at the peaks of the potential energy but at upward and downward hillside as illustrated in Figure 2-17. Instead of Eq.2.135, for $|t| < \frac{T_{\rm int}}{2}$,

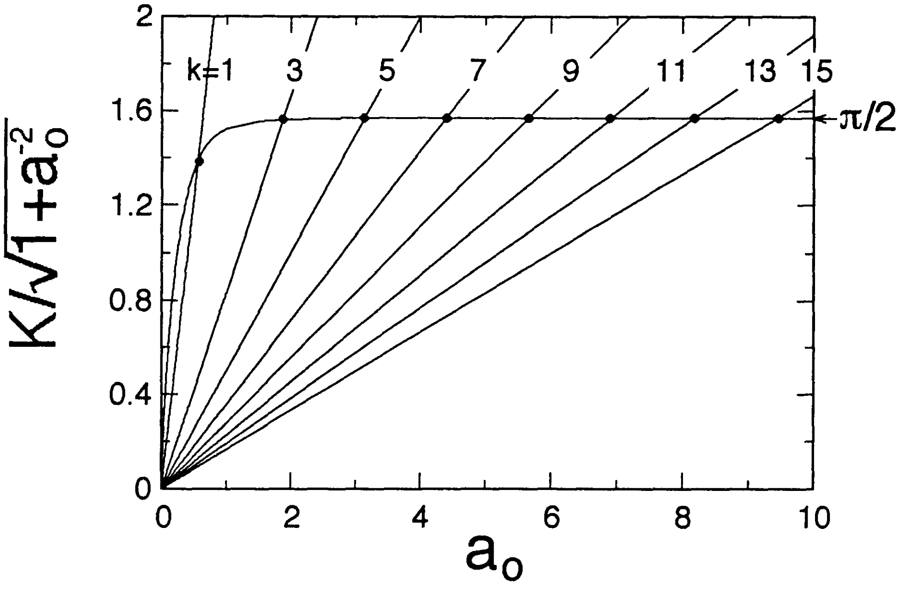

Figure 2-15: The solutions of Eq.2.146 are obtained from the intersecting points in the plot. For this example, we assume $g_oT_{int} = 5$.

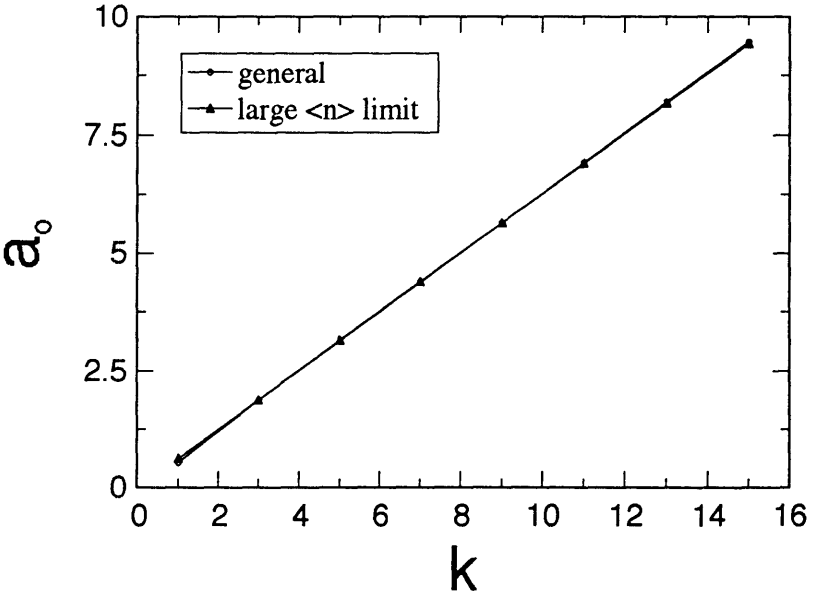

Figure 2-16: The solution under the assumption of large photon number and the solution without such assumption. Here the cavity damping is neglected and $g_oT_{int} = 5$.

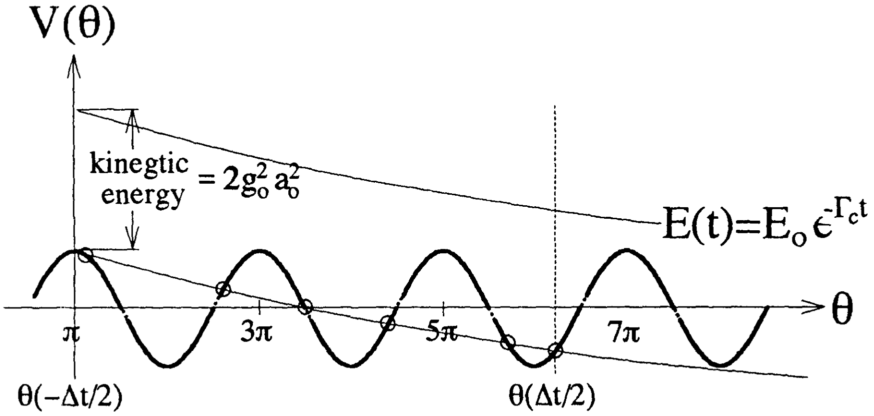

Figure 2-17: The one-atom laser as a pendulum in the presence of cavity damping. For simplicity we assume $\Delta t = T_{int}$ (exactly one-atom operation).

$$\frac{d}{dt}E(t) = \frac{d}{dt}\left(\frac{1}{2}\dot{\theta}^2 - g_o^2\cos\theta\right) = -\frac{1}{2}\Gamma_c\dot{\theta}^2 \ . \tag{2.149}$$

Large Photon Number Limit

If $a^2(t) \gg 1$, approximately $a(t) \approx$ constant $= a_o$ for $|t| < T_{int}/2$. We can rewrite Eq.2.149 as

$$\frac{d}{dt}E(t) \approx -\frac{1}{2}\Gamma_c\left(2g_oa_o\right)^2 \approx -\Gamma_cE(t) \ . \tag{2.150}$$

Hence

$$E(t) \approx E(-T_{int}/2)\ \mathrm{e}^{-\Gamma_c(t+T_{int}/2)} \ , \tag{2.151}$$

or

$$\begin{aligned} E(T_{int}/2) &= \frac{1}{2}\dot{\theta}^2(T_{int}/2) - g_o^2\cos\theta(T_{int}/2) \\ &= \left[\frac{1}{2}\dot{\theta}^2(-T_{int}/2) - g_o^2\cos\theta(-T_{int}/2)\right]\ \mathrm{e}^{-\Gamma_cT_{int}} \ , \end{aligned} \tag{2.152}$$

which reduces to

$$2g_o^2a_{n+1}^2(T_{int}/2) - g_o^2\cos\theta(T_{int}/2) = \left[2g_o^2a_{n+1}^2(-T_{int}/2) + g_o^2\right]\ \mathrm{e}^{-\Gamma_cT_{int}} \tag{2.153}$$

Since

$$a_{n+1}(\pm T_{int}) = a_{n+1}(\pm\Delta t/2)\ \mathrm{e}^{-\pm\frac{\Gamma_c}{2}(\Delta t-T_{int})/2} \ , \tag{2.154}$$

Eq.2.153 becomes

$$\begin{aligned}
&2g_o^2 a_{n+1}^2(\Delta t/2)\ \mathrm{e}^{\Gamma_c(\Delta t - T_{int})/2} - g_o^2\cos\theta(T_{int}/2) \\
&= \left[2g_o^2 a_{n+1}^2(-\Delta t/2)\ \mathrm{e}^{-\Gamma_c(\Delta t - T_{int})/2} + g_o^2\right]\ \mathrm{e}^{-\Gamma_c T_{int}} \\
&2g_o^2 \alpha_{n+1}^2\ \mathrm{e}^{\Gamma_c(\Delta t - T_{int})/2} - g_o^2\cos\theta(T_{int}/2) \\
&= \left[2g_o^2 \alpha_n^2\ \mathrm{e}^{-\Gamma_c(\Delta t - T_{int})/2} + g_o^2\right]\ \mathrm{e}^{-\Gamma_c T_{int}}\ ,
\end{aligned} \tag{2.155}$$

which is further simplified to

$$\alpha_{n+1}^2 - \frac{1}{2}\cos\theta(T_{int}/2) \approx \alpha_n^2\ \mathrm{e}^{-\Gamma_c \Delta t} + \frac{1}{2}\ , \tag{2.156}$$

or

$$\begin{aligned}
\alpha_{n+1}^2 &= \alpha_n^2\ \mathrm{e}^{-\Gamma_c\Delta t} + \cos^2\left[\frac{\theta(T_{int}/2)}{2}\right] \\
&= \alpha_n^2\ \mathrm{e}^{-\Gamma_c\Delta t} + \cos^2\left[\frac{\pi}{2} + g_o\alpha_n T_{int}\right] \\
&\approx \alpha_n^2(1-\Gamma_c\Delta t) + \sin^2(g_o\alpha_n T_{int}) \equiv f(\alpha_n^2)\ ,
\end{aligned} \tag{2.157}$$

which is a new recursion relation for the field amplitude. We assumed $\Gamma_c\Delta t \ll 1$ in the last step of Eq.2.157. The relation describes the evolution of the field as a function of the number of atoms traversing the cavity as shown in Figure 2-18.

Convergent solutions can be found by letting $\alpha_n = \alpha_{n+1} = \alpha_\infty$ in Eq.2.157.

$$\alpha_\infty^2 = \frac{\sin^2(g_o\alpha_\infty T_{int})}{\Gamma_c\Delta t}\ . \tag{2.158}$$

The mean time interval between atoms, Δt, is related to the mean number of atoms in the mode, $\langle N_{atom}\rangle$, by

$$\langle N_{atom}\rangle = \frac{T_{int}}{\Delta t} \tag{2.159}$$

for the step-wise cavity mode as shown in Figure 2-10. Note that we do not have the $\frac{1}{2}$factor due to the $\sin^2 kz$ dependence of the coupling constant because we assumed that all the atoms are located at the anti-nodes of the cavity field mode. Using this

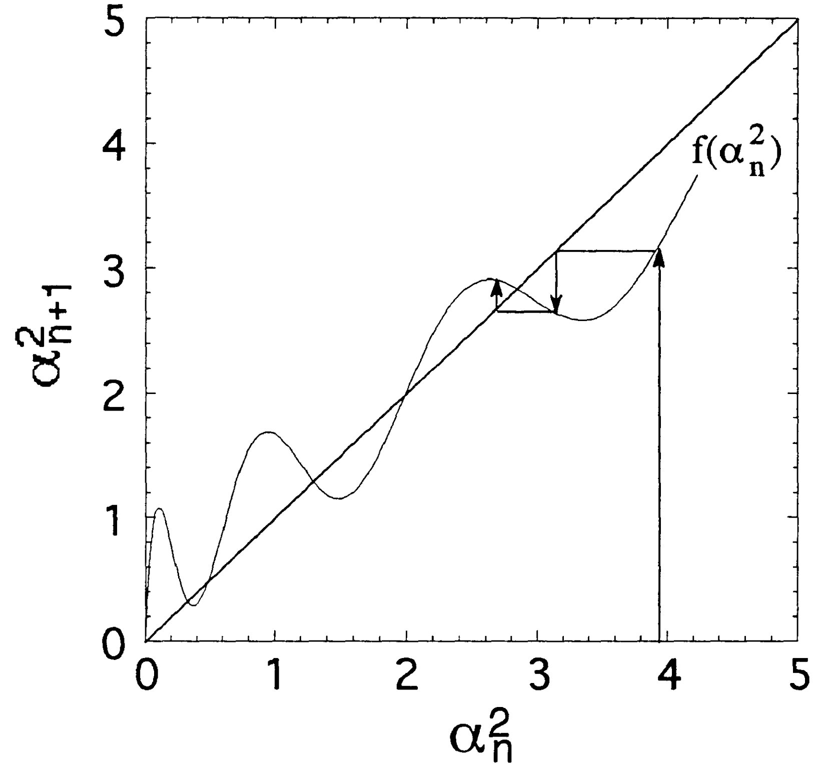

Figure 2-18: Evolution of $a(t)$ in the presence of cavity damping. We assume that g_oT_{int}=5 and $\Gamma_c\Delta t = 0.25$.

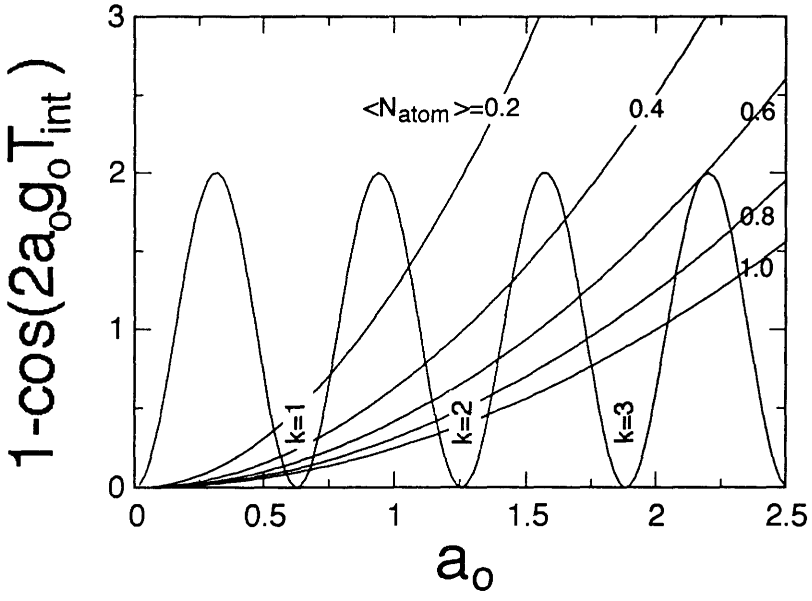

Figure 2-19: Convergent solutions including the cavity decay. Only a few α_∞ solutions exist in contrast with the no-damping case, where infinite number of α_∞ solutions exist. Here we assume $g_oT_{int} = 5$ and $\Gamma_c\Delta t = 0.25$.

notation,

$$\frac{\Gamma_c T_{int}}{\langle N_{atom}\rangle}\alpha_\infty^2 = \sin^2\left(g_o\alpha_\infty T_{int}\right) . \tag{2.160}$$

The solutions can be found by plotting both sides of the equation and finding a crossing point as shown in Figure 2-19.

Stability Condition

In the absence of the cavity damping, $\beta^{(k)}$ solutions in Eq.2.145 are stable when approached from lower amplitude side whereas it is unstable when approached from the other side. When the damping is included, almost all the a_o solutions of Eq. 2.158 or 2.160 are unstable no matter how they are approached as illustrated in Figure 2-20. Among the a_o solutions, only the ones satisfying the following condition are stable against small fluctuations.

$$\left|\left.\frac{df}{dx}\right|_{x=a_o^2}\right| < 1 , \tag{2.161}$$

where

$$f(x) = x\left(1-\Gamma_c\Delta t\right) + \sin^2\left(g_o\sqrt{x}T_{int}\right) .$$

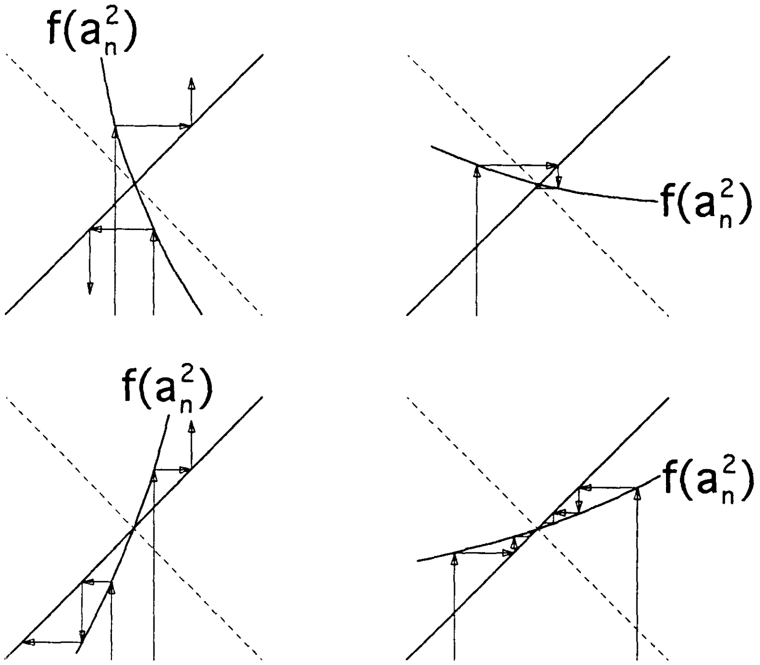

Figure 2-20: Among a_o solutions, only the ones satisfying Eq.2.161 are stable solutions. The other solutions are unstable when subject to field fluctuations

If we consider $a_o > 0$ solutions and denote the solutions of Eq.2.160 by $\beta^{(1)}$, $\beta^{(2)}$, $\beta^{(3)}$, and so on in the order of increasing amplitude, it is obvious from Fig.2-20 that all the odd-numbered solutions are unstable whereas the even-numbered solutions can be stable as the number increases. The largest solution, which is even-numbered, has the best chance to be stable. If the largest one is not stable, no solutions are stable. In this case, the system will become highly unstable, continuously fluctuating. If the largest one is stable, it may be possible that a few more smaller even-numbered solutions are also stable. Let's consider a case, $\Gamma_c \Delta t \ll 1$, which we are mostly interested in. The largest a_o solution, denoted by a_N, gets fairly large, and it approximately satisfies

$$g_o a_N T_{int} \approx (2N+1)\frac{\pi}{2}, \quad N \gg 1 \ . \tag{2.162}$$

The next largest one, a_{N-1}, is also approximately

$$g_o a_{N-1} T_{int} \approx (2N-1)\frac{\pi}{2} \ ,$$

and hence

$$\frac{\delta a_N^2}{a_N^2} \equiv \frac{a_N^2 - a_{N-1}^2}{a_N^2} = \frac{2N}{\left(N+\frac{1}{2}\right)^2} \approx \frac{2}{N} \ll 1 \; . \tag{2.163}$$

Though many stable a_o solutions can be allowed, they are very closely spaced, and therefore practically indistinguishable from each other when the field fluctuations are present.

Semiclassical Photon Statistics

Interestingly this multiplicity of the field amplitude provides a classical description of the photon statistics.

$$\frac{\Delta n}{\langle n \rangle} \sim \frac{\delta a_N^2}{a_N^2} \sim \frac{1}{N} \sim \frac{1}{g_o T_{int}} \frac{1}{\sqrt{\langle n \rangle}} \; . \tag{2.164}$$

For a Poissonian photon statistics

$$\frac{\Delta n}{\langle n \rangle} = \frac{1}{\sqrt{\langle n \rangle}} \; . \tag{2.165}$$

Therefore in the semiclassical model the photon statistics becomes super-Poissonian with $g_o T_{int} \ll 1$, sub-Poissonian with $g_o T_{int} \gg 1$, and Poissonian with $g_o T_{int} \sim 1$. Of course this description should be considered being qualitative. Only the quantum-mechanical model described in Sec.1 can give correct results. In Figure 2-21 predictions based on the quantum-mechanical model are shown for various $\Theta = 2 g_o T_{int}$. The parameter σ in the plot is defined as

$$\sigma \equiv \frac{\Delta n}{\sqrt{\langle n \rangle}} = \frac{\sqrt{\langle n^2 \rangle - \langle n \rangle^{\,2}}}{\sqrt{\langle n \rangle}} \tag{2.166}$$

Interestingly the semiclassical model provides qualitative description on the photon statistics as demonstrated in the plot.

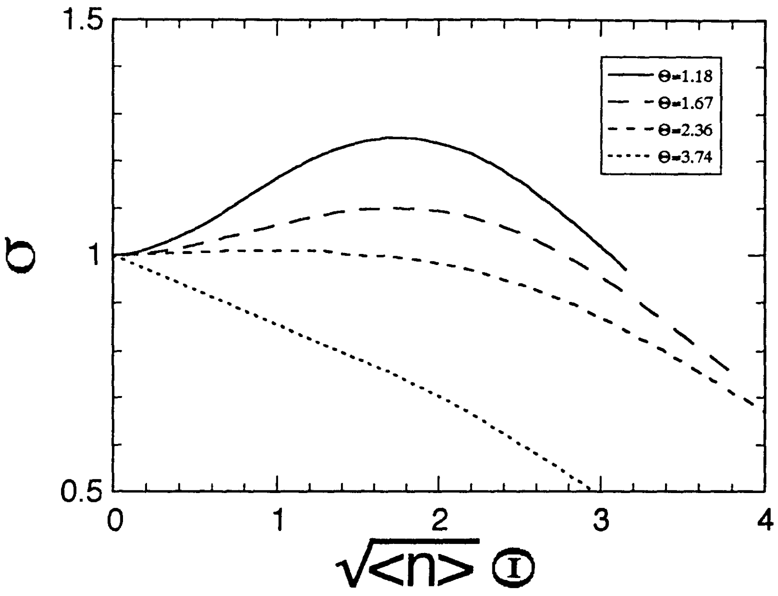

Figure 2-21: Photon number variances based on the quantum-mechanical theory described in Sec.1 for various $\Theta = 2g_oT_{int}$.

Physical Solution

When more than one solutions satisfy the stability condition, Eq.2.161, it is not obvious whether all the stable solutions are observable or not. If Δx_o is a displacement of x parameter from its stable point x_o due to fluctuation at a certain moment, the subsequent displacement will be

$$\Delta x_n = \left(\frac{df}{dx}\bigg|_{x=x_o} \right)^n \Delta x_o \, .$$

Therefore the smaller the slope is the faster x converges back to x_o. If the slope is slightly less than one, the convergence of x can be very slow. In this case x is likely to have additional fluctuation during the process of convergence. It can be displaced farther away from x_o and eventually jumps to a larger stable point. If x_o is the largest stable solution, x does not have a larger stable point to jump to. Furthermore largest stable point has the smallest slope and hence it is most robust against fluctuations. Therefore what we observe in an experiment would be statistical average of the all stable solutions. This average would depend on the very details of the fluctuations and the evolution of the field. We can numerically solve the recursion relation, Eq.2.157, under random fluctuations and can calculate a time average. This time average is equivalent to the above statistical average. This average, however, would approximately equal to the largest stable solution because the field amplitude stays close to it most of time under the fluctuations. Although we do not attempt to prove this claim in this work, we will compare the experimental data with the stable solutions given by the theory in the next chapter.

2.2.3 Gaussian Mode Coupling in Large Photon Number Limit

In this section we again consider a general case, where the coupling constant is not a stepwise function but is a gaussian given by Eq.2.115. A pump laser field is treated generally, given by Eq.2.116. We start with a formal solution of the coupled Maxwell-Schrödinger equations, which can be obtained from Eq.2.124 and 2.125.

$$\dot{a}(t) + \frac{\Gamma_c}{2} a(t) = -\frac{1}{2} g(t) \sin\left\{ \int_{-\infty}^{t} \left[2g(t')a(t') + \Omega_R(t')\right] dt' \right\} . \tag{2.167}$$

Multiply $a(t)$ to the both sides and integrate the result over Δt.

$$\begin{aligned} &\frac{1}{2} a^2(t)\Big|_{-\Delta t/2}^{\Delta t/2} + \frac{\Gamma_c}{2} \int_{-\Delta t/2}^{\Delta t/2} a^2(t')dt' \\ &= -\frac{1}{2} \int_{-\Delta t/2}^{\Delta t/2} dt\ g(t)a(t) \sin\left\{ \int_{-\infty}^{t} \left[2g(t')a(t') + \Omega_R(t')\right] dt' \right\} , \end{aligned} \tag{2.168}$$

where $\langle n \rangle$ is defined by Eq.2.129. Using the boundary condition in Eq.2.143 and α_n notation therein, Eq.2.168 reduces to

$$\begin{aligned} &\alpha_{n+1}^2 - \alpha_n^2 + \Gamma_c \int_{-\Delta t/2}^{\Delta t/2} a^2(t')dt' \\ &= -\int_{-\Delta t/2}^{\Delta t/2} dt\ g(t)a(t) \sin\left\{ \int_{-\infty}^{t} \left[2g(t')a(t') + \Omega_R(t')\right] dt' \right\} . \end{aligned} \tag{2.169}$$

Now we assume

$$\left|\frac{a(t)-a(-\Delta t/2)}{a(t)}\right| = \left|\frac{a(t)-\alpha_n}{a(t)}\right| \ll 1 \quad \text{for } |t| < \frac{\Delta t}{2} \, . \tag{2.170}$$

Then

$$\begin{aligned}
&\alpha_{n+1}^2 - \alpha_n^2 + \Gamma_c \Delta t \alpha_n^2 \\
&\quad \approx \;\; -\alpha_n \int_{-\Delta t/2}^{\Delta t/2} dt \; g(t) \sin\left\{\int_{-\infty}^{t} [2g(t')\alpha_n + \Omega_R(t')]\, dt'\right\} \\
&\quad = \;\; -\alpha_n \int_{-\Delta t/2}^{\Delta t/2} dt \; g_o \, \mathrm{e}^{-\left(\frac{vt}{w_m}\right)^2} \sin\left\{\int_{-\infty}^{t}\left[2g_o \, \alpha_n \, \mathrm{e}^{-\left(\frac{vt'}{w_m}\right)^2} + \Omega_R^o \, \mathrm{e}^{-\left(\frac{v(t'-t_o)}{w_P}\right)^2}\right] dt'\right\} \\
&\quad = \;\; -\alpha_n \int_{-\Delta t/2}^{\Delta t/2} dt \; g_o \, \mathrm{e}^{-\left(\frac{vt}{w_m}\right)^2} \\
&\qquad\qquad \times \sin\left\{2g_o \, \alpha_n t_m \mathrm{Err}\left(\frac{vt}{w_m}\right) + \Omega_R^o t_p \mathrm{Err}\left(\frac{v(t-t_o)}{w_p}\right)\right\} \, ,
\end{aligned}$$

where t_m and t_p are the transit time and the pumping time respectively defined as,

$$t_{m,p} \equiv \frac{\sqrt{\pi} w_{m,p}}{v} \tag{2.171}$$

and

$$\mathrm{Err}(x) \equiv \frac{1}{\sqrt{\pi}} \int_{-\infty}^{x} \mathrm{e}^{-x^2} dx \, . \tag{2.172}$$

Noting $t_{int} = t_m$ and substituting $q = \frac{vt}{w_m}$,

$$\begin{aligned}
\alpha_{n+1}^2 \;\; = \;\; & \alpha_n^2(1-\Gamma_c \Delta t) - g_o \alpha_n \frac{w_m}{v} \int_{-\frac{v\Delta t}{2w_m}}^{\frac{v\Delta t}{2w_m}} dq \; \mathrm{e}^{-q^2} \\
& \times \sin\left\{2g_o \, \alpha_n t_{int} \mathrm{Err}(q) + \Omega_R^o t_p \mathrm{Err}\left(\frac{q-q_o}{w_p/w_m}\right)\right\} \, .
\end{aligned} \tag{2.173}$$

Defining $x_n = \alpha_n^2$, $q_o = x_o/w_m$, and

$$\Delta q \;=\; \frac{v\Delta t}{2w_m}$$

$$\Theta_m \;=\; 2g_o t_{int} \tag{2.174}$$

$$\Theta_p \;=\; \Omega_R t_p \, , \tag{2.175}$$

We obtain a recursion relation,

$$\begin{aligned}
x_{n+1} &= x_n(1-\Gamma_c\Delta t) \\
&\quad + \frac{\Theta_o\sqrt{x_n}}{2\sqrt{\pi}}\int_{-\Delta q}^{\Delta q} dq\ \mathrm{e}^{-q^2} \\
&\qquad \times \sin\left\{\Theta_o\sqrt{x_n}\mathrm{Err}(q) + \mathrm{Sign}(\alpha_n)\left[\Theta_p\mathrm{Err}\left(\frac{q-q_o}{w_p/w_m}\right)-\pi\right]\right\} \\
&\equiv f(x_n)\,, \qquad (2.176)
\end{aligned}$$

where

$$\begin{aligned}
\mathrm{Sign(x)} &= +1\ ,\ \text{if}\ x \geq 0 \\
&= -1\ ,\ \text{if}\ x < 0\,. \qquad (2.177)
\end{aligned}$$

For a spatial distribution of an atomic beam as considered in the preceding section, the time interval Δt is related to an effective number of atoms in the field mode as

$$\Delta t = \left(\frac{t_{int}}{\sqrt{2}\,\langle N_{atom}\rangle}\right)\,.$$

Note that we do not have the $\frac{1}{2}$ factor due to the $\sin^2 kz$ dependence of the coupling constant because we assumed that all the atoms are located at the anti-nodes of the cavity field mode. Any convergent solutions of Eq.2.176 are obtained by letting $x_{n+1} = x_n = a_o^2$ and solving a resulting equation.

$$a_o = \sqrt{\frac{2}{\pi}\frac{g_o}{\Gamma_c}}\,\langle N_{atom}\rangle\int_{-\Delta q}^{\Delta q} dq\ \mathrm{e}^{-q^2}\sin\left\{\Theta_o a_o\mathrm{Err}(q) + \left[\Theta_p\mathrm{Err}\left(\frac{q-q_o}{w_p/w_m}\right)-\pi\right]\right\}\,. \qquad (2.178)$$

Among the solutions, only the ones satisfying the following condition are stable against small fluctuations.

$$\left|\left.\frac{df}{dx_n}\right|_{x_n=a_o^2}\right| < 1\,.$$

Only these solutions are physically meaningful solutions, which are observable in experiments.

Reduction to Stepwise Coupling Case

If the coupling constant is stepwise as shown in Fig. 2-10, the solution above is greatly simplified. First notice that Eq.2.167 reduces to

$$\dot{a}+\frac{\Gamma_c}{2}a=-\frac{1}{2}g_o\sin\left(2g_0\int_{-T_{int}/2}^{t}a(t')dt'+\pi\right)=\frac{1}{2}g_o\sin\left(2g_0\int_{-T_{int}/2}^{t}a(t')dt'\right)\ , \tag{2.179}$$

from which

$$\begin{aligned}\alpha_{n+1}^2 &\approx \alpha_n^2(1-\Gamma_c\Delta t)+g_o\alpha_n\int_{-T_{int}/2}^{T_{int}/2}\sin\left[2g_o\alpha_n\left(t+T_{int}/2\right)\right]dt\\ &= \alpha_n^2(1-\Gamma_c\Delta t)-\frac{1}{2}\cos\left[2g_o\alpha_n\left(t+T_{int}/2\right)\right]\Big|_{-T_{int}/2}^{T_{int}/2}\\ &= \alpha_n^2(1-\Gamma_c\Delta t)+\frac{1}{2}\left[1-\cos\left(2g_o\alpha_nT_{int}\right)\right]\\ &= \alpha_n^2(1-\Gamma_c\Delta t)+\sin^2\left(g_o\alpha_nT_{int}\right)\ ,\end{aligned} \tag{2.180}$$

which is nothing but Eq.2.157.

Results: Pump Position Dependence

Using Eq.2.167, we can study the effects of the pump laser when is placed near and even in the cavity. Figure 2-22 shows the predicted mean number of photons as a function of the position of the pump laser. Interestingly there are two solutions for some values of the pump position. If the pump field overlaps with the cavity field mode even slightly, the resulting pump pulse area in Eq.2.176 is less than π, and hence there are two different recursion relations, one corresponding to positive α_n and the other to negative α_n. According to the discussion in Sec.2.2.2, a largest stable solution of each recursion relation approximately corresponds to a physically observable solution. Since a fluctuation cannot change the sign of the field amplitude unless it is very small, the two photon number solutions are legitimate solutions and should be physically observable. The larger photon number solution corresponds to a cavity field antiparallel to the pump laser field and the smaller one to the field parallel to the pump field. When the pump field does not overlap with the cavity mode, these

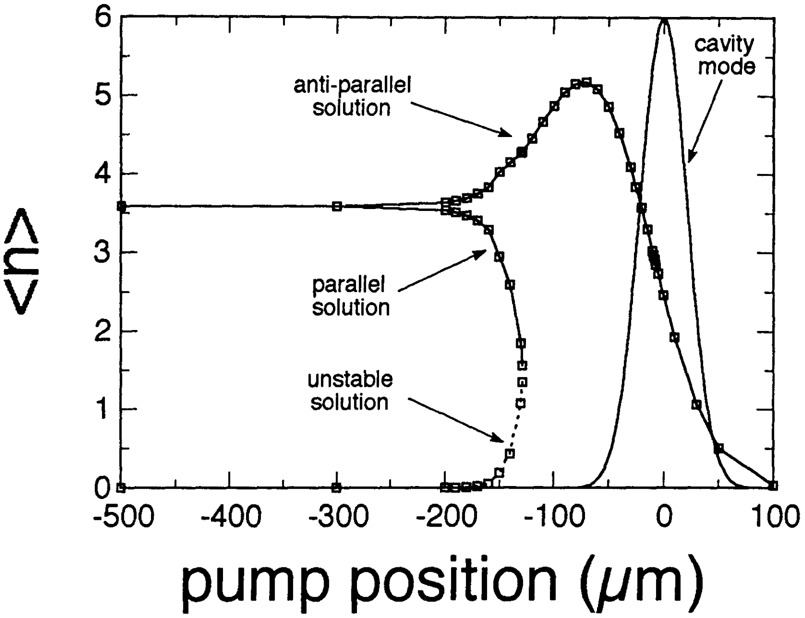

Figure 2-22: Dependence of the position of the pump laser. Notice that the photon buildup is maximized when the pump laser is placed just outside the cavity mode. we assumed $\langle N_{atom} \rangle = 1$, $g_o/\Gamma_c = 2.4$, $\Theta_m = 1.1$, $\Theta_p = \pi$, $w_p = 90\mu m$, and $w_m = 42\mu m$.

two solutions are degenerate. In Chapter 3 we will compare this prediction with the data.

Interestingly the largest $\langle n \rangle$ can be generated when the pump laser is placed just outside the cavity mode, i.e., $x_o \approx -w_m$. This is due to the fact that the photon build-up is maximized when the atoms are prepared in a superposition state of the two energy levels as discussed in page 56 in Sec.2.1.5. As shown in Fig.2-9, the maximum occurs when the atomic state is 30 % – 70 % mixture of the lower level and the upper level. When the pump is just outside of the mode, the atoms in the cavity mode have not undergone a complete π-excitation, and hence they are in a superposition state while interacting with the cavity field mode. Notice that $\langle n \rangle$ is relatively small when the pump laser is right inside the cavity. Recall that the atomic population is maximally created at the end of the pumping process. However at the end of the π-excitation the atoms are exiting the cavity, and hence do not have any chance to interact with the field. If the pump is place past the cavity mode, $\langle n \rangle$ cannot build up since the atoms entering the cavity are not excited at all.

2.3 Semiclassical Theory of Many-Atom Laser

2.3.1 Model

The quantum theory in Sec.2.1.1 and the semiclassical model in Sec.2.2 assume at most only one atom is present in the cavity. Experimentally, however, we can continuously increase the atomic beam flux until more than one atom are present in average. Although it would be extremely difficult to derive a quantum theory for a few atoms interacting with the same cavity field, it is relatively easy to formulate the operation with a large number of atoms. We can define macroscopic quantities averaged over unit volume, replacing variables associated with individual atoms.

Suppose a beam of excited atoms entering the cavity at a same velocity v. The dimension of the atomic beam in the direction perpendicular to the cavity axis, denoted by h, is assume to be much smaller than the waist of the cavity mode, w_m, and the dimension along the cavity axis, denoted by l, is supposed to be much shorter than the cavity length as depicted in Figure 2-23. As discussed before, the coupling constant between an atom and the field mode depends on the position of the atom. The $\sin^2 kz$ dependence can be taken into account by an effective mean number of atoms in the mode. So for simplicity of calculation, we assume that all the atoms are located at the anti-nodes of the cavity field mode. The Maxwell-Schrödinger equations for such system are

$$
\begin{aligned}
\dot{\sigma}_k + \frac{\Gamma_a}{2}\sigma_k &= -(g_k a + \Omega_R^k/2)N_k && (2.181)\\
\dot{a} + \frac{\Gamma_c}{2}a &= -\sum_k^{\infty} g_k\sigma_k && (2.182)\\
\dot{N}_k + \Gamma_a(N_k+1) &= 4(g_k a + \Omega_R^k/2)\sigma_k\ , && (2.183)
\end{aligned}
$$

where g_k is the coupling constant at the position of the k-th atom and Ω_R^k is the Rabi frequency of the pump laser at the same position.

Let's consider a small volume ΔV, which encloses a small number of atoms and moves along with the atoms in it at a velocity v. We introduce polarization density

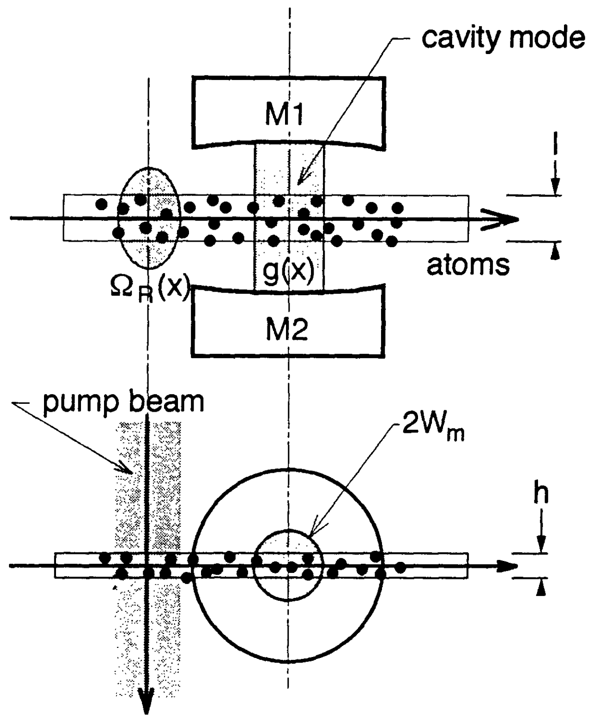

Figure 2-23: Many-atom laser

$\sigma(t;x_o)$ and inversion density $n(t;x_o)$ defined as

$$\sigma(t;x_o) \equiv \frac{1}{\Delta V}\sum_{\text{at } x=vt+x_o}^{\Delta V} \sigma_k(t) \tag{2.184}$$

$$n(t;x_o) \equiv \frac{1}{\Delta V}\sum_{\text{at } x=vt+x_o}^{\Delta V} N_k(t)\,. \tag{2.185}$$

Then the Maxwell-Schrödinger equations reduce to

$$\frac{d\sigma(t;x_o)}{dt}+\frac{\Gamma_a}{2}\sigma(t;x_o) = -\left(g(x)a(t)+\frac{\Omega_R(x)}{2}\right)\Bigg|_{x=vt+x_o} n(t;x_o) \tag{2.186}$$

$$\frac{dn(t;x_o)}{dt}+\Gamma_a\left[n(t;x_o)+n_o\right] = 4\left(g(x)a(t)+\frac{\Omega_R(x)}{2}\right)\Bigg|_{x=vt+x_o} \sigma(t;x_o) \tag{2.187}$$

$$\begin{aligned}\frac{da}{dt}+\frac{\Gamma_c}{2}a &= -\sum_{\Delta V}^{\infty} g(x)|_{x=vt+x_o}\,\sigma(t;x_o)\Delta V \\ &\rightarrow -lh\int_{-\infty}^{\infty} g(x)|_{x=vt+x_o}\,\sigma(t;x_o)dx_o\,,\end{aligned} \tag{2.188}$$

where n_o is defined as

$$n_o = \frac{1}{\Delta V} \sum_{\text{at } x=vt+x_o}^{\Delta V} 1 \,. \tag{2.189}$$

2.3.2 Negligible Atomic Damping

First we consider a case in which the atomic spontaneous emission decay is negligible compared to the time evolution of the system. There exists a constant of motion,

$$4\sigma \frac{d\sigma}{dt} + n \frac{dn}{dt} = 0 \,, \tag{2.190}$$

or

$$4\sigma^2(t;x_o) + n^2(t;x_o) = \text{constant} = n_o^2 \,. \tag{2.191}$$

The value of the constant is determined by an initial condition,

$$4\sigma^2(-\infty;x_o) + n^2(-\infty;x_o) = n^2(-\infty;x_o) = n_o^2 \,.$$

Eq.2.191 suggests the following substitution.

$$n(t;x_o) = -n_o \cos\theta(t;x_o) \tag{2.192}$$

$$\sigma(t;x_o) = \frac{n_o}{2} \sin\theta(t;x_o) \,. \tag{2.193}$$

Substituting Eq.2.193 into Eq.2.186, we find

$$\frac{d\theta(t;x_o)}{dt} = \left[2g(x)a(t) + \Omega_R(x)\right]_{x=vt+x_o} \,, \tag{2.194}$$

Stepwise Cavity Mode

If the cavity mode is described by a stepwise function,

$$\begin{aligned} g(x) &= g_o \,, \quad |x| < w_m \\ & \ 0 \,, \quad \text{otherwise,} \end{aligned}$$

and if the pump laser is placed well before the cavity, Eq.2.194 is simply

$$\frac{d\theta(t;x_o)}{dt} = 2g_o a(t)\ , \tag{2.195}$$

and hence

$$\theta(t;x_o) = 2g_o \int_{-\frac{w_m - x_o}{v}}^{t} a(t')dt' + \pi \tag{2.196}$$

for $-\frac{w_m - x_o}{v} < t < \frac{w_m - x_o}{v}$. Eq.2.188 is then reduced to

$$\begin{aligned} \frac{da(t)}{dt} + \frac{\Gamma_c}{2}a(t) &= -lhg_o \int_{-w_m - vt}^{w_m - vt} \sigma(t;x_o)dx_o \\ &= \frac{1}{2}lhg_o n_o \int_{-w_m - vt}^{w_m - vt} \sin\left[2g_o \int_{-\frac{w_m + x_o}{v}}^{t} a(t')dt'\right] dx_o\ . \end{aligned} \tag{2.197}$$

Multiply $a(t)$ to the both sides and integrate from $-T_{int}/2$ to $T_{int}/2$.

$$\begin{aligned} &\frac{1}{2}\left[a\left(\frac{T_{int}}{2}\right) - a\left(-\frac{T_{int}}{2}\right)\right] + \frac{\Gamma_c T_{int}}{2}\langle n\rangle \\ &= \frac{1}{2}lhg_o n_o \int_{-\frac{T_{int}}{2}}^{\frac{T_{int}}{2}} a(t)\left\{\int_{-w_m - vt}^{w_m - vt} \sin\left[2g_o \int_{-\frac{w_m + x_o}{v}}^{t} a(t')dt'\right] dx_o\right\} dt\ , \end{aligned} \tag{2.198}$$

where

$$\langle n\rangle = \frac{1}{T_{int}} \int_{-\frac{T_{int}}{2}}^{\frac{T_{int}}{2}} a^2(t)dt\ .$$

We assume that $\langle n\rangle \gg 1$ so that

$$a(t) \approx a\left(-\frac{T_{int}}{2}\right) \equiv a_i\ ,\quad -\frac{3T_{int}}{2} < t < \frac{T_{int}}{2}\ .$$

Therefore, with a notation, $a_f \equiv a\left(\frac{T_{int}}{2}\right)$, we obtain

$$\begin{aligned} &\left(a_f^2 - a_i^2\right) + \Gamma_c T_{int} a_i^2 \\ &= lhg_o n_o a_i \int_{-\frac{T_{int}}{2}}^{\frac{T_{int}}{2}} dt \int_{-w_m - vt}^{w_m - vt} \sin\left[2g_o a_i\left(t + \frac{w_m + x_o}{v}\right)\right] dx_o \\ &= lhg_o n_o a_i \int_{-\frac{T_{int}}{2}}^{\frac{T_{int}}{2}} dt \left\{-\frac{\cos\left[2g_o a_i\left(t + \frac{w_m + x_o}{v}\right)\right]}{2g_o a_i/v}\right\}\Bigg|_{-w_m - vt}^{w_m - vt} \end{aligned}$$

$$
\begin{aligned}
&= lhn_o v \int_{-\frac{T_{int}}{2}}^{\frac{T_{int}}{2}} dt \left[\frac{1-\cos\left(2g_o a_i T_{int}\right)}{2}\right] \\
&= lhn_o v T_{int} \sin^2\left(g_o a_i T_{int}\right) \\
&= 2lhw_m n_o \sin^2\left(g_o a_i T_{int}\right) \qquad (2.199)
\end{aligned}
$$

Recall that all the atoms are assumed to be located at the anti-nodes of the cavity mode and n_o is the density of such atoms. Since $2lhw_m$ is the volume of the atomic beam in the cavity mode, the total number of atoms in the cavity, $\langle N_{atom}\rangle$, is $2lhw_m n_o$. Then Eq.2.199 becomes

$$
a_f^2 = a_i^2\left(1-\Gamma_c T_{int}\right) + \langle N_{atom}\rangle \sin^2\left(g_o a_i T_{int}\right) \ , \qquad (2.200)
$$

which is a recursion relation, describing a time evolution of the field as a function of the number of groups of $\langle N_{atom}\rangle$ atoms. Any convergent solutions, whether they are stable or not, are obtained by letting $a_i = a_f = a_\infty$.

$$
a_\infty^2 = \frac{\langle N_{atom}\rangle}{\Gamma_c T_{int}} \sin^2\left(g_o a_\infty T_{int}\right) \ . \qquad (2.201)
$$

A stability condition is

$$
\left|\left.\frac{df}{dx}\right|_{x=a_\infty^2}\right| < 1 \ , \qquad (2.202)
$$

where

$$
f(x) = x\left(1-\Gamma_c T_{int}\right) + \langle N_{atom}\rangle \sin^2\left(g_o\sqrt{x}T_{int}\right) \ . \qquad (2.203)
$$

Gaussian Cavity Mode

In experiments, the cavity and the pump laser are described by gaussian mode functions.

$$
\begin{aligned}
g(x) &= g_o\, \mathrm{e}^{-\left(\frac{x}{w_m}\right)^2} \\
\Omega_R(x) &= \Omega_R^o\, \mathrm{e}^{-\left(\frac{x-x_p}{w_p}\right)^2} \ .
\end{aligned}
$$

In this case Eq.2.194 becomes

$$
\begin{aligned}
\frac{d\theta(t;x_o)}{dt} &= 2g_o\,\mathrm{e}^{-\left(\frac{vt+x_o}{w_m}\right)^2} a(t) + \Omega_R^o\,\mathrm{e}^{-\left(\frac{vt+x_o-x_p}{w_p}\right)^2} && (2.204)\\
\theta(t;x_o) &= \int_{-\infty}^{t}\left[2g_o\,\mathrm{e}^{-\left(\frac{vt'+x_o}{w_m}\right)^2} a(t') + \Omega_R^o\,\mathrm{e}^{-\left(\frac{vt'+x_o-x_p}{w_p}\right)^2}\right] dt'\,. && (2.205)
\end{aligned}
$$

$$
\begin{aligned}
&\frac{da(t)}{dt} + \frac{\Gamma_c}{2}a(t)\\
&= -lh\int_{-\infty}^{\infty} g(x=vt+x_o)\sigma(t;x_o)dx_o\\
&= -\frac{1}{2}lhg_on_o\int_{-\infty}^{\infty}\mathrm{e}^{-\left(\frac{vt+x_o}{w_m}\right)^2}\\
&\quad\times\sin\left\{\int_{-\infty}^{t}\left[2g_o\,\mathrm{e}^{-\left(\frac{vt'+x_o}{w_m}\right)^2} a(t') + \Omega_R^o\,\mathrm{e}^{-\left(\frac{vt'+x_o-x_p}{w_p}\right)^2}\right] dt'\right\} dx_o\,. \quad (2.206)
\end{aligned}
$$

Multiply $a(t)$ to the both sides and integrate from $-t_{int}/2$ to $t_{int}/2$.

$$
\begin{aligned}
&\frac{1}{2}\left[a\left(\frac{t_{int}}{2}\right)^2 - a\left(-\frac{t_{int}}{2}\right)^2\right] + \frac{\Gamma_c}{2}\int_{-\frac{t_{int}}{2}}^{\frac{t_{int}}{2}} a^2(t)dt\\
&= -\frac{1}{2}lhg_on_o\int_{-\frac{t_{int}}{2}}^{\frac{t_{int}}{2}} a(t)\int_{-\infty}^{\infty}\mathrm{e}^{-\left(\frac{vt+x_o}{w_m}\right)^2}\\
&\quad\times\sin\left\{\int_{-\infty}^{t}\left[2g_o\,\mathrm{e}^{-\left(\frac{vt'+x_o}{w_m}\right)^2} a(t') + \Omega_R^o\,\mathrm{e}^{-\left(\frac{vt'+x_o-x_p}{w_p}\right)^2}\right] dt'\right\} dx_odt\,. \quad (2.207)
\end{aligned}
$$

The first gaussian function is negligibly small when $|x_o + vt| > w_m$, and hence the x_o integration is appreciable only in a range,

$$-w_m - vt < x_o < w_m - vt\,.$$

Similarly t' integration is important only in a range,

$$-w_m - x_o < vt' < w_m - x_o\,.$$

Since t is varied from $-t_{int}/2$ to $t_{int}/2$, the significant range of x_o is at largest

$$-2w_m < x_o < 2w_m \ ,$$

and hence the important range of t' is at largest

$$-\frac{3t_{int}}{2} < t' < t < \frac{t_{int}}{2} \ .$$

Now we assume that $a(t)$ in this time interval can be approximated as the value at the midpoint of the interval,

$$a(t) \approx a\left(t = -\frac{t_{int}}{2}\right) \equiv a_i \ . \tag{2.208}$$

With a notation, $a\left(t = \frac{t_{int}}{2}\right) \equiv a_f$, Eq.2.207 then becomes

$$\begin{aligned}
&\left(a_f^2 - a_i^2\right) + a_i^2 \Gamma_c t_{int} \\
&= \ -lhg_o n_o a_i \int_{-\frac{t_{int}}{2}}^{\frac{t_{int}}{2}} \int_{-\infty}^{\infty} \mathrm{e}^{-\left(\frac{vt+x_o}{w_m}\right)^2} \\
&\quad \times \sin\left\{ \int_{-\infty}^{t} \left[2g_o \, \mathrm{e}^{-\left(\frac{vt'+x_o}{w_m}\right)^2} a_i + \Omega_R^o \, \mathrm{e}^{-\left(\frac{vt'+x_o-x_p}{w_p}\right)^2} \right] dt' \right\} dx_o dt \\
&= \ -lhw_m g_o n_o a_i \int_{-\frac{t_{int}}{2}}^{\frac{t_{int}}{2}} \int_{-\infty}^{\infty} \mathrm{e}^{-q^2} \\
&\quad \times \sin\left[2g_o a_i \frac{w_m}{v} \int_{-\infty}^{q} \mathrm{e}^{-q'^2} dq' + \Omega_R^o \frac{w_p}{v} \int_{-\infty}^{\frac{q-q_p}{w_p/w_m}} \mathrm{e}^{-q''^2} dq'' \right] dq dt \ ,
\end{aligned}$$

where

$$q' \equiv \frac{vt' + x_o}{w_m} \ , \ dq' = \frac{v}{w_m} dt' \tag{2.209}$$

$$q'' \equiv \frac{vt'' + x_o - x_p}{w_p} \ , \ dq'' = \frac{v}{w_p} dt'' \tag{2.210}$$

$$q \equiv \frac{x_o + vt}{w_m} \ , \ dq = \frac{1}{w_m} dx_o \ . \tag{2.211}$$

Using the definition of $\mathrm{Err}(x)$ in Eq.2.172,

$$\begin{aligned}
&\left(a_f^2 - a_i^2\right) + a_i^2 \Gamma_c t_{int} \\
&= -lhw_m g_o n_o a_i t_{int} \int_{-\infty}^{\infty} \mathrm{e}^{-q^2} \sin\left[2 g_o a_i t_{int} \mathrm{Err}(q) + \Omega_R^o t_p \mathrm{Err}\left(\frac{q - q_p}{w_p / w_m}\right)\right] dq \\
&= -\frac{1}{2} lhw_m n_o a_i \Theta_m \int_{-\infty}^{\infty} \mathrm{e}^{-q^2} \sin\left[\Theta_m a_i \mathrm{Err}(q) + \Theta_p \mathrm{Err}\left(\frac{q - q_p}{w_p / w_m}\right)\right] dq \ , \qquad (2.212)
\end{aligned}$$

where Θ_m and Θ_p are defined by Eqs.2.174 and 2.175 respectively. Recall that the atoms are assumed to be at the anti-nodes of the field mode. So the density n_o is the density of such specially distributed atoms. Then an effective mean number of atoms in the mode is

$$\langle N_{atom} \rangle = n_o \int_{-\infty}^{\infty} dx \int_{-h/2}^{h/2} dy \int_{l/2}^{l/2} dz \ \mathrm{e}^{-2\left(\frac{x}{w_m}\right)^2} = n_o \left(hlw_m \sqrt{\frac{\pi}{2}} \right) \ . \qquad (2.213)$$

As in reality, if the atoms are randomly distributed in the beam,

$$\begin{aligned}
\langle N_{atom} \rangle &= n_{o,all} \int_{-\infty}^{\infty} dx \int_{-h/2}^{h/2} dy \int_{l/2}^{l/2} dz \ \mathrm{e}^{-2\left(\frac{x}{w_m}\right)^2} \cos^2 kz \\
&\approx n_{o,all} \int_{-\infty}^{\infty} dx \int_{-h/2}^{h/2} dy \ \mathrm{e}^{-2\left(\frac{x}{w_m}\right)^2} \ \frac{l}{2} \\
&= n_{o,all} \left(\frac{hlw_m}{2} \sqrt{\frac{\pi}{2}} \right) \ , \qquad (2.214)
\end{aligned}$$

with $n_{o,all}$ being the density associated with any atoms, which can be measured in experiments. Hence

$$\begin{aligned}
a_f^2 &= a_i^2 \left(1 - \Gamma_c t_{int}\right) + \frac{\langle N_{atom} \rangle \, \Theta_m a_i}{\sqrt{2\pi}} \int_{-\infty}^{\infty} \mathrm{e}^{-q^2} \\
&\times \sin\left\{ \Theta_m a_i \mathrm{Err}(q) + \left[\Theta_p \mathrm{Err}\left(\frac{q - q_p}{w_p / w_m}\right) - \pi \right] \right\} dq \ , \qquad (2.215)
\end{aligned}$$

which is a recursion relation, describing a time evolution of the field in a time scale of t_{int}. From a field amplitude at time t, a field amplitude at time $t + t_{int}$ is given by the relation.

Any convergent solutions, whether they are stable or not, are obtained by letting

$a_i = a_f = \alpha_\infty$.

$$\begin{aligned}\alpha_\infty &= \frac{g_o}{\Gamma_c}\sqrt{\frac{2}{\pi}}\,\langle N_{atom}\rangle \int_{-\infty}^{\infty} \mathrm{e}^{-q^2} \\ &\quad \times \sin\left\{\Theta_m \alpha_\infty \mathrm{Err}(q) + \left[\Theta_p \mathrm{Err}\left(\frac{q-q_p}{w_p/w_m}\right) - \pi\right]\right\} dq\,. \qquad (2.216)\end{aligned}$$

A stability condition is

$$\left|\frac{df}{dx}\bigg|_{x=a_\infty^2}\right| < 1\,, \qquad (2.217)$$

where

$$\begin{aligned}f(x) &= x\left(1-\Gamma_c t_{int}\right) + \frac{\langle N_{atom}\rangle\,\Theta_m \sqrt{x}}{\sqrt{2\pi}} \int_{-\infty}^{\infty} \mathrm{e}^{-q^2} \\ &\quad \times \sin\left\{\Theta_m \sqrt{x}\,\mathrm{Err}(q) + \mathrm{Sign}(\alpha_\infty)\left[\Theta_p \mathrm{Err}\left(\frac{q-q_p}{w_p/w_m}\right) - \pi\right]\right\} dq \qquad (2.218)\end{aligned}$$

where

$$\begin{aligned}\mathrm{Sign}(x) &= +1\ ,\ \text{if}\ x \geq 0 \\ &= -1\ ,\ \text{if}\ x < 0\,. \qquad (2.219)\end{aligned}$$

If the pump is positioned well before the cavity ($q_p \rightarrow -\infty$),

$$\mathrm{Err}\left(\frac{q-q_p}{w_p/w_m}\right) \rightarrow \mathrm{Err}(\infty) = 1\,.$$

So if $\Theta_p = \pi$, the second term in the sine function vanishes.

$$\alpha_\infty = \frac{g_o}{\Gamma_c}\sqrt{\frac{2}{\pi}}\,\langle N_{atom}\rangle \int_{-\infty}^{\infty} \mathrm{e}^{-q^2} \sin\left[\Theta_m \alpha_\infty \mathrm{Err}(q)\right] dq\,. \qquad (2.220)$$

2.3.3 Non-negligible Atomic Damping

A. Mean Field Representation

When the atomic damping is not negligibly small, $n^2 + 4\sigma^2$, which was a constant of motion in the case of negligible atomic damping, is not constant any more. Consequently the pulse area $\theta(t;x_o)$ is not a useful parameter to work with. In this limit, time-averaged Maxwell-Schrödinger equations instead provide useful insights on the system.

We consider a steady-state solution of the Maxwell-Schrödinger equations. In a steady state the explicit time dependence in $n(x,t)$, $\sigma(x,t)$ and $a(t)$ all disappear, where $n(x,t)$ and $\sigma(x,t)$ are related to $n(t;x_o)$ and $\sigma(t;x_o)$ in the following way.

$$\begin{aligned} n(x,t) &= n(x=vt+x_o,t) \equiv n(t;x_o) \\ \sigma(x,t) &= \sigma(x=vt+x_o,t) \equiv \sigma(t;x_o)\,. \end{aligned} \tag{2.221}$$

Absence of any explicit time dependence means

$$\begin{aligned} n(x,t) &\rightarrow n(x=vt+x_o) \\ \sigma(x,t) &\rightarrow \sigma(x=vt+x_o) \\ a(t) &\rightarrow a_o\,. \end{aligned} \tag{2.222}$$

Then the Maxwell-Schrödinger equations are

$$v\frac{d\sigma(x)}{dx}+\frac{\Gamma_a}{2}\sigma(x) = -(g(x)a_o+\Omega_R(x)/2)n(x) \tag{2.223}$$

$$v\frac{dn(x)}{dx}+\Gamma_a\left[n(x)+n_o\right] = 4(g(x)a_o+\Omega_R(x)/2)\sigma(x) \tag{2.224}$$

$$a_o = -\frac{2lh}{\Gamma_c}\int dx g(x)\sigma(x)\,. \tag{2.225}$$

For simplicity, lets consider a pump laser positioned far away from the cavity and a cavity mode described by a stepwise function, which is $g(x)=g_o$ if $|x|<w_m$, and $g(x)=0$ otherwise. Integrating Eq.2.223 from $x=-w_m$ to $x=w_m$,

$$v\sigma(x)|_{-w_m}^{w_m}+\frac{\Gamma_a}{2}\int_{-w_m}^{w_m}\sigma(x)dx = -g_oa_o\int_{-w_m}^{w_m}n(x)dx\,. \tag{2.226}$$

and defining spatially averaged variables

$$\bar{\sigma} \equiv \frac{1}{2w_m}\int_{-w_m}^{w_m} \sigma(x)dx \tag{2.227}$$

$$\bar{n} \equiv \frac{1}{2w_m}\int_{-w_m}^{w_m} n(x)dx \ , \tag{2.228}$$

we then obtain

$$\Gamma_{tr}\left[\sigma(w_m) - \sigma(-w_m)\right] + \frac{\Gamma_a}{2}\bar{\sigma} = -a_o g_o \bar{n} \ , \tag{2.229}$$

where Γ_{tr} is a transit time broadening rate, defined as

$$\Gamma_{tr} \equiv \frac{1}{T_{int}} = \frac{v}{2w_m} \ . \tag{2.230}$$

Similarly we can rewrite Eqs.2.187 and 2.188 as

$$\Gamma_{tr}\left[n(w_m) - n(-w_m)\right] + \Gamma_a\left[\bar{n} + n_o\right] = 4a_o g_o \bar{\sigma} \tag{2.231}$$

$$a_o = -4lhw_m \frac{g_o}{\Gamma_a}\bar{\sigma}. \tag{2.232}$$

Recall that all the atoms are assumed to be located at the anti-nodes of the cavity mode and n_o is the density of such atoms. Since $2lhw_m$ is the volume of the atomic beam in the cavity mode, the total number of atoms in the cavity, N_o, is $2lhw_m n_o$. Similarly we can define a total inversion and a total induced dipole in the cavity as

$$S(x) \equiv (2lhw_m)\sigma(x) \tag{2.233}$$

$$N(x) \equiv (2lhw_m)n(x) \tag{2.234}$$

$$\bar{S} \equiv (2lhw_m)\bar{\sigma} \tag{2.235}$$

$$\bar{N} \equiv (2lhw_m)\bar{n} \ . \tag{2.236}$$

Assuming that the pump laser is adjusted for π-pulse excitation so that $N(-w_m) = N_o$ and $S(-w_m) = 0$, we can rewrite the Maxwell-Schrödinger equations as

$$\Gamma_{tr}S_f + \frac{\Gamma_a}{2}\bar{S} = -ag_o\bar{N} \tag{2.237}$$

$$\begin{aligned}\Gamma_{tr}(N_f - N_o) + \Gamma_a\left[\bar{N} + N_o\right] &= 4ag_o\bar{S} \qquad (2.238)\\ \Gamma_c a &= -2g_o\bar{S}\ , \qquad (2.239)\end{aligned}$$

where $S_f \equiv S(w_m)$ and $N_f \equiv N(w_m)$.

Reduction to Negligible Damping Limit

We can recover Eq.2.201 by letting $\Gamma_a \to 0$ in the above equations. This means that Eqs.2.237,2.238 and 2.239 are still equivalent the original Maxwell-Schrödinger equations, Eqs.2.186, 2.187 and 2.188. In order to show this, first note that in a steady state Eq.2.194 reads

$$v\frac{d\theta}{dx} = 2g_o a_o \text{ for } |x| < w_m\ , \qquad (2.240)$$

and hence

$$\theta(x) = 2g_o a_o\left(\frac{x + w_m}{v}\right) + \pi\ , \text{for } |x| < w_m\ . \qquad (2.241)$$

Then

$$\begin{aligned}\bar{S} &= \frac{1}{2w_m}\int_{-w_m}^{w_m}\frac{N_o}{2}\sin\theta(x)dx\\ &= \frac{N_o}{4w_m}\int_{-w_m}^{w_m}\sin\left[2g_o a_o\left(\frac{x + w_m}{v}\right) + \pi\right]dx\\ &= -\frac{N_o}{4w_m}\int_{-w_m}^{w_m}\sin\left[2g_o a_o\left(\frac{x + w_m}{v}\right)\right]dx\\ &= -\frac{N_o}{4w_m}\left\{-\frac{\cos\left[2g_o a_o\left(\frac{x+w_m}{v}\right)\right]}{2g_o a_o/v}\right\}\Bigg|_{-w_m}^{w_m}\\ &= -\frac{N_o}{2g_o a_o T_{int}}\frac{1 - \cos\left(2g_o a_o T_{int}\right)}{2}\\ &= -\frac{N_o}{2g_o a_o T_{int}}\sin^2\left(g_o a_o T_{int}\right)\ .\end{aligned}$$

From Eq.2.239 we then obtain

$$a_o^2 = -\frac{2g_o a_o}{\Gamma_c}\bar{S}$$

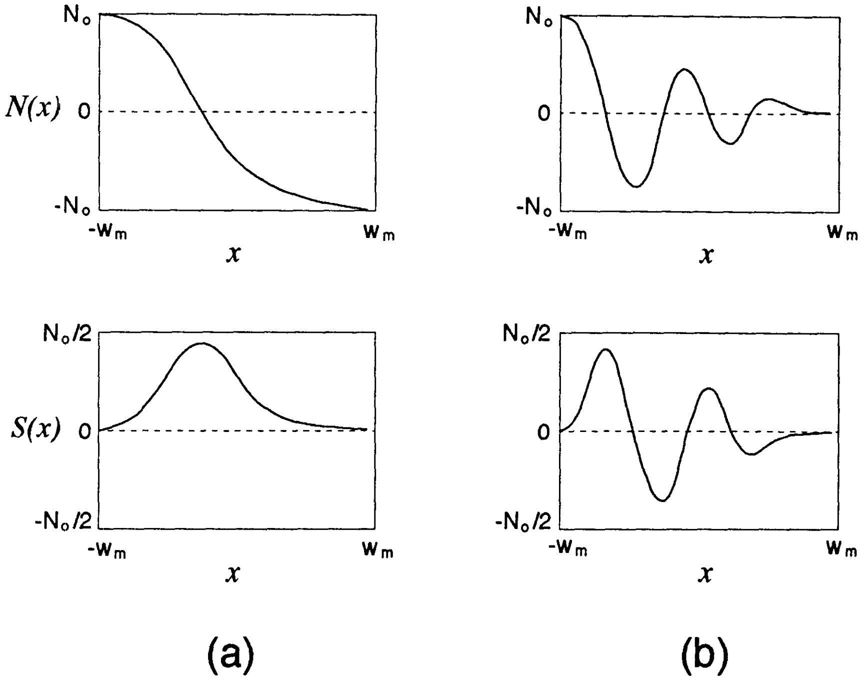

Figure 2-24: Rate equation approximation can be applied to two limiting cases, which are (a) over-damping and (b) saturation limits.

$$= \frac{N_o}{\Gamma_c T_{int}} \sin^2 (g_o a_o T_{int}) \ , \tag{2.242}$$

which is nothing but Eq.2.201.

B. Rate Equation Approximation

If the atomic damping is not negligible, the dephasing of atomic dipole moments will diminish the collective behavior of the dipoles appearing in Eqs.2.216 and 2.201. Consequently Rabi oscillation characteristics in the total dipole moment would be washed away at the end of the interaction, resulting in a constant S_f, which is insensitive to the details of the atom-field interactions. This assumption is equivalent to "rate equation approximation, which is often used in the analyses of conventional lasers. In this rate equation limit, we can think of two limiting cases of interest as illustrated in Figure 2-24. One case is *over-damping* limit, where the atomic damping leads to complete decay of the total atomic dipole and population at the end of the interaction, so $S_f = 0$ and $N_f = -N_o$. Another interesting limit is *saturation* limit, in which the atoms are fully saturated during the interaction, and therefore leaving the cavity either in the excited state or in the ground state with equal probabilities. In this case N_f as well as S_f are vanishing.

In both cases Eqs.2.237, 2.238 and 2.239 reduce to familiar rate equations. Substituting Eq.2.239 into Eq.2.237, we obtain

$$\Gamma_a \Gamma_c a = 4 a g_o^2 \bar{N}$$

or

$$\frac{4g_o^2}{\Gamma_a} \langle n \rangle \bar{N} - \Gamma_c \langle n \rangle = 0 \rightarrow \frac{d \langle n \rangle}{dt} , \tag{2.243}$$

which can be thought as a rate equation for the mean number of photons, $\langle n \rangle$. From Eq.2.238, on the other hand,

$$-\eta N_o \Gamma_{tr} + \Gamma_a \left[\bar{N} + N_o \right] = 4 a g_o \bar{S} \tag{2.244}$$

or

$$N_o \left(\frac{\eta \Gamma_{tr}}{2} - \frac{\Gamma_a}{2} \right) - \frac{\Gamma_a}{2} \bar{N} - \frac{4g_o^2}{\Gamma_a} \langle n \rangle \bar{N} = 0 \rightarrow \frac{dN}{dt} , \tag{2.245}$$

where $\eta = 2$ for over-damping limit, and $\eta = 1$ for saturation limit. Eq.2.245 can be thought as a rate equation for the total population inversion, N. We can identify a pumping term,

$$N_o \left(\frac{\eta \Gamma_{tr}}{2} - \frac{\Gamma_a}{2} \right) \rightarrow R_p$$

and a laser coupling coefficient, K,

$$\frac{4g_o^2}{\Gamma_a} \rightarrow K$$

which appear in the rate equations for the conventional lasers in Ref.[52]. It is easily seen from Eq.2.243 that $\bar{N} K \left(\frac{L}{c} \right)$ is nothing but a *saturated* single-pass gain in a laser.

$$K \bar{N} = \frac{4g_o^2}{\Gamma_a} \bar{N} = \Gamma_c$$

Since an absorption cross section is given by

$$\sigma_o = \frac{4\pi\mu^2\omega}{\hbar\frac{\Gamma_a}{2}c},$$

and

$$g_o = \frac{\mu}{\hbar}\sqrt{\frac{2\pi\hbar\omega}{V}},$$

we find

$$\begin{aligned} 1 &= \frac{\frac{4g_o^2}{\Gamma_a}\bar{N}}{\Gamma_c} \\ &= \frac{\bar{N}\sigma_o c}{V\Gamma_c} \\ &= \frac{\bar{N}\sigma_o c}{V2\frac{c}{2L}(1-R)} \\ &= \frac{\frac{\bar{N}}{V}\sigma_o L}{1-R} \end{aligned}$$

The numerator, $\frac{\bar{N}}{V}\sigma_o L$ is nothing but a single pass gain while $(1-R)$ is a loss due to cavity decay. The equality means that the single pass gain saturates to the value that exactly compensates the loss in the system. This is a well-known steady-state behavior of conventional lasers above threshold [53].

The rate equations, Eqs.2.243 and 2.245 have an exact solution.

$$\langle n\rangle = \frac{\eta\Gamma_{tr}}{2\Gamma_c}\left(1-\frac{\Gamma_a}{\eta\Gamma_{tr}}\right)(N_o - N_{th}) \tag{2.246}$$

where N_{th} is a threshold value for the number of atoms for laser oscillation,

$$N_{th} \equiv \frac{\left(\frac{\Gamma_a}{2g_o}\right)^2\left(\frac{\Gamma_c}{\eta\Gamma_{tr}}\right)}{1-\left(\frac{\Gamma_a}{\eta\Gamma_{tr}}\right)} \tag{2.247}$$

For an example, under our experimental conditions, N_{th} is about 8×10^{-4} and the constant multiplied to N_o is about 3.1 if we assume the over-damping limit, so

$$\langle n\rangle \approx 3.1\left(N_o - 8\times10^{-4}\right)$$

This result will be compared with the experimental data and the predictions of other models in Chapter 3.

Chapter 3

Experimental Study of the One-Atom Laser

In this chapter, the experimental study of the one-atom laser is presented. In a nut shell, the one-atom laser is composed of a beam of two-level atoms, a high-Q supercavity resonator, a pump laser to excite the atoms into the upper energy level, and photon-counting detectors, as illustrated in Figure 1-1. In addition we need a vacuum chamber that houses both the resonator and an atomic beam oven, and a setup for stabilizing the pump laser frequency and locking the frequency of it to the two-level transition frequency. First, in-depth coverage on each component is presented, followed by the description of the one-atom laser experiment. The results of the experiment are presented, and then comparison with the predictions by the theories studied in the preceding chapter are given.

3.1 Components of Experiment

3.1.1 Two-Level Atom

Candidates

The theories developed in Chapter 2 require that only two levels of an atom be coupled to a cavity field and the decay rates of both levels be much smaller than the rate of atom-field Rabi oscillation. An appreciable buildup of the cavity field requires negligible cavity damping as well as a coupling constant g_o much greater than the decay rates of the cavity and the atom. If atoms are generated from an oven, readily obtainable source of atoms will be a thermal atomic beam. These atoms would have a mean velocities in the range of 300 m/s to 500 m/s depending on the temperature of the oven as well as the masses of the atoms. Typical mode waist of a supercavity resonator is about 50 μm, so the atom-field interaction time, t_{int}, would be order of 0.2 μsec. A significant buildup of the cavity field occurs if $g_o t_{int} \gtrsim 1$, and hence the coupling constant should be greater than 5×10^6 rad/sec or about 1 MHz. The cavity and the atomic decay during t_{int} also should be negligibly small.

If the velocities of atoms are modified, these requirements scale accordingly. With slower atoms the atomic and the cavity decay rates need to be smaller whereas g_o needs to be larger. However, since g_o^2 is proportional to the atomic radiative decay rate Γ_a (both g and Γ_a are proportional to μ^2), the conditions on the coupling constant and the decay rate cannot be satisfied at the same time if the velocity is set too small. With faster atoms, on the other hand, the decay rates can be larger, and g_o can be smaller. But since a larger g_o is more desirable, we can have both a larger decay rates and a larger coupling constant satisfying the requirements. Only problem is that the practical number for the increase in velocity is about twice or so with a simple velocity selector or with a supersonic atomic beam.

Since we want to build a laser, the transition frequency between the two levels must be in the optical regime. A quick glance of the periodic table reveals that only low-lying energy levels of atoms can be used. If the lower level is not a ground state of an atom, the requirement on the decay rates of the lower and the upper levels are not easily satisfied. Usually the upper level decays strongly to the other lower levels. If the lower level is a ground state, only the upper level decay need be slow enough. Table 3.1 summarizes a survey of possible candidates [54].

Among alkali atoms only cesium is listed since the other alkali atoms require an ultra-fast atomic beam. Even cesium atom requires velocities three to four times larger than a mean thermal velocity. On the other hand either barium or ytterbium

atom	barium	ytterbium	cesium
transition	$6^1S_0 \leftrightarrow 6^3P_1$	$6^1S_0 \leftrightarrow 6^3P_1$	$6^2S_{\frac{1}{2}} \leftrightarrow 6^2P_{\frac{3}{2}}$
wavelength (nm)	791	556	852
$\Gamma_a/2\pi$ (MHz)	0.050	0.19	5.1
typical velocity (m/s)	320	270	250
$\Gamma_a t_{int}$ (w_m=50 μm)	0.086	0.37	1.1

Table 3.1: Candidates for two-level atom

atom can be used with a thermal atomic beam. As far as the loss due to the atomic decay is concerned, barium is better than ytterbium. However ytterbium permits a larger coupling constant for a given geometry of the cavity since its decay rate is larger. In this sense, both atoms are equally good if same cavity decay rates are assumed. However in practice a higher finesse can be achieved at a longer wavelength with the present supercavity technology. The bottleneck in achieving a high finesse mirror is the scattering off the mirror surface. Such scattering is mostly Rayleigh scattering, the strength of which is proportional to $\frac{1}{\lambda^4}$ with λ being the wavelength which the mirror is coated for. Therefore an atom with a longer transition wavelength is favored as far as a finesse is concerned. From all these considerations, we have chosen barium as the atom for our experiment.

Barium Energy Levels

Figure 3-1 illustrates the low-lying energy levels of atomic barium. A two-level atom is realized by exciting $^1S_0 \leftrightarrow {}^3P_1$ transition, the wavelength of which is 791.1 nm (12636 cm^{-1} wavenumber). The Einstein A coefficient of the transition is about 50 kHz [55, 54, 56]. The $^3P_1$ state can decay to $^1S_0$, a ground state, $^3D_2$ and $^3D_1$ state with a branching ratio of 1.0:0.97:0.37 [57], resulting in 1.4 μsec lifetime. The D states are metastable states since $^3D \leftrightarrow {}^1S$ transition is forbidden in the dipole approximation.

The most frequently studied transition in atomic barium is $^1S_0 \leftrightarrow {}^1P_1$. It has a

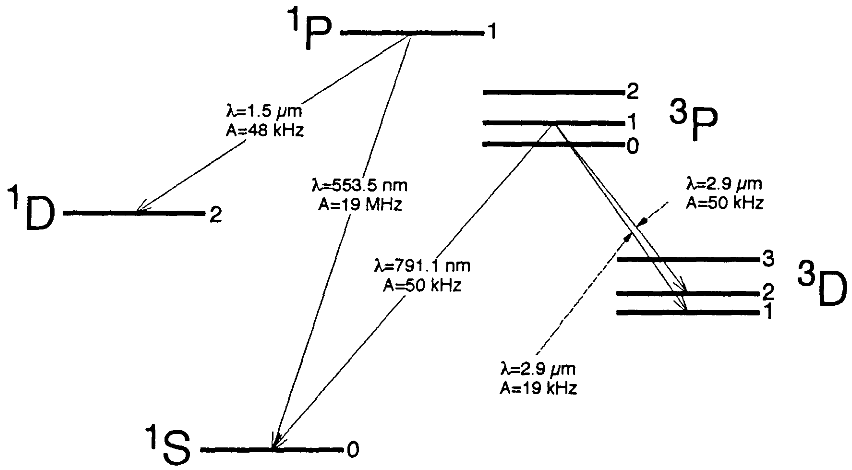

Figure 3-1: Low-lying energy levels of atomic barium. The ${}^1S_0 \leftrightarrow {}^3P_1$ transition was used to form a two-level atom.

wavelength of 553 nm and a linewidth of 19 MHz. Figure 3-2 show fluorescence signals from various barium isotopes in naturally abundant barium sample [1]. Because of its visibility and transition strength, it will be used in the procedure of calibrating the density of barium atoms in the cavity.

3.1.2 Resonator

Finesse Requirement

In selecting a type of resonator which will be used in the experiment, there are two major issues to consider. First how high finesse should be and secondly how strong a coupling constant should be.

The finesse requirement is determined by the cavity decay rate allowed in the experiment. For barium atoms in an effusive atomic beam a mean thermal velocity is about 300 m/sec. We can think of two kinds of resonators. One is a degenerate-mode resonator such as a confocal or a concentric resonator, and the other is a single-mode resonator such as a supercavity resonator. The mode waist and the cavity decay rate of each type is summarized in Table 3.2, where r_o is the radius of curvature of the

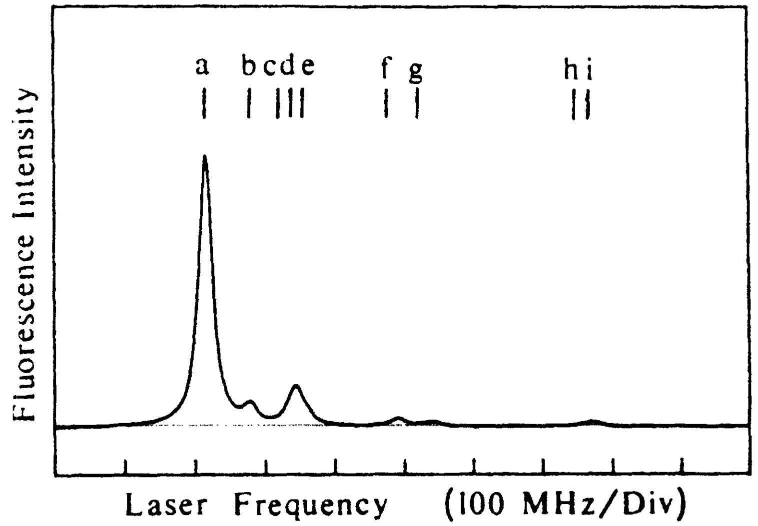

Compt.	Isotope	F_{upper}	Relative Frequency (MHz)
a	^{138}Ba	1	0
b	^{137}Ba	5/2	65
c	^{135}Ba	5/2	105
d	^{136}Ba	1	125
e	^{134}Ba	1	140
f	^{137}Ba	3/2	260
g	^{135}Ba	3/2	305
h	^{135}Ba	1/2	535
i	^{137}Ba	1/2	555

Figure 3-2: Isotopic and hyperfine structure of the $^1S_0 \leftrightarrow {}^1P_0$ transition of atomic barium. Excerpted from Ref.[1], p 124.

mirrors and L is the distance between the mirrors, and $\mathcal{F}$ is a finesse given by

$$\mathcal{F} = \frac{\pi}{1-R} \, . \tag{3.1}$$

with $R = \sqrt{R_1 R_2}$ a geometric mean of the reflection coefficients of the mirrors.

For a single-mode resonator notice that the waist is a very slow function of r_o and L. Therefore for rough estimation we can pick up some representative values for r_o and L. If we use 10 cm for r_o and 0.1 cm for L, the waist is about 40 μm. The atom-field interaction time, t_{int}, is then about 0.2 μsec. Since the cavity decay should be negligibly small during t_{int} ($\Gamma_c t_{int} \ll 1$), the finesse has to be much greater than $\frac{\pi c t_{int}}{L} \sim 2 \times 10^5$. For a confocal resonator, a typical value for r_o might be 5 cm, which gives a waist of 80 μm and t_{int} of 0.1 μsec. Then a finesse has to be much greater than 4×10^4.

A concentric resonator has a diffraction-limited waist, w'_m, within which atoms can couple to the mode [1].

$$w'_m = \sqrt{\frac{\lambda r_o}{8\mathcal{F}}} \, . \tag{3.2}$$

type	mode waist	Γ_c
single-mode	$\left(\frac{r_o L \lambda^2}{2\pi^2}\right)^{\frac{1}{4}}$	$\frac{\pi c}{L\mathcal{F}}$
confocal	$\sqrt{\frac{\lambda L}{2\pi}}$	$\frac{\pi c}{2L\mathcal{F}}$
concentric	$\sqrt{\frac{\lambda r_o}{8\mathcal{F}}}$	$\frac{\pi c}{L\mathcal{F}}$

Table 3.2: Mode waist and cavity decay rate of various types of resonators. r_o is a radius of curvature of the mirrors and L is a distance between the mirrors, and $\mathcal{F}$ is a finesse.

Then the finesse has to satisfy

$$\mathcal{F}^{\frac{3}{2}} >> \frac{2\pi c\sqrt{\lambda r_o}}{\sqrt{2}vL} , \tag{3.3}$$

which translates $\mathcal{F} \gg 4 \times 10^6$ for a r_o of 5 cm.

Based on these estimations, a confocal resonator appears the most favorable choice. A finesse of 10^5 would be adequate. However, such a high finesse over the waist of the degenerate mode on the mirror surface is extremely difficult to realize. Roughly speaking, a highest finesse value attainable is inversely proportional to the mode waist on the mirror. For a single-mode resonator, the mode waist on the mirror is about the same as w_m for $L \ll z_o \equiv \sqrt{\frac{r_o L}{2}}$. The mode waist for a confocal resonator, on the other hand, is given by

$$w''_m = \left(\frac{L^3\lambda}{2\mathcal{F}}\right)^{\frac{1}{4}} , \tag{3.4}$$

which turns out to be 200 μm for our example. If a finesse of 10^6 is a highest achievable finesse value for a single-mode resonator, a highest finesse for a confocal resonator over 200 μm spot would be $10^6 \times \left(\frac{40}{200}\right)^2 = 4 \times 10^4$, which does not well satisfy the requirement (We need 10^5 or even higher). In other words, a confocal resonator is not any better or perhaps worse than a single-mode resonator. A concentric resonator is the worst one since the mode waist on the mirror is the largest and the required finesse alone is the highest among the three types . All these considerations lead us to choose a single-mode resonator as the resonator in the experiment.

Coupling Constant

The atom-field coupling constant, g_o, was defined by Eq.2.84 as

$$g_o = \frac{\mu}{\hbar}\sqrt{\frac{2\pi\hbar\omega}{V}} .$$

For a single-mode resonator a mode volume V is given by

$$V = \frac{1}{4} w_m^2 L .$$

Using the expression for w_m from Table 3.2, we can rewrite g_o as

$$\frac{g_o}{2\pi} = \left(\frac{3}{2\sqrt{2}\pi^2}\right)^{\frac{1}{2}} \sqrt{\frac{c\lambda}{\sqrt{r_o L^3}}\left(\frac{\Gamma_a}{2\pi}\right)} . \tag{3.5}$$

Once a type of two-level atom is chosen, only adjustable parameters are r_o and L. Since a larger g_o induces a stronger cavity field build up, r_o and L should be made as small as possible.

The mirrors used in the experiment have been fabricated at PMS electro-optic [58]. They use super-polishing technique to produce mirror substrates with extremely high surface figures. Then they use multi-layer ion beam coating technology to yield very low transmission coefficients. In order to achieve very high finesse, not only the transmission but also the scattering loss, either from coating material or from coating-substrate interface, should be minimized. According to PMS, the scattering loss is closely related to the radius of curvature of the mirror mostly because the smaller the curvature is, the more difficult is to realize a high surface figure. If the curvature is too deep, it is also difficult to maintain coating material uniformly deposited during coating processes. Prior to our mirror production, typical r_o they had used was 100 cm. The highest finesse attained so far with that radius of curvature was 2×10^6 with a transmission (T) of 0.5×10^{-6} and an absorption/scatter (A) of 1×10^{-6} at 850 nm [7]. If we assume that A is mostly scattering and it is mainly due to Rayleigh scattering, we can predict that A with the same radius of curvature at 791 nm would be $1 \times 10^{-6} \times (850/791)^4 = 1.3 \times 10^{-6}$ and therefore the finesse would be $\frac{\pi}{0.5+1.3} \times 10^6 = 1.7 \times 10^6$. Since a workable smallest distance in general might be 1 mm, $g_o/2\pi$ then would be 200 kHz and $\Gamma_c/2\pi$ would be 90 kHz, satisfying a strong-coupling condition, $2g_o \gg \Gamma_c, \Gamma_a$. However the projected finesse value by PMS was only around 5×10^5 based on their previous experience. Then $\Gamma_c/2\pi$ would be 300 kHz instead, which is not much smaller than $2g_o/2\pi$. Therefore we chose a shorter radius of curvature, 10 cm instead of 100 cm, obtaining $g_o/2\pi$ of 360 kHz.

Actual finesse values have been measured using a ringdown technique, which will be described later. The measurement has been performed on 20 mirrors from a same batch, yielding a result of about 1×10^6. During the actual experiment, the finesse value gradually changed because the barium atoms that were scattered off an aperture in front of the resonator continuously deposited on the surface. Eventually the finesse settled down to 8×10^5. At this finesse value, $\Gamma_c/2\pi$ becomes 190 kHz, therefore satisfying

$$2g_o \ : \ \Gamma_c \ : \ \Gamma_a = 14.4 \ : \ 3.8 \ : \ 1 \,, \tag{3.6}$$

thereby safely satisfying the strong-coupling condition.

We can vary r_o and L while still satisfying the condition. However the ranges over which we can vary those are quite limited. If we change L by a factor of ξ, the above ratio becomes

$$2g_o \ : \ \Gamma_c \ : \ \Gamma_a = \frac{14.4}{\xi^{\frac{3}{4}}} \ : \ \frac{3.8}{\xi} \ : \ 1 \,. \tag{3.7}$$

If we want to keep $2g_o$ at least three times larger than $\Gamma_{c,a}$, an allowed range of ξ is only between 0.94 and 8.0. However we cannot make the length too long since cavity linewidth then becomes too narrow to perform any cavity locking/stabilization. As shown later, cavity locking/stabilization requires that a locking laser should have

atom	^{138}Ba
transition	$6\ ^1S_0 \leftrightarrow 6\ ^3P_1$
wavelength, λ	791 nm (16316.000 cm^{-1})
$\Gamma_a/2\pi$	50 kHz
cavity length, L	1 mm
finesse, $\mathcal{F}$	8×10^5
$\Gamma_c/2\pi$	190 kHz
g_o/π	720 kHz

Table 3.3: Summary of specifications on atom and cavity.

narrow linewidth than cavity linewidth. In our setup a laser stabilization technique enabled us to achieve about 50 kHz laser linewidth (The details of the stabilization will be discussed later). Then a smallest cavity linewidth might be 150 kHz for successful cavity frequency locking unless we further improve the stability of the probe laser. However there are types of experiment which do not require frequency locking of the cavity. A resonator can be designed to have free-running stability better than 50 kHz without any active stabilization (see the next section). In that case we are allowed to increase the cavity length up to 3–4 mm for the same finesse value. However for the present experiment we have chose the length to be 1 mm.

Table 3.3 summarizes the specifications on our one-atom laser based on the discussions so far.

Stability

design of resonator

When we design a resonator for the one-atom laser, the most important issue is the mechanical stability of the resonator. A frequency shift due to resonator length change is given by

$$\delta\nu = \nu\frac{\delta L}{L} = \frac{c}{2L}\frac{\delta L}{\lambda/2}\ . \tag{3.8}$$

For a length of 1 mm, the free spectral range is 150 GHz, so even 1 Å change in the length induces 38 MHz frequency shift. This length change is due to global displace-

material	ρ (g/cm^3)	Y (10^{12} dyne/cm^2)	$\omega_o/2\pi$ (kHz)
fused silica	2.2	1.5	130
stainless steel	7.9	4.0	110
rubber	1.0	0.066	40
PZT (type 5A)	7.7	0.60	40

Table 3.4: Physical properties of material used in our resonator. ω_o is a typical mechanical resonance frequency obtained from Eq.3.9 with C=D/cm=1.

ment of the mirror surface, and it should not be confused with thermal vibrations of individual molecules. Such vibrations can be easily as large as a few Å but they are random and not globally correlated, and therefore there is no net effect on the field inside the resonator. However mechanical vibration of the mirror substrate will certainly induce global displacement of the surface, and hence causing frequency shift of the field inside. We can estimate such global displacement due to thermal energy at room temperature. We can easily show that a mechanical resonance frequency of a solid object is given by

$$\omega_o = C\sqrt{\frac{Y}{\rho D^2}}\,, \tag{3.9}$$

where Y and ρ are the Young's modulus and the density of the object, respectively, D is a typical dimension the object, and of C is a constant of order of unity depending on a shape of the object. The physical properties of various material used in our resonator are listed in Table 3.4. For example, a normal mode frequency of a mirror made of fused silica with a dimension of 1 cm would be 130 kHz. In a thermal equilibrium, according to the classical partition theorem, we have

$$\frac{1}{2}k_BT = \frac{1}{2}M\omega_o^2\left\langle x^2\right\rangle .$$

where x is the displacement of the mirror surface. Then at a room temperature

$$\sqrt{\langle x^2\rangle} = \sqrt{\frac{k_BT}{\rho V\omega_o^2}} \sim 2\times 10^{-13}\ \text{cm} = 2\times 10^{-5}\ \text{Å}.$$

Therefore a frequency shift is immeasurably small. In other words, if the resonator is mechanically isolated, the frequency shift due to thermal energy is immeasurably small. Therefore Any design of a resonator and its mount should concentrate on how to isolate the resonator from the outside world.

Sources of mechanical vibrations in the resonator are entirely external. A laboratory is full of sounds from various sources such as air-conditioner and cooling fans in power supplies. It is not immediately clear how much effects these noises would have on the frequency stability of a resonator. We found out an answer in a hard way. Our first resonator, designed with emphasis on functionality, could not meet the stability requirement. In that design a pair of supercavity mirrors were held by aluminum holders. One of the holders was glued to a piezoelectric transducer (PZT) to allow change of cavity length. The PZT was mounted on a flange, tilt of which was adjustable by three micrometers. Figure 3-3 illustrates the dimensions of the mirrors and the schematic of the resonator assembly. The material used for the mount was super Invar. We measured the transmission of the resonator while slowly scanning the frequency of a probe laser. Many sharp resonances occurred over 100 MHz range. Since the linewidth of the cavity is known to be 190 kHz by the ringdown measurement, which will be discussed later, and since the stability of the probe laser is at worst less than 2–3 MHz, the broad resonance or frequency excursion in the transmission is entirely due to the vibrations of the resonator itself. According to our previous estimation, the amplitude of the vibrations is only 5 Å. We could reduce the frequency excursion down to 30 MHz with extra care in eliminating the sources of noise sound and in mounting the resonator assembly on a rigid support with teflon spacers in between. However such level of the frequency excursion was far from being acceptable. Simply put, our first attempt was a total failure.

With this experience, a new resonator was designed with the stability in mind. We eliminated all the parts needed for mirror alignment except a PZT as shown in Figure 3-4. The mirrors were glued directly on stainless steel holders. The holders were machined with precision of 0.0005 inches. When a mirror is inserted into a holder, the mirror touches the holder on three symmetrically protruded parts snuggly.

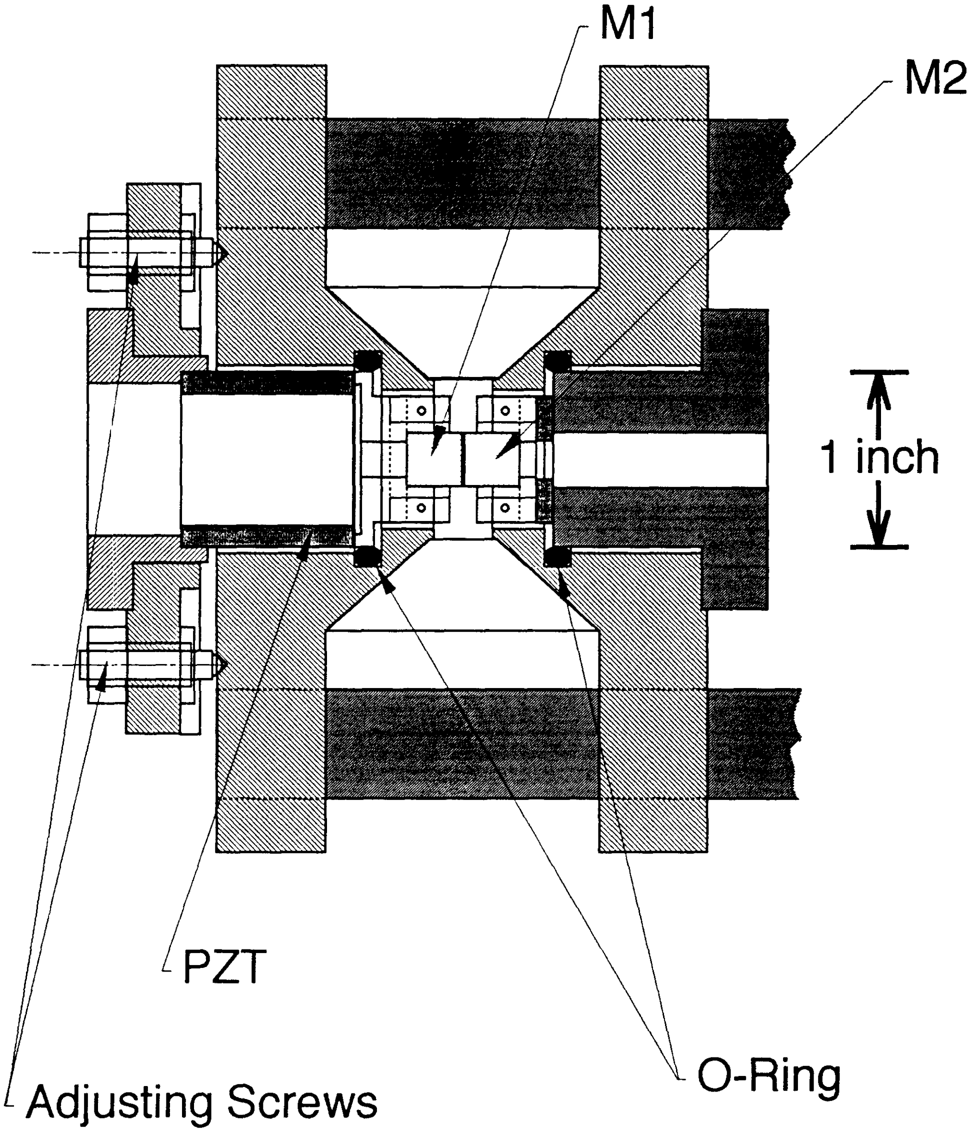

Figure 3-3: Schematic of our first resonator assembly. The design failed to meet the requirements on frequency stability. However this mirror mount was used in assembling our new resonator, which is described next.

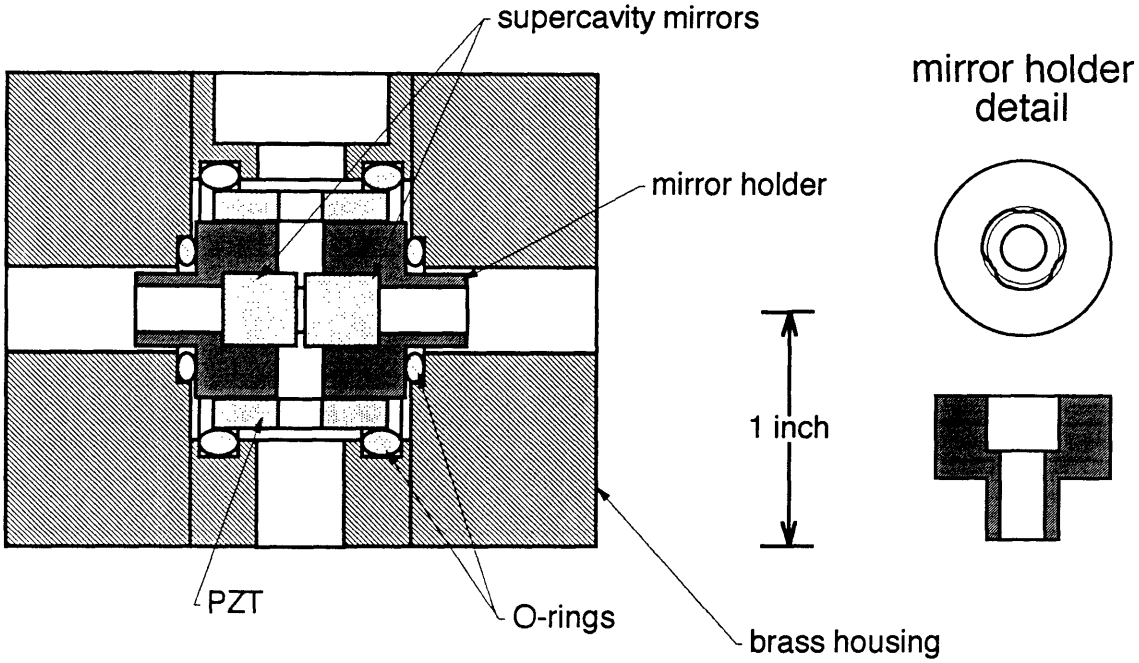

Figure 3-4: Schematic of our new resonator.

Small amount of Torr Seal epoxy was applied between the mirror and the recessed part of the holder. By mounting the mirrors on the holders symmetrically in radial direction, possibility of stress-induced birefringence was reduced. We modified the old resonator and used it as a tool for assembling the new resonator. The new mirror holder has a protruded part on the opposite side to the mirror. That part has an exactly same dimensions as the mirror so that it can fit the old holder perfectly. In this way the new holders with the mirrors installed were mounted on the old mount and the distance between the mirrors and the tilt of one mirror relative to the other were adjusted.

We used a He–Ne laser beam to align the mirrors to be parallel. Since the high reflection coating at 791 nm is of narrow band (50 nm wide) two surfaces of a mirror have about 4 % reflectance at visible wavelengths. While the coated surface has a curvature of 10 cm, the other surface is flat and is wedged at 4 °. When two curved surfaces are perfectly aligned, a ring pattern is reflected back onto the incoming He–Ne laser beam. Once the mirrors were aligned, the flange holding one of the holder was removed from the mount.

A PZT tube (type PZT-5A from Vernitron) with a length of 3/4" was used to allow the length change of the resonator. The tube has four holes in the middle for the clear passage of an atomic beam and a pump laser beam. Torr-Seal epoxy was applied onto the inner surface of the PZT tube at both ends. Only 1/3 of the length of the PZT was free of the glue, so free to expand or contract. The tube was inserted into the mount so that, when the flange was placed back, the mirror holders were glued into the PZT tube as shown in Fig.3-5. The old mount was made precisely and rigidly so that when the flange was put back, we did not loose the mirror alignment. After overnight hardening of the epoxy, the resonator assembly was removed from the old mount. We then verified the alignment and measured the frequency excursion. When it was gently clamped between teflon V-blocks, the frequency excursion was about 4 MHz without much care in reducing external perturbation. This improvement, better than ten-fold, is due to the simplicity and rigidity of the new resonator.

The resonator assembly was housed in a brass enclosure with a large inertia. There were two Viton o-rings between the PZT and the enclosure, and two smaller o-rings between the mirror holders and the end plates of the enclosure so that the assembly was in touch only with four o-rings, suspended inside the enclosure. Then the enclosure was gently clamped by two 1" thick aluminum plates with 1/4" thick teflon spacers in between. The plates were mounted on the inner wall of a vacuum chamber with three teflon screws (Figure 3-5). These three-fold protection by the o-rings and the teflon spacers and screws could effectively isolate the resonator assembly from external perturbation. The excursion measurement resulted in only 2–3 MHz at largest when the measurement was repeated many times. Most of time the excursion was less than 1 MHz. Later we identified that this excursion was actually due to the instability of the probe laser. When the probe laser was stabilized in frequency, the typical excursion was about 300 kHz. However even this value was due to the mechanical resonance of the probe laser itself. The resonance was measured to be 660 Hz. Hence for a time interval shorter than a millisecond the frequency excursion of the resonator was much smaller, being about 50 kHz. This small excursion, much

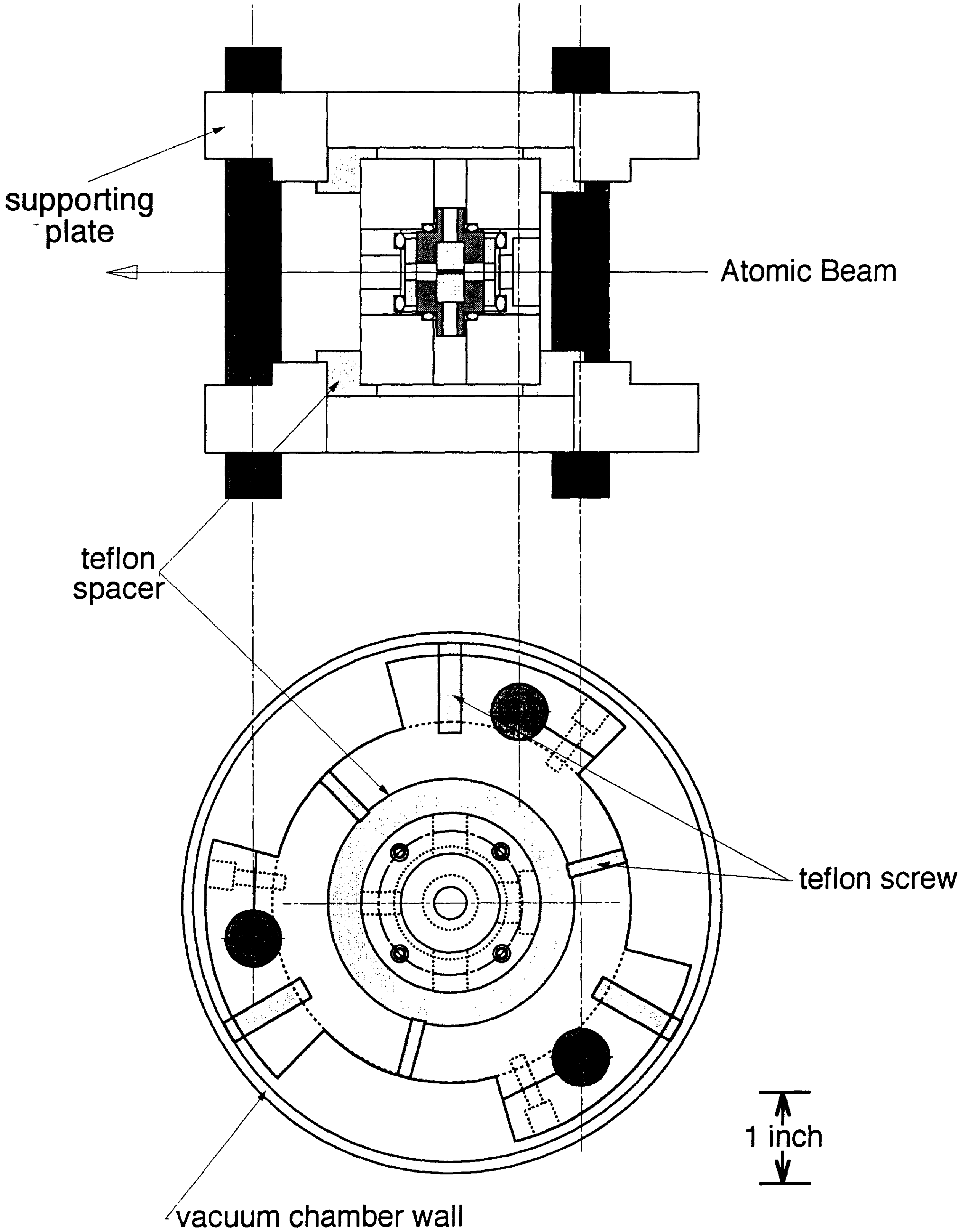

Figure 3-5: Mount for a new resonator. With this mount the resonator demonstrated a free-running frequency jitter of only 50 kHz.

less than the cavity linewidth, is certainly acceptable for the experiment.

PZT resonances

In the experiment, at least for initial alignment, it is necessary to maintain the frequency of the resonator in resonance with the atomic transition. For this we employed a side-band locking scheme, in which the resonance frequency of the cavity is locked to a probe laser frequency, which is in turn locked to the atomic transition. The details of the locking scheme will be discussed later. Only thing to mention in this section is that an error signal proportional to the frequency difference between the laser and the cavity is continuously fed back to the resonator PZT to compensate the error. If the bandwidth of a feedback loop is infinite, any error is instantly corrected. However if the loop has a component with a low resonance frequency, the bandwidth of the loop should be made much lower than the resonance frequency since across the resonance the sign of the feedback changes, resulting in amplification of the error rather than suppression. For this reason the mechanical resonances of the PZT was studied.

We measured the response of the PZT as a function of the frequency of a sinusoidal driving voltage applied to the PZT with the resonator installed in place. The result is shown in Figure 3-6 indicating a strong resonance at 20 kHz. Therefore any feedback loop should be designed to have a band cutoff frequency well below 20 kHz to avoid any amplification of the error signal. Then our resonator with the present PZT cannot correct any frequency errors above the cutoff frequency. However we have found that the rigid structure of the resonator with the three-fold vibration isolation scheme practically does not show frequency components higher than 10 kHz. Therefore it is possible to design a feedback loop that stabilize and lock the cavity frequency to a reference frequency.

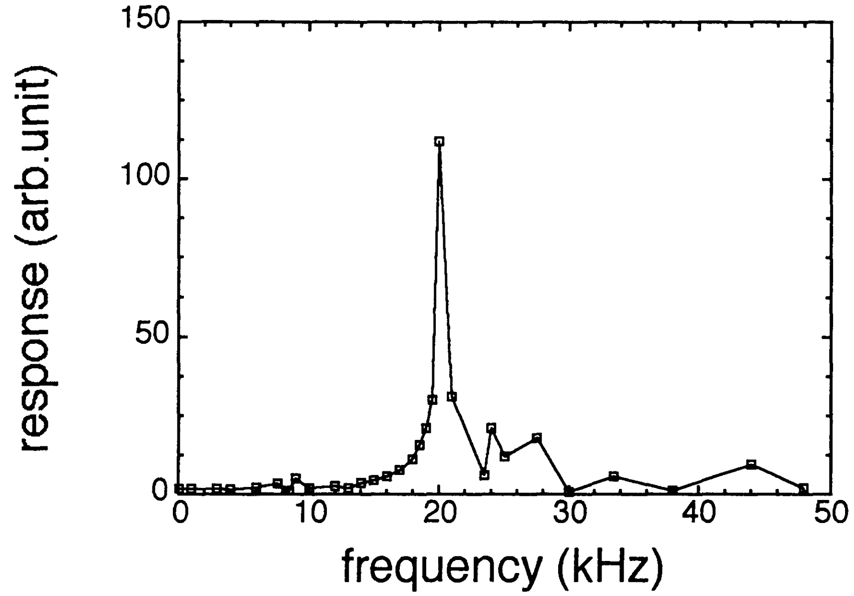

Figure 3-6: Frequency sensitivity of PZT (Vernitron PZT-5A)

3.1.3 Characterization of Resonator

Transmission Modes

The measurement of cavity transmission provides information on various aspects of a resonator such as degree of alignment, cavity length, finesse and throughput. In order to excite a single cavity mode, which is just a TEM_{00} mode of the resonator in our experiment, not only a probe laser should be aligned along the cavity axis, but also it should be focussed down to the waist of the cavity mode to maximize the coupling of the probe laser into the mode. We used a CW Ti:Sapphire laser (Coherent CR 899-29) as a probe laser. The direction of the cavity axis was identified with a He-Ne laser beam as described earlier. When the He-Ne laser was well aligned along the cavity axis, a concentric ring pattern was reflected back onto the incident laser beam. Then the probe beam was superimposed on top of the He-Ne laser beam.

The transmitted beam was measured by a photo diode while the resonator was scanned by applying a voltage ramp to the PZT. This voltage was derived from a scan drive output of a Tektronix 555 oscilloscope. The signal from the photo diode

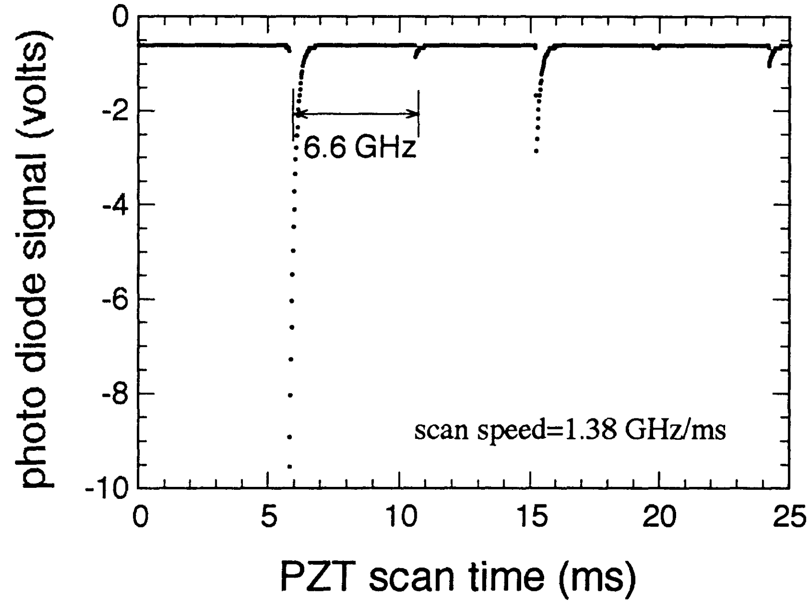

Figure 3-7: Typical cavity scan signal. The largest peak corresponds to TEM_{00} mode. The following modes are $TEM_{1,0}$, $TEM_{2,0}$, $TEM_{3,0}$, and so on.

was then measured synchronously on the oscilloscope. The amplitude of the ramp was 130 V. This voltage corresponds to 60 GHz scan range of the resonance frequency of the cavity. Since the free spectral range of the cavity is 150 GHz, at most only one longitudinal mode can be displayed on the scope. If necessary, a DC offset voltage was added to the ramp voltage to bring a longitudinal mode on display. If the mirrors are not perfectly aligned or alternatively the probe laser is not properly coupled into the cavity mode, the transverse modes with the same principle mode number as the longitudinal mode appear at slightly higher frequencies. A typical cavity scan is shown in Figure 3-7. The largest peak corresponds to the TEM_{00} mode. The following peaks are transverse modes, $TEM_{1,0}$, $TEM_{2,0}$, $TEM_{3,0}$, and so on. If the cavity has perfect axial symmetry, any $TEM_{n,m}$ with $n + m = k$ is degenerate with $TEM_{k,0}$. We found the frequency differences among the $TEM_{n,m}$ modes with $n + m = k$, if any, were smaller than a MHz, indicating the cavity was fairly axial-symmetric. Furthermore, the reflection as well as the transmission of the He-Ne beam also showed symmetric concentric ring patterns. This suggests that the mirrors were quite parallel. The presence of all the transverse modes then should be due to improper coupling of the probe laser beam. Actually we could demonstrate that the relative heights of the transverse modes changed as the probe laser beam direction was slightly tilted. The slight tilt of the probe laser led to favorable excitation of $\mathrm{TEM}_{2k+1,0}$ modes ($k = 0, 1, \ldots$). If the focus of the probe was changed slightly, we observed $\mathrm{TEM}_{2k,0}$ modes ($k = 1, 2, \ldots$) were selectively excited. These are understandable since $\mathrm{TEM}_{2k+1,0}$ mode represents $\mathrm{TEM}_{n,m}$ with $n+m = 2k+1$, which are asymmetric whereas $\mathrm{TEM}_{2k,0}$ mode corresponds to $\mathrm{TEM}_{n,m}$ with $n + m = 2k$, which are axially symmetric. In fact we could reduce the heights of all the transverse modes down to less than 5 % of the height of $\mathrm{TEM}_{0,0}$ by carefully adjusting the direction and the focus of the probe laser.

The mode structure in the transmission signal provides not only the information on alignment but also a way of measuring the cavity length. The transverse modes in a cavity such as our supercavity resonator are separated in frequency by [59]

$$\Delta\nu_t = \frac{c}{2\pi z_o} , \quad \text{if } r_o \gg L , \tag{3.10}$$

where z_o is a confocal parameter given by

$$z_o = \sqrt{\frac{r_o L}{2}} . \tag{3.11}$$

As shown in Fig.3-7, the transverse mode spacing for our cavity was 6.6 GHz. We calibrated the frequency scale by shifting the frequency of the probe laser by a known amount and observing the position change of the modes on the scope while the cavity was repeatedly scanned in real time. From the spacing we found the cavity length was 1.05 ± 0.05 mm and z_o=0.72 cm.

Finesse Measurement

A resonator finesse can be measured in two ways. One is to measure a transmission lineshape and the other is to measure a cavity decay time. The measurement of a resonator lineshape is desirable if the resonator linewidth is much broader than the linewidth of a probe laser. If not, the cavity decay is more useful tool. In our case, when the probe laser was not stabilized, the resonator linewidth ($\sim$ 200 kHz) was narrower than the probe linewidth (500 kHz $\sim$ 2 MHz), so the decay measurement was more favorable one. However, when the probe was stabilized, its linewidth was only 50 kHz, and therefore a resonator linewidth could also be measure. The results of both measurements yielded 190 kHz FWHM consistently. This linewidth corresponds to a finesse of $(7.9 \pm 0.1) \times 10^5$.

The measurement of the cavity decay utilizes a ringdown of the field inside. An empty cavity is filled up by a pulse of electromagnetic field, and then the decay of the field is monitored in time. In a usual setup, a probe laser which is resonant with a cavity is introduced into the cavity at a certain time only for a brief moment. The duration of excitation is much shorter than a cavity decay time so that the excitation can be considered being a delta function. To simulated a delta function, an acousto-optic modulator (AOM) is used as a shutter. Initially the shutter is opened and the cavity is allowed to drift slowly toward the resonance frequency. When the cavity becomes resonant with the laser, a field builds quickly in the cavity. The buildup is monitored through cavity transmission. When a transmission signal reaches a certain threshold, the AOM is immediately switched off, and the subsequent field decay is measured as a function of time. This technique has been used by other group [7] to measure a finesse as high as 2×10^6 at 850 nm.

We have developed a much simpler technique, which does not require a AOM and a trigger circuit to switch the AOM off at a right moment. Instead we utilize a fact that the cavity is resonant with the probe laser only for a short time if the cavity is quickly scanned. This short resonance time in effect achieves a delta function excitation. By controlling the scan speed, we can adjust how much field can build up in the cavity before the cavity becomes out of resonance with the laser. The cavity is scanned repeatedly while the field decay is measured on an oscilloscope in real time. There is one caveat though, that is the cavity decay curve shows an amplitude modulation, which depends on the scan speed as

$$T_M = \left(\sqrt{2}-1\right)\sqrt{\left(\frac{2L_o}{c}\right)\left(\frac{\lambda}{v}\right)}\,, \tag{3.12}$$

where T_M is a time interval between the first and the second local minima due to the modulation. The origin of the modulation is the interference between the probe laser and the intra-cavity field. Since one of the mirrors is moving, the intra-cavity field, which had built up when the cavity was resonant with the probe laser, continuously acquires frequency shift caused by the Doppler effect while its amplitude decays. Although the probe laser is no longer resonant with the cavity in a steady-state sense, it can still get into the cavity because of the transmittance of the mirror it is incident upon. Because the probe and the intra-cavity field have different frequencies, they exhibit a beating in the transmission. The algebraic expression for the decay curve as well as the above formula are derived in Appendix A.

For our cavity, typical decay time was order of 1 μsec. We used a 300 MHz digital oscilloscope (Lecroy 9310M) to capture a decay curve by a single scan. A voltage ramp to drive the PZT was obtained from the Tektronix 555 oscilloscope. A 185 Ω terminator was used at the input of the digital oscilloscope to override 1 MΩ input impedance and therefore to shorten its RC response time. With the terminator the RC time is only 30 ns so that its effect on the decay time can be neglected. A typical decay curve is shown in Figure 3-8. A straight line is an exponential fit by a least-square fit algorithm [50], resulting in a decay time of 1.14 μsec or a finesse of 1.03×10^6. For that data the cavity was scanned at a speed of 14.5 GHz/ms. From this value, we can estimate the velocity at which the mirror on the PZT was scanned.

$$v = \frac{\lambda/2}{c/2L} \times 14.5\text{GHz/ms} = 3.8 \times 10^{-3}\text{cm/s}\,.$$

The cavity-field resonance time in this case is $190kHz \times \frac{1ms}{14.5GHz} \sim 13ns$, which is

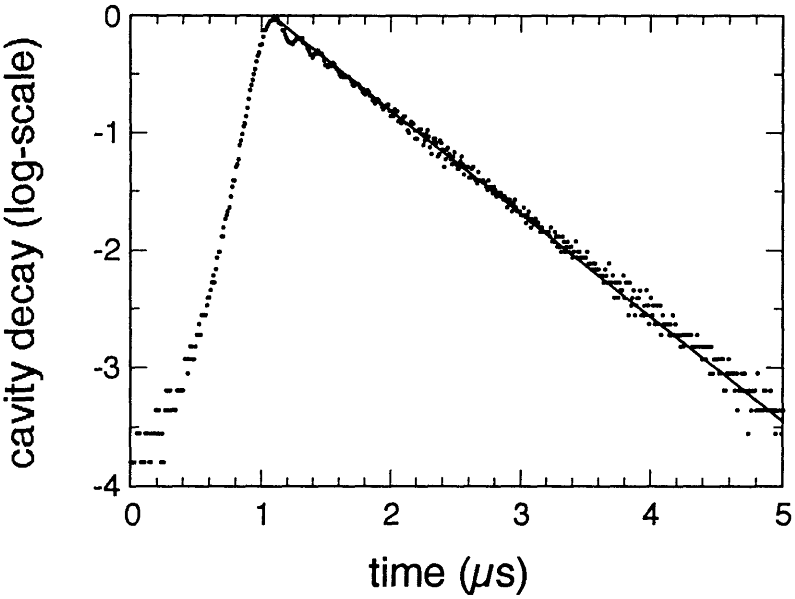

Figure 3-8: Typical cavity decay curve by the ringdown technique explained in the text.

much shorter than usual decay times. According to Eq.3.12, the modulation period T_M is about 150 ns, which is consistent with the data. If the cavity is scanned more slowly, the modulation becomes more pronounced. The decay curve in Figure 3-9 was obtained with a scan speed of 1.45 GHz/ms, corresponding to a velocity of 3.8 μm/sec and a T_M of 490 ns, which is again consistent with the data.

Among a total of 20 supercavity mirrors specially made for the experiment, only a half of them were tested. First a pair of mirrors were randomly selected from the batch. The pair were mounted on our old resonator mount. Even thought the mount does not have acceptable long-term stability, during the time of finesse measurement, which is only a few μsec, the mount can be considered being stable. By using the old mount we could easily disassemble and reassemble a resonator. Once the finesse of the two mirrors were known, one of the mirrors was replaced with a new mirror while the other one was kept in position, and the finesse of this newly formed resonator was measured. We repeated this process for the half of the batch relative to the fixed mirror. A new resonator was then formed out of the two mirrors that gave the highest finesse values. This resonator should have the highest finesse value. In fact

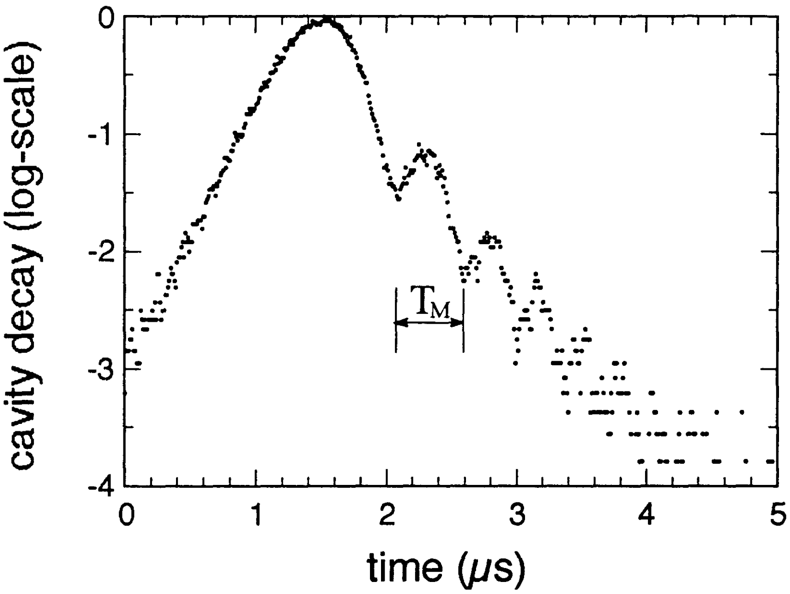

Figure 3-9: A cavity decay curve with a slow scan speed shows an amplitude modulation. The period T_M, defined in Eq. 3.12, is 0.51 μsec, resulting in a mirror velocity of 3.4μm/sec.

the variation in the finesse values was only 10 % of their mean value, 1×10^6. The finesse with the best pair was $(1.05 \pm 0.05) \times 10^6$. We also measured the finesse at various probe laser wavelengths and the result is shown in Figure.3-10.

During the experiment, the finesse of the resonator changed gradually, possibly due to accidental deposition of barium atoms on the surfaces of the mirrors. Interestingly the finesse initially increased (sometimes up to 1.2×10^6) and then decreased. The initial increase might be because barium atoms act as *getter* material, lowering vacuum pressure and possibly removing small dust particles. Barium atoms inevitably would deposit on the resonator as the experiment was repeated over a long period of time, resulting in the gradual decrease of the finesse. Sometimes the finesse dropped unacceptably low so that we needed to clean the mirror surfaces. The cleaning was performed without taking out the resonator. A tightly folded lens tissue with a clean drop of acetone was inserted between the mirrors and gently swapped against the mirror surfaces. This process was repeated with a new tissue every time until an acceptable finesse value was obtained.

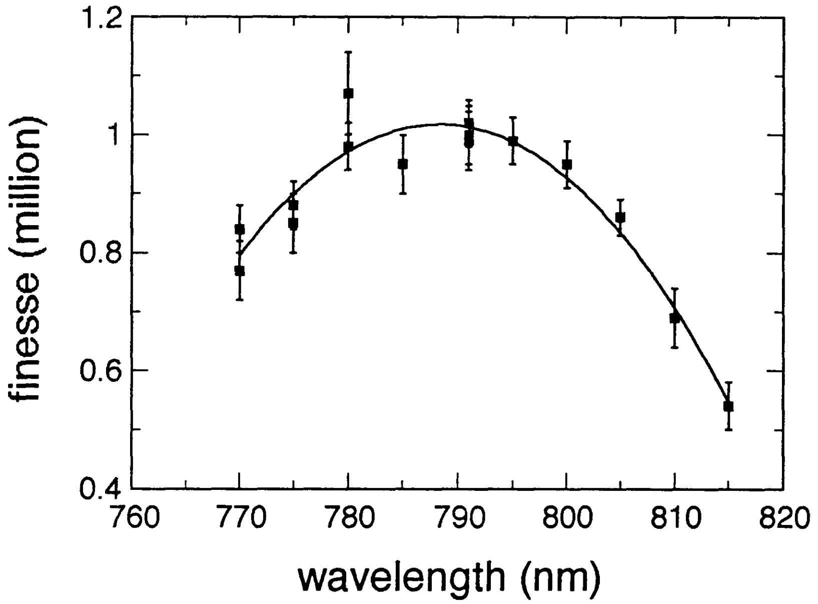

Figure 3-10: Finesse as a function of probe laser wavelength.

Throughput

A cavity throughput is a ratio of the power transmitted through a cavity to the power incident on it. It can be expressed in terms of a transmittance, T, and an absorption and scatter, A, as $\left(\frac{T}{T+A}\right)^2$. Since a finesse measurement determines the value of $1 - R = T + A$, an additional throughput measurement can completely determines both T and A. A throughput measurement also connects a mean number of photons inside the resonator to the rate of photon emission out the ends of the resonator:

$$\langle \dot{n} \rangle = \langle n \rangle \, \Gamma_c \left(\frac{T}{T + A} \right) , \tag{3.13}$$

For the throughput measurement, an avalanche photo diode (EG&G C30902S, S/N 8490) was used with a bias voltage of 216 VDC (see Table 3.5). According to the test data sheet supplied by EG&G, the photodiode has a response of 128 A/W at 830 nm at this bias voltage. This value scales to a response of 119 A/W at 791 nm. A laser beam from a Ti:Sapphire laser was attenuated to a few μW and the transmitted power through the resonator was measured. With a 10 kΩ terminator the photo diode registered a few tenth of a volt, resulting in a throughput of $(7.9 \pm 0.4) \times 10^{-2}$ and hence $\frac{T}{T+A} = 0.28 \pm 0.01$. This measurement and the finesse measured by the ringdown technique ($\mathcal{F} = (7.9 \pm 0.1) \times 10^5$) completely determines T and A: $T=(1.1 \pm 0.1) \times 10^{-6}$ and $A=(2.9 \pm 0.1) \times 10^{-6}$.

Birefringence

Supercavity resonators with high finesse values like ours are often subject to birefringence. Even though mirrors can be fabricated free of birefringence, improper mounting can cause unbalanced stress on the multi-layer dielectric coating and can induce birefringence [7]. When we designed the new resonator, we took an extra care to prevent such birefringence. The mirror holder was designed with three clutching parts that fit a mirror with an accuracy of 0.0005" (Fig.3-5). Glue was applied to the regions between the clutching parts so that when the glue dried, any resulting stress must be symmetric, hence eliminating any preferred direction. We studied the cavity transmission with different probe polarization directions, but could not find any substructure in the TEM_{00} mode. However the transverse modes showed more than one resonances. The separations were often a few MHz. Such birefringence, however, does not affect our experiment because only TEM_{00} mode is excited.

We also studied a very short cavity, which was just two mirrors glued together face to face at four points on the mirror edges. The purpose of the study was to examine the possibility of building a cavity, relying on the parallelism of the rounded edge of the mirror to the curved spot in the center. The distance of the cavity was about 200 μm. Interestingly, this cavity showed a large birefringence possibly due to the unequal stress exerted by unequal amount of the glue at the four contact points. The cavity lineshape measured as a function of probe polarization is presented in Figure 3-11 for the sake of a record.

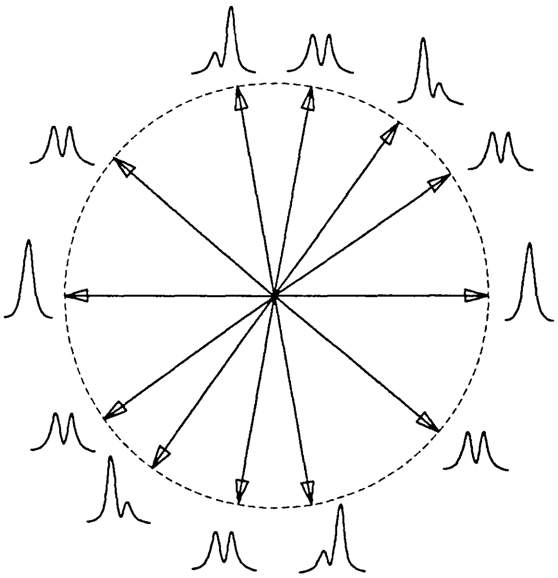

Figure 3-11: Birefringence shown in a cavity with two mirrors directly glued face to face. The cavity transmission lineshape was measured as a function of the probe polarization direction. The cause of the birefringence is possibly the stress exerted by unequal amount of glue at four contact points.

3.1.4 Pump Laser Stabilization and Locking

Requirement

For a π-pulse excitation the intensity and the waist of the pump laser should be adjusted so that $\Omega_R t_p = \pi$ (see Eq.2.35). In addition, the loss of atoms by spontaneous emission during the pumping process should be minimized. If A_{tot} denotes the total spontaneous emission rate of the $^3P_1$ state, it is therefore required that $A_{tot}t_p \ll 1$. Since $A_{tot} \sim 100$ kHz, we obtain $w_p \ll 290$ μm. In fact we used a w_p of 50 μm in the experiment, and consequently Ω_R or the intensity of the pump was adjusted to satisfy the π-excitation condition.

The small spot size of the pump laser inevitably introduces transit time broadening in the interaction with atoms. As long as the frequency of the pump stays well within the broadening, the pumping process is not much affected by the frequency uncertainty of the pump laser. If $\Gamma_a w_o/v \ll 1$, which is the case in our experiment, the transit time broadening is given by

$$\Delta\nu_{tr}(\mathrm{FWHM}) = \frac{2\sqrt{2\ln 2}}{\pi}\frac{v}{2w_p} \cong 0.75\frac{v}{2w_p}\ . \tag{3.14}$$

Assuming v=320 m/s and w_p=50 μm, we can estimate $\Delta\nu_{tr}$ =2.4 MHz. We require the frequency fluctuations of the pump laser should be much less than $\Delta\nu_{tr}$. However the original Ti:Sapphire laser used in the experiment did not conform to this requirement. When its frequency was locked to its built-in reference cavity, frequency jitter was about 2–3 MHz, mostly due to instability of the reference cavity. We needed to reduce the jitter to use the laser as a pump laser. Therefore we had to perform frequency stabilization as well as frequency locking of the Ti:Sapphire laser.

A stabilization method most widely used has been a two-step locking scheme, in which the frequency of a laser is locked to a stable reference cavity first, then the frequency of the cavity is locked to an atomic/molecular transition [60]. If the cavity just drifts slowly without much frequency jitter, the cavity length can be corrected by an error signal derived from the atomic transition. We did not use this technique since we found a much simpler method, that is, an one-step scheme. We applied the frequency modulation (FM) spectroscopy to a Lamb dip setup to obtain a dispersion-type error signal, which was applied to the Ti:Sapphire laser control box in negative feedback to correct the frequency error.

FM Spectroscopy

Modulation spectroscopy such as the lock-in detection has a capability of isolating a small signal from a large background. In the lock-in technique, for example, a system to be studied is excited by an amplitude-modulated probe laser and its fluorescence or absorption (equivalently transmission) is measured. Then a lock-in amplifier can extract only the signal component that is modulated in the same way as the probe laser. Large background, which is not modulated at all, is completely rejected. We can get the same effect by modulating a component of the system that the signal directly depends upon instead of modulating the probe laser. The bandwidth of lock-in detection is limited by the modulation frequency. In practice the amplitude modulation is done by a mechanical shutter or a AOM shutter with a modulation frequency lower than 10 kHz for a mechanical shutter and perhaps up to 100 kHz for a AOM shutter.

A much higher bandwidth is available with the frequency modulation (FM) spectroscopy. Instead of modulating the amplitude of a probe laser, its frequency is modulated. Typically modulation frequency lies between 10 MHz and 1 GHz, achieving 2–4 orders of magnitude improvement in bandwidth. The optical FM spectroscopy has been widely used since its invention [61]. When combined with saturation spectroscopy, it turns into the Doppler-free high resolution spectroscopy. The principle of the FM spectroscopy is best understood by noting that frequency modulation of a probe laser results in generating two side bands in the probe spectrum with opposite phases.

$$\begin{aligned} E(t) &= E_o \cos(\Omega t + M \sin \omega_m t) \\ &= \frac{1}{2} E_o \sum_{n=-\infty}^{\infty} J_n(M)\, \mathrm{e}^{i(\Omega + n\omega_m)t} + \text{c.c.}\,, \end{aligned} \tag{3.15}$$

where $J_n(x)$ is the Bessel function. If $M \ll 1$,

$$J_o(M) \cong 1 \;\text{ and }\; J_{\pm 1}(M) \cong \pm \frac{M}{2}$$

So

$$E(t) \cong E_o \cos \Omega t + \frac{M}{2} E_o \cos(\Omega + \omega_m)\, t - \frac{M}{2} E_o \cos(\Omega - \omega_m)\, t\,. \tag{3.16}$$

If we send this probe through a medium, the resulting field amplitude in complex notation is

$$E'(t) = E_o \left[T_o\, \mathrm{e}^{i\Omega t} + T_1 \left(\frac{M}{2}\right) \mathrm{e}^{i(\Omega + \omega_m)t} - T_{-1} \left(\frac{M}{2}\right) \mathrm{e}^{i(\Omega - \omega_m)t} \right]$$

where $T_n = \mathrm{e}^{-\delta_n - i\phi_n}$ with δ_n and ϕ_n accounting for the absorption/gain and the phase change experienced by the probe at $\Omega + n\omega_m$, respectively. The intensity of the probe is then

$$I'(t) \propto \; e^{-2\delta_0}\Big\{1 + \Big[\, e^{\delta_0-\delta_1}\cos(\phi_0-\phi_1) - \; e^{\delta_0-\delta_{-1}}\cos(\phi_0-\phi_{-1})\Big] M\cos\omega_m t \\ + \Big[\, e^{\delta_0-\delta_1}\sin(\phi_0-\phi_1) - \; e^{\delta_0-\delta_{-1}}\sin(\phi_0-\phi_{-1})\Big] M\sin\omega_m t\Big\} \;,$$

which simplifies to

$$I'(t) \cong \; e^{-2\delta_0}\left[1 + (\delta_{-1}-\delta_1)\, M\cos\omega_m t + (\phi_1+\phi_{-1}-2\phi_0)\, M\sin\omega_m t\right] \qquad (3.17)$$

if

$$|\phi_0-\phi_1|,\; |\phi_o-\phi_{-1}| \ll 1$$
$$|\delta_0-\delta_1|,\; |\delta_0-\delta_{-1}| \ll 1 \;.$$

If ω_m is much larger than a typical range of a spectral structure, the FM spectroscopy can map out two aspects of the spectral structure: absorption and dispersion. In this case, if one of the sidebands is placed near the structure as illustrated in Figure 3-12, the intensity is simply

$$I'(t) = I_o\; e^{-2\bar{\delta}}\left[1 \mp \Delta\delta M\cos\omega_m t + \Delta\phi M\sin\omega_m t\right] \;, \qquad (3.18)$$

where $\bar{\delta}$ and $\bar{\phi}$ are off-resonance values of δ_n and ϕ_n, respectively. These values can be considered as baselines relative which an absorption coefficient $\Delta\delta$ and a dispersion coefficient $\Delta\phi$ are measured. The minus/plus sign above corresponds to the $\Omega \pm \omega_m$ sideband, respectively. Then it becomes obvious that we can selectively measure the absorption or the dispersion coefficient by applying a phase-sensitive detection scheme, in which a raw signal is multiplied by $\cos\omega_m t$ or $\sin\omega_m t$ and averaged over a period of $\frac{1}{\omega_m}$.

In experiments, the phase-sensitive detection is electronically performed by a balanced mixer, which is a specially balanced pair of diodes with nonlinear response [62]. A frequency modulation is done by an electro-optic modulator (EOM) driven by a

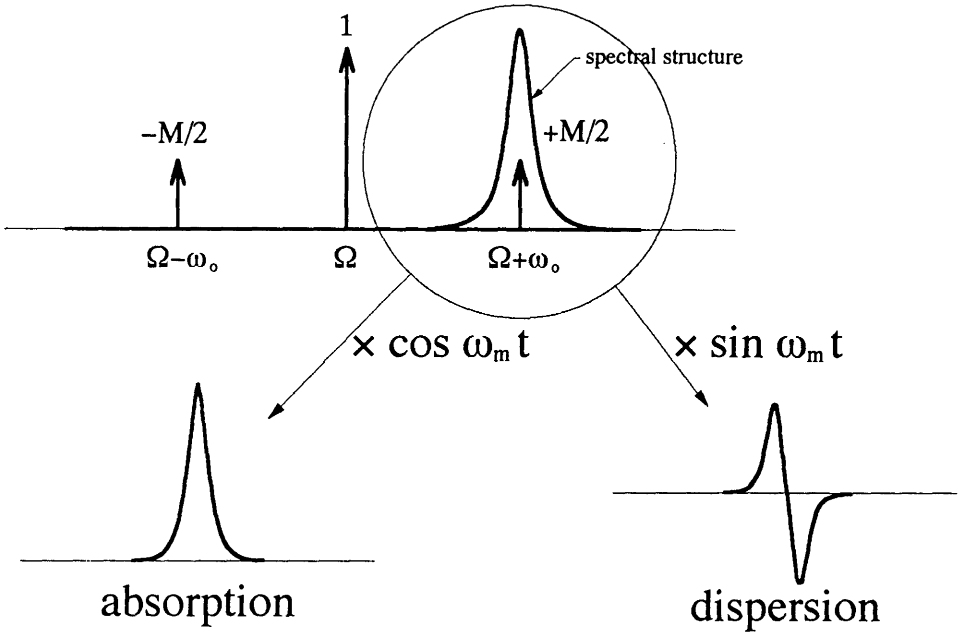

Figure 3-12: FM spectroscopy can reveal absorption as well as dispersion lineshape of a resonance line.

local oscillator, which is often a function generator. A transmission signal through a sample is measured by a fast detector, the bandwidth of which is much larger than the modulation frequency. The signal from the detector is sent to the RF (radio frequency) input of a balanced mixer, where the signal is mixed with a signal at LO (local oscillator) input. The resulting signal has two frequency components: $2\omega_m$ and DC. The $2\omega_m$ component is rejected by the mixer and only the DC component is available at its IF (intermediate frequency) output. We can select sine or cosine quadrature by controlling the relative phase between the input signal to RF and the local oscillator signal to LO input.

Lamb Dip

In a Lamb dip measurement, a pump and a probe beam with a same frequency traverse an atomic (or molecular) vapor cell. The atoms in the cell have different velocities according to the Maxwell-Boltzmann velocity distribution. The pump laser saturates a velocity group, which satisfies $\omega_o + kv_+ = \Omega$ with Ω the frequency of the laser and ω_o the frequency of the transition of interest. Then the probe propagating in

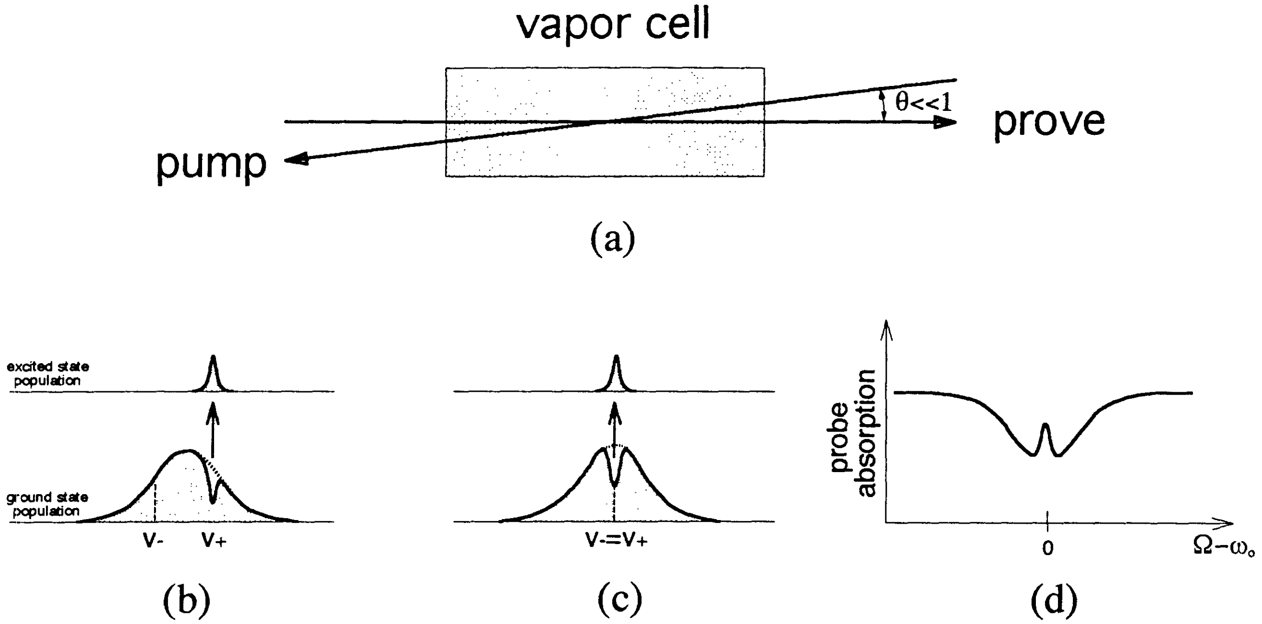

Figure 3-13: Lamb dip experiment. (a) configuration, (b) a velocity group with a velocity of v_+ is excited by a pump whereas a probe laser interacts with a velocity group with a velocity of v_-, where $v_\pm = \pm\frac{\Omega-\omega_o}{k}$, (c)the velocity group with $v_+ = v_- = 0$ is excited by both the probe and the pump laser if $\Omega = \omega_o$, (d) resulting probe absorption signal as a function of laser-atom detuning, $\Omega - \omega_o$.

the opposite direction will be resonant with a velocity group satisfying $\omega_o - kv_- = \Omega$. Since $v_+ = -v_- = \frac{\Omega-\omega_o}{k}$, two velocity groups do not share common atoms so the probe laser will measure unsaturated absorption profile of the vapor sample. However if Ω is tune to ω_o within the homogeneous linewidth of a velocity group, the probe will interact with the same velocity group atoms with zero velocity as the pump laser does. Since the intense pump laser depletes the ground state population of the zero-velocity group by exciting the atoms to an excited state, the probe laser interacts with less number of ground state atoms, and therefore its intensity will be attenuated less. This saturation effect results in a dip in an ordinary absorption profile as illustrated in Figure 3-13. The linewidth of the dip is the homogeneous linewidth of the atoms, including natural linewidth, collisional broadening and power broadening.

A barium vapor cell used in the experiment was made of 3/4" stainless steal tubing. The length of the cell was about 30 cm and the both ends had windows.

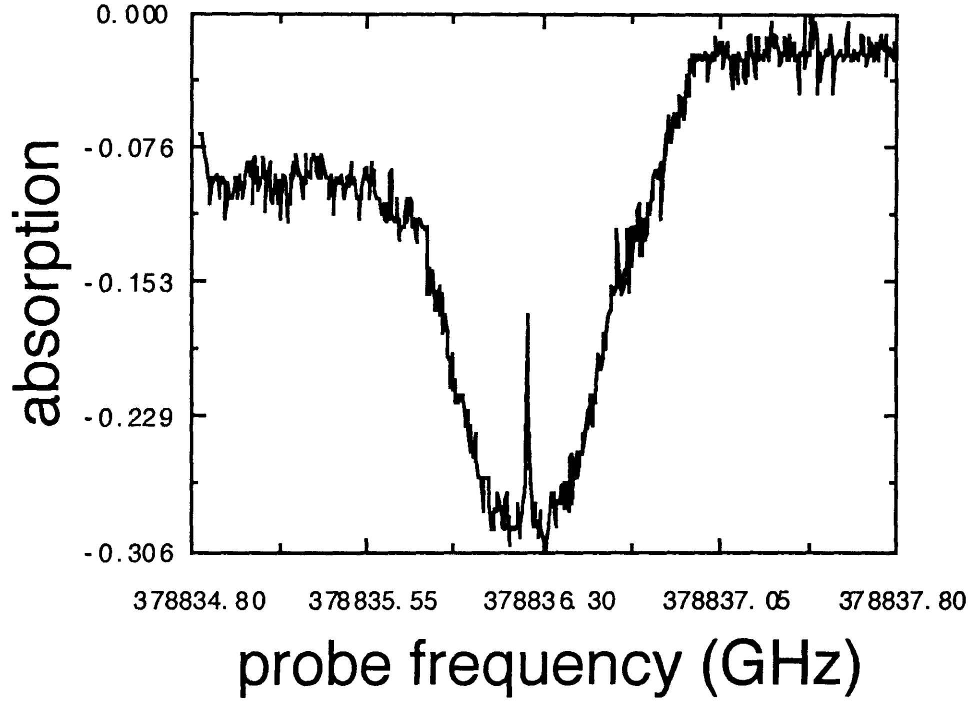

Figure 3-14: Typical Lamb-dip signal of the $^1S_0 \leftrightarrow {}^3P_1$ transition of atomic barium. The asymmetry in the baseline arose because the power of the probe laser changed as it was scanned.

The central 5 cm long part of the cell was heated by a non-contact cylindrical heater surrounding the cell. The heater had nichrome wires wound in a zig-zag pattern so that stray magnetic field inside was minimized. The vapor pressure was a few mTorr, at which the collisional broadening was in the order of 10 kHz. We used the $^1S_0 \leftrightarrow {}^3P_1$ transition, which has a 50 kHz linewidth. However the linewidth of the Lamb dip was about 2 MHz. We found that a slight misalignment ($\lesssim$ 0.5 mrad) between the pump and probe laser beams contributed a inhomogeneous broadening of 0.5 MHz to the measured linewidth. The most broadening came from the power broadening of the transition by the pump laser. In fact we could set the homogeneous linewidth to a value we wanted by adjusting the pump laser intensity. A typical pump intensity was 10 mW, giving rise to a Lamb-dip linewidth of 2.5 MHz (Figure 3-14).

With the FM spectroscopy, we can map out not only the absorption lineshape but also the dispersion lineshape of a spectral line. The Lamb dip itself can be though as a spectral line. Therefore if we replace the probe in the Lamb dip experiment with a frequency-modulated laser beam while keeping the pump laser unmodulated, we can obtain a dispersion lineshape of the Lamb dip. For this, we assume that the modulation frequency is much smaller than the linewidth of the Doppler profile but much larger than the homogeneous linewidth of the dip. Since the FM signal is proportional to the difference between the absorption coefficient at one sideband and the coefficient at the other sideband (Eq.3.17), the signal is very small if none of the sideband is resonant with the Lamb dip transition. Therefore the FM signal does not contain the broad Doppler profile. Only the dispersion or absorption lineshape of the Lamb dip is revealed.

For the experiment, we used an EOM (INRAD 651-254) driven by a quartz-tuned function generator (Standford Research DS-3100) at 25.000000 MHz. The FM signal was measured by a silicon photodiode (EG&G FND100), which was biased at -90 V to have a rise time of 2 ns with 50 Ω impedance. The current from the photodiode was directed to the RF port of a balanced mixer (VARI-L CM-4). As discussed before, depending on the phase of the local oscillator signal in the balanced mixer relative to the phase of the FM signal, either a dispersion lineshape or an absorption lineshape is selected from the FM signal. In order to adjust the phase difference, we varied the length of the BNC cable connecting the function generator and the LO port of the mixer. Since the speed of light in a BNC cable is 2×10^8 m/s, a 2π phase change is obtained by a length change of $\frac{2\text{x}10^8 m/s}{25\text{MHz}} = 8$ m. The output at the IF port of the mixer was amplified by a homemade DC amplifier (Figure 3-15) and then displayed and digitized on a digital scope (Lecroy 9310M). Figure 3-16 shows a typical FM Lamb-dip signals as a function of the laser-atom detuning $(\Omega - \omega_o)$. The curve consists of three dispersive resonances at $\Omega = \omega_o, \omega_o \pm \omega_m/2$. Note that a same velocity group can be excited by the pump laser and probed by the probe laser if

$$\begin{aligned} kv_+ = \omega_o - \Omega = kv_- &= \Omega \pm \omega_m - \omega_o \text{ ,for sidebands} \\ &= \Omega - \omega_o \text{ ,} \qquad \text{for carrier} \end{aligned} \tag{3.19}$$

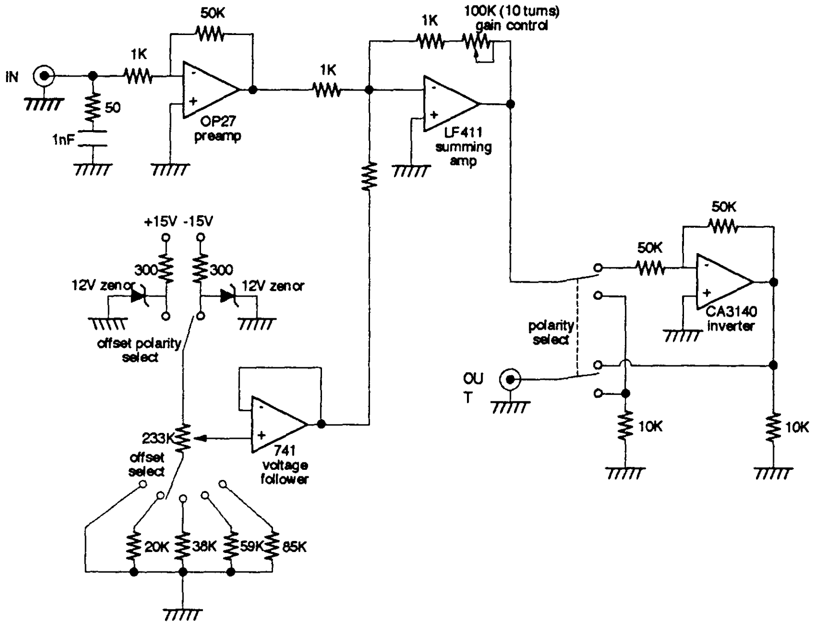

Figure 3-15: A homemade DC amplifier circuit used in the FM Lamb-dip measurement.

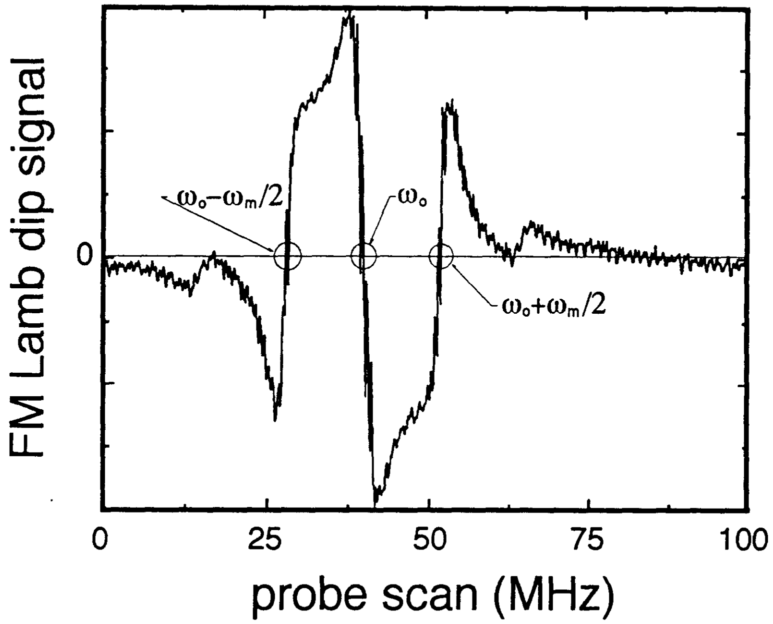

Figure 3-16: A typical FM Lamb-dip signal. It consists of three dispersive resonances at $\Omega = \omega_o, \omega_o \pm \omega_m$.

and therefore,

$$\Omega = \omega_o, \omega_o \mp \frac{\omega_m}{2} \, . \tag{3.20}$$

FM Laser Stabilization/Locking

The dispersion lineshape of the Lamb dip shown in Fig 3-16 was measured as a function of the laser-atom detuning. We are interested in the central straight segment of the curve, where the FM signal is directly proportional to the difference between the laser and the atom frequencies. In other words, the FM signal itself can be a direct indicator of a frequency error when we want to make the laser frequency the same as the atom frequency. Therefore the laser can be stabilized as well as locked relative to the atom by nullifying the error signal. This nullification can be done in real time by forming a negative feedback loop composed of the laser, the Lamb-dip setup and an amplifier for the FM signal with a properly chosen polarity.

The laser system we used in the experiment had a reference cavity, to which the frequency of the laser was locked. An error signal generated by the reference cavity was processed in a so-called 'control box' to provide necessary voltage signals for the frequency-correcting elements in the laser head. There are two such elements with different bandwidths, a tweeter mirror driven by a PZT ($\gtrsim$ 1 kHz) and a tipping plate driven by a galvo drive ($\lesssim$ 1 kHz). The control circuitry includes a cross-over network to generate drive signals with proper bandwidth for the elements.

We could lock the laser to the atom simply by substituting the error signal from the reference cavity with the FM Lamb-dip signal. We still utilized the control box for the signal processing. The homemade amplifier circuit shown in Fig.3-15 was used as a pre-amplifier for the FM signal, also providing a correct polarity for the negative feedback. The FM signal was amplified by the circuit to a voltage level comparable to the error signal from the reference cavity. In this way the FM signal fed to a differential amplifier in the control box could be in a proper input range ($\sim$ 50 mV RMS). The frequency range of the straight segment in the FM Lamb-dip signal was identical to the homogeneous linewidth of the Lamb dip, about being 2.5 MHz. The peak-to-peak height of the segment was 250 mV. Hence the slope of the straight segment was 10 kHz/mV.

With a switch box, we could choose the source of the error signal to be either the reference cavity or the FM Lamb-dip signal. When the reference cavity was used for locking, even if we initially placed the laser at the atomic resonance, the laser slowly drifted away from the resonance. Furthermore due to random fluctuations in the laser frequency the the FM signal swung up to the full height of the straight segment, indicating the frequency error up to 2–3 MHz. This large fluctuation was mostly at low frequencies ($\lesssim$ 10 Hz), and its source appeared to be the reference cavity. The FM signal also had underlying fast frequency components ($\gtrsim$ 100 Hz), but their amplitudes were about 30 mV RMS, corresponding to excursions of 300 kHz RMS. These fluctuations were greatly reduced when the FM Lamb-dip signal was used in the feedback loop instead of the reference cavity signal. When the laser was locked to the resonance, the size of the FM error signal was about 15 mV RMS, corresponding to frequency fluctuations with an excursion of 150 kHz RMS. These fluctuations,

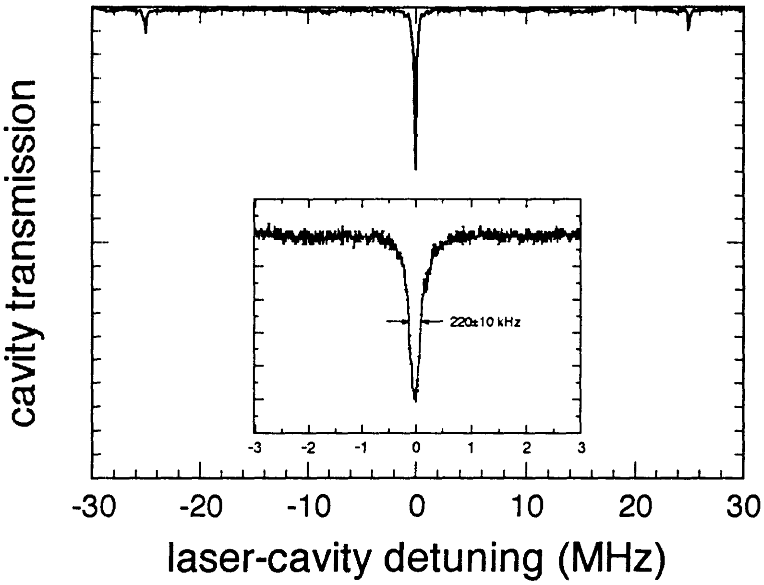

Figure 3-17: Laser spectrum when it is stabilized by the FM scheme described in the text. It was measured by a scanning Fabry-Perot with a linewidth of 110 kHz ($\mathcal{F} = 1.3 \times 10^6$). The Fabry-Perot was scanned fast enough so that the laser fluctuations at 660 Hz did not affect the measurement. The measured linewidth of 220 kHz therefore corresponds to a laser linewidth of 110 kHz, or 55 kHz RMS.

however, were regular, mostly at 660 Hz. Later we found that this frequency was associated with the mechanical resonance of the galvo-driven tipping plate in the laser head. Except this frequency component, the size of the FM error signal was 5 mV RMS, resulting in an excursion of 50 kHz RMS. Figure 3-17 shows the spectrum of this frequency-stabilized laser probed by a scanning Fabry-Perot, which was in fact the supercavity resonator used in the experiment. The Fabry-Perot was scanned fast enough so that the laser fluctuations at 660 Hz did not affect the measurement. The two peaks on the side were due to the sidebands by the frequency modulation at 25 MHz. These sidebands actually serve as frequency marks for calibrating of the frequency scale. The linewidth of the central peak is 220 kHz. Since the resonator had a linewidth of 110 kHz FWHM ($\mathcal{F} = 1.3 \times 10^6$) for this measurement, the contribution from the laser was 110 kHz or 55 kHz RMS, which is consistent with the estimation based on the FM error measurement.

We did not attempt to eliminate the noise at 660 Hz since its excursion, 300 kHz, was acceptably small for the one-atom laser experiment. In the experiment this laser is used as a pump laser, which is focussed down to 50 μm spot. The transit time broadening in this case is 2.5 MHz, and therefore the 300 kHz frequency uncertainty of the pump has practically no effects on the pumping process. However this uncertainty certainly affects the performance of cavity locking, which is the subject of the next section.

3.1.5 Cavity Locking

Locking the frequency of the resonator to that of the pump laser is not compulsory in the experiment in the sense that the resonator at its free-running state has only 50 kHz frequency jitter. Of course the resonator frequency is slowly changing but is in a predictable way. Its frequency drifts slowly and linearly at a rate of about 1 MHz/sec. The direction of the drift and the exact drift rate depend on the history of the resonator, such as stress on the PZT, temperature and vacuum pressure which the resonator has been exposed to. An important fact is that the resonator undergoes any change of state very slowly and linearly if it is not under sudden perturbation. Therefore when we perform the experiment, the resonator is simply let to drift toward the atomic resonance, and the output of the one-atom laser is measured as a function of atom-cavity detuning. However it is convenient to have the resonator locked to the atom (and the pump laser) whenever the one-atom laser is aligned from a scratch or re-aligned for some reason. With the resonator locked, we can monitor the output of the one-atom laser in real time while we adjust the rest of parameters such as the angle between the atomic beam and the resonator axis and the position of the pump laser relative to the cavity mode. With eliminating the uncertainty on the resonator frequency, the phase space that alignment process to cover is greatly reduced.

For the locking, we used a scheme similar to the cavity-side-lock method [63]. In our scheme, an error signal, which to be fed back to the PZT of the supercavity resonator, was obtained by subtracting a reference voltage from a signal measuring the transmitted power of a locking laser through the resonator (Figure 3-18). The locking

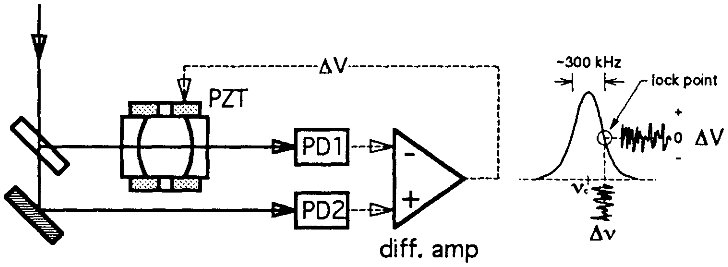

Figure 3-18: Cavity Locking Scheme used in the experiment

beam was obtained from the frequency-stabilized Ti:Sapphire laser, so was the pump beam. An silicon avalanche photodiode (EG&G C30902S) at -230 V bias was used to measure the transmitted power. The reference voltage was in fact obtained from a silicon photodiode (EG&G FND-100) measuring a reference laser beam intensity. 100 kΩ load resistances were used to convert photocurrent to voltage for both photodiodes. A differential amplifier measured the difference between the transmission signal and the reference voltage. The intensity of the reference beam was adjusted with a polarizer so that the output of the differential amplifier became zero when the resonator was detuned to a side of the transmission lineshape. The amount of detuning was equal to the half width of the lineshape so that the resulting transmission was 50 % of its maximum. At the half-height point the output of the differential amplifier was proportional to the frequency difference between the resonator and the locking laser. Therefore the output could be used as an error signal for the cavity locking. Figure 3-19 show a circuit which generates a feedback signal from the photocurrents of the two photodiodes.

A drawback of this scheme is that the cavity is locked to the atomic resonance with an offset frequency, which is equal to the half width of the transmission lineshape. However the offset was only 150 kHz, which is much smaller than a gain bandwidth of the one-atom laser, 3 MHz. This bandwidth is due to the transit time broadening associated with the small waist of the cavity field mode. So the 150 kHz offset did not affect the output of the one-atom laser. This locking scheme is insensitive to the power fluctuations in the laser beams because both the reference and the locking beam are derived from a same source, a Ti:Sapphire laser. Therefore any power fluctuations in

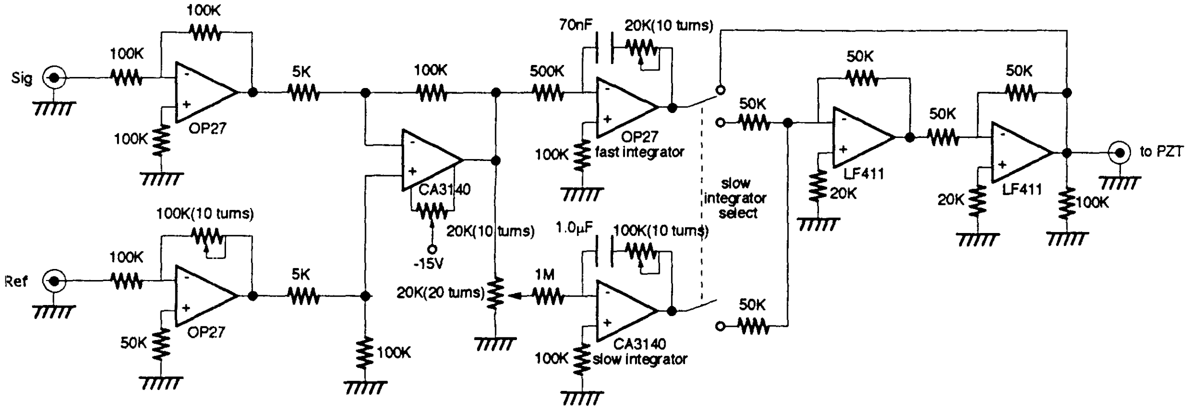

Figure 3-19: A homemade circuit used to lock the cavity

the source equally affect the reference and the locking beam, so the frequency offset remained unchanged.

The performance of the cavity locking was mostly limited by the frequency stability of the locking laser. As discussed before, the stabilized Ti:Sapphire laser had 660 Hz noise coming from its tipping plate of the laser. The noise excursion was 150 kHz RMS. Since the locking laser was derived from the Ti:Sapphire laser, the error signal contained the 660 Hz noise, inducing the feedback circuit to react to this error. As a result, the 660 Hz noise were transferred to the resonator. The feedback loop performed admirably in reducing the apparent frequency error below 100 kHz. However it is only relative error between the cavity and the locking laser. Absolute frequency error between the cavity and the atom could be larger than that. Therefore we intentionally kept the feedback gain at its minimum requirement in order not to reduce the cavity-locking laser error too much. In this way we could minimize the transfer of noise from the locking beam to the cavity, thereby keeping the cavity frequency as near to the atomic resonance as possible.

Whenever the resonator is locked to the locking laser, the laser beam has to go through the resonator. This beam, however, will interact with the atoms in the resonator and disturb the one-atom laser operation. This problem can be avoided by alternating the cavity locking and the one-atom laser operation rapidly enough that the cavity locking is still maintained. We used an acousto-optic modulator (AOM,

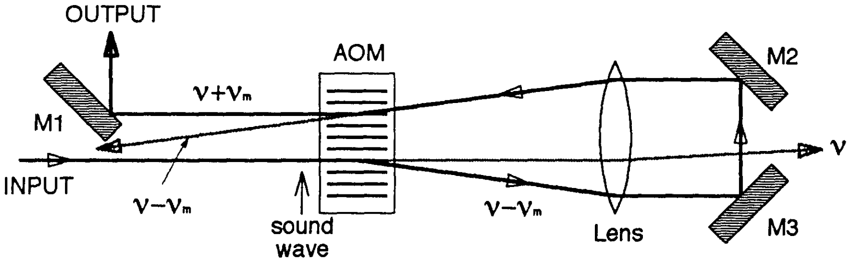

Figure 3-20: A double-pass configuration of a AOM without a frequency shift. It was used in the experiment to modulate the amplitude of the locking laser beam.

Isomet 1206C) in a double-pass configuration shown in Figure 3-20 to control the locking beam. In this configuration the first passage of the locking beam through the AOM undergoes an $m = -1$ order diffraction accompanying a downward frequency shift by an amount of the AOM modulation frequency (80 MHz). The second passage, on the other hand, undergoes an $m = +1$ diffraction, inducing a upward shift by the same amount as the first shift, therefore exactly canceling the frequency shift. The diffractions take place only when a TTL high-logic signal is applied to the modulation input of the RF driver circuit (Isomet DB320). By applying a TTL clock signal to the input, therefore, we can modulate the amplitude of the probe beam as needed.

The various values of the period of the clock signal have been tested. A good performance of the locking was obtained with a clock which turns on the probe for 383 μsec and turns it off for 127 μsec, resulting in a duty cycle of 25 %. We used this setting later through out the one-atom laser experiment.

3.1.6 Detector

Avalanche Photodiode

Photo multiplier tubes (PMTs) have been the choice of detector for the photon counting for many years. PMTs with multi-alkali photocathode have good quantum efficiencies in the visible region, particularly at 350∼550 nm. Quantum efficiencies of 10 ∼ 20 % are common. As the wavelength approaches 800 nm, however, the quantum efficiency of multi-alkali photocathode quickly drops below 1 %. In this wavelength

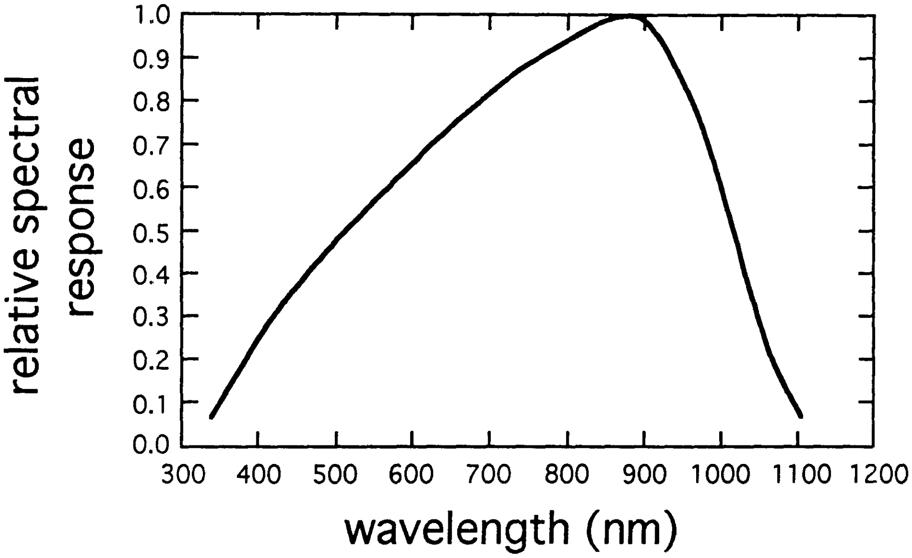

Figure 3-21: Relative spectral response and corresponding quantum efficiency of silicon photodiode, excerpted from EG&G Short Form Catalog (1992). The quantum efficiency is proportional to the spectral response divided by wavelength

region, GaAs is the best material for photocathode. At 791 nm the efficiency of GaAs photocathode is up to 10 % [64]. In order to use GaAs photocathod in photon counting mode, elaborate cooling down to −20 ~ −30 °C is essential.

As far as quantum efficiency is concerned, silicon photodiode is much better than PMTs, particularly for longer wavelengths. It can have up to 100 % efficiency around at 900 nm. However silicon photodiode has only a gain of unity and its background counts are unacceptably high ($\sim 10^{5-6}$ cps). For this reason silicon photodiode is more suitable in measuring large photon flux ($\gg 10^6$ cps) not in photon counting mode but in current mode.

Recent developments in avalanche photodiode (APD) have offered researchers a new option for photon counting detectors. A silicon avalanche photodiode has a high quantum efficiency just like an ordinary silicon photodiode (Figure 3-21). It also features high amplification gain owing to electron avalanche process just like PMTs. Therefore even a single-photon event can generate a macroscopic current pulse. According to our measurement, which is described below, the quantum efficiency at 791 nm is more than 36 %, far superior than PMTs.

category	Det 1	Det 2	Det 3
model	C30902S	C30902S-TC	C30902S-TC
serial No.	8490	163	166
operating temperature	22 °C	-20 °C	-20 °C
breakdown bias voltage	221.7 V	202.5 V	157.0 V
operating bias	216.0 V (?)	212.9 V	167.2 V
dark counts	–	3000 cps	300 cps
usage	cavity transmission	density calibration	signal count

Table 3.5: The characteristics of the APDs used in the experiment.

The APDs used in the experiment were EG&G C30902S and C30902S-TC, where the latter model has a detector core mounted on a miniature thermo-electric cooler. The cooler drew a current of about 1 A, at which the temperature could be lowered to -20 °C. When the APDs were cooled, dark counts, which is the counts with no light incident on them, were reduced to 300 $\sim$ 3000 counts/sec depending on the models. They require bias voltage of about 200 VDC. Exact required bias voltage varies from detector to detector. Usually it is set at a voltage larger than a breakdown voltage by 10 V. The breakdown voltage is a bias voltage at which the avalanche processes start to occur. Table 3.5 summarizes the characteristics of the APDs used in the experiment.

One of the general characteristics of APDs is temporal saturation of the detectors just after an avalanche process. an APD can be modeled by an equivalent circuit shown in Figure 3-22. When an electron avalanche occurs, the APD becomes conductive. In the equivalent circuit, the switch S is closed, the internal capacitor of the APD, C_i, is quickly discharged, and the switch reopens. The whole sequence takes about a few nsec. Then no further avalanche occurs until C_i is fully recharged so that a full bias voltage is applied to the APD. The recharging time is about a few μsec. During that time, the detector is not capable of photon counting. This property limits the number of photons that the detector can handle. The maximum number of counts per second the detector can handle is about 10^4 cps ($\sim 10^5$ photons/sec). Therefore it is necessary to *quench* the internal capacitor as soon as a signal pulse has been generated. We used a passive-quenching scheme, in which the internal capacitor

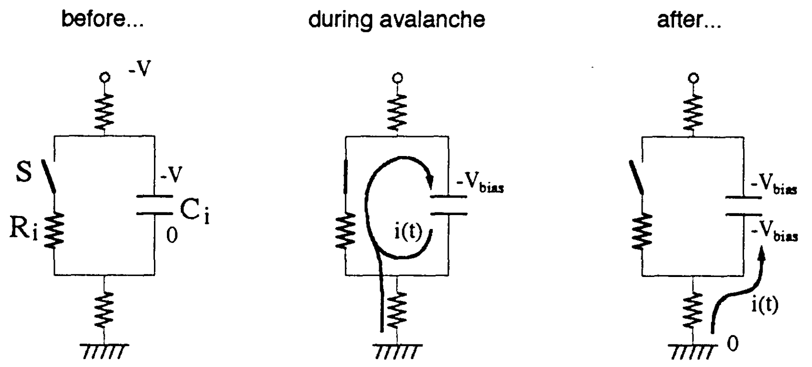

Figure 3-22: An equivalent circuit for an avalanche photodiode.

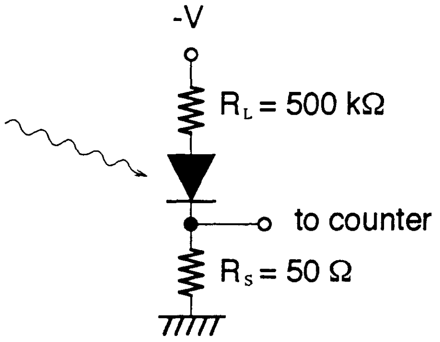

Figure 3-23: A passive-quenching circuit for the APDs used in the photon counting mode.

is passively discharged all the time by a resistor with a small value in series to the APD. Figure 3-23 show a passive-quenching circuit used in the experiment.

Efficiency Measurement

In an experiment, a useful parameter representing a detector efficiency is not the quantum efficiency but a counting efficiency, that is how many clicks are registered on an electronic photon counter for a given number of photons incident on a detector. The counting efficiency depends not only the quantum efficiency of a detector but also other electrical parameters, most importantly a discriminator level setting on a photon counter. If the discriminator setting is too low, we may get a maximum counting efficiency, but also a lot of noise pulses owing to dark current can be maximally counted. An optimal discriminator setting can be obtained by the pulse-height analysis, in which the discriminator level is continuously varied under nominal light condition while the rate of counter clicks on the photon counter is measured. Figure 3-24 shows the result of the pulse-height analysis on one of the APDs when used with a photon counter (Stanford Research System SR-400). The discriminator level was set where counting distribution is flat (at -50 mV). The dark counts listed in Table 3.5 are based on this discriminator setting.

With this discriminator setting we have measured counting efficiencies of the two APDs with a cooler. A probe laser beam with a wavelength of 553 nm was attenuated by an overall factor of 3×10^{-11}. The attenuation was done by neutral density filters with high optical densities and a prism polarizer at a right angle to the probe polarization. The filters were intentionally tilted relative to each other in order to prevent interference among filters. Since the attenuated beam is too weak to be measured by a power meter (Coherent model 212), the sensitivity of which is 0.01 μW at best, the filters were grouped in two and the attenuation by each group was measured separately. A typical incident power on an APD detector was in the order of 1×10^{-12} W. We varied the bias voltage on the detector and measured the number of counts per second. From the incident power we can estimate the number of photons incident on the detector per second. The ratio of these two rates is the counting efficiency of the combined system of the detector and the photon counter. Figure 3-25 shows the counting efficiency of one of the APDs for various bias voltages. The bias voltage was later fixed at a value larger than the breakdown voltage by 10 V for the one-atom laser experiment. The counting efficiency at 791 nm were then calculated based on the spectral response of silicon APDs shown in Fig. 3-21 and the efficiency at 553 nm. The counting efficiency, which is proportional to the quantum efficiency, is related to the spectral response in the following way.

$$\text{spectral response} \propto \frac{\dot{N}\eta_{QE}}{\dot{N}\hbar\omega} = \frac{\eta_{QE}}{\hbar\omega} ,$$

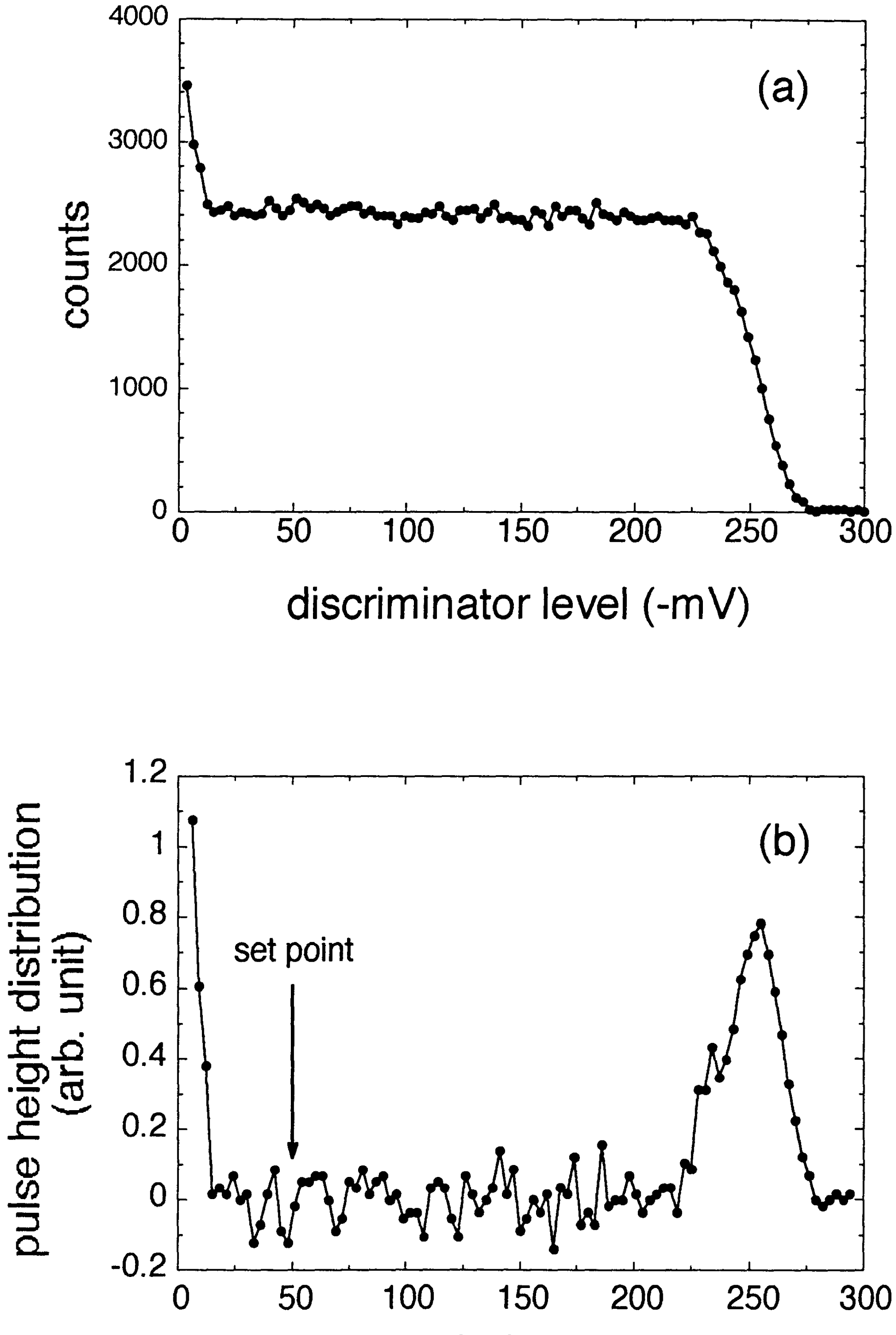

Figure 3-24: A typical result of the pulse-height analysis on an APD detector (S/N 166) at -20 °C. (a) Number of counts vs. discriminator level and (b) a pulse-height distribution, which is just the derivative of curve-(a).

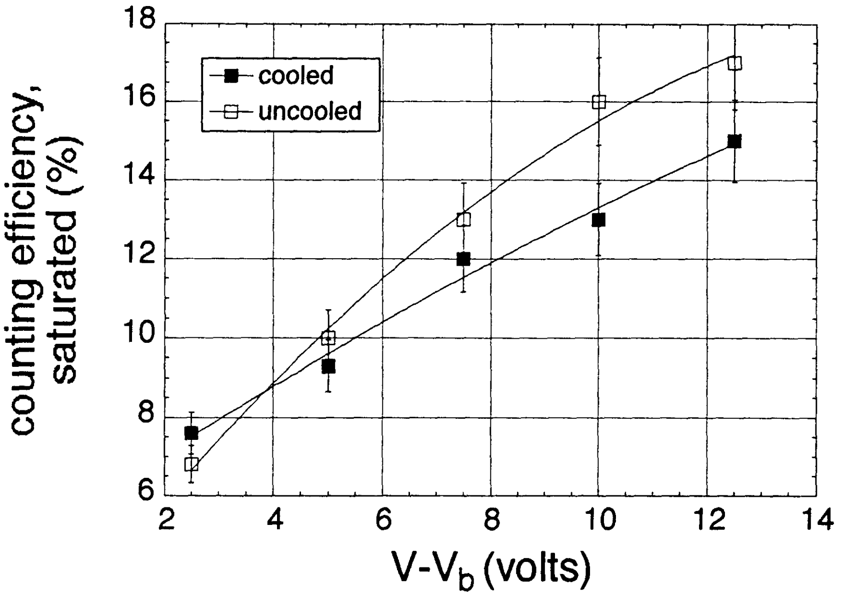

Figure 3-25: Counting efficiency of an APD detector (S/N 166) at 553 nm as a function of bias voltage. Counting efficiencies corrected for detector saturation are shown in Figure 3-27.

where $\dot{N}$ is the number of photons incident on the detector per second.

The counting efficiency also depend on the number of photons incident on the detectors. Even with the quenching circuit the detectors start to saturate at about 4×10^5 counts/sec (the number of photons$\sim 10^6$ /sec). In fact the counting rate at which the counting efficiency had been measured was in the order of 10^5 counts/sec, so we had to suspect that an actual efficiency might be higher that the value quoted before. In order to study the detector saturation, we used the detector to measure the fluorescence from barium atoms in an atomic beam. Throughout the measurement, the detector was set up to image a fixed volume. The number of atoms in the volume were varied by changing the current through an atomic beam oven. The atoms were excited by a probe laser, which was resonant to the $^1S_0 \leftrightarrow {}^1P_1$ transition (553 nm). The probe laser intensity were kept well below the saturation intensity of the transition, 16 mW/cm^2. For a fixed oven current, we recorded the number of signal counts per sec for various probe intensity. The number of counts then should be proportional to the probe intensity as long as the intensity is kept well below the saturation intensity. Any

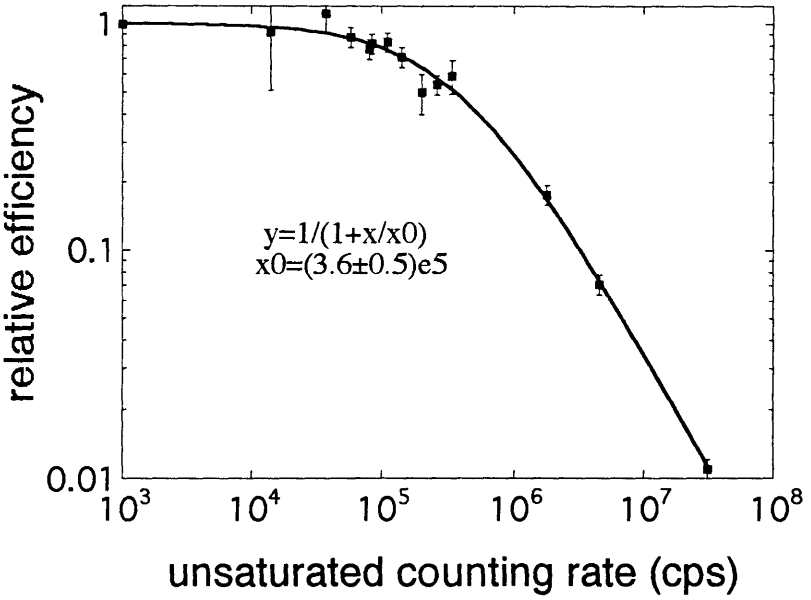

Figure 3-26: Saturation effect of an APD detector (S/N 166).

deviation from the linearity should be attributed to the saturation of the detector. We repeated the measurements for various oven currents to cover an extensive range of the number of counts. The result is shown in Figure 3-26. As seen in the figure, the saturation effect of the detector can be summarized by an empirical formula

$$y = \frac{x}{\left(1 + \frac{x}{(3.6 \pm 0.5) \times 10^5}\right)}, \tag{3.21}$$

where y is a saturated counting rate and x is a unsaturated counting rate. Both are in counts per second. Using this formula, we can correct the previously measured counting efficiencies. The result is summarized in Figure 3-27. We repeated the efficiency measurement of the other APD detector (S/N 163) and obtained about the same result within experimental error. Therefore we conclude that the counting efficiencies of the APD detectors used in the one-atom experiment are 32 ± 4 % at 553 nm and 36 ± 4 % at 791 nm. The corresponding quantum efficiencies should be greater than the counting efficiencies.

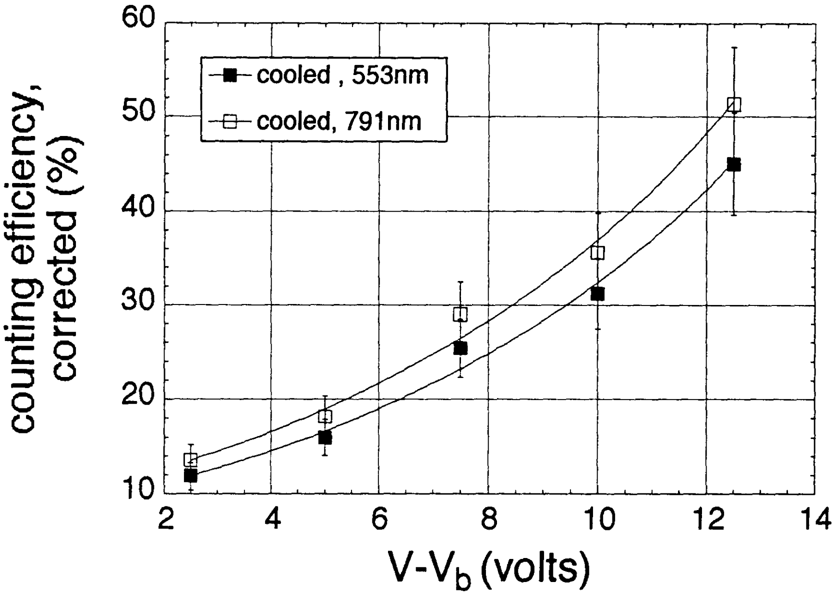

Figure 3-27: Counting efficiencies of an APD detector (S/N 166) corrected for detector saturation as a function of bias voltage.

3.1.7 Vacuum System

A Vacuum chamber system houses the supercavity resonator and an atomic beam oven. It consists of two chambers, one containing the oven and the other surrounding the resonator. These chambers are connected by two tubular lines, one for an atomic beam and the other for efficient pumping of the resonator chamber through the oven chamber (Figure 3-28). The chamber system was designed with possible use with the laser slowing and trapping in mind. It features four extended view ports at 90 degrees, allowing to set up six orthogonal laser beams when combined with two large view ports at the top and the bottom. The tubular line for pumping is made of a stainless steel flexible tubing so that its length and degree of bending are easily adjustable. The other line for the atomic beam is a rigid tubing with four view ports for diagnosis of the atomic beam. Both lines are connected to the sub-chambers by Conflat flanges so that rearranging of the chamber parts, when necessary, is easily done. The atomic beam line can be replaced with an auxiliary chamber, which may houses a velocity selector for future experiment, for example.

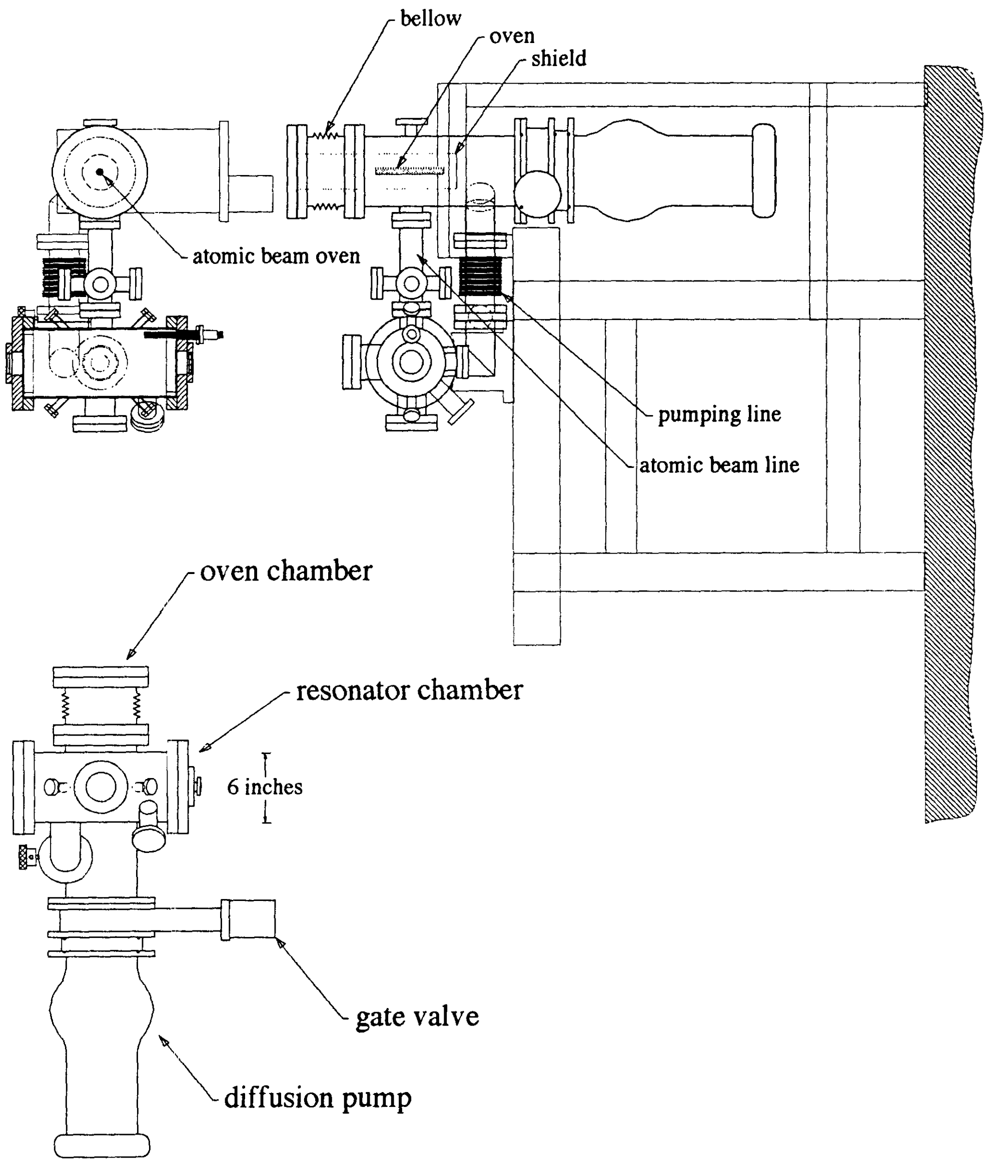

Figure 3-28: A vacuum chamber system for the supercavity resonator and an atomic beam oven.

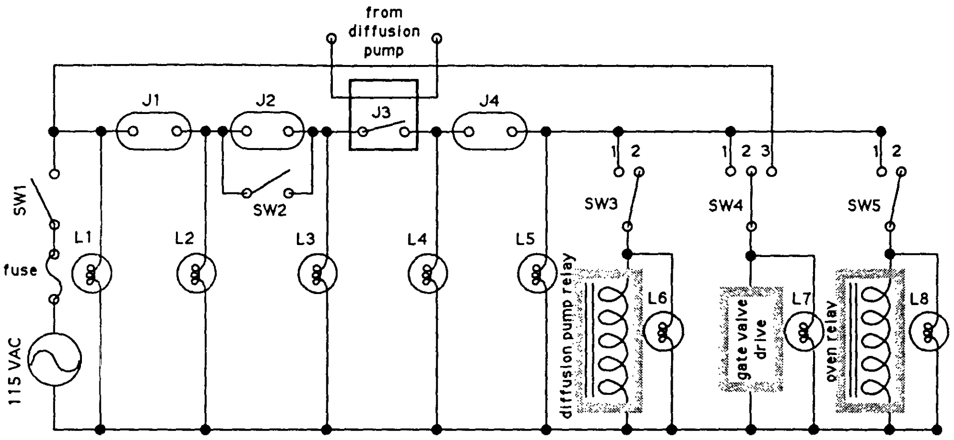

J1: on/off relay, backing pressure
J2: on/off relay, chamber pressure
J3: on/off switch, diffusion pump overheating
J4: on/off relay, flow switch for cooling water

L1: power on/off indicator
L2: backing pressure OK
L3: chamber pressure OK
L4: diffusion pump tempterature OK
L5: cooling water flow OK
L6: diffusion pump on/off indicator
L7: gate valve open/close indicator
L8: oven on/off indicator

SW1: power switch
SW2: ion gauge override (on for diffusion pump isolated operation)
SW3: diffusion pump mode switch
  1=interlock engaged
  2=off
SW4: gate valve mode switch
  1=automatic
  2=manual close (off)
  3=manual open (on)
SW5: oven switch
  1=on
  2=off

Figure 3-29: An interlock circuit controlling the vacuum system.

The oven chamber is connected to an inlet of a diffusion pump (Varian VHS-4) through a pneumatically driven gate valve (MDC GV-50000) and a water-cooled optical-dense baffle (Varian BFxxx), which prevents pump oil backstream. The gate valve as well as the diffusion pump are controlled by a homemade interlock circuit shown in Figure 3-29, which closes the valve and shuts off the pump if the vacuum pressure rises beyond a certain set point. The interlock circuit also monitors the cooling water flow to the atomic beam oven and the diffusion pump as well as the backing pressure at the diffusion pump exhaust maintained by a mechanical rough pump. The circuit also allows a user to turn on the oven only when all the check points are satisfied. If anything goes wrong, the circuit immediately shuts down the vacuum system. The rough pump is running all the time and its backing pressure is lower than 50 mTorr.

The pumping speed (S) of the diffusion pump is 1000 l/s. The total volume (V) and the surface area (A) of the chamber system are about 30 liters and 1 m^2 respectively. Typical vacuum pressure when the experiment was performed was 5 ×

10^{-8} Torr. A outgassing rate q of all the components in the chamber system including the chamber wall can be estimated from these values.

$$\begin{aligned} q &= \frac{dN}{dt}\frac{k_B T}{A} \\ S &= \frac{dV}{dt} = \frac{dN}{dt}\frac{k_B T}{P} \\ \text{therefore } q &= \frac{SP}{A} = 7 \times 10^{-6} W/m^2 \end{aligned}$$

The vacuum system was designed with Claris CAD on a Macintosh computer. The major parts of the chamber system were fabricated by MDC [65].

3.1.8 Atomic Beam Oven

The technique we used to generate barium atomic beam is to heat up a piece of barium metal in an oven above 500 °C in vacuum. The barium oven was simply a tantalum tubing with a small aperture in the center. The tubing was $6\frac{1}{2}$" long with 1/32" wall thickness and the diameter of the oven aperture was 340 μm. The both ends of the tubing were sealed by clamping them tightly and 250–400 amps of AC current ran through the tubing, heating it up to 500 - 700 °C. Such high current was converted from an 240 VAC/30 A line by a step-down transformer with a turn ratio of 71 : 1.

The thermal radiation from the oven needed to be blocked by a water-cooled copper shield surrounding the oven. An oven assembly consisted of the oven, the shield and electrodes supplying the current. The assembly was mounted on 8" Conflat flange, which also serves as a top cover of the oven chamber. A flexible bellow with three adjusting screws was placed between the flange and the body of the oven chamber so that the position of the oven could be adjusted whenever necessary (see Figure 3-28).

The atomic beam was collimated by four additional apertures. Their locations and diameters are summarized in Table 3.6. The last aperture was place just in front of the resonator. The distance between them was 2 cm. A maximum divergence angle

ID	distance from oven	diameter
oven aperture	0	340 μm
aperture 1	5.5 cm	8.1 mm
aperture 2	10 cm	7.1 mm
aperture 3	34.5 cm	1.5 mm
aperture 4	40.5 cm	340 μm

Table 3.6: Atomic beam apertures used in the experiment

(half angle) of the atomic beam at the resonator was 0.8 mrad, solely determined by the sizes of the oven aperture (340 μm) and the last aperture (340 μm) as well as the distance between the oven and the resonator (43 cm). This divergence gives rise to a maximum Doppler broadening of 640 kHz (full width) in the coupling between the atom and the cavity field. However an effective broadening is only a half of that, a full width of 320 kHz, because of the averaging over all possible angles as explained below. This Doppler broadening did not affect the performance of the one-atom laser since the gain bandwidth of the excited atoms by the π-pulse excitation field was larger than the broadening by an order of magnitude.

We performed Monte Carlo simulation to find the distribution of the Doppler broadening, and the results are shown in Figure 3-30. The FWHM of the distribution depends very weakly on the smaller aperture of the two apertures, the oven and the last aperture. The relative sizes of the two apertures, however, determine the shape of the distribution. When they are about equal, the distribution resembles a gaussian distribution whereas its shape is close to a half circle when they are different much. The half-circle distribution can be understood in the following way. Let's consider a cone, which has a height much larger than a base radius (Figure 3-31). We can think the end point as a very small aperture and the base as a large aperture. We want to know the angular distribution of the lines drawn from any points on the base to the end point. An important angle is the angle between such a line and a plane bisecting the cone because we can assume that the resonator axis is perpendicular to the plane and so is the propagation direction of the cavity field. Any points on a line which is parallel to the plane and lies on the disk correspond to the same angle. Then it is

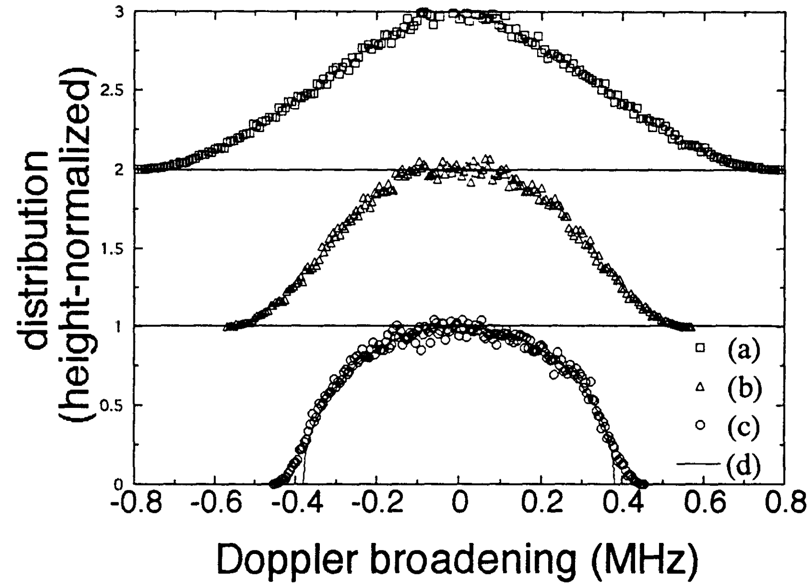

Figure 3-30: Distribution function of the Doppler broadening for a diverging atomic beam obtained by Monte Carlo simulation. The diameter of the oven aperture is 340 μm whereas the diameter of the last aperture is varied among (a) 340, (c) 150, and (c) 50 μm. In (d) a perfect semi-circle distribution is shown for comparison with (c).

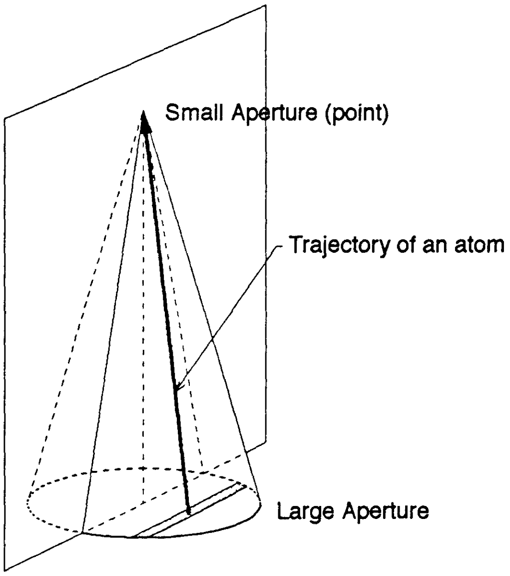

Figure 3-31: Origin of the half-circle distribution

obvious that the distribution of such angle is proportional to the length of the line, resulting in a shape of a half circle with the diameter of the circle is exactly the acute angle of the cone.

Density Calibration

It is important to know the density of the atoms since the output signal of the one-atom laser critically depends on the average number of atoms in the resonator. We used atomic fluorescence to calibrate the density. The atoms in the resonator were excited by a probe laser beam tuned to the ${}^1S_0 \leftrightarrow {}^1P_1$ transition of atomic barium. The probe beam was obtained from a CW single-mode dye laser (Coherent CR599-21). The probe beam propagated along the resonator axis and focussed down to a small spot with a waist of about 50 μm inside the resonator by a lens with a 30 cm focal length. Since we could not measure the waist directly there, we made a dummy setup outside the vacuum chamber simulating the lens and the one of the resonator mirror. The distance between the dye laser and the dummy lens was made the same as the distance between the laser and the real lens so that both setup were subject to identical laser beam divergence. The focussed waist just after the dummy mirror was 99 μm. The volume defined by the laser beam and the atomic beam in the resonator was then 1.0×10^{-5} cm^3. Since the saturation intensity of the transition is 16 mW/cm^2, the corresponding saturation power was 4.9 μW.

The probe was polarized vertically relative to the resonator axis and the atomic beam. Hence the fluorescence was maximally radiated on a plane defined by the probe and the atomic beam. A cooled avalanche photodiode (S/N 163) with a counting efficiency of 34 % was placed at 10 degree off the atomic beam (see Figure 3-32). It could not be placed in the atomic beam direction because the strong radiation from the atomic beam oven propagated along the atom beam, not blocked by all the collimating apertures at all. An interference filter peaked at 550 nm and a 50 μm aperture were placed in front of the detector to reduce the radiation from the oven and the scattering off the resonator mirror surfaces. The background counts with those installed was about 3000 counts/sec. Without them the background counts

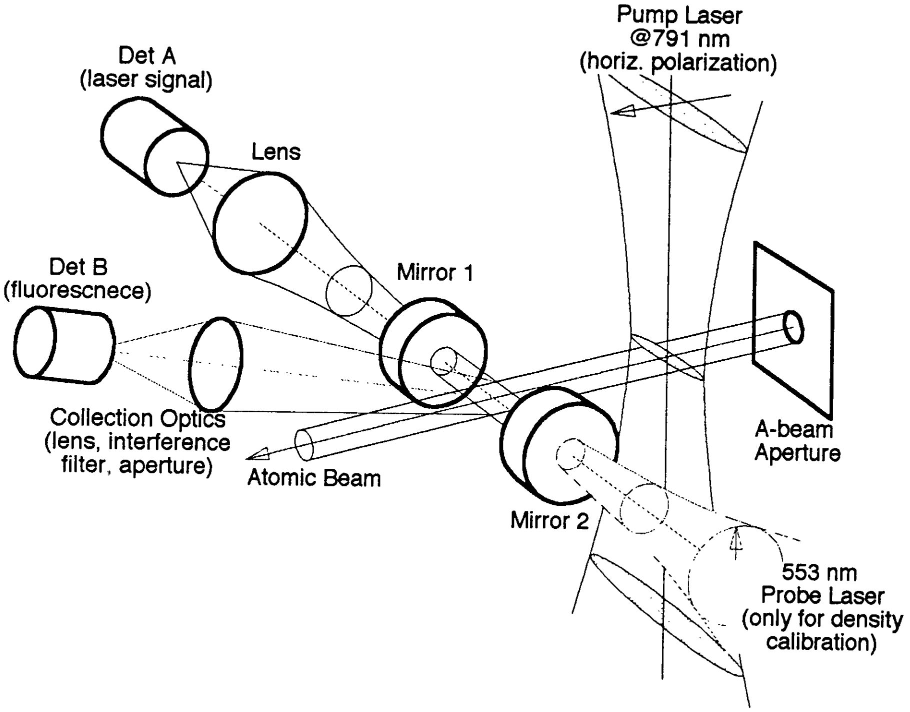

Figure 3-32: Experimental setup. For density calibration a probe laser beam was focussed in the resonator, propagating along the resonator axis with vertical polarization. Det B was a cooled avalanche photodiode (S/N 163), placed 10 degree off the atomic beam axis.

were as large as the signal counts, 10^5 counts/sec. The efficiency of the filter and the aperture for the fluorescence signal were found by measuring the signal with only one of them or both of them installed. The efficiencies of the filter and the aperture were 0.67 ± 0.06 and 0.51 ± 0.4, respectively.

The magnitude of the fluorescence signal can be expressed as

$$F = N_u V n \Gamma_a \left(\frac{3}{8\pi} \Delta\Omega \right) \eta_o \eta_c \ , \tag{3.22}$$

where V is the volume defined by the laser and atomic beam, n is the density, $\Delta\Omega$ is a solid angle, into which the fluorescence is collected by imaging lenses and detected by the detector, η_o is the efficiency of collection optics, η_c is the efficiency of photon counting system ($= 0.32 \pm 0.04$), and N_u is an upper-state population, $N_u = \frac{1}{2} P/P_s$, with P_s being the saturation power if $P/P_s \ll 1$. The volume V could be regarded as a point source since the dimension of the volume was much smaller than the size of the imaging lenses and the distance between the volume and the lenses. The solid angle $\Delta\Omega$ then could be obtained from the distance and the usable aperture size of the lenses, and the result was 1.0×10^{-2} rad. The efficiency η_o was associated with the transmission through the imaging lenses, the interference filter and the aperture, and its value was $(0.96)^8 \times (0.67 \pm 0.06) \times (0.51 \pm 0.04) = 0.25 \pm 0.08$. With all these known parameters the fluorescence signal is given by

$$F = \left[n/\mathrm{cm}^{-3} \right] \frac{[P/\mu\mathrm{W}]}{80 \pm 40} \quad \text{counts/sec} \ ,$$

from which the density can be found. The overall systematic error in the estimation of all those parameters was as much as 50 %. Figure 3-33 shows the density measured as a function of the oven current.

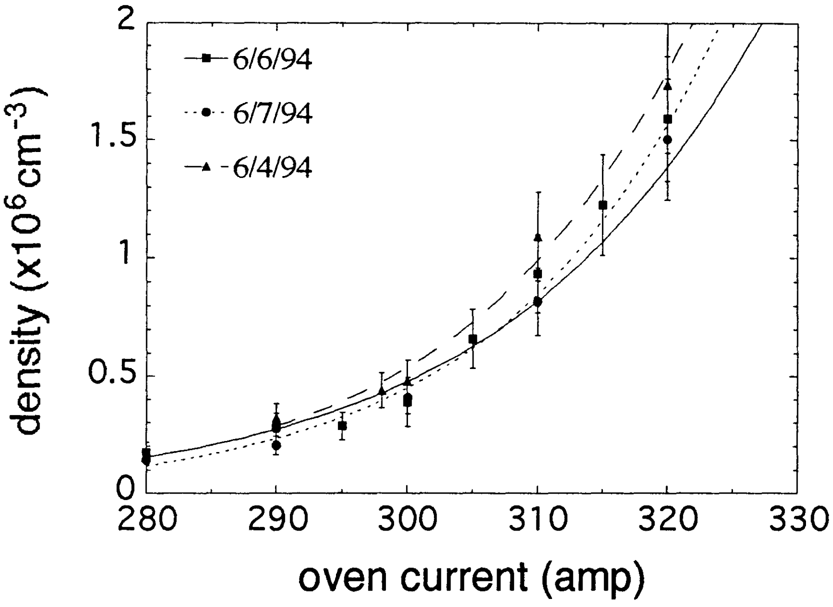

Figure 3-33: Atomic density as a function of oven current.

3.2 One-Atom Laser Experiment

3.2.1 Setup

Basic concept of the one-atom laser experiment is quite simple as illustrated in Fig. 1-1, but the stringent requirements on the resonator and the pump laser added extra complexity in the setup and the result is shown in Figure 3-34. A more detailed view of the configuration around the resonator is also illustrated in Fig.3-32.

The Lamb-dip setup in Fig.3-34 generated a frequency correction signal for the control box of *Laser 1*, a CW Ti:Sapphire laser, and the laser frequency was locked to the atom frequency, as described in Sec.3.1.4 in detail. Hence any part of the laser output in the setup had its frequency stabilized. When we needed to calibrate the atomic density, a probe beam from a dye laser was introduced along the resonator axis to induce fluorescence at 553 nm ($^1S_0 \leftrightarrow {}^1P_1$) of the atoms in the resonator. The polarization of the laser beam was perpendicular to a plane defined by the atomic beam direction and the resonator axis. The fluorescence then was emitted maximally on the plane and detected by a APD detector, denoted by *detector B*, which was

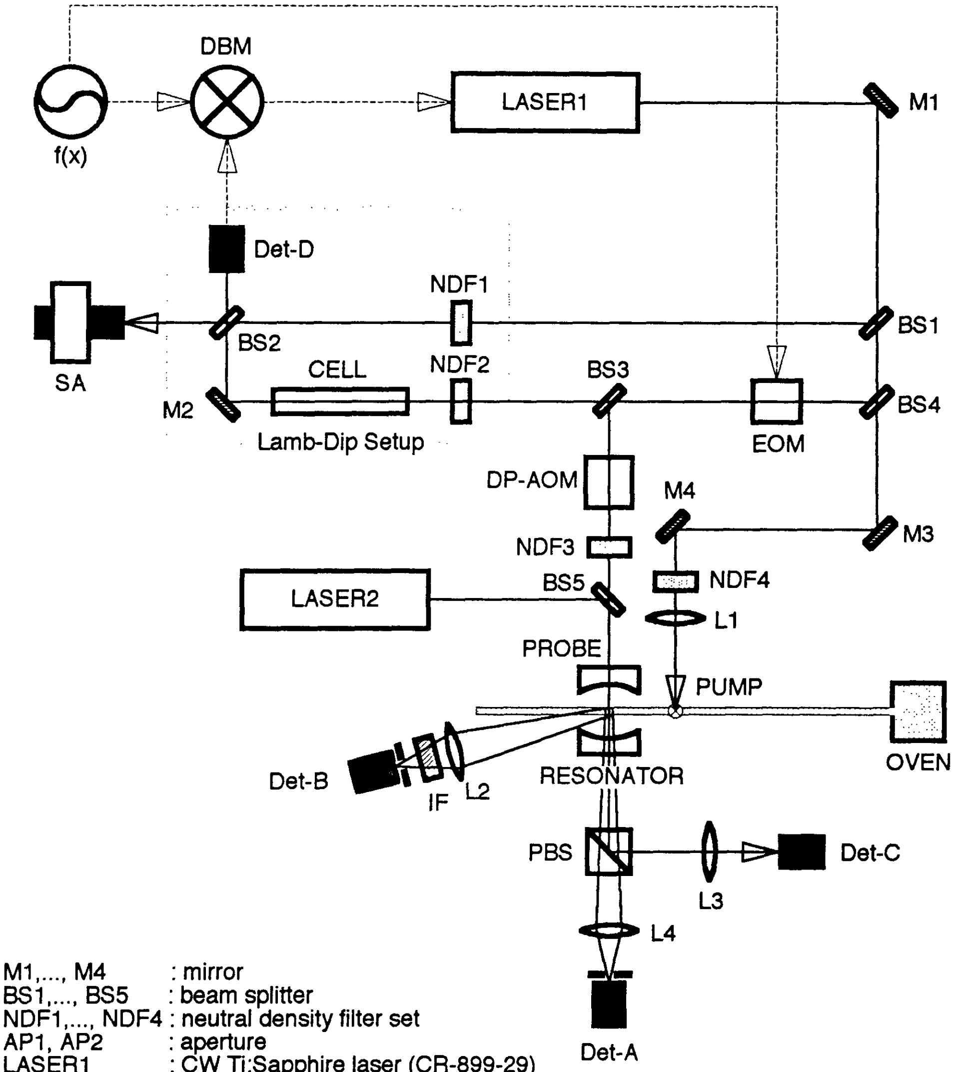

M1,..., M4 : mirror
BS1,..., BS5 : beam splitter
NDF1,..., NDF4 : neutral density filter set
AP1, AP2 : aperture
LASER1 : CW Ti:Sapphire laser (CR-899-29)
LASER2 : CW dyelaser (CR599-21)
Det-A, Det-B : photon counting APD, EG&G C30902S-TC
Det-C : current-mode APD, EG&G C30902S
Det-D : photodiode, EG&G FND 100
f(x) : function generator, SRS DS-3100
DBM : double-balanced mixer, VARI-L CM-4
EOM : electro-optic modulator, 25MHz, Inrad 651-254
DP-AOM : double-pass acousto-optic modulator as a shutter
IF : interference filter, 790 nm or 550 nm
SP : spectrum analyzer
CELL : barium vapor cell
OVEN : barium atomic beam oven
RESONATOR : supercavity resonator

Figure 3-34: Schematic of the actual one-atom laser experiment.

slightly off the plane by about 10 degrees. When we needed to measure the resonator finesse, we used a 791 nm probe beam and performed the ringdown measurement while the resonator was scanned quickly and repeatedly. The probe beam was vertically polarized and therefore most of the transmitted power was reflected by a polarizing prism to a current-mode APD, denoted by *detector C*. The same probe laser with a much smaller intensity and the same detector were used to perform the cavity locking. The probe laser beam was turned on and off rapidly by an AOM in a double-pass configuration (*DP-AOM*), the details of which are illustrated in Fig.3-20. The probe laser, often referenced as a locking laser, was also frequency-modulated even though the modulation was not necessary in the cavity locking process. In fact, the sidebands generated by the modulation were utilized in calibrating the cavity detuning relative to the atom in the experiment. The cavity locking was only used in the alignment phase of the experiment because of its limited performance (300 kHz jitter).

3.2.2 Angular Alignment

There are basically two important angles to pay attention to: the angle between the atomic beam and the cavity axis, denoted by *angle A*, and the angle between the pump beam and the atomic beam, denoted by *angle B* hereafter. The accuracy required for the success of the experiment is different for each angle. It is relatively easy to understand how accurate angle B should be. Since the spot waist of the pump on the atomic beam was about 50 μm, a corresponding transit time broadening was 2.4 MHz. If the pump beam intersects the atomic beam at an angle different from 90 degrees, the excitation process will suffer from a Doppler broadening proportional to the angular misalignment. As long as the Doppler broadening is much smaller than the transit time broadening, this misalignment effect can be neglected. This consideration suggests that the angular misalignment should be much less than 6 mrad.

The requirement on the other angle, *angle A*, is more subtle. If the angle is misaligned by a small angle, the frequencies of the radiation from a moving atom into the resonator mode will be up- or down-shifted in the laboratory frame relative to the

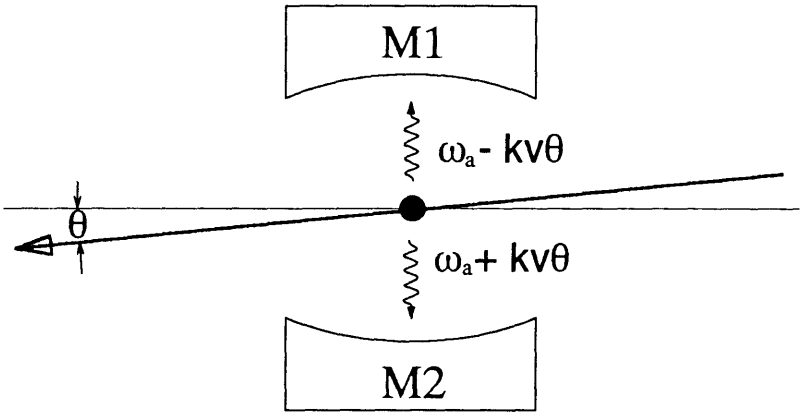

Figure 3-35: Effect of misalignment in the angle between the atomic beam and the cavity axis.

atom frequency depending on the direction of the emission as illustrated in Figure 3-35. The photons at these frequencies will still be reflected by the mirrors as many as $\frac{1}{1-R}$ times in the same way as the photons at the exact atom frequency are since the bandwidth of the mirror reflectivity is quite broad (~30 nm). These photons will also interact with the atom without any degradation as long as the shift is far less than the transit time broadening, which is present in the atom-field interaction even for perfect angular alignment. The magnitude of the transit-time broadening was 2.8 MHz, determined by the cavity mode waist of 43 μm and a mean thermal velocity of 320 m/s. According to the quantum mechanical micromaser theory overviewed in Chapter 2, the one-atom laser will have a laser linewidth much smaller than the transit-time broadening. We expect two peaks in the spectrum of the one-atom laser if the *angle A* is misaligned by more than the one-atom laser linewidth but much less than the transit-time broadening. If we just measure the total output power of the one-atom laser, as we did in the experiment, such misalignment has negligible effects on the results since the detector measures all the spectral contents. Hence the requirement, as far as the total power is concerned, is that the angle should be accurate within 5 mrad. However if we are interested in measuring the laser linewidth, the misalignment should be made much less than an expected laser linewidth. In this case not only the angular alignment is important but also the divergence of the atomic beam itself becomes critical; the Doppler broadening associated with the divergence itself was 320 kHz for the present experiment.

In addition, there is one more condition that should be satisfied by *angle A*. Because of the standing-wave mode structure of the cavity, the atomic beam should not move from one node to another while it traverses the cavity. More specifically, any transverse displacement should be much less than $\lambda/2$. Therefore *angle A* has to be much less than $\frac{\lambda/2}{2w_m} \approx 5$ mrad.

In order to align the pump laser beam and the cavity axis relative to the atomic beam, we utilized the 553 nm fluorescence of atomic barium. The linewidth of the transition is 19 MHz, so 2–3 MHz broadening due to the angular misalignment could be easily noticeable. A 553 nm probe beam from the dye laser was used to measure the fluorescence lineshape of the transition. For angle A alignment, the beam intersected the atomic beam along the resonator axis. We varied the direction of the atomic beam relative to the resonator axis until the linewidth was minimized. The smallest linewidth was 23 MHz. The extra broadening might be due to a transit-time broadening since the probe was focussed as it was in the density calibration measurement. When we used a unfocused probe beam, the linewidth was further reduced to 21 MHz, confirming projection. The extra 2 MHz in this case seemed to come from the frequency jitter of the probe. For *angle B*, a probe beam at 553 nm was introduced without any focusing, replacing the pump laser, and the linewidth was minimized by adjusting its angle relative to the atomic beam. In this case the smallest linewidth approached was 20 MHz.

Once the best alignments for the two probe beams were found, the pump laser was superimposed on the probe beam that had replaced the pump beam before, and the probe beam was blocked. Next we engaged the cavity locking and monitored the transmitted power of the locking laser on detector A. Since the locking laser filled up the TEM_{00} mode of the resonator, the output of the one-atom laser, which also originates from the same mode, should be in the same direction as the locking laser. The locking laser was vertically polarized so that most of the power was reflected to detector C and only small fraction of it ($\sim 10^{-3}$) was transmitted through the prism

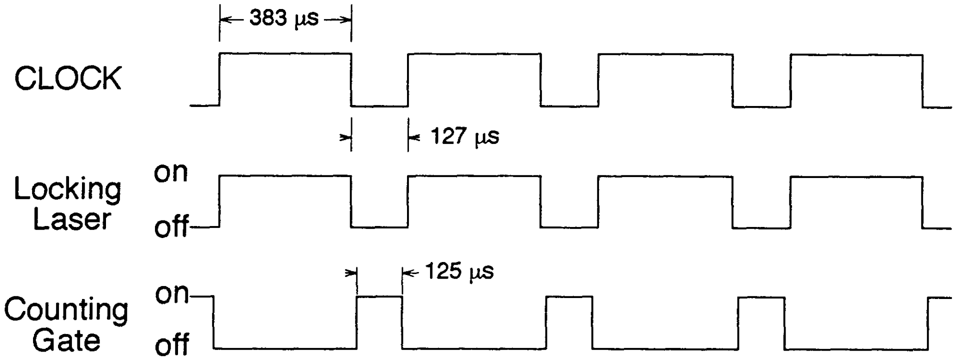

Figure 3-36: Timing diagram of photon counter and AOM

polarizer (PBS). We adjusted the position of the detector and the focus of lens L4 in Fig.3-34 until the signal registered on the detector was maximized. Later once we got the output signal these parameters were readjusted for the maximum signal. We found that the final settings were not much different from the presetting based on the locking laser beam.

Once the system was pre-aligned as described so far, the atomic beam oven was turned up to produce about 10 to 100 times more than the density actually needed for single atom operation. Then the spot size and the intensity of the pump beam were preset as a π-pulse. The beam was first placed well before the cavity mode and then translated toward the mode in a 10 μm step until a laser signal was registered on detector A. Signal counting was done only when the locking laser was turned off. Once the signal was obtained, all the adjustable parameters were fine tuned again one by one to maximized the signal.

3.2.3 Data Aquisition

The photon counting signal from detector A was processed by a digital photon counter (SRS, SR400). The counter was triggered by a TTL clock signal, which controls the AOM in DP-AOM setup. A gate feature of the counter was enabled so that the signal was counted only when the cavity-locking laser was turned off (see Figure 3-36). The counter was active for 125 μsec per each period of the clock. The signal was accumulated for 100 or 200 periods depending on the signal size and the result was converted to a voltage by a digital-to-analog converter in the counter. A typical conversion factor was $10^3 \sim 10^4$ counts/volt. This voltage signal was then recorded on a digital oscilloscope (Lecroy 3100M). A typical data consisted of 1000 data points and it was recorded as a function of the cavity-atom detuning. The cavity locking laser was still present because it could be used as a frequency mark in the cavity-atom detuning. When any of the three frequency components of the locking laser was resonant with the cavity, detector A recorded a large counts relative to off-resonance background counts although the locking laser was turned off during the counting time. This large counts was due to the fact that the cavity could store the locking laser beam for a while after it was turned off. Therefore, during the scan, the locking laser was completely blocked by a beam stop over 10 MHz range around the resonance. Otherwise, the central frequency component of the locking laser would have caused the detector to become blind temporarily.

3.3 Results

3.3.1 Dependence on Atom-Cavity Detuning for Various Number of Atoms

For the data that will be presented next, the cavity locking was disengaged and the resonator was allowed to drift slowly across the atom-cavity resonance. Then the output of the one-atom laser was measured as a function of the cavity-atom detuning. The drift of the resonator was uniform in time and its rate was about 1 MHz/sec. The linearity error of this free-run scan was later confirmed to be less than 400 kHz over a 50 MHz scan range.

Some early data is shown in Figure 3-37. The mean number of atoms was about one. The signal was barely seen buried in a large background. There are two problems with this data: the peak power occurred when the cavity was detuned by about -6 MHz, and the signal size was two orders of magnitude smaller than an estimation

April 25, 1994

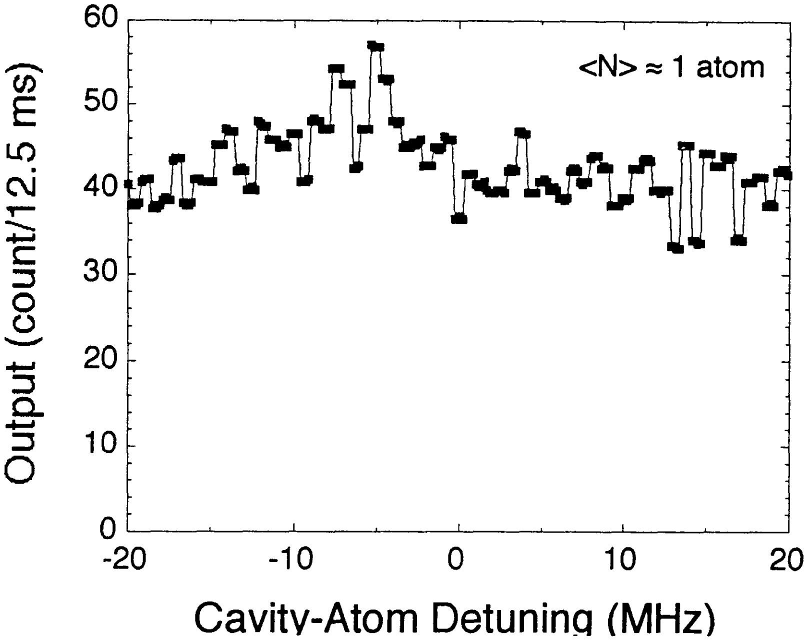

Figure 3-37: Some early data influenced by a local magnetic field.

based on the quantum theory in Chapter 1. After a series of diagnostic experiments, we found that a few gauss local magnetic field, apparently pointing in the direction of the cavity axis, induced the atoms to be excited mostly to the $m = \pm 1$ sublevels of the $^3P_1$ state and very little to the $m = 0$ sublevel. Recall that the polarization direction of the pump laser was supposed to defined the z-axis, or the quantization axis in the one-atom laser so that only the $\Delta m = 0$ transition ($^1S_0$, m=0 $\leftrightarrow$ $^3P_1$,m=0) would be excited. The local field was strong enough to redefine the quantization axis, thereby disrupting the excitation of the atoms in a proper state. Presumably, the origin of the local field was the earth magnetic field as well as a stray magnetic field from the atomic oven driven by a high current ($\sim$300 A). Although we tried to eliminate the stray field by twisting the cable pair delivering the current to the oven, the field appeared to be a few gauss.

This problem was solved by a keeper field in the same direction as the pump laser polarization. The keeper field is a modest-strength DC magnetic field defining a quantization axis. The keeper field was generated by a pair of Helmholtz coils placed outside the vacuum chamber. The strength of the field was about 10 gauss. The

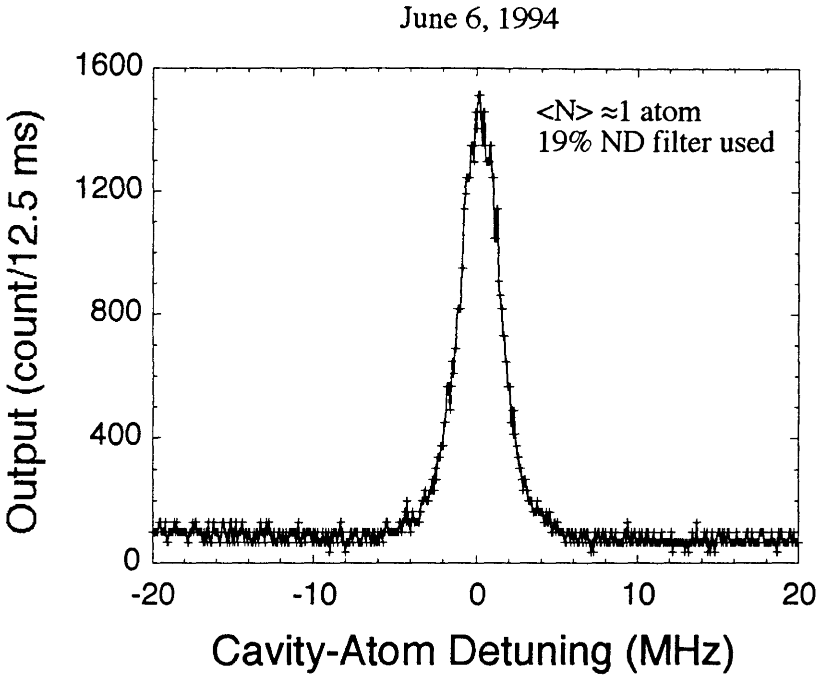

Figure 3-38: After a keeper field is added to the system. It was taken under the same condition as the data in Fig.3-37 except for the keeper field.

keeper field not only eliminated the frequency shift but also it boosted the output signal as shown in Figure 3-38, where the data was taken under the same condition as the data in Fig.3-37 except for the keeper field.

The output signal was reasonably strong even when the average number of atoms in the resonator was as small as 0.1, yielding a count rate of 7×10^3 count/sec. Some representative data are shown in Figure 3-39, where the average number of atoms were varied from 0.10 to 1.0. Rapid growth of the output power as a function of the average number of atoms is easily noticeable in Figure 3-40. Neutral density filters were used to attenuate the signal on the detector whenever counting rate, the counts per bin divided by the counting time, was more than 10^5 count/sec because of the detector saturation effect (see Sec.3.1.6). We can also plot the peak values of these curves as a function of the average number of atoms in the resonator mode, or equivalently the average number of photons in the mode as a function of the average number of atoms. The average number of photons is related to the count rate of the

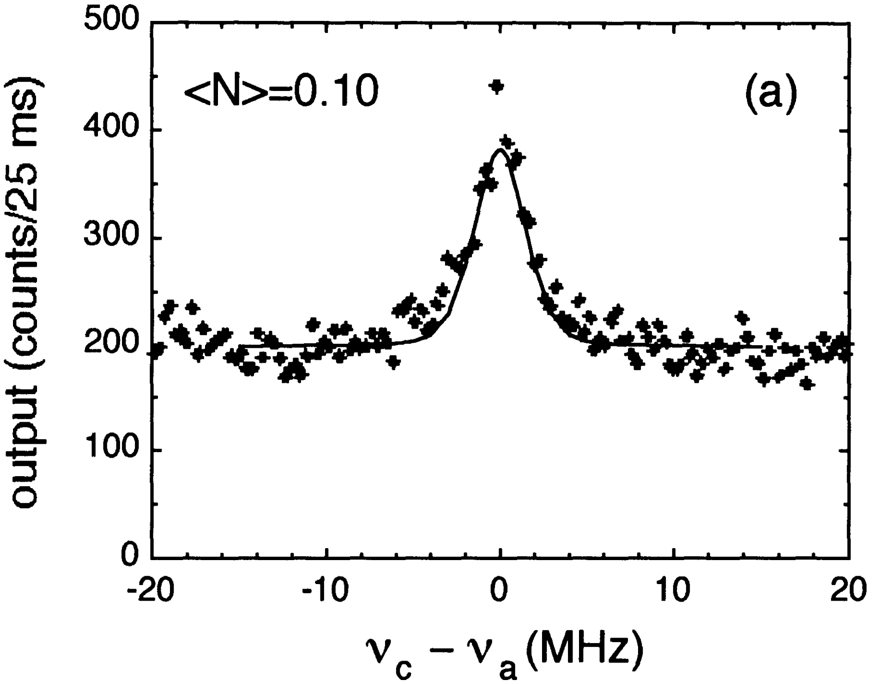

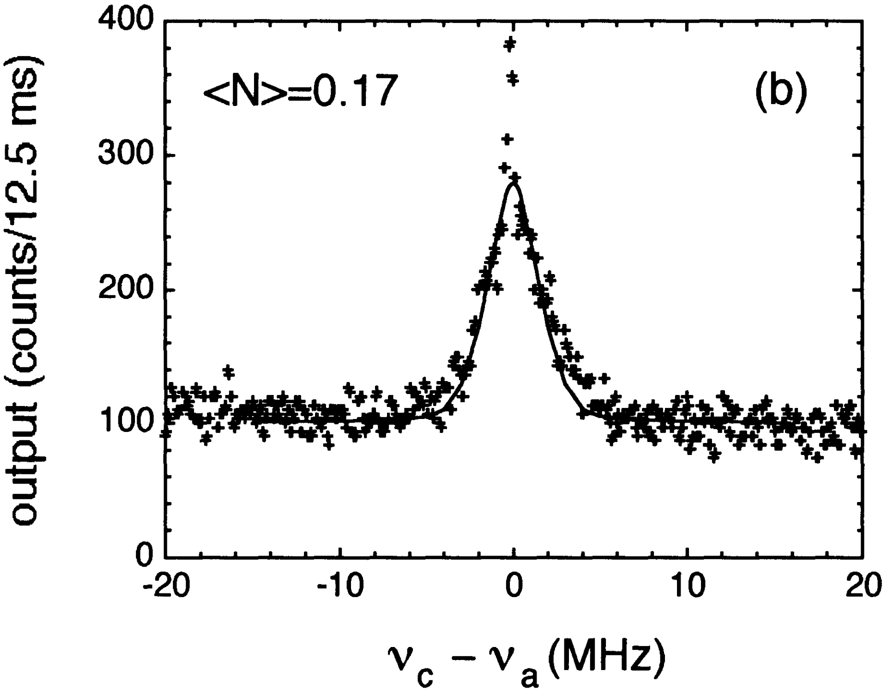

Figure 3-39: Output of the one-atom laser as a function of the cavity-atom detuning. Average number of atoms in the cavity mode was (a) 0.10, (b) 0.17, (c) 0.23, (d) 0.38, (e) 0.71 and (f) 1.0. Counting time per bin was 25 ms for (a)~(c) and 12.5 ms for (d)~(f). Solid lines are based on Eq. 2.82, the modified quantum recursion relation, and Eqs. 2.90 and 2.85 for the definition of the average number of atoms.

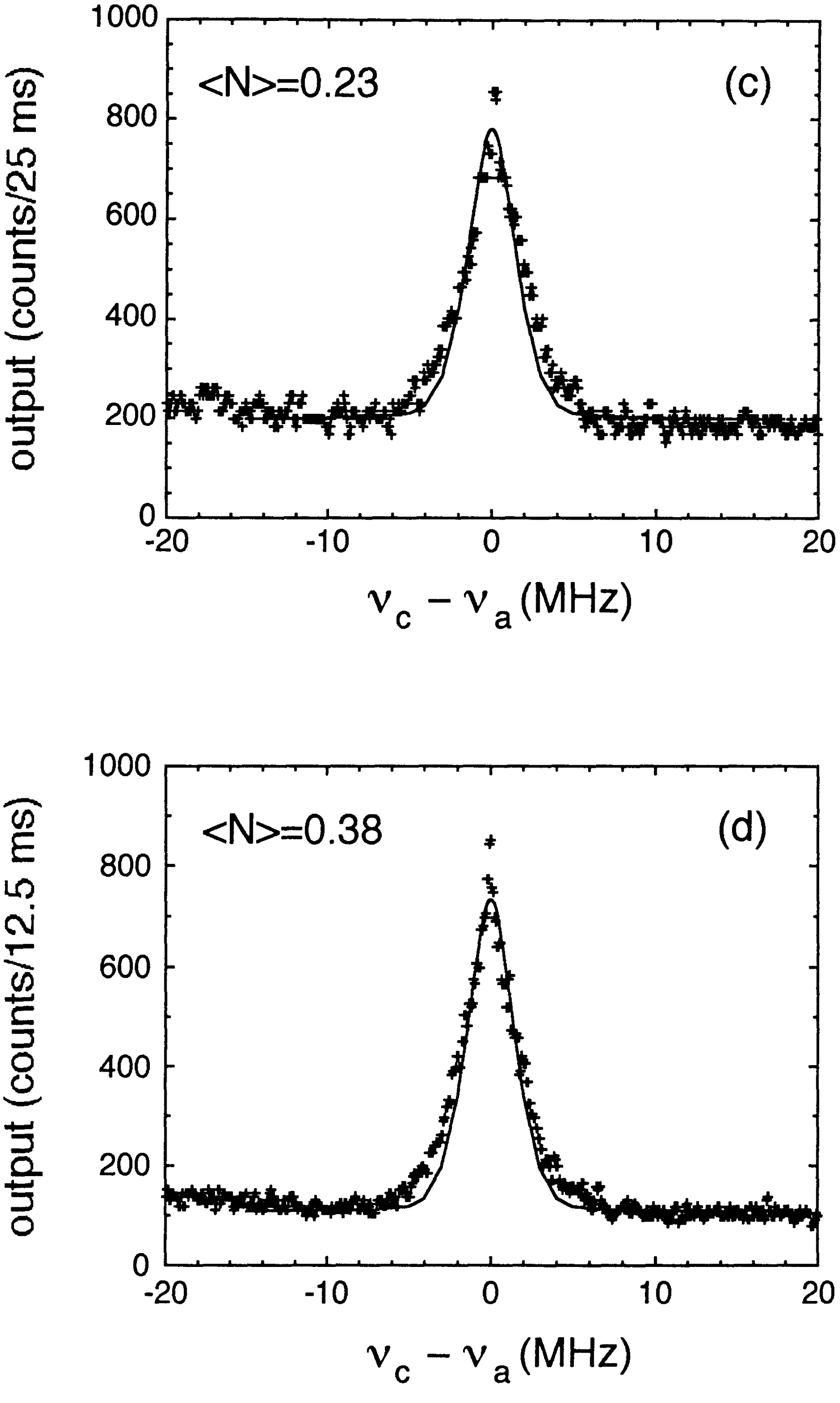
output (counts/25 ms)
1000
800
600
400
200
0
<N>=0.23
(c)
-20
-10
0
10
20
$\nu_c - \nu_a$ (MHz)
output (counts/12.5 ms)
1000
800
600
400
200
0
<N>=0.38
(d)
-20
-10
0
10
20
$\nu_c - \nu_a$ (MHz)

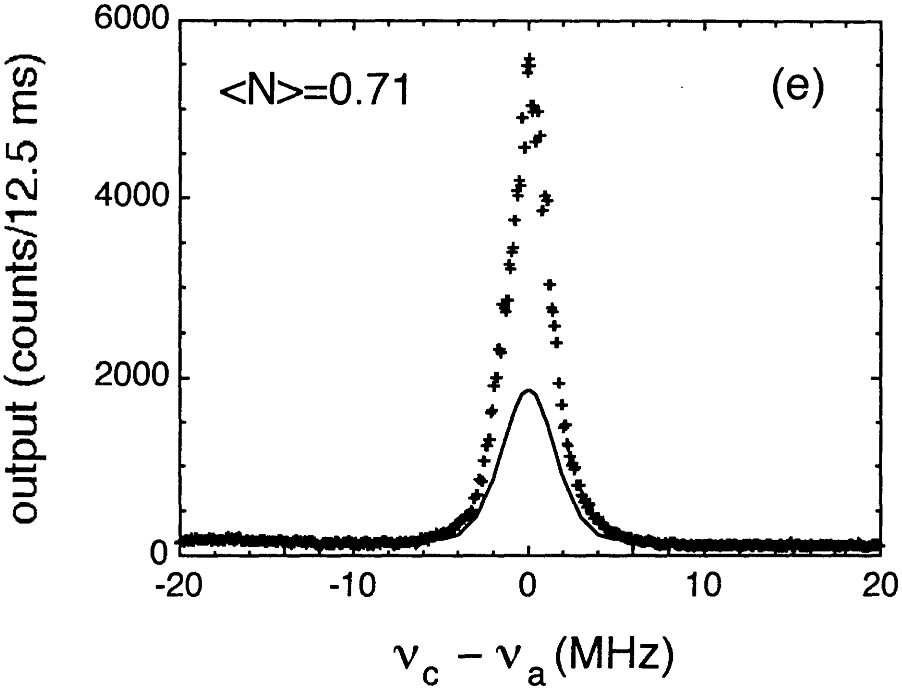
6000
4000
2000
0
output (counts/12.5 ms)
<N>=0.71
(e)
-20
-10
0
10
20
$\nu_c - \nu_a$ (MHz)

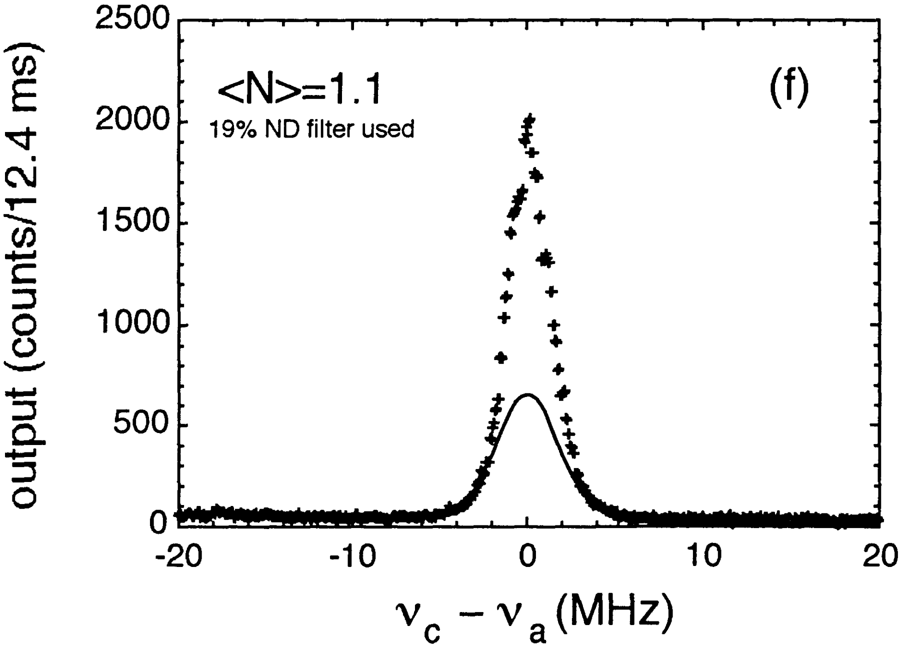
2500
2000
1500
1000
500
0
output (counts/12.4 ms)
<N>=1.1
19% ND filter used
(f)
-20
-10
0
10
20
$\nu_c - \nu_a$ (MHz)

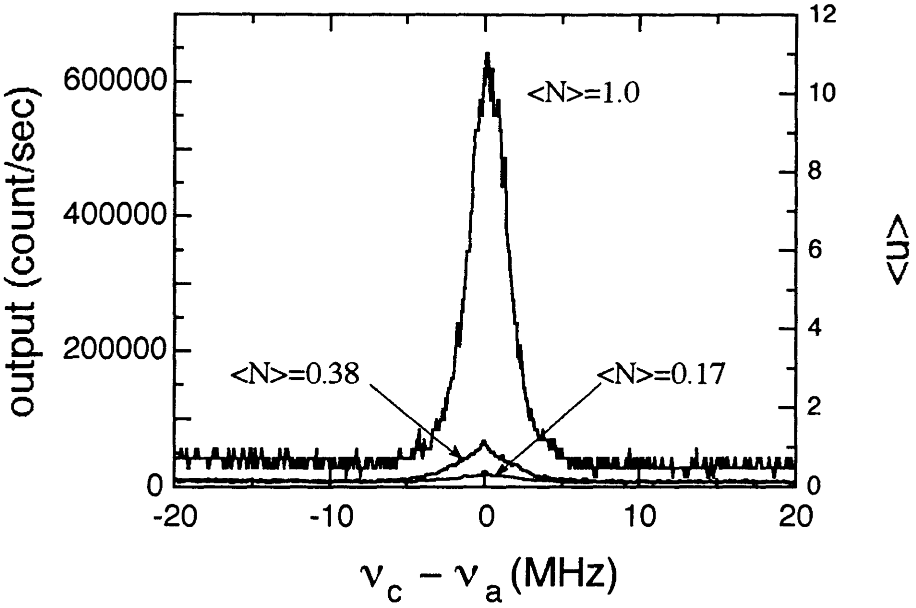

Figure 3-40: Output count rates for various average number of atoms in the mode are compared.

output signal, S, by

$$S = \frac{1}{2}\langle n\rangle\, \Gamma_c \left(\frac{T}{T+A}\right) \eta_c \eta_o \,, \tag{3.23}$$

where η_c is the counting efficiency of the detector, 0.36 ± 0.04, η_o is the efficiency of collection optics, mostly due to a total of 7 uncoated surfaces of optical components, and $T/(T+A)$ is the throughput factor, which was measured to be 0.32 ± 0.02 earlier in Sec.3.1.3. Hence

$$\langle n\rangle = \frac{S}{6.3 \times 10^4 \text{count/sec}} \,.$$

Figure 3-41 shows the results. This data is compared with the theories developed in Chapter 1, and the result is shown in Figure 3-42. A curve denoted by `QM(<n>,v-av)` is based on Eq.2.82, the modified quantum recursion relation, and Eqs.2.90 and eq:N-Dt-corrected for the definition of the average number of atoms. It also accounts for the velocity distribution in the atomic beam (i.e., the results were averaged over the velocity distribution). The solid lines in Fig.3-39 are based on the same model.

The curve denoted by `micromaser theory` is the prediction by the micromaser theory. For this the number of thermal photons was set zero ($n_b = 0$) and the re-

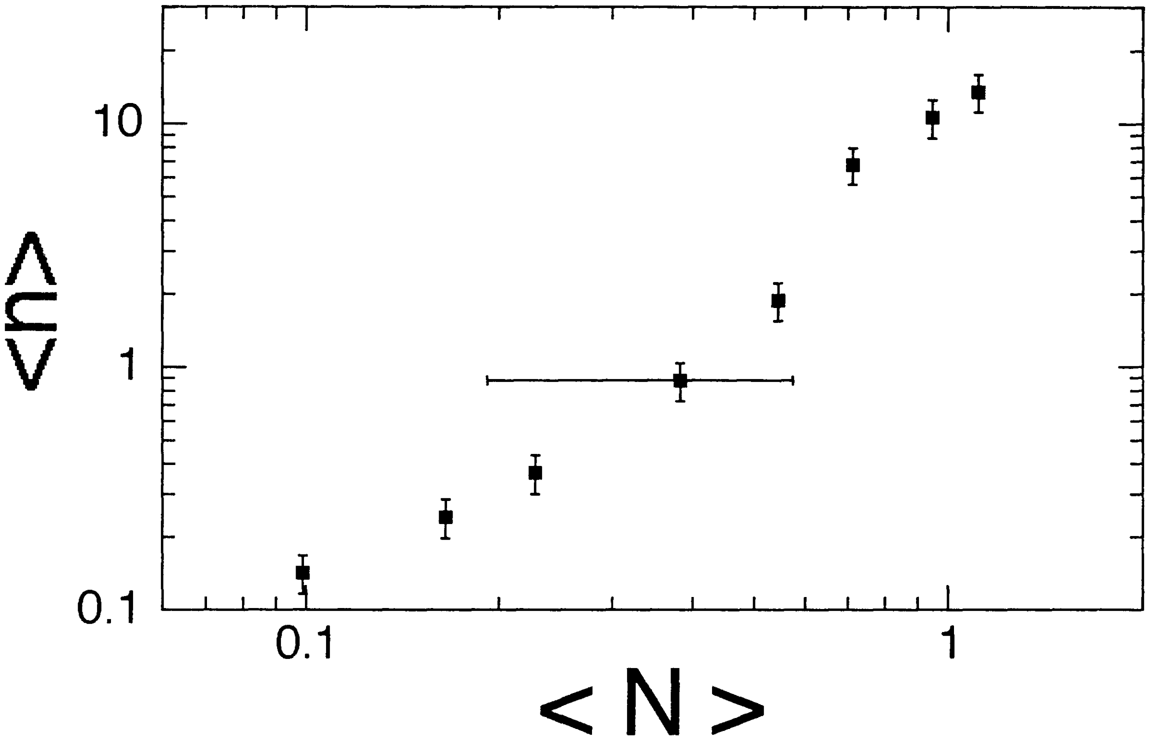

Figure 3-41: Average number of photons in cavity mode as a function of average number of atoms in the mode. The average number of atoms were measured by fluorescence technique explained in Sec.3.1.8, and it is subject to 50 % systematic error as denoted by error bars.

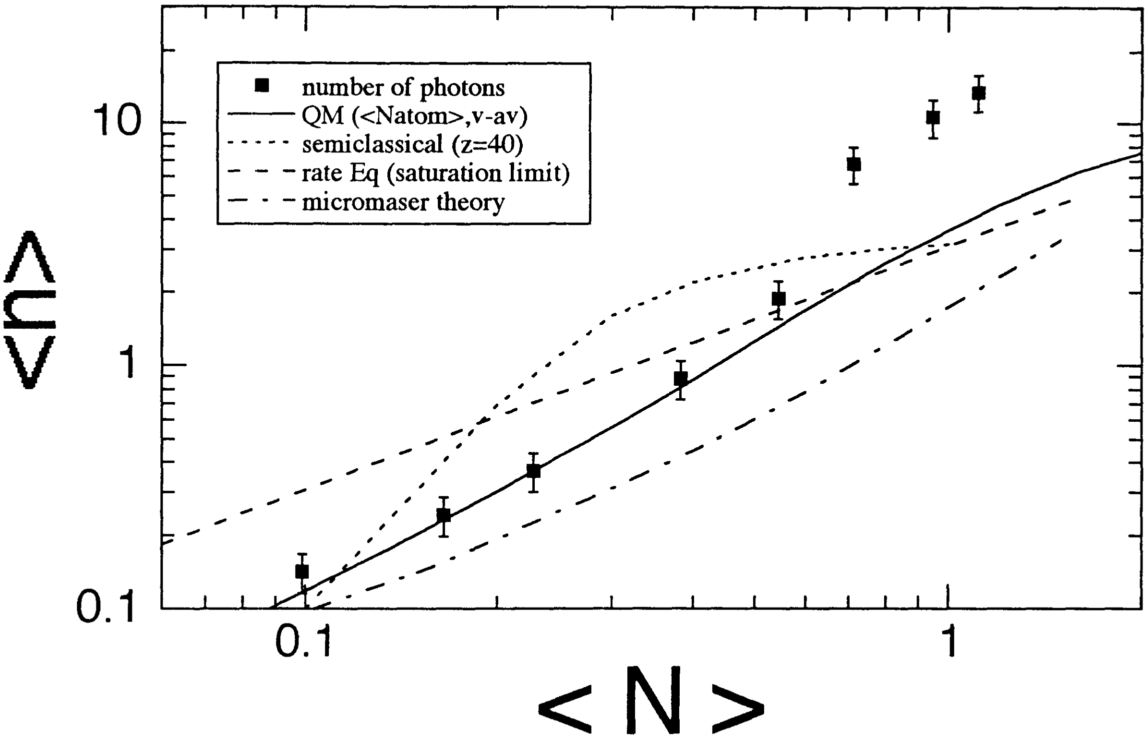

Figure 3-42: The same data as in Fig.3-41 is compared with the various theories developed in Chapter 1. See the text for detail.

sults were averaged over the velocity distribution. Recall that the micromaser theory assumes that the off-diagonal elements of the field density operator are vanishing. This assumption, as discussed before, does not hold in our experiment, and therefore the predicted signal is smaller than the actual signal roughly by factor of two. The discrepancy gets larger as the mean number of atoms approaches one.

In addition, the predictions by the rate equation formulae, Eqs.2.246 and 2.247, as well as by the semiclassical model in Sec.2.2.3, particularly Eq.2.178, are also plotted. It is interesting that the one-atom semiclassical model behaves worse than the rate equation model. As far as the signal size is concerned, the semiclassical model is the worst one. However, this model has some success in other areas. It will be shown later that the model can explained the dependence of the output power on the pump position at least qualitatively.

The rate equation formalism is supposedly good for a large number of atoms if it could ever fit the data. In fact, it performs respectably for relatively large mean number of atoms. It deviates from the data further and further as the mean number decreases.

It is surprising that even the prediction denoted by the fully quantized theory is totally off the mark when the average number of atoms is comparable to one. The agreement between the data and the theory is good only when the number of atoms and the mean photon number are much less than one. This disagreement between the theory and the data might be attributed to the fact that the quantum mechanical recursion relation and the corresponding fully quantum mechanical theory in Sec. 2.1 is basically one-atom theory. In other words the theory assumes that at most only one atom interacts with the cavity field at any instance. This assumption obviously breaks down if the mean number of atoms is comparable to one. In this case actual number of atoms can be more than one with appreciably high probabilities due to statistical fluctuations.

The quantum mechanical treatment of the micromaser with a few atoms has been sparse [66]. A complete theory has yet to be developed. However, it is not obvious whether a yet-to-be-developed few-atom quantum mechanical theory could explain the anomalously large output power of the one-atom laser. The experimental data clearly shows that there is rapid change in the slope as the number of atoms approaches one. Can this slope change be explainable by a few-atom theory?

The most reasonable explanation, however, perhaps comes from the peculiar way that the standing wave nature of the cavity mode was handled in the theory. In reality atoms can travel anywhere in the standing wave structure of the cavity mode, some near the anti-nodes enjoying maximum coupling strength whereas some near the nodes experiencing no coupling at all. In our theory we simplified situation in such a way that the half of the atoms are at the nodes and the rest of the atoms are at the anti-nodes. This approximation may be reasonably a good approximation as long as the number of photons in the cavity mode is relatively small, as confirmed by the experimental data. However the approximation might break down if the photon number gets quite large. In that case even the atoms moving near the nodes will benefit from the large photon number mostly generated by the atoms traveling near the anti-node. For those atoms near the nodes, even though coupling is reduced by

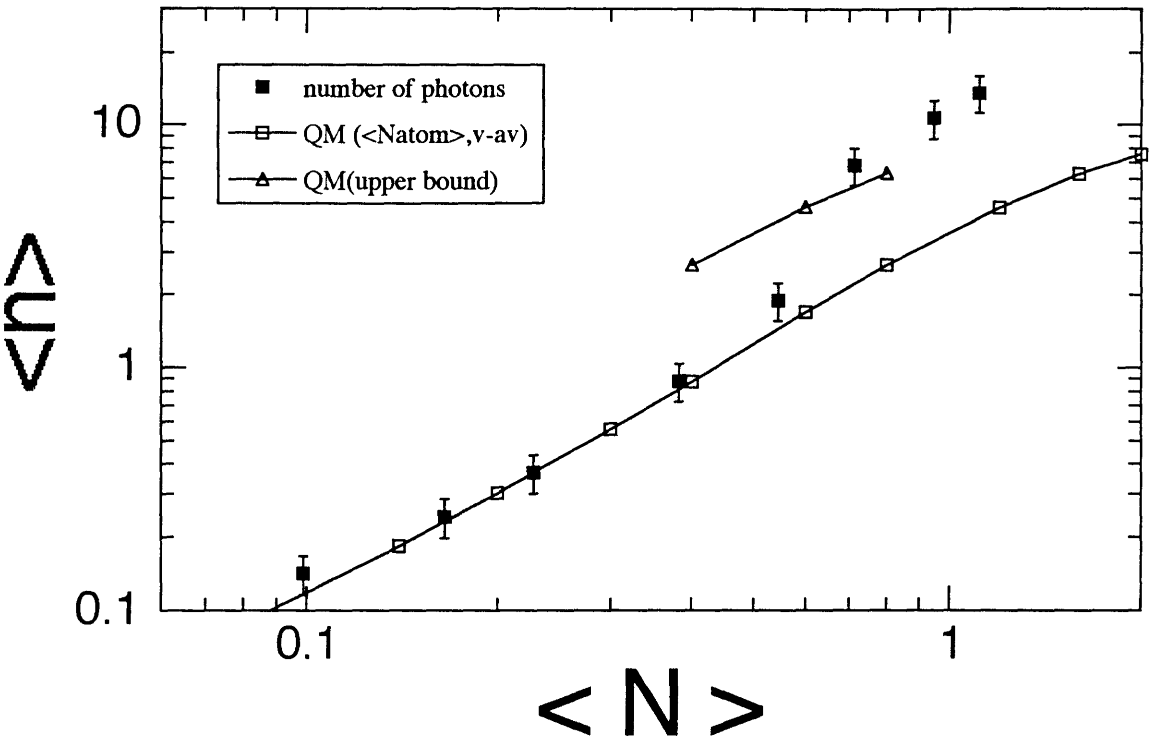

Figure 3-43: Experimental data is plotted again in comparison with the curve indicating the upper bound of the output power based on the argument in the text.

the *coskz* function, Rabi frequency that governs the tendency of photon emission from the atoms is boosted by $\sqrt{n+1}$ factor with n much larger than one. So except the atoms traveling exactly along the nodes, effectively all the atoms participate in photon emission. The upper bound of the laser output caused by this saturation effect should be the what we would find if there were no sinusoidal dependence on the position along the cavity axis, and if all the atoms assumed the full strength of the coupling constant. In this case the number of atoms participating in the laser oscillation is simply doubled. In Figure 3-43 the experimental data is compared with the curve indicating the upper bound of the output power based on this argument. This rather heuristic argument, even though it is far from rigorous, qualitatively explains the signal size. More reliable explanation, however, would be possible only when one solves the quantum mechanical master equation including the standing wave nature and allowing more than one atom in the cavity. It appears that such solution will not be available in a near future due to its extreme complexity. For the time being one can rely on numerical simulations, particularly Monte Carlo simulation.

But this simulation has to be done in such a way the time dependent solution is followed for long sequence of atom-field interactions with random atomic position per interaction. The solution will gradually approach the real solution after large number of interactions.

3.3.2 Dependence on Pump Position

The data presented before were taken for a pump laser position just outside of the cavity mode so that the pump field did not overlap with the resonator mode significantly. At that position the output signals were maximized as expected. However, we repeated the output measurement for various pump positions in order to demonstrate that the system works as it should. For a fixed pump position the resonator was allowed to drift slowly across the resonance and the output was measured as a function of cavity-atom detuning as usual. The measurement was repeated for different pump positions as shown in Figure 3-44. If we plot the peak power of each scan as a function of pump laser position, we then obtain Figure 3-45. The solid lines are the prediction based on the one-atom semiclassical model presented in Sec. 2.2. The pump beam waist used in the calculation was 50 μm and the intensity of the beam corresponded to a π-pulse excitation. The waist of the resonator was assumed to be 43 μm as it should be. The curve denoted by `Semiclassical(N=0.2,F=0.79)` in Fig.3-45 is the prediction when the actual finesse and an estimated average number of atoms were used. The result agrees with the data only when the pump beam is inside the cavity mode ($z = -2w_m \sim w_m$ with z defined in the plot.). In order to get the observed position dependence, we had to adjust both the finesse value and the average number of atoms to be 1.0×10^6 and 1.0 respectively whereas the actual finesse and average number of atoms were 0.79×10^6 and 0.2, respectively. Although the semiclassical theory could reproduced the observed position dependence with these new parameters, the magnitude given by the theory was 3.3 times larger than the actual value. We believe this discrepancy is due to the inherent problem of the semiclassical theory. Since the average number of photons was very small (less than one for the data shown here), it is not totally unexpected that the semiclassical theory

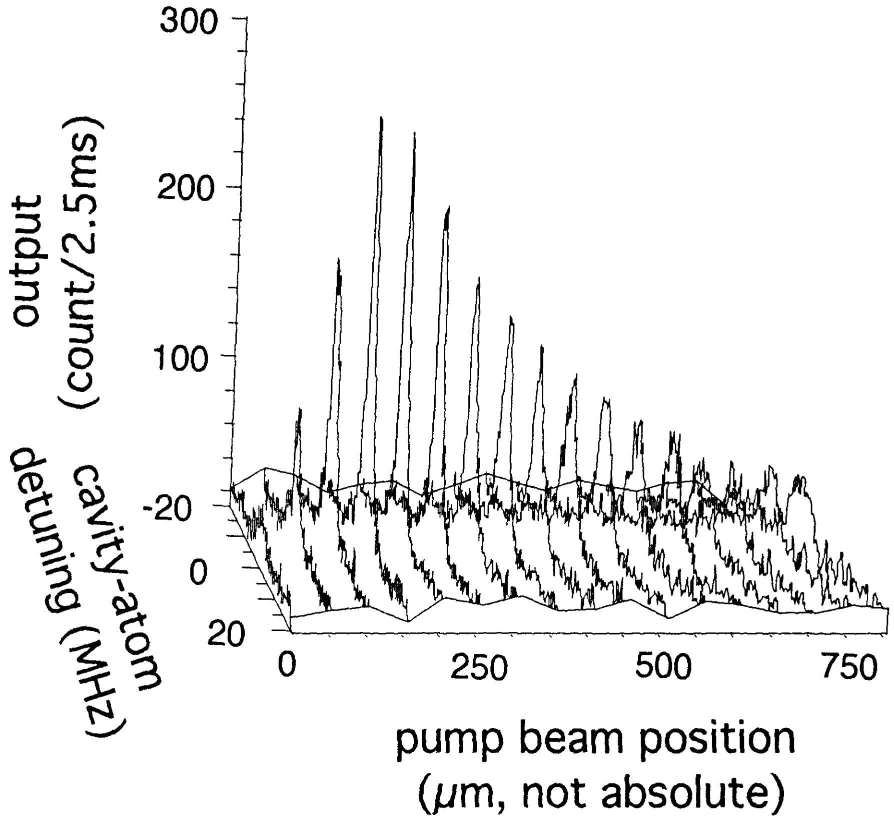

Figure 3-44: Output power (counts) as a function of pump beam position and cavity-atom detuning for $\langle N \rangle \approx 0.3$.

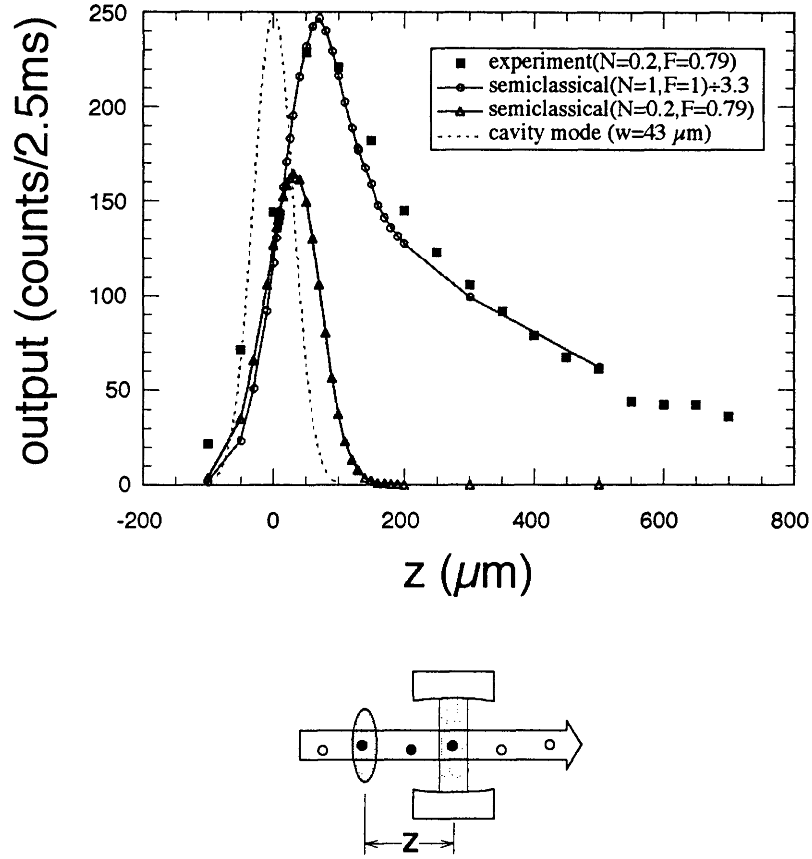

Figure 3-45: Peak output as a function of pump beam position

cannot describe the experiment in every detail. The semiclassical theory treats the cavity field classically. This treatment is reasonable only when the number of photons in the resonator is enormously large. The semiclassical theory used to calculate the position dependence assumes that the photon number is indeed much larger than one (see Sec.2.2.3). Therefore it is understandable that the theory cannot produce a right amplitude for the cavity field.

Another point which should be noted in the plot is the exponential-like decrease of the output as the pump beam moves away from the resonator. If an atom is excited far prior to the cavity mode, the excited state population will be lost much by the spontaneous emission process while it is traveling toward the cavity mode. As noted in Sec 3.1.1, $^3P_1$ state of atomic barium decays to $^1S_0$ ground state as well as ^{3}D state with about equal probabilities. The total decay rate is hence about twice of the radiative linewidth of $^1S_0 \leftrightarrow {}^3P_1$ transition, resulting in a lifetime of 1.5 μsec. This lifetime corresponds to 500 μm of flight distance with a mean thermal velocity of 320 m/s, and therefore the output signal drops to $1/e$ of the maximum at that distance as shown in the plot.

3.3.3 Dependence on Pump Power

All the data presented so far have been taken with the pump laser field supposedly adjusted for the π-pulse excitation of the most probable velocity group of the atoms. In actual experiment, however, the output power of the one-atom laser was maximized as the intensity of the pump laser was varied with the position of the pump well outside the cavity mode. The pump intensity corresponding to the maximum output was then tagged as a π-pulse excitation intensity. To demonstrate this convention was indeed the correct one, we measured the output power as a function of the cavity-atom detuning for various pump laser power. For this measurement the pump beam was positioned at $z = 100$ μm with z defined in Fig. 3-45. Since the cavity mode waist and the pump beam waist were 43 μm (determined by resonator geometry) and about 50 μm (from data fitting such as Fig.3-45, respectively, the pump laser at that position was was reasonable outside the cavity mode. The peak power of such scans are plotted as a function of the square root of the pump laser powers in Figure 3-46, and the result is compared with a fitting by the modified quantum recursion relation, Eq.2.82, in the same spirit as `QM(<N>,v-av)` in Sec.3.3.1, accounting for the standing wave nature of the cavity mode. As seen in the plot, the theory predicts that the output power is in fact maximized when the pump intensity about 90 % of the intensity corresponding to the π-pulse excitation of the most probable velocity group (pulse area $\approx 0.8\pi$). The reduction in the output power when the intensity is set for the π-pulse excitation is about 5 %, comparable to the experimental error in the plot. Therefore for practical purposes we can consider that the output power is maximized when the pump intensity is set for the π-pulse excitation. In that sense the experimental data well agrees with the theory, exhibiting saturation behavior when the pump intensity far greater than the intensity for the π-pulse excitation.

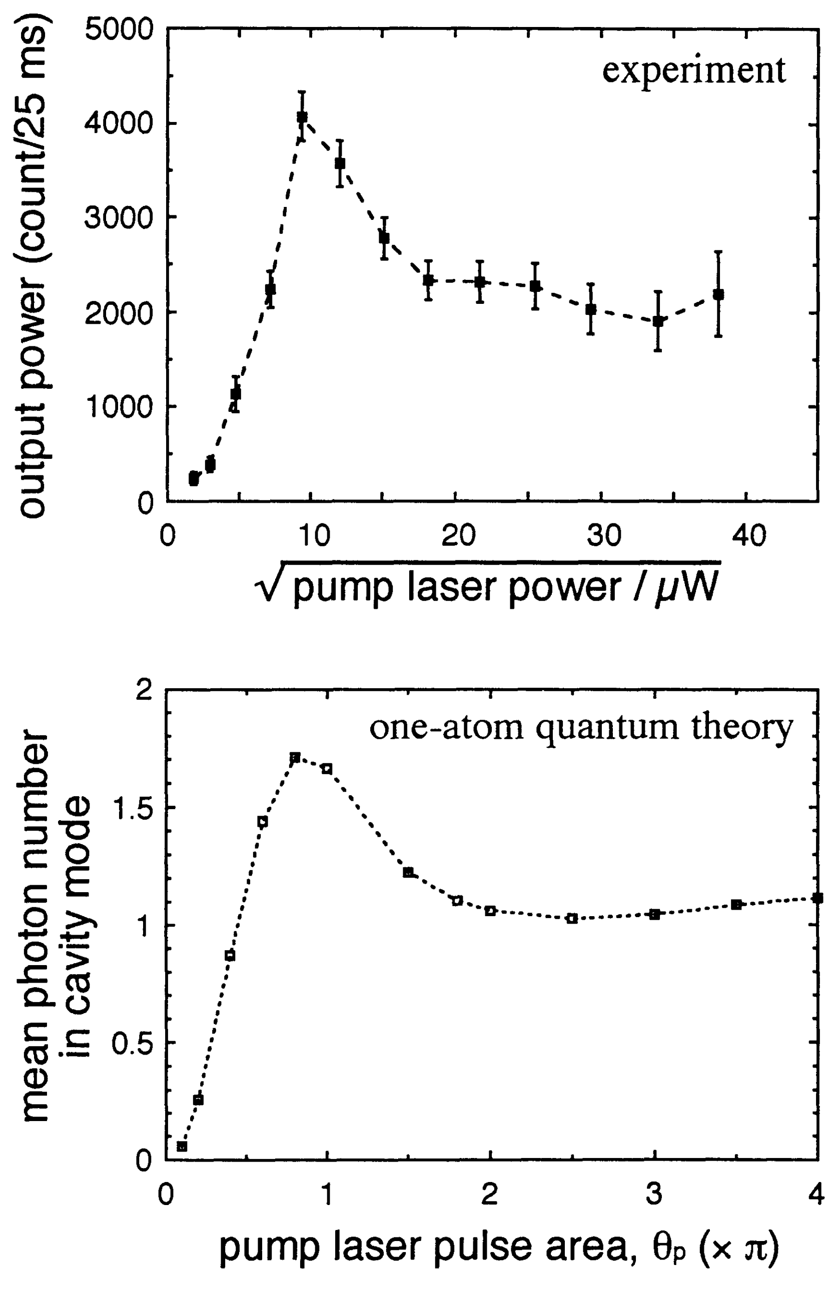

Figure 3-46: Peak output power as a function of pump beam power. Experimental data is compared with the prediction based on the quantum recursion relation.

Chapter 4

Discussion and Conclusion

Standing-Wave Cavity Mode

In the previous chapter, the standing wave mode structure of the cavity used in the experiment introduced an ambiguity in evaluating the effective number of atoms in the cavity. We used a rather heuristic argument to explain the origin of the anomalously large signal size with some success. As pointed out there, however, a more reliable explanation would be obtained only when one solves the quantum mechanical master equation including the standing wave nature and allowing more than one atom in the cavity. There exists a numerical method which might be suitable for this kind of calculation. It is called quantum trajectory approach [67, 68, 69, 70], and it has been used to obtain the fluorescence spectrum of an atom in an optical trap [71]. In this approach a time dependent solution is followed for long sequence of atom-field interactions with random atomic position per interaction. The solution will gradually approach an equilibrium solution after large number of interactions.

Alternatively one can think of using a ring cavity instead. There will be no nodes and anti-nodes in this case, and hence the coupling constant is uniform over the entire cavity, eliminating the complexity in the theory associated with the position dependence in the coupling constant. Since we use only one of the two waves traveling in the opposite directions, the magnitude of the coupling constant is reduced to the half of the maximum coupling constant for a standing-wave cavity. However, such a cavity will not be trivial to construct, and furthermore, it is questionable if we can achieve a finesse as high as we do with a standing-wave cavity.

Superposition State Excitation

If atoms are prepared in a superposition state of the two levels instead of being completely excited to the excited state, the coherence in the atoms can be transferred to the cavity field. In this case the field density matrix has non-vanishing off-diagonal elements, as illustrated in Fig. 2-3, and even the diagonal elements are redistributed accordingly. As pointed out in Sec. 2.1.5, a maximum, $\langle n \rangle$, is achieved not when the atoms are fully inverted but when they are prepared in a superposition state initially. Note that $\langle n \rangle$ is just the first moment of the field density matrix. Obviously the second moment, $\langle n^2 \rangle$, will also change if the field density matrix changes. Note that a simple measure of the photon statistics is the variance of the photon number, $\Delta n \equiv \sqrt{\langle n^2 \rangle - \langle n \rangle^2}$. Therefore, the photon statistics for a superposition-state excitation can be quite different from the photon statistics with the π-pulse excitation.

In order to create atoms in a superposition state, one should control the interaction time between the atoms and the pump field more precisely. For this a mono-energetic atomic beam is required. One way to select a single-velocity group of atoms out of a thermal atomic beam is to use the laser-beam deflection technique [72]. We can use the strong 553 nm transition ($^1S_0 \leftrightarrow {}^1P_1$) for this technique.

Detection of Atomic State

In our experiment, we detected only the photons emitted from the system. Equivalently, atoms can be counted in a state-selective manner. An idea similar to the atomic shelving technique [73, 74, 75], for example, can be applied to the V-transition consisting of $^1S_0$, $^1P_1$ and $^3P_1$ states. The idea is as follows. In our experiment an atom is first excited by a π-pulse laser beam at 791 nm ($^1S_0 \leftrightarrow {}^3P_1$). The atom undergoes an interaction with the cavity field and exists the cavity either in the ground state or in the excited state. This exiting atom is then probed by a laser beam at 553 nm ($^1S_0 \leftrightarrow {}^1P_1$). The duration of the probing is set much longer than the lifetime of the

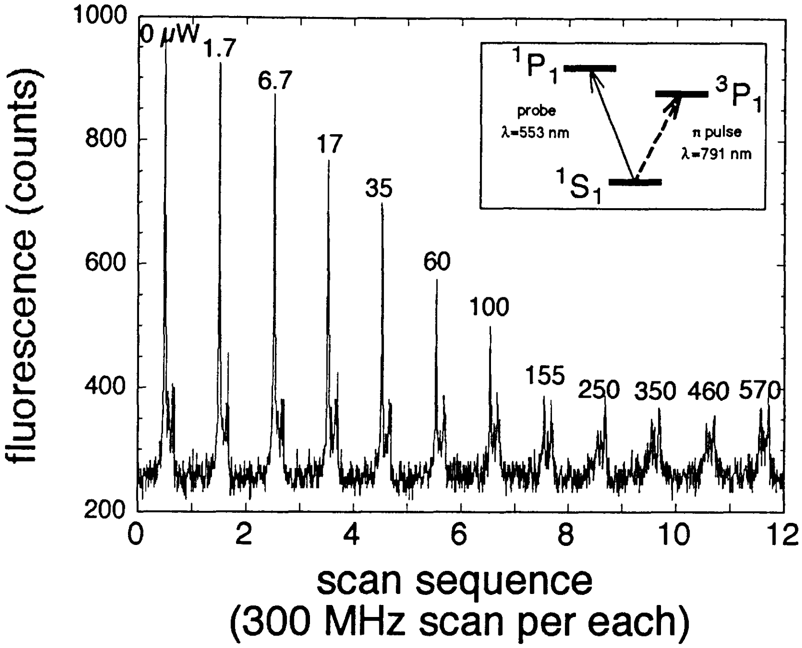

Figure 4-1: A preliminary data demonstrating an atomic shelving technique, which can be used in our experiment to count atoms in a state-selective wave. See the text for explanation.

$^1P_1$ state but much shorter than the lifetime of the $^3P_1$ state. If the atom is in the $^3P_1$ state, it will stay there for the duration of the probing, and hence it does not interact with the probe laser. On the other hand, if the atom is in the ground state, it can be excited by the probe and emits a photon spontaneously. Since the duration of the probing is much longer than the lifetime of the $^1P_1$, this excitation-emission cycling occurs many times, generating many fluorescence photons at 553 nm. By monitoring the fluorescence, therefore, we can tell if the atom exits the cavity in the ground state or in the excited state. Some preliminary data was taken to test this idea, and it is shown in Fig. 4-1. For this data we did not have the cavity. Instead, the pump laser intensity was varied around the intensity for the π-pulse excitation and the resulting atomic states were probed. The data is composed of 12 fluorescence scans by the probe, displayed in a sequence. The numbers on the individual curves represent the power of the 791 nm pump laser. Note that the fluorescence signal is proportional to the population in the ground state. Clearly, when the pump pulse area approaches π, the fluorescence signal decreases. It is interesting to note that only the fluorescence peak corresponding to ^{138}Ba changes. The peaks due to the other isotopes remain the same since the pump laser was not resonant with the $^1S_0 \leftrightarrow {}^3P_1$ transition of the isotopes.

4.0.4 Future Study

One of the most important subject to study will be the statistics of the photons as well as atoms in the one-atom laser. According to many theories on the micromaser, the photon and atom statistics can be highly nonclassical, often exhibiting sub/super-Poissonian number distributions [47, 42]. These results for the micromaser are readily applicable to our microlaser with a few modifications. Squeezing [44, 46, 49] has been also predicted for the micromaser.

Laser linewidth measurement will be also quite interesting. With a stronger coupling constant or a longer interaction time to satisfy $2gt_{int} \gg 1$, the linewidth deviates from the Schawlow-Townes limited linewidth. A long interaction time can be achieved by selecting a slow-velocity group of atoms out of the thermal beam. Connection between the linewidth and the photon statistics will be a interesting subject. Experimentally, the angular alignment between the atomic beam and the cavity axis as well as the divergence of the atomic beam itself have to be improved by an order of magnitude to successfully measure the linewidth. Otherwise, the emission linewidth will be broadened by the Doppler shift.

Rabi dynamics can also be studied in a more direct way. The velocity selection permits control of the interaction time t_{int} precisely. Due to the Rabi-oscillation nature of the atom-cavity field interaction, the output of the one-atom laser is expected to oscillate as a function of the atom-field interaction time t_{int} as shown in Fig. 4-2.

4.0.5 Summary

In this work we have realized an one-atom laser for the first time. The laser oscillation was obtained with the mean number of atom in the cavity mode varied between 0.1 and 1.0, resulting in the mean photon number in the cavity changing from 0.14 to

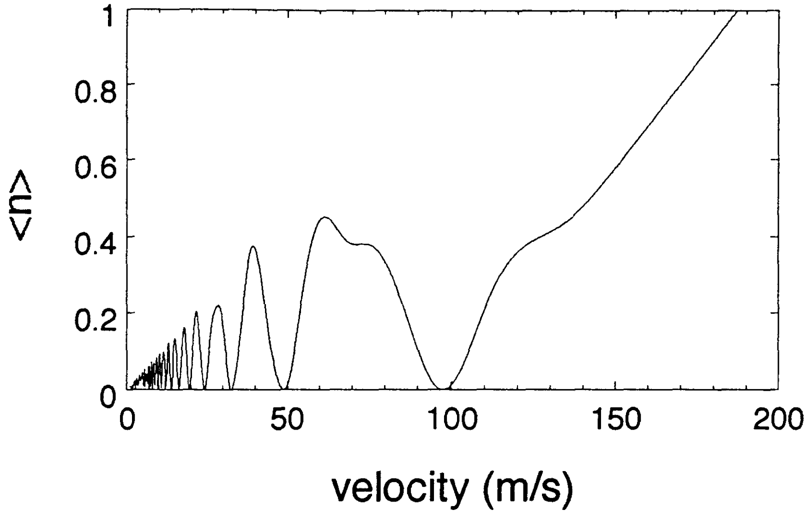

Figure 4-2: The mean number of photons as a function of the atomic velocity. All the experimental parameters were assumed to be the same as those of the present experiment except the finesse (increased to 1.2×10^6), the cavity length (decreased to 300 μm) and the velocity (varied from zero to 200 m/s).

11. In the present setup, the one-atom laser can emit up to 10^7 photons per second. We observed no distinct threshold behavior as the number of atoms were varied. We found that the measured mean photon number agreed with a fully quantized one-atom theory (to be described in Chap.2) as long as the mean number of atoms was much less than unity. However, the measured mean photon number was much larger than the prediction of the one-atom theory when the number of atoms was comparable to unity. This discrepancy was explained by incorporating the standing-wave nature of the cavity mode into the theory.

Appendix A

Derivation of Ringdown Formulae

Suppose a monochromatic plane-wave laser field is incident on a Fabry-Perot resonator. We assume that the distance between mirrors is changing in time:

$$L(t) = L_o + vt\ . \tag{A.1}$$

The velocity v is assumed to be so small that for a time interval we consider $\frac{vt}{L} \ll 1$ or $L(t) \approx L_o$. Both mirrors have a reflectivity of r and transmitivity of t. Then the electric field inside the resonator at any instance is given by

$$\begin{aligned} E_{in}(t) &= tE_o\,\mathrm{e}^{ikz-\omega t} \\ &+ tr^2E_o\,\mathrm{e}^{ik\left[z+2L\left(t-\frac{L_o}{c}\right)\right]-i\omega t} \\ &+ tr^4E_o\,\mathrm{e}^{ik\left[z+2L\left(t-\frac{3L_o}{c}\right)+2L\left(t-\frac{L_o}{c}\right)\right]-i\omega t} \\ &+ \cdots \\ &+ tr^{2n}E_o\,\mathrm{e}^{ik\left[z+\sum_{m=1}^{n}2L\left(t-\frac{(2m-1)L_o}{c}\right)\right]-i\omega t} \\ &+ \cdots\ . \end{aligned} \tag{A.2}$$

The summation in the exponent is simplified as

$$\sum_{m=1}^{n} 2L\left(t-\frac{(2m-1)L_o}{c}\right) = \sum_{m=1}^{n} 2L(t) - 2v\frac{(2m-1)L_o}{c}$$

$$
\begin{aligned}
&= 2nL(t) - 2L_o\left(\frac{v}{c}\right)\sum_{m=1}^{n}(2m-1) \\
&= 2nL(t) - 2L_o\left(\frac{v}{c}\right)n^2 \\
&= 2n\left[\left(1-n\frac{v}{c}\right)L_o + vt\right] . \qquad \text{(A.3)}
\end{aligned}
$$

So the field inside is

$$
E_{in}(t) = E_o\, \mathrm{e}^{i(kz-\omega t)} \sum_{n=0}^{\infty} r^{2n}\, \mathrm{e}^{i2nk\left[\left(1-n\frac{v}{c}\right)L_o+vt\right]} . \qquad \text{(A.4)}
$$

We assume the resonator becomes resonant with the incident field at $t = 0$ so

$$
kL_o = N\pi , \qquad \text{with } N = rminteger . \qquad \text{(A.5)}
$$

We also assume that the round trip time, $\frac{2L}{v}$, is much smaller than the cavity decay time so that an arbitrary time t can be expressed as $t = \frac{2L_o}{c}l$ with l being an integer. Then the phase factor in Eq.A.3 becomes

$$
\begin{aligned}
2nk\left[\left(1-n\frac{v}{c}\right)L_o + vt\right] &= 2nk\left[\left(1-n\frac{v}{c}\right)L_o + v\frac{2L_o}{c}l\right] \\
&= 2nk\left[L_o + (2l-n)\frac{v}{c}L_o\right] \\
&= 2nN\pi + kv\left(\frac{2L_o}{c}\right)n(2l-n)
\end{aligned}
$$

so that

$$
E_{in}(t) = E_o\, \mathrm{e}^{i(kz-\omega t)} \sum_{n=0}^{\infty} r^{2n}\, \mathrm{e}^{ikv\left(\frac{2L_o}{c}\right)n(2l-n)} . \qquad \text{(A.6)}
$$

The intensity then is

$$
I_{in}(t) \propto \left|\sum_{n=0}^{\infty} r^{2n}\, \mathrm{e}^{ikv\left(\frac{2L_o}{c}\right)n(2l-n)}\right|^2 . \qquad \text{(A.7)}
$$

The phase factor in the exponent can be written as a quadratic function of n, which is stationary when $n \approx l$. Only the terms with $n \approx l$ contribute to the summation constructively. As a lowest order approximation, we can treat r^{2n} factor as a constant and take it out of the summation. Then the intensity decays exponentially for large l.

$$\begin{aligned} I_{in}(t) &\propto |r|^{4l} \left| \sum_{n=0}^{\infty} \mathrm{e}^{ikv\left(\frac{2L_o}{c}\right)n(2l-n)} \right|^2 \\ &\propto R^{2l} = \mathrm{e}^{\ln R^{2l}} = \mathrm{e}^{2l \ln[1-(1-R)]} \approx \mathrm{e}^{-2(1-R)l} \\ &= \mathrm{e}^{-2(1-R)\frac{ct}{2L}} = \mathrm{e}^{-\Gamma_c t} . \end{aligned} \tag{A.8}$$

However in general the intensity exhibits a modulation on its exponential decay. We can rewrite Eq.A.6 as

$$\begin{aligned} I_{in}(t) &\propto \left| \sum_{n=0}^{\infty} r^{2n} \, \mathrm{e}^{ikv\left(\frac{2L_o}{c}\right)\left[l^2-(n-l)^2\right]} \right|^2 \\ &= \left| \sum_{n'=-l}^{\infty} r^{2(n'+l)} \, \mathrm{e}^{ikv\left(\frac{2L_o}{c}\right)\left[l^2-n'^2\right]} \right|^2 \\ &= \left| r^{2l} \, \mathrm{e}^{ikv\left(\frac{2L_o}{c}\right)l^2} \right|^2 \left| \sum_{n'=-l}^{\infty} r^{2n'} \, \mathrm{e}^{-ikv\left(\frac{2L_o}{c}\right)n'^2} \right|^2 \\ &= R^{2l} \left| \sum_{n'=-l}^{\infty} r^{2n'} \, \mathrm{e}^{-ikv\left(\frac{2L_o}{c}\right)n'^2} \right|^2 \\ &= R^{2l} \left| \sum_{n''=1}^{l} r^{-2n''} \, \mathrm{e}^{-ikv\left(\frac{2L_o}{c}\right)n''^2} + \sum_{n'=0}^{\infty} r^{2n'} \, \mathrm{e}^{-ikv\left(\frac{2L_o}{c}\right)n'^2} \right|^2 , \end{aligned} \tag{A.9}$$

where the second term is just a constant corresponding to a field amplitude at $t = 0$ whereas the first term corresponds to a modulation on the amplitude as a function of l or t. The modulation occurs because of the sinusoidal nature of the exponential function in the first term. The summation oscillates as a function of l. When l correponds to 2π of the phase factor of the exponential function, a first minimum of the decay curve occurs.

$$\begin{aligned} kv\left(\frac{2L_o}{c}\right) l^2 &= 2\pi \\ l &= \sqrt{\frac{\lambda c}{2L_o v}} . \end{aligned}$$

Therefore

$$t = \sqrt{\left(\frac{2L_o}{c}\right)\left(\frac{\lambda}{v}\right)} \,. \tag{A.10}$$

A k-th mininum occurs when

$$kv\left(\frac{2L_o}{c}\right)l^2 = 2k\pi \,,$$

so

$$t_k = \sqrt{k\left(\frac{2L_o}{c}\right)\left(\frac{\lambda}{v}\right)} \,. \tag{A.11}$$

Therefore, the time interval between the first minimum and the second one is

$$T \equiv t_2 - t_1 = \left(\sqrt{2}-1\right)\sqrt{\left(\frac{2L_o}{c}\right)\left(\frac{\lambda}{v}\right)} \,. \tag{A.12}$$

Appendix B

Computer Programs

B.1 Main Program

```
/****************************************************************/
/*                                                              */
/*                           ml3_5.c                            */
/*                                                              */
/****************************************************************/

/****************************************************************/
/* About program:                                               */
/* Qunatum recursion relation with off-diagonal field matrix    */
/* elements.  The standing wave nature of the cavity mode is    */
/* accounted for by an effective Delta_t.  Calculation is done */
/* for a given atomic velocity in the velocity distribution and */
/* the result is averaged over the distribution.               */
/*                                                              */
/* Last modified on 8-13-94                                     */
/****************************************************************/

#include <stdio.h>
#include <math.h>
#include <time.h>

/****************************************************************/
/* A header file contains constant and macro definitions.       */
/* It also include numerical recipe library files.              */
/****************************************************************/
#include "micro_header3.c"

/****************************************************************/
/* Global variables are defined here                            */
/****************************************************************/
double  _Ga_over_2g, _Nex, _theta, _alpha;
double _w0, _u_th, _N_atom, _Omega_R=1.0, _Gc_over_2pi, _g_over_2pi;
int _choice=1, _UseLastQ=0;
double _last_p[N_MAX+1][N_MAX+1], _last_q[N_MAX+1][N_MAX+1];
double _Delta_over_2g, _EXP=1.;

/****************************************************************/
/* _MAX_ITERATION is the maximum number of iteration in         */
/* calculating the density matrix elements.                     */
/* _N_CUTOFF is the largest n index of the density matix        */
/* elements.                                                    */
/* _TOLERANCE is the relative error in the numerical            */
```

```
/* integration.                                                */
/* EPS and K controls precision of numerical integration       */
/* NOTE: EPS and K are defined in the header file.             */
/**************************************************************/
int _MAX_ITERATION, _N_CUTOFF;
double _TOLERANCE;

main(argc, argv)
int argc;
char *argv[];
{
double n_mean[MAX_DATA_PNT], n_u_th[MAX_DATA_PNT];
double Ga_over_2pi, lambda, r0, finesse;
double z0, L, f, fsr;
int i, dothis=0;
int make_input_only=0, c;
FILE *inputfile, *parafile, *logfile;
double T1, T2;
double pnt[MAX_DATA_PNT];
int n_data_pnt;
double R, t_int_over_Delta_t;
long *tp;
FILE *errfile;

void set_to_vacuum();
double integrand_with_choice();
double f_MB();

while ((c = getopt (argc, argv, "ih")) != EOF)
switch (c) {
case 'i':
make_input_only=1;
break;
case 'h':
fprintf(stderr, "   Usage: ml3.5 [-ih]\n");
fprintf(stderr, "   This version allows you to choose...\n");
fprintf(stderr, "\t2_ changing Natom w/ velocity averaging\n");
fprintf(stderr, "\t3_ changing W_R w/ velocity averaging\n");
fprintf(stderr, "\t4_ changing detuning w/ velocity averaging\n");
exit(2);
break;
case '?':
fprintf(stderr, "Usage: ml3.5 [-ih]\n");
fprintf(stderr, "where -i  makes input file only\n");
fprintf(stderr, "      -h  displays user choices\n");
exit(2);
break;
}

/* open log file */
if (DEBUG) {
   if ((errfile=fopen(ERR_FILE, "w"))==NULL) {
perror(ERR_FILE);
exit();
}
   fclose(errfile);
   }
if (LOGGING) {
   if ((logfile=fopen(LOG_FILE, "a"))==NULL) {
perror(LOG_FILE);
exit();
}
   time(&tp);
   fprintf(logfile, "-----------------------------------------------------\n");
   fprintf(logfile, "%s\n", ctime(&tp));
   fclose(logfile);
   }

if ((inputfile=fopen(INPUTFILE, "w"))==NULL) {
```

```
perror(INPUTFILE);
exit();
}

/* PARA_FILE is read */
if ((parafile=fopen(PARA_FILE, "r"))==NULL) {
perror(PARA_FILE);
exit();
}
fscanf(parafile, "%d", &_UseLastQ);
fscanf(parafile, "%d", &_N_CUTOFF);
fscanf(parafile, "%d", &_MAX_ITERATION);
fscanf(parafile, "%lf", &_TOLERANCE);
fscanf(parafile, "%lf", &EPS);
fscanf(parafile, "%d", &K);
fclose(parafile);


/*************************User Input****************************/

fprintf(stderr, "Welcome to %s...\n", program_name);
fprintf(stderr, "This version allows averagin over velocity distribution\n");
fprintf(stderr, "as well as the cavity-atom detuning.\n\n");
fprintf(stderr, "Enter Ga/2pi in kHz:\n");
scanf("%lf", &Ga_over_2pi);
fprintf(stderr, "Enter wavelength in nanometer:\n");
scanf("%lf", &lambda);
fprintf(stderr, "Enter radius of curvature in cm:\n");
scanf("%lf", &r0);
fprintf(stderr, "Enter finesse in million:\n");
scanf("%lf", &finesse);
fprintf(stderr, "Enter thermal veleocity of atoms in m/s:\n");
scanf("%lf", &_u_th);
fprintf(stderr, "Enter cavity length in cm:\n");
scanf("%lf", &L);

fprintf(stderr, "Choose...with W_R=pump Rabi frequency...\n");
fprintf(stderr, "2_ changing Natom with velocity and spatial averaging\n");
fprintf(stderr, "3_ changing W_R with velocity averaging\n");
fprintf(stderr, "4_ changing detuning with velocity averaging\n");

scanf("%d", &dothis);

fprintf(inputfile, "%.3lf\n", Ga_over_2pi);
fprintf(inputfile, "%.3lf\n", lambda);
fprintf(inputfile, "%.3lf\n", r0);
fprintf(inputfile, "%.3lf\n", finesse);
fprintf(inputfile, "%.3lf\n", _u_th);
fprintf(inputfile, "%.3lf\n", L);
fprintf(inputfile, "%d\n", dothis);

if (dothis==2) {
   fprintf(stderr, "Enter number of Natom values to be entered:\n");
   scanf("%d", &n_data_pnt);
   fprintf(inputfile, "%d\n", n_data_pnt);
   fprintf(stderr, "Enter Natom values in sequence:\n");
   for (i=0; i<n_data_pnt; ++i) {
scanf("%lf", &pnt[i]);
fprintf(inputfile, "%lf\n", pnt[i]);
}
   }
else if (dothis==3) {
   fprintf(stderr, "Enter number of (W_R/W_pi) values to be entered:\n");
   scanf("%d", &n_data_pnt);
   fprintf(inputfile, "%d\n", n_data_pnt);
   fprintf(inputfile, "%d\n", n_data_pnt);
   fprintf(stderr, "Enter (W_R/W_pi) values in sequence:\n");
```

```
   for (i=0; i<n_data_pnt; ++i) {
scanf("%lf", &pnt[i]);
fprintf(inputfile, "%lf\n", pnt[i]);
}
   }
else if (dothis==4) {
   fprintf(stderr, "Enter number of detuning values to be entered:");
   scanf("%d", &n_data_pnt);
   fprintf(inputfile, "%d\n", n_data_pnt);
   fprintf(stderr, "Enter detuning values in sequence:");
   for (i=0; i<n_data_pnt; ++i) {
scanf("%lf", &pnt[i]);
fprintf(inputfile, "%lf\n", pnt[i]);
}
   }
else {
   fprintf(stderr, "*** Wrong choice !!  Terminated...\n");
   exit();
   }
if (!(dothis==2)) {
   fprintf(stderr, "Enter number of atoms inside cavity:\n");
   scanf("%lf", &_N_atom);
   fprintf(inputfile, "%.3lf\n", _N_atom);
   }
if (!(dothis==3)) {
   fprintf(stderr, "Enter W_R/W_pi:\n");
   scanf("%lf", &_Omega_R);
   fprintf(inputfile, "%.3lf\n", _Omega_R);
   }

fclose(inputfile);
if (make_input_only) exit();

/**************************End of Input**************************/

T1=clock();

/* calculated once. does not depend on Natom nor velocity  */
z0=sqrt(r0*L/2.); /* in cm */
fsr=3.e4/2./L; /* in MHz */
_w0=sqrt(lambda*10.*z0/pi); /* in micron */
f=3./4.*sqr(lambda/pi/_w0)*1.e-6;
_Gc_over_2pi=fsr/finesse/1.e6; /* in MHz */
_g_over_2pi=sqrt(2./pi*fsr*f*Ga_over_2pi/1000.); /* in MHz */
_Ga_over_2g=Ga_over_2pi/1000./2./_g_over_2pi;

/* generate common header information */
printf("# This file was generated by %s.\n", program_name);
printf("# Ga/2pi=%.2lf kHz  lambda=%.2lf nm  r0=%.2lf cm\n",
Ga_over_2pi, lambda, r0);
printf("# u=%.2lf m/s  length=%.2lf cm  finesse=%.2lf million\n",
_u_th, L, finesse);
printf("# z0=%.2le cm  w0=%.2le micron  f=%.2le\n", z0, _w0, f);
printf("# Gc/2pi=%.2le MHz  g/2pi=%.2le MHz\n", _Gc_over_2pi, _g_over_2pi);
printf("# max_iteration=%d    tolerance=%.2le    _N_CUTOFF=%d\n",
_MAX_ITERATION, _TOLERANCE, _N_CUTOFF);
printf("# EPS=%.2le   JMAX=%d   K=%d\n", EPS, JMAX, K);

if (dothis==2) {
   printf("# N_atom is varied...W_R/W_pi=%.2le  w/ velocity ", _Omega_R);
   printf("and spatial averaging...\n");
   printf("# N_atom      t_int/Delta_t  n(averaged)   n(v=u_th)\n");
   }
else if (dothis==3) {
   printf("# W_R/W_pi is varied...N_atom=%.2le  w/ velocity ",
_N_atom);
   printf("and spatial averaging...\n");
```

```
   printf("# W_R/W_pi    n(averaged)    n(v=u_th)\n");
   }
else if (dothis==4) {
   printf("# detuning is varied...N_atom=%.2le  W_R/W_pi=%.2le  ",
_N_atom, _Omega_R);
   printf("/w velocity and spatial averaging\n");
   printf("# detuning    n(averaged)    n(v=u_th)\n");
   }

set_to_vacuum(_last_p, _last_q);

if (dothis!=2) {
t_int_over_Delta_t = _N_atom*sqrt(2.);
/* _EXP=exp(t_int_over_Delta_t); */
}
if (dothis!=4) _Delta_over_2g = 0.;

if (dothis==2) {
   for (i=0; i<n_data_pnt; ++i) {
_N_atom=pnt[i];
t_int_over_Delta_t = _N_atom*sqrt(2.);
/* _EXP=exp(t_int_over_Delta_t); */

/*_Omega_R = 1.;*/
_choice=1;

n_mean[i]=qromo(integrand_with_choice, _TOLERANCE, 1.0, midpnt)
+ qromo(integrand_with_choice, 1.0, INFINITY, midinf);

n_u_th[i]=integrand_with_choice(1.0)/f_MB(1.0);

printf("%.4le   %.4le   %.4le   %.4le\n",
_N_atom, t_int_over_Delta_t, n_mean[i], n_u_th[i]);

if (LOGGING) {
   logfile=fopen(LOG_FILE, "a");
   fprintf(logfile, "TOLERANCE=%.2le  EPS=%.2le  N_CUTOFF=%d\n",
_TOLERANCE, EPS, _N_CUTOFF);
   fprintf(logfile,
"N_atom=%.3le t_int/Delta_t=%.3le <n>=%.4le n_u_th=%.4le\n",
pnt[i], t_int_over_Delta_t, n_mean[i], n_u_th[i]);
   fprintf(logfile, "............................................\n");
   fclose(logfile);
   }
fprintf(stderr, "+");
}
   fprintf(stderr, "\n");
   }
else if (dothis==3) {
   for (i=0; i<n_data_pnt; ++i) {
_Omega_R = pnt[i];

_choice=1;

n_mean[i]=qromo(integrand_with_choice, _TOLERANCE, 1.0, midpnt)
+ qromo(integrand_with_choice, 1.0, INFINITY, midinf);

n_u_th[i]=integrand_with_choice(1.0)/f_MB(1.0);

printf("%.4le   %.4le   %.4le\n", _Omega_R, n_mean[i], n_u_th[i]);
if (LOGGING) {
   logfile=fopen(LOG_FILE, "a");
   fprintf(logfile, "TOLERANCE=%.2le  EPS=%.2le  N_CUTOFF=%d\n",
_TOLERANCE, EPS, _N_CUTOFF);
   fprintf(logfile, "Omega_R=%.3le  <n>=%.4le  n_u_th=%.4le\n",
pnt[i], n_mean[i], n_u_th[i]);
   fprintf(logfile, "............................................\n");
   fclose(logfile);
```

```
   }
fprintf(stderr, "+");
}
   fprintf(stderr, "\n");
   }
else if (dothis==4) {
   for (i=0; i<n_data_pnt; ++i) {
_Delta_over_2g = pnt[i]/(2.*_g_over_2pi);

/*_Omega_R = 1.;*/
_choice=1;

n_mean[i]=qromo(integrand_with_choice, _TOLERANCE, 1.0, midpnt)
+ qromo(integrand_with_choice, 1.0, INFINITY, midinf);

n_u_th[i]=integrand_with_choice(1.0)/f_MB(1.0);

if (LOGGING) {
   logfile=fopen(LOG_FILE, "a");
   fprintf(logfile, "TOLERANCE=%.2le  EPS=%.2le  N_CUTOFF=%d\n",
_TOLERANCE, EPS, _N_CUTOFF);
   fprintf(logfile, "detuning=%.3le <n>=%.4le  n_u_th=%.4le\n",
pnt[i], n_mean[i], n_u_th[i]);
   fprintf(logfile, "..........................................\n");
   fclose(logfile);
   }
fprintf(stderr, "+");
}
   fprintf(stderr, "\n");

   for (i=n_data_pnt-1; i>0; --i)
printf("-%.4le  %.4le   %.4le\n", pnt[i], n_mean[i], n_u_th[i]);
   for (i=0; i<n_data_pnt; ++i)
printf("%.4le   %.4le   %.4le\n",  pnt[i], n_mean[i], n_u_th[i]);
   }

T2=clock();
printf("It has taken %lf sec\n", (T2-T1)*1.e-6);
fprintf(stderr, "It has taken %lf sec\n", (T2-T1)*1.e-6);

} /* end of main */

#include "micro_integrand3.c"
#include "micro_Q_core5.c"
```

B.2 Included File 1

```
/*****************************************************************/
/*                                                               */
/*                       micro_header3.c                         */
/*                                                               */
/*****************************************************************/

/*****************************************************************/
/* 2^{JMAX-1} is the max number of divisions allowd in the       */
/* numerical integration                                         */
/*****************************************************************/
#define JMAX 10

/*****************************************************************/
/* PARA_FILE contains the value of EPS, and K, which             */
/* control the numerical integration                             */
/*****************************************************************/
#define PARA_FILE "ml3.PARA"
```

```
/****************************************************************/
/* N_MAX+1 is the row and column size of p and q arrays.        */
/* So N_MAX is the largest N_CUTOFF allowed.                    */
/* MAX_DATA_PNT is the max number of data point to calculate    */
/****************************************************************/
#define N_MAX 102
#define MAX_DATA_PNT 100

/****************************************************************/
/* If DEBUG is defined, ERROR file is generated. The ERROR file */
/* contains p[i][i] values and number of iteration.             */
/****************************************************************/

#define ERR_FILE "ml3.ERROR"
#define LOG_FILE "ml3.LOG"
#define INPUTFILE "ml3.INPUT"
#define DEBUG 1
#define LOGGING 1
#define DOTS_FROM_QROMO 1

double EPS=0;
int K=0;

#include "../numrec/nrutil.c"
#include "../numrec/polint.c"
#include "../numrec/midpnt.c"
#include "../numrec/midinf.c"

#include "../numrec/Qromo.c"

#define sqr(x) ((x)*(x))
#define program_name "ml3_5.c"
#define INFINITY  1.e30
#define         pi              3.141592
```

B.3 Included File 2

```
/*********************************************************************/
/*                                                                   */
/*                        micro_integrand3.c                         */
/*                                                                   */
/*********************************************************************/

double integrand_with_choice(x)
double x;
/*********************************************************************/
/* The following parameters should be set before calling this routine. */
/*  _w0, _Natom, _Omega_R, _Gc_over_2pi, _g_over_2pi,                */
/* _Ga_over_2g,  _power                                             */
/* This routine will set the following parameters before it calls   */
/* calculate...routines.                                             */
/*  _alpha, _Nex, _theta                                             */
/* If _choice=1 or 2, <n> or <n2> is returned.                       */
/* If _choice=3, <FW> is returned.                                   */
/* If _choice=4, integral of f_MB(v) is returned. test purpose       */
/* In form, this routine is a one-variable function.                 */
/*********************************************************************/
{
double t_int, R, n;
double p[N_MAX+1][N_MAX+1], q[N_MAX+1][N_MAX+1];

int calculate_Q();
double calculate_n_to_p_average();
double f_MB();
void print_to_stdout();
```

```
t_int=sqrt(pi)*_w0/x/_u_th; /* in microsecond */

/***********************************************************************/
/* for effective atom number argument                                  */
R=_N_atom/t_int*sqrt(2.);                       /* million per second  */
/***********************************************************************/

_alpha=sqr(sin(pi/2./x*_Omega_R));
_Nex=R/(2.*pi*_Gc_over_2pi);
_theta=sqrt(_Nex)*_g_over_2pi*t_int*2.*pi;

calculate_Q(p, q, _TOLERANCE);

if (_choice==1) { /* <n> */
n = calculate_n_to_p_average(1., p);
return n*f_MB(x);
}
else if (_choice==4) return f_MB(x);  /* test purpose */
else if (_choice==5) {
print_to_stdout(p, q);
n = calculate_n_to_p_average(1., p);
return n*f_MB(x);
}

}

double f_MB(x)
double x;
/***********************************************************************/
/* This function calculates Maxwell-Boltzman velocity distribution    */
/* Before calling _u_th should be set.                                 */
/***********************************************************************/
{
return 4.*sqr(x)*exp(-sqr(x))/sqrt(pi);
}

void print_to_stdout(p, q)
double (*p)[N_MAX+1], (*q)[N_MAX+1];
{
int i, j;
double  norm[N_MAX+1][N_MAX+1];

for (i=0; i<=_N_CUTOFF; ++i) {
for (j=0; j<=_N_CUTOFF; ++j) {
if (i>j) printf("%.2le  ", norm[j][i]);
else if (i==j) printf("%.2le  ", p[i][i]);
else if (i<j) {
norm[i][j]=sqrt(sqr(p[i][j])+sqr(q[i][j]));
printf("%.2le  ", norm[i][j]);
}
}
printf("\n");
}
}
```

B.4 Included File 3

```
/***************************************************************************/
/*                                                                         */
/*                           micro_Q_core5.c                               */
/*                                                                         */
/***************************************************************************/

/***************************************************************************/
/* This file is included by ml3_5.c.                                       */
```

```
/* It contains low-level routines used in the program.                     */
/* It is based on a recursion relation for field density matrix elements.  */
/* It replaces micro_core.c and micro_new_core.c .                         */
/* Last modification on 7/3/94                                             */
/**************************************************************************/

void    terminate(s)
char    *s;
{
FILE    *errfile;

if (DEBUG) {
        errfile=fopen(ERR_FILE, "a");
        fprintf(errfile, "*** too many iterations in calculating %s(>%d)\n",
                        s, _MAX_ITERATION);
        fclose(errfile);
        }
fprintf(stderr, "*** too many iterations in calculating %s(>%d)\n",
                        s, _MAX_ITERATION);
exit();
}


double C(n)
int n;
{
if (n<0) return 1.; /* if n == -1 */
else return cos(_theta/sqrt(_Nex)*sqrt(n+1.+sqr(_Delta_over_2g)));
}

double Sd(n)
int n;
{
double S, X;

if (n<0) return 0;
if (_Delta_over_2g==0.) return 0.;
X=sqrt(n+1.+sqr(_Delta_over_2g));
S=sin(_theta/sqrt(_Nex)*X);
S*=( _Delta_over_2g/X);
return S;
}

double Sk(n)
int n;
{
double S, X;

if (n<0) return 0;
X=sqrt(n+1.+sqr(_Delta_over_2g));
S=sin(_theta/sqrt(_Nex)*X);
if (_Delta_over_2g==0.) return S;
S*=(sqrt(n+1.)/X);
return S;
}

void iterate_Q(p, q)
double (*p)[N_MAX+1], (*q)[N_MAX+1];
/**************************************************************************/
/* This routine calculates next higher order approximation of Q array from */
/* inital approximation given by p and q.                                  */
/*                                                                         */
/* p+iq =inital/next order approximation of Q array                        */
/**************************************************************************/
{
double rho_aa, rho_bb, rho_ab, p0[N_MAX+1][N_MAX+1], q0[N_MAX+1][N_MAX+1];
double A, B, c, D, E, F, G, x, y, Z;
int n, m;
double C_n, C_m, C_n_1, C_m_1, Sd_n, Sd_m, Sd_n_1, Sd_m_1, Sk_n, Sk_m,
```

```
Sk_n_1, Sk_m_1;

rho_aa = _alpha;
rho_bb = 1.- rho_aa;
rho_ab = sqrt(rho_aa*rho_bb);

for (n=0; n<=_N_CUTOFF; ++n)
for (m=0; m<=_N_CUTOFF; ++m) {
p0[n][m]=p[n][m];
q0[n][m]=q[n][m];
}
for (n=0; n<=_N_CUTOFF; ++n) {
C_n=C(n);
C_n_1=C(n-1);
Sd_n=Sd(n);
Sd_n_1=Sd(n-1);
Sk_n=Sk(n);
Sk_n_1=Sk(n-1);

for (m=n; m<=_N_CUTOFF; ++m) {
C_m=C(m);
C_m_1=C(m-1);
Sd_m=Sd(m);
Sd_m_1=Sd(m-1);
Sk_m=Sk(m);
Sk_m_1=Sk(m-1);

A = rho_aa*(C_n*C_m + Sd_n*Sd_m)
   + rho_bb*(C_n_1*C_m_1+Sd_n_1*Sd_m_1);
x = A*p0[n][m];
y = A*q0[n][m];

if (m>n) {
A= rho_aa*(C_n*Sd_m-C_m*Sd_n)
   + rho_bb*(C_n_1*Sd_m_1-C_m_1*Sd_n_1);
x += A*q0[n][m];
y += -A*p0[n][m];
}

if ((m<_N_CUTOFF)&&(n<_N_CUTOFF)) {
B = rho_bb*Sk_n*Sk_m
+ sqrt((double)((n+1.)*(m+1.)))/_Nex*_EXP;
x += B*p0[n+1][m+1];
y += B*q0[n+1][m+1];
}

if ((m>0)&&(n>0)) {
c = rho_aa*Sk_n_1*Sk_m_1;
x += c*p0[n-1][m-1];
y += c*q0[n-1][m-1];
}

if (n<_N_CUTOFF) {
D = rho_ab*Sk_n*C_m;
x += -D*p0[n+1][m];
y += -D*q0[n+1][m];
D = rho_ab*Sk_n*Sd_m;
x += -D*q0[n+1][m];
y += D*p0[n+1][m];
}

if (m<_N_CUTOFF) {
E = rho_ab*C_n*Sk_m;
x += -E*p0[n][m+1];
y += -E*q0[n][m+1];
E = rho_ab*Sd_n*Sk_m;
x += E*q0[n][m+1];
y += -E*p0[n][m+1];
}
```

```
if (m>0) {
F =  rho_ab*C_n_1*Sk_m_1;
x += F*p0[n][m-1];
y += F*q0[n][m-1];
F =  rho_ab*Sd_n_1*Sk_m_1;
x += F*q0[n][m-1];
y += -F*p0[n][m-1];
}

if (n>0) {
G =  rho_ab*Sk_n_1*C_m_1;
x += G*p0[n-1][m];
y += G*q0[n-1][m];
G =  rho_ab*Sk_n_1*Sd_m_1;
x += -G*q0[n-1][m];
y += G*p0[n-1][m];
}

Z = (1.+ 0.5/_Nex*(double)(n+m))*_EXP;
p[n][m] = x/Z;
q[n][m] = y/Z;

if (n!=m) {
p[m][n] = p[n][m]; /* hermitian */
q[m][n] = -q[n][m];
}
}
}
}

double normalize_Q(p, q)
double (*p)[N_MAX+1], (*q)[N_MAX+1];
/*************************************************************************/
/* This routine normalizes input Q array                                 */
/*                                                                       */
/* p+iq =input/output Q array                                            */
/*************************************************************************/
{
double sum=0.;
int i, j;

for (i=0; i<=_N_CUTOFF; ++i) sum+=p[i][i];
for (i=0; i<=_N_CUTOFF; ++i)
for (j=0; j<=_N_CUTOFF; ++j) {
p[i][j]=p[i][j]/sum;
q[i][j]=q[i][j]/sum;
}
return sum;
}

void initialize_Q(p, q, p2, q2)
double (*p)[N_MAX+1], (*p2)[N_MAX+1], (*q)[N_MAX+1], (*q2)[N_MAX+1];
/***********************************************************************/
/* Q is initialized using Q2                                           */
/***********************************************************************/
{
int i, j;

for (i=0; i<=_N_CUTOFF; ++i)
for (j=0; j<=_N_CUTOFF; ++j) {
p[i][j]=p2[i][j];
q[i][j]=q2[i][j];
}
}

void set_to_vacuum(p, q)
double (*p)[N_MAX+1], (*q)[N_MAX+1];
/***********************************************************************/
```

```
/* Q is initialized to vacuum                                             */
/*************************************************************************/
{
int i, j;

for (i=0; i<=_N_CUTOFF; ++i)
for (j=0; j<=_N_CUTOFF; ++j) {
p[i][j]=0.;
q[i][j]=0.;
}
p[0][0]=1.;
}

int calculate_Q(p, q, error)
double (*p)[N_MAX+1], (*q)[N_MAX+1], error;
/*****************************************************************************/
/* This routine calculates Q array for given initial condition by Q0 until */
/* desired convergence specified by error is obtained.                      */
/*                                                                          */
/* p+iq =inital/final Q array                                               */
/* error=allowed error                                                      */
/* number of iteration is returned                                         */
/*****************************************************************************/
{
double norm, dp_00, old_p_00, dp_NN;
int i, n=0, negative_Q=0;
FILE *errfile;

if (_UseLastQ) initialize_Q(p, q, _last_p, _last_q);
else set_to_vacuum(p, q);

old_p_00=p[0][0];
do {
iterate_Q(p, q);
norm=normalize_Q(p, q);
dp_00=fabs(p[0][0]/old_p_00-1.);

if (n>_MAX_ITERATION/4) dp_NN=fabs(p[_N_CUTOFF][_N_CUTOFF]/p[0][0]);
else dp_NN=p[0][0];

old_p_00=p[0][0];

for (i=0; i<=_N_CUTOFF; ++i) {
if (p[i][i]<0) negative_Q=1;
}
++n;
if (n>_MAX_ITERATION) terminate("calculate_Q");
} while ((dp_00 > error)&&(dp_NN > error/2)&&(!negative_Q));
if (DEBUG) {
errfile=fopen(ERR_FILE, "a");
if (n>_MAX_ITERATION/4) {
fprintf(errfile, "%3d", n);
for (i=0; i<=_N_CUTOFF; ++i)
fprintf(errfile, "|%.3le", p[i][i]);
fprintf(errfile, "\n");
}
fclose(errfile);
}

if (_UseLastQ) initialize_Q(_last_p, _last_q, p, q);

if (negative_Q) n=-1;

return n;
}

double calculate_n_to_p_average(x, p)
double x, (*p)[N_MAX+1];
/*****************************************************************************/
```

```
/* This routine calculates <n^p> for given velocity v                    */
/*                                                                       */
/* p+iq =final Q array                                                   */
/* <n^x> is returned                                                     */
/*************************************************************************/
{
double sum=0.;
int i;

for (i=0; i<=_N_CUTOFF; ++i) sum += pow((double)i, x)*p[i][i];
return sum;
}
```

Bibliography

[1] D. J. Heinzen, Ph.D. thesis, Massachusetts Institute of Technology, 1986.

[2] E. T. Jaynes and F. W. Cummings, Proc. IEEEE **51**, 89 (1963).

[3] R. J. Thompson, G. Rempe, and H. J. Kimble, Phys. Rev. Lett. **64**, 2499 (1992).

[4] D. Meschede, H. Walther, and G. Muller, Phys. Rev. Lett. **54**, 551 (1985).

[5] P. G. Kwiat, A. M. Steinberg, R. Y. Chiao, P. H. Eberhard, and M. D. Petroff, Phys. Rev. A **48**, R867 (1993).

[6] J. Krause, M. O. Scully, T. Walther, and H. Walter, Phys. Rev. A **39**, 1915 (1989).

[7] G .Rempe, R. J. Thompson, and H. J. Kimble, Opt. Lett. **17**, 363 (1992).

[8] A. L. Schawlow and C. H. Townes, Physcal Review **112**, 1940 (1958).

[9] A. E. Siegman, *Lasers* (University Science Books, Mill Valley, CA, 1986), pp. 453–454.

[10] M. Sargent III, M. O. Scully, and W. E. Lamb, Jr., *Laser Physics* (Addison-Wesley, Reading, Mass, 1974), pp. 335–339.

[11] *Cavity Quantum Electrodynamics*, edited by P. Berman (Academic Press, Inc., NY, 1993).

[12] E. M. Purcell, Phys.Rev. **69**, 681 (1946).

[13] P. Goy, J. M. Raimond, M. Gross, and S. Haroche, Phys. Rev. Lett. **50**, 1903 (1983).

[14] R. G. Hulet, E. S. Hilfer, and D. Kleppner, Phys. Rev. Lett. **55**, 2137 (1985).

[15] W. Jhe, A. Anderson, E. A. Hinds, D. Meschede, L. Moi, and S. Haroche, Phys. Rev. Lett. **58**, 666 (1987).

[16] D. J. Heinzen, J. J. Childs, J. E. Thomas, and M. S. Feld, Phys. Rev. Lett. **58**, 1320 (1987).

[17] F. De Martini, G. Innocenti, G. R. Jacobovitz, and P. Mataloni, Phys. Rev. Lett. **59**, 2955 (1987).

[18] D. J. Heinzen and M. S. Feld, Phys. Rev. Lett. **59**, 2623 (1987).

[19] M. Brune, S. Haroche, V. Lefevre, J. M. Raimond, and N. Zagury, Phys. Rev. Lett. **65**, 976 (1990).

[20] M. Brune, P. Nussenzveig, F. Schmidt-Kaler, F. Bernardot, A. Maali, J. M. Raimond, and S. Haroche, Phys. Rev. Lett. **72**, 3339 (1994).

[21] Y. Kaluzny, P. Goy, M. Gross, J. M. Raimond, and S. Haroche, Phys. Rev. Lett. **51**, 1175 (1983).

[22] M. G. Raizen, R. J. Thompson, R. J. Brecha, H. J. Kimble, and H. J. Carmichael, Phys. Rev. Lett. **63**, 240 (1989).

[23] Y. Zhu, D. J. Gauthier, S. E. Morin, Q. Wu, H. J. Carmichael, and T. W. Mossberg, Phys. Rev. Lett. **64**, 2499 (1990).

[24] J. J. Childs, Kyungwon An, R. R. Dasari, and M. S. Feld, in *Cavity Quantum Electrodynamics*, *Advances in Atomic,Molecular, and Optical Physics*, edited by P. Berman (Academic Press, Inc., NY, 1993).

[25] S. Haroche and D. Kleppner, Physics Today __, 24 (1989).

[26] Steven E. Morin, Qilin Wu, and Thomas W. Mossberg, Optics & Photonics News __, 1992 (1992).

[27] K. An, J. J. Childs, R. R. Dasari, and M. S. Feld, *Single-atom emission in an optical resonator: cavity-QED laser*, International Laser Science Conference, Albuquerque, NM 1992, paper no. TuN5.

[28] Y. Mu and C. Savage, Phys. Rev. A **46**, 5944 (1992).

[29] Christian Ginzel, Hans-Jurgen Briegel, Ullrich Martini, Berthold-Georg Englert and Axel Schenzle, Phys. Rev. A **48**, 732 (1993).

[30] T. Pellizzari and H. Ritsch, Journal of Modern Optics **41**, 609 (1994).

[31] T. Pellizzari and H. Ritsch, Phys. Rev. Lett. **72**, 3973 (1994).

[32] J. Kimble, *Quantum optics with atoms trapped in a cavity*, Americal Physcial Society Meeting, Crystal City, Virginia (1994), paper np. F3.2.

[33] T. W. Mossberg, private communication., 1994.

[34] S. Qamar and M. S. Zubairy, Phys. Rev. A **44**, 7804 (1991).

[35] M. O. Scully, H. Walther, G. S. Agarwal, T. Quang, and W. Schleich, Phys. Rev. A **44**, 5992 (1991).

[36] K. Vogel, W. P. Schleich, M. O. Scully, and H. Walther, Phys. Rev. A **48**, 813 (1993).

[37] T. Quang, G. S. Agarwal, J. Bergou, M. O. Scully, and H. Walther, Phys. Rev. A **48**, 803 (1993).

[38] N. Lu, Phys. Rev. A **47**, 1347 (1993).

[39] P. Filipowicz, J. Javanainen, and P. Meystre, J. Opt. Soc. Am. **B3**, 906 (1986).

[40] J. C. Retamal, L. Roa, and C. Saavedra, Phys. Rev. A **45**, 1876 (1992).

[41] G. Rempe, H. Walther, and N. Klein, Phys. Rev. Lett. **58**, 353 (1987).

[42] G. Rempe, M. O. Scully, and H. Walther, Physica Scripta **T34**, 5 (1991).

[43] J. Krause, M. O. Scully, and H. Walther, Phys. Rev. A **36**, 4547 (1987).

[44] P. Meystre and M. S. Zubairy, Physics Letters **89A**, 390 (1982).

[45] M. Sargent III, M. O. Scully, and W. E. Lamb, Jr., *Laser Physics* (Addison-Wesley, Reading, MA, 1974), pp. 230–236.

[46] A. Heidmann, J. M. Raimond, and S. Reynaud, Phys. Rev. Lett. **54**, 326 (1985).

[47] P. Filipowicz, J. Javanaine, and P. Meystre, Phys. Rev. A **34**, 3077 (1986).

[48] J. Krause, M. O. Scully, and H. Walther, Phys. Rev. A **34**, 2032 (1986).

[49] J. R. Kuklinski and J. L. Madajczyk, Phys. Rev. A **37**, 3175 (1988).

[50] W. H. Press, B. P. Flannery, S. A. Teukolsky, and W. T. Vetterling, *Numerical Recipes in C* (Cambridge University Press, Cambridge, 1988), pp. 111–141.

[51] W. H. Beyer, *CRC standard mathematical tables*, 25 ed. (CRC Press Inc., Palm Beach, Fla, 1978), pp. 433–435.

[52] A. E. Siegman, *Lasers* (University Science Books, Mill Valley, CA, 1986), pp. 505–509.

[53] A. E. Siegman, *Lasers* (University Science Books, Mill Valley, CA, 1986), pp. 510–522.

[54] A. A. Radzig and B. M. Smirnov, *Reference Data on Atoms, Molecules, and Ions*, *Chemical Physics 31* (Springer-Verlag, New York, Berlin, ———), pp. 219, 229.

[55] W. H. Parkinson and F. S. Tomkins, J. Opt. Soc. Am. **68**, 535 (1978).

[56] Daniel J. Gauthier, Yifu Zhu, and T. W. Mossberg, Phys. Rev. Lett. **66**, 2460 (1991).

[57] ———, *Atomic data and Nuclear data table* (———, ———, 1968), Vol. 1, p. 1.

[58] R. Lalezari, PMS Electro-Optics, 1855 South 57th Court, Boulder, Colorado 80301; private communication.

[59] A. Yariv, *Quantum Electronics*, 2 ed. (John Wiley & Sons, Inc., New York, 1975), p. 141.

[60] W. P. Drever, J. L. Hall, F. V. Kowalski, J. Hough, G. M. Ford, A. J. Munley, and H. Ward, Appl. Phys. B **31**, 97 (1983).

[61] G. C. Bjorklund, Opt. Lett. **5**, 15 (1980).

[62] P. Horowitz and W. Hill, *The art of electronics*, 2 ed. (Cambridge University Press, Cambridge, _), pp. 885–886.

[63] Leo Hollberg, in *Dye laser principles with applications*, *Quantum electronics-principle and applications*, edited by F. J. Duarte and L. W. Hillman (Academic Press, Inc., Boston, 1990), pp. 214–216.

[64] Hamamatsu PMT catalog, 1991.

[65] S. Harvell, MDC Vacuum Products Corporation, 23842 Cabot Boulevard, Hayward, CA 94545-1651; private communication.

[66] M. Orszag and R. Ramirez, Phys. Rev. A **49**, 2933 (1994).

[67] K. Molmer, K. Berc-Sorensen, Y. Castin, and J. Dalibard, *Monte Carlo wave-function method in quantum optics*, International Laser Science Conference, Albuquerque, NM 1992, paper no. MFF1.

[68] P. Zoller, *Monte Carlo simulation of the quantum master equation for vacuum thermal and squeezed reservoirs*, International Laser Science Conference, Albuquerque, NM 1992, paper no. MFF2.

[69] L. Tian and H. J. Carmichael, *Quantum trajectory calculations in cavity QED*, International Laser Science Conference, Albuquerque, NM 1992, paper no. TuJJ1.

[70] H. J. Carmichael, L. Tian, and P. Kochan, *Decay of quantum coherence using quantum trajectories*, International Laser Science Conference, Albuquerque, NM 1992, paper no. MFF4.

[71] P. D. Lett, *Monte Carlo wavefunction solution of the spectrum of Rb in a 1-D optical molasses*, International Laser Science Conference, Albuquerque, NM 1992, paper no. MFF5.

[72] J. Nellessen, J. H. Müller, K. Sengstock, and W. Ertmer, J. Opt. Soc. Am. **B6**, 2149 (1989).

[73] W. Nagourney, J. Sandberg, and H. Dehmelt, Phys. Rev. Lett. **56**, 2797 (1986).

[74] Th. Sauter, W. Neuhauser, R. Blatt, and P. E. Toschek, Phys. Rev. Lett. **57**, 1696 (1986).

[75] J. C. Bergquist, R. G. Hulet, W. M. Itano, and D. J. Wineland, Phys. Rev. Lett. **57**, 1699 (1986).